Examination of channel catfish (*Ictalurus punctatus*) leukocyte immune-type receptor-mediated crosstalk regulation of phagocytosis

by

Chenjie Fei

A thesis submitted in partial fulfillment of requirements for the degree of

Doctor of Philosophy

in

Physiology, Cell, and Developmental Biology

Department of Biological Sciences

University of Alberta

ABSTRACT

Across vertebrates, innate immune cells are capable of initiating a range of potent effector responses that are designed to destroy or contain foreign microbial invaders. The execution and regulation of various innate cellular responses is mediated by a dedicated repertoire of cell surface-expressed immune receptor proteins. These specialized receptors, known as immunoregulatory receptors, sense extracellular stimuli and activate intracellular signaling cascades that elicit appropriate effector responses.

Channel catfish (*Ictalurus punctatus*) leukocyte immune type receptors (IpLITRs) belong to a polygenic and polymorphic immunoregulatory receptor family. These teleost proteins are structurally and phylogenetically related to several mammalian immunoregulatory proteins within the immunoglobulin super family (IgSF). The IpLITR family consists of multiple members that exist as generally as putative inhibitory or stimulatory types. Functional characterization of representative IpLITR-types using heterologous overexpression approaches has shown that these teleost proteins are capable of mediating various innate effector responses via classical as well as unique intracellular signaling networks. Previously, it was shown that IpLITR 2.6b activates phagocytosis and degranulation in rat basophil leukocytes (RBL-2H3) using a canonical ITAM-dependent signaling pathway; whereas a putative inhibitory IpLITR-type (i.e. IpLITR 1.1b) functioned as a potent inhibitor of NK cell-mediated cytotoxicity via an ITIM-mediated phosphatases recruitment as well as a distinct ITIM-independent signaling pathway. Moreover, specific triggering of IpLITR 1.1b in myeloid cells activate the phagocytic responses, likely through activation of an alternative ITAM-independent signaling cascade. This unique ability of IpLITR 1.1b to exert both inhibitory and stimulatory effects is likely dependent on selective recruitments of intracellular effectors. To further understand mechanistic details

underlying this functional plasticity, the overall objectives of my thesis study was to use IpLITR 1.1b as an alternative vertebrate immunoregulatory receptor model to further explore the signaling potential of this unique teleost protein. Specifically, my research aims were; i) to examine IpLITR 1.1b-mediated integrated control of phagocytic responses using a new flow cytometry-based platform; ii) to investigate the potential IpLITR-mediated receptor crosstalk regulation of the phagocytic response; and iii) to dissect the molecular details underlying the inhibitory actions of IpLITR 1.1b on IpLITR 2.6b activated phagocytosis

Overall, my thesis research demonstrates the utility of imaging flow cytometry as a valuable platform to investigate the dynamic signaling potential of IpLITR-types during their regulation of immune cell effector responses. My results further support the notion that engagement of IpLITR 1.1b results in selective recruitments of intracellular effectors for the intricate tuning of effector processes in a context-dependent manner. I also show for the first time that IpLITR types can not only function independently, but that they also integrate proximal signaling events downstream via receptor crosstalk to modulate innate effector responses. Specifically, I have shown that IpLITR 1.1b is capable of cross-inhibiting IpLITR 2.6b-mediated phagocytosis when co-expressed in AD293 cells and this inhibitory effect is likely dependent on down-regulating phosphotyrosine signaling cascades. Furthermore, I show that two tyrosine-based motifs (ITIMs and Csk-binding motif) in the cytoplasmic tail of IpLITR 1.1b are minimally required for sustaining the inhibitory effects on IpLITR 2.6b-mediated phagocytosis. My biochemical studies revealed the coordinated recruitments of endogenous Csk and SHP2 molecules to IpLITR 1.1b during receptor crosstalk, which act in concert to sustain the inhibitory effects on IpLITR 2.6b-mediated phagocytosis. Overall, this research represents the first report of IpLITR-mediated integrated control of phagocytosis via receptor crosstalk and provides the

basis for further understanding the mechanistic details underlying this important regulatory process.

PREFACE

This thesis is the original work of Chenjie Fei. No animals were used during the completion of this research; therefore, no ethics committee approval was required. Chapter II herein is published in part as Chenjie Fei, Joshua G. Pemberton, Dustin M.E. Lillico, Myron A Zwosdesky and James L. Stafford (2016). Biochemical and functional insights into the integrated regulation of innate immune cell responses by teleost leukocyte immune-type receptors. *Biology* 5(1), 13. Chapter IV herein is published in part as Chenjie Fei, Dustin M.E. Lillico, Brian Hall, Aja M. Rieger and James L. Stafford (2017). Connected component masking accurately identifies the ratio of phagocytosed and cell-bound particles in individual cells by imaging flow cytometry. *Cytometry Part A* 91:372–381. I collected and analyzed all data and wrote this manuscript. Dr. James Stafford contributed philosophical, conceptual and technical guidance and edited this manuscript. I supervised one undergraduate student, Luke Gerla (499).

ACKNOWLEDGEMENTS

I would first like to thank my supervisor Dr. James Stafford and thanks for having me as a member of the Stafford lab. Thanks for being a wonderful supervisor that helps me understanding what PhD really means and also being a nice friend who I can crack jokes with even though I'm still trying to get the hang of it. I could not have asked a better supervisor and I will certainly miss these days I spent here.

I would like to thank my committee members Dr. John Chang and Dr. Patrick Hanington for all suggestions, ideas and supports over the past six years. To Dr. Debbie McKenzie and Dr. Paige Lacy, thanks for being on my candidacy exam. To Dr. Aja Rieger, thanks for helping me to set up the analysis template and to train me on the flow cytometry. To Dr. Daniel Barreda and Dr. Eva Bengten, thanks for being a part of my defense.

To those lovely people in the Stafford lab: Myron (really miss those days when we generated pDisplay constructs and the time we spent by the imaging flow cytometry); Dustin (thanks for helping me with the confocal imaging and sharing your experience as a graduate student, and also those hilarious jokes really make my day); Lena (still remember when you talk about how it feels to be a parent and now I have a little girl too); the "bubble tea team", Hima and Yemaya (thanks for "distracting" me every ten minutes in the lab so we can go on a trip to fetch liquid candies which really boost my productivity by having a sugar high); Rikus (young blood in the Stafford lab and I hope I trained you well so you can carry on with the AD293 system and make it great again).

To my friends: Enezi, thanks for bringing me to the world of bouldering which really helps me with my flexibility, and also being a great person to talk to with all those funny stories and inspiring conversations; Kang, thanks for giving me a ride every Friday (grocery shopping night yay) which save me from the freezing cold weather here and also those foodie trips to find the best fried chicken in the town will be one of those good memories; Wei Li, Feiteng, Dapeng, Xin Wang, Daoxiang and Huayang, it's really nice to see the size of your family is growing over the past six years and we will hang out more often when I settle down back home.

To my parents and in-laws: thanks for being so supportive when I decided to pursue a degree abroad instead of settling down to have a normal life like most people do. It is your undivided love and support that make this journey possible.

To my beloved wife Ying and my little girl Wansheng: we met each other at our best age, and it is amazing that we have been having this great chemistry since then. I can't express my gratitude enough for the love, patience and support you give me, and I think it is time for me to repay all of these with all my heart.

TABLE OF CONTENTS

ABSTRACT..... ii
PREFACE..... v
ACKNOWLEDGEMENTS..... vi
TABLE OF CONTENTS.....vii
LIST OF TABLES..... x
LIST OF FIGURES..... xi
LIST OF ABBREVIATIONS..... xiii

CHAPTER I

INTRODUCTION

1.1 Introduction..... 1
1.2 Objective of thesis.....3
1.3 Outline of thesis.....4

CHAPTER II

LITERATURE REVIEW

2.1 Overview..... 6
2.2 Examination of Stimulatory IpLITR-Mediated Responses.....10
2.2.1 Stimulatory Immunoregulatory Receptors.....10
2.2.2. Stimulatory IpLITRs Demonstrate a Unique Ability to Associate with Intracellular Signaling Adaptors.....11
2.2.3 Induction of Intracellular Signaling and Immune Cell Activation by a Stimulatory IpLITR-Adaptor Protein Complex..... 12
2.3. Examination of Inhibitory IpLITR-Mediated Responses.....15
2.3.1 Inhibitory Immunoregulatory Receptors..... 15
2.3.2. Inhibitory IpLITRs Contain ITIMs and Recruit Protein Tyrosine Phosphatases..... 15
2.3.3. Inhibitory IpLITRs Abrogate the NK Cell Killing Response via Both SHP-1-Dependent and -Independent Signaling Pathways..... 16
2.4. Examination of IpLITR-Mediated Functional Plasticity..... 18
2.4.1. Functional Plasticity and Immunoregulatory Receptors..... 18
2.4.2. Induction of Phagocytosis and Stimulatory Signaling by an Inhibitory IpLITR..... 20
2.4.3. IpLITRs Activate Distinct Phagocytic Modes: Further Insights into 1.1b$^{WT\ CYT}$ -Mediated Functional Plasticity..... 24
2.5. Conclusions..... 28

CHAPTER III

MATERIALS AND METHODS

3.1 Cells, antibodies and constructs..... 53
3.1.1 Cells..... 53
3.1.2 Antibodies..... 53
3.1.3 Constructs..... 54

3.2 Generation of AD293 cell lines stably expressing IpLITR constructs..... 55
3.3 Scanning electron microscopy analysis of IpLITR phagocytic responses..... 57
3.4 Standard flow cytometry vs. imaging flow cytometry for differentiating surface-bound from phagocytosed targets during IpLITR-mediated phagocytosis..... 58
3.5 Imaging flow cytometry-based assays..... 59
3.5.1 Investigation of impacts of experimental conditions on IpLITR-mediated phagocytosis 59
3.5.2 Independent activation of 2.6b$^{ITAM\ CYT}$ and 1.1b $^{WT\ CYT}$ constructs in co-expression AD293 cell lines..... 60
3.5.4 Examining the impact of IpLITR-mediated receptor crosstalk on phagocytosis..... 61
3.5.5 Examining the phosphorylation state of intracellular molecules during IpLITR-mediated receptor crosstalk..... 62
3.6 Confocal microscopic examination of the recruitment of intracellular molecules during IpLITR-mediated crosstalk regulation of phagocytosis..... 63
3.6.1 Examining the recruitment of phosphotyrosine molecules at phagocytic cups..... 63
3.6.2 Examining selective recruitments of Csk and pSHP-2 to the CYT region of 1.1b$^{WT\ CYT}$ during IpLITR-mediated receptor crosstalk regulation of phagocytosis..... 64
3.7 Magnetic beads-based co-immunoprecipitation assays..... 65
3.8 Time course examination of intracellular signaling molecule recruitments following the co-crosslinking of 2.6b$^{ITAM\ CYT}$ with various 1.1b^{CYT} constructs..... 67
3.9 Statistical analysis..... 68

CHAPTER IV

CONNECTED COMPONENT MASKING ACCURATELY IDENTIFIES THE RATIO OF PHAGOCYTOSED AND SURFACE-BOUND PARTICLES IN INDIVIDUAL CELLS BY IMAGING FLOW CYTOMETRY

4.1 Introduction..... 70
4.2 Results..... 74
4.2.1 Generation of IpLITRs-expressing AD 293 cell lines..... 74
4.2.2 Standard flow cytometry lacks the resolution to discriminate cells in double positive population..... 75
4.2.3 Connected component masking accurately discriminate surface-bound from internalized beads within individual cells..... 76
4.2.4 Quantitative examination of IpLITR-mediated phagocytosis using imaging flow cytometry-based method..... 77
4.3 Discussion.....78

CHAPTER V

EXAMINATION OF THE POTENTIAL RECEPTOR CROSSTALK BETWEEN TWO IPLITR-TYPES IN THE CONTROL OF THE PHAGOCYTIC RESPONSE

5.1 Introduction..... 93
5.2 Results..... 96

5.2.1 Co-expression of different IpLITR-types in AD 293 cell lines for the examination of potential receptor crosstalk..... 96
5.2.2 Cross-inhibition of 2.6b$^{ITAM\ CYT}$ -mediated phagocytosis by 1.1b$^{WT\ CYT}$..... 99
5.2.3 Co-crosslinking of 2.6b $^{ITAM\ CYT}$ with 1.1b $^{WT\ CYT}$ down-regulates 2.6b $^{ITAM\ CYT}$-induced phosphotyrosine signaling.....100
5.3 Discussion..... 103

CHAPTER VI

CROSS-INHIBITION OF ITAM-DRIVEN PHAGOCYTOSIS THROUGH COORDINATE RECRUITMENTS OF CSK AND SHP-2 TO 1.1B$^{WT\ CYT}$ DURING RECEPTOR CROSSTALK

6.1 Introduction..... 128
6.2 Results..... 131
6.2.1 Generation of stable AD 293 cells co-expressing 2.6b $^{ITAM\ CYT}$ with various 1.1b ^{CYT} tyrosine mutant constructs..... 131
6.2.2 Tyrosine 453 and ITIMs in the CYT of 1.1b$^{WT\ CYT}$ are minimally required for sustaining the inhibitory effects on 2.6b$^{ITAM\ CYT}$-mediated phagocytosis..... 131
6.2.3 Coordinated recruitment of pSHP-2 and Csk molecules to the CYT of 1.1b $^{WT\ CYT}$ during crosstalk inhibition of the phagocytic response.....133
6.2.4 Reduction in phosphorylation of Erk1/2 but not Akt during crosstalk inhibition of the phagocytic response.....135
6.3 Discussion..... 137

CHAPTER VII

GENERAL DISCUSSION AND FUTURE DIRECTIONS

7.1 Summary of thesis findings..... 169
7.2 Future directions..... 178
7.2.1 Characterization of the role of Csk and SHP-2 in 1.1b$^{WT\ CYT}$-mediated cross-inhibition of phagocytosis..... 178
7.2.2 Unbiased screen of potential effector molecules recruited to 2.6b$^{ITAM\ CYT}$ -1.1b$^{WT\ CYT}$ signaling complex during receptor crosstalk..... 180
7.2.3 Establishing in vivo models for studying LITRs biology..... 181
7.2.4 Identification of IpLITR ligands..... 182
7.3 Final summary..... 184
REFERENCES..... 186
APPENDIX..... 205

LIST OF TABLES

Table 2.1. Protein basic local alignment search tool (BLASTp) searches for vertebrate immunoregulatory receptor-like sequences and intracellular signaling proteins in the Channel catfish (*Ictalurus punctatus*).....36

Table 2.2. Protein BLAST searches for human immunoregulatory receptor-like sequences in teleost fishes.....45

Table 3.1. Primers used in this thesis.....68

LIST OF FIGURES

Figure 2.1. Proposed inhibitory and stimulatory (Ictalurus punctatus) leukocyte immune-type receptors (IpLITR) 1.1b-mediated intracellular signaling events. 32
Figure 2.2 Proposed mechanism for an ITAM-independent target acquisition and engulfment pathway facilitated by pLITR 1.1b. 34
Figure 4.1. Generation, transfection and stable expression of N-terminal HA-tagged IpLITR 1.1b CYT region expression constructs in AD 293 cells. 85
Figure 4.2. SEM analysis of IpLITR-mediated phagocytic responses in AD 293 cells. 86
Figure 4.3. Schematic representation of the phagocytic assay. 87
Figure 4.4. Standard flow cytometry lacks the resolution to discriminate cells of different phenotypes in the double positive population. 88
Figure 4.5. Imaging flow cytometry allows analysis of cells with bound and phagocytosed beads. 90
Figure 4.6. Phagocytic analysis of 1.1b$^{ITAM\ CYT}$ and 1.1b$^{WT\ CYT}$ using imaging flow cytometry-based method. 92
Figure 4.7. Experimental conditions affect phagocytic activities in AD 293 heterologous expression system. 93
Figure 5.1. Generation and stable co-expression of N-terminal HA and FLAG epitope-tagged IpLITR constructs in AD293 cells. 114
Figure 5.2. Specific activation of 1.1b$^{WT\ CYT}$ and 2.6b$^{ITAM\ CYT}$ in co-expressing AD 293 cells. 116
Figure 5.3. Optimal concentration of αHA and αFLAG mAbs opsonized on phagocytic targets to crosslink 2.6b$^{ITAM\ CYT}$ and 1.1b^{CYT} constructs with similar binding avidity. 118
Figure 5.4. Schematics of examining potential IpLITRs-mediated crosstalk. 119
Figure 5.5. Inhibition of 2.6b$^{ITAM\ CYT}$-mediated phagocytosis following co-crosslinking with 1.1b$^{WT\ CYT}$. 120
Figure 5.6. Examination of phosphotyrosine signaling events using imaging flow cytometry.. 122
Figure 5.7. Down-regulation of 2.6b$^{ITAM\ CYT}$-mediated phosphotyrosine signaling following co-crosslinking with 1.1b$^{WT\ CYT}$ 124
Figure 5.8. Confocal microscopy analysis of signaling molecules recruited to phagocytic cups. 128
Figure 6.1. Generation and stable co-expression of N-terminal HA and FLAG epitope-tagged IpLITR constructs in AD293 cells 149
Figure 6.2. Csk-binding motif (tyrosine 453) and ITIMs (tyrosine 477 and 499) in the cytoplasmic region of 1.1b$^{WT\ CYT}$ are required to sustain the inhibition on 2.6b$^{ITAM\ CYT}$-mediated phagocytosis. 154
Figure 6.3. Selective recruitments of Csk and pSHP-2 molecules to tyrosine 453 and ITIMs in the CYT of 1.1b$^{WT\ CYT}$ following co-crosslinking with 2.6b$^{ITAM\ CYT}$. 156
Figure 6.4. Confocal microscopy analysis of Csk recruitments to phagocytic cups following co-crosslinking of IpLITR constructs 159

Figure 6.5. Confocal microscopy analysis of pSHP-2 recruitments to phagocytic cups following co-crosslinking of IpLITR constructs. 164
Figure 6.6. Examination of Erk1/2 activation in IpLITR-activated AD 293 cells. 166
Figure 6.7. Hypothesized mechanism of 1.1b$^{WT\ CYT}$-mediated cross-inhibition of ITAM-driven phagocytosis. 168
Appendix Figure A1. Masking description for connected component strategy. 206

LIST OF ABBREVIATIONS

- Abl Abelson murine leukemia viral oncogene homolog
- AF488 AlexaFluor488
- AF647 AlexaFluor647
- Akt AK strain transforming
- aNKIS activating natural killer cells immunological synapse
- ASB Antibody staining buffer
- BCR B cell receptor
- CD cluster of differentiation
- cdc42 cell division cycle 42
- cDMEM complete Dulbecco's minimum essential medium
- cDNA complementary deoxyribonucleic acid
- CEACAM carcinoembryonic antigen-related cell adhesion molecule
- CHIR chicken Ig-like receptor
- CO2 carbon dioxide
- Crk chicken tumour virus regulator of kinase
- Csk C-terminal Src kinase
- cSMAC central supramolecular activation cluster
- CTL cytotoxic T lymphocyte
- CYT cytoplasmic tail
- DAP DNAX-activation protein
- DNA deoxyribonucleic acid
- Dok downstream of tyrosine kinase
- EAT2 EWS/FLI1-activated transcript 2
- ED extracellular domain
- EDTA ethylenediaminetetraacetic acid
- ERK extracellular signal-regulated kinase
- F-actin filamentous actin
- FBS fetal bovine serum
- FcR fragment crystallizable receptor

- FcRL fragment crystallizable receptor-like
- Fgr feline Gardner-Rasheed sarcoma viral oncogene homolog
- Fwd forward
- Fyn Src/Yes-related novel oncogene homolog
- G418 geneticin
- Gab Grb2-associated-binding protein
- GAP GTPase activating protein
- GEF guanine exchange factor
- Grb growth factor receptor-bound
- GST glutathione S-transferase
- GTPase guanosine triphosphatase
- HA hemagglutinin
- Hck hematopoietic cell kinase
- HEK human embryonic kidney
- HRP horseradish peroxidase
- IFN interferon
- Ig immunoglobulin
- IgSF immunoglobulin superfamily
- IL interleukin
- ILR Ig-like receptor
- IP immunoprecipitation
- IP_3 inositol 1,4,5-trisphosphate
- IpLITR Ictalurus punctatus leukocyte immune-type receptor
- IS immunological synapse
- ITAM immunoreceptor tyrosine-based activating motif
- ITAMi inhibitory immunoreceptor tyrosine-based activating motif
- ITIM immunoreceptor tyrosine-based inhibitory motif
- ITSM immunoreceptor tyrosine-based switch motif
- JNKs c-Jun N-terminal kinases
- KD knockdown

- kDa kilo-Dalton
- KIR killer cell Ig-like receptor
- LILR leukocyte Ig-like receptor
- LRC leukocyte receptor complex
- LY light yellow
- Lyn Lck/Yes-related novel protein tyrosine kinase
- mAb monoclonal antibody
- MAPK mitogen-activated protein kinase
- Nck non-catalytic region of tyrosine kinase adaptor protein
- NCR natural cytotoxicity receptor
- NF-κB nuclear factor kappa in B cells
- NITR novel immune-type receptor
- NK natural killer
- NKIS natural killer cell immunological synapse
- pAb polyclonal antibody
- PBS phosphate buffered saline
- PCR polymerase chain reaction
- PECAM platelet endothelial cell adhesion molecule
- PH plekstrin homology
- PI-3,4-P2 phosphatidylinositol 3,4-bisphosphate
- PI-3,4,5-P3 phosphatidylinositol 3,4,5-trisphosphate
- PI-4,5-P2 phosphatidylinositol 4,5-bisphosphate
- PI3K phosphoinositide 3-kinase
- PIR paired Ig-like receptor
- PKA protein kinase A
- PKC protein kinase C
- PLC phospholipase C
- PLD phospholipase D
- pSMAC peripheral supramolecular activation cluster
- PTB phosphotyrosine binding

- PTM post-translational modification
- Rac Ras-related C3 botulinum toxin substrate
- Ras rat sarcoma viral oncogene homolog
- RBL rat basophilic leukemia
- Rho Ras homolog
- ROS reactive oxygen species
- Rvs reverse
- SAP SLAM-associated protein
- SDS-PAGE sodium dodecyl sulfate polyacrylamide gel electrophoresis
- SFK Src family kinase
- SH2 Src homology 2
- SH3 Src homology 3
- Shc SH2 domain-containing transforming protein
- SHIP SH2 domain-containing inositol 5'-phosphatase
- SHP SH2 domain-containing phosphatase
- SLAM signaling lymphocytic activation molecule
- Sos son of sevenless
- Src sarcoma viral oncogene homolog
- Syk spleen tyrosine kinase
- TCR T cell receptor
- TLR Toll-like receptor
- TM transmembrane
- TNF tumor necrosis factor
- Vav guanine nucleotide exchanger factor
- vSrc viral Src kinase
- WASp Wiskott Aldrich syndrome protein
- WAVE WASp family verprolin homologous
- WT wild-type
- YF tyrosine-phenylalanine
- YG yellow green

CHAPTER I

INTRODUCTION

1.1 Introduction

Across vertebrates, innate immunity consists of a complex assortment of highly specialized cells capable of unleashing potent effector responses designed to destroy or mitigate foreign pathogens. The execution of various innate cellular behaviors such as phagocytosis, degranulation, or cell-mediated cytotoxicity are functionally indistinguishable when being performed by immune cells isolated from humans or teleost fishes; vertebrates that diverged from one another more than 450 million years ago (1–4). This suggests that vital components of the vertebrate innate defense machinery are conserved and investigating such processes in a range of model systems provides an important opportunity to identify fundamental features of vertebrate immunity.

Vertebrate cellular immune responses are dependent on specialized immunoregulatory receptors that sense environmental stimuli and initiate intracellular cascades that can elicit appropriate effector responses. Although a wide variety of immunoregulatory receptor families have been extensively studied in mammals, and many have been identified as cell- and function-specific regulators of a range of innate responses, much less is known in fish. However, the growing database of genomic information has recently allowed for the identification of several immunoregulatory receptor gene families in teleost (5–7). Many of these putative immunoregulatory receptors have yet to be assigned any specific role(s), and much of what is known has been based solely on structural and/or phylogenetic relationships with mammalian receptor families. As an attempt to address some of these shortcomings, this thesis research will focus on our growing understanding of the functional roles played by specific members of the

channel catfish (*Ictalurus punctatus*) leukocyte immune-type receptors (IpLITRs), which appear to be important regulators of several innate cellular responses via classical as well as unique biochemical signaling networks.

In an effort to understand the conserved and divergent aspects of immunoregulatory receptors and associated signaling events in regulating innate immunity, my thesis research focuses on further investigating the immunoregulatory roles of distinct IpLITR-types. This polymorphic and polygenic receptor family shares basic structural and phylogenetic relationships with several families involved in the regulation of innate immunity (e.g. phagocytosis). This includes mammalian FcR proteins and a variety of other immunoregulatory proteins located within the Leukocyte Receptor Complex (the LRC is a conserved genomic region and encodes for a variety of related-genes that participate in regulating multiple aspects of innate immunity) (7,8). Although it is proposed that IpLITRs and other immunoregulatory proteins in mammals have diverged from a common ancestral gene(s), orthology between IpLITRs and their relatives has not been established; in part, due to the unknown nature of their endogenous ligand(s) (7,8). Regardless, recent studies from our lab has shed new insights into the biology of IpLITRs that helps to uncover new details in the regulation of innate immune cell effector responses (4,9–16). Each IpLITR-type contains one or more extracellular immunoglobulin-like domains, a transmembrane (TM) segment, and a variable length of cytoplasmic tails (CYT) (7). Stimulatory IpLITR-types associate with immunoreceptor tyrosine-based activation motif (ITAM)-containing adaptor proteins. When fused together as a receptor-adaptor chimera, one of these constructs (i.e. IpLITR 2.6b) promote canonical ITAM-dependent intracellular signaling that triggers degranulation, cytokine secretion, and phagocytosis in a manner similar to mammalian FcRs (4,11,13). In comparison, IpLITR 1.1b is a putative inhibitory receptor-type that possesses a long

CYT with six tyrosine (Y) residues distributed among its proximal and distal segments. The distal CYT region contains two immunoreceptor tyrosine-based inhibitory motifs (ITIMs) located at Y^{477} and Y^{499} that function to abrogate NK cell-mediated responses via recruitment of Src Homology 2 (SH2) domain-containing phosphatases (SHPs) (10). Unexpectedly, the proximal CYT region also inhibits NK cell responses despite the fact it does not recruit SHPs. This novel SHP-independent mechanism is regulated by Y^{453} and involves the recruitment of C-terminal kinase (Csk) (12). Interestingly, IpLITR 1.1b also activates the phagocytic response when stably transfected in the rat basophilic leukemia (RBL)-2H3 myeloid cell line (4,11). Detailed examination of IpLITR 1.1b-mediated phagocytosis revealed the engagement of distinct signaling pathways. This ability of IpLITR 1.1b to exert both inhibitory and activating effects on effector responses is likely due to selective recruitments of intracellular effector molecules in a context-dependent manner. Therefore, to further understand mechanistic details underlying this signaling versatility, my thesis studies focus on further investigating the signaling potential of IpLITR 1.1b 1.1 using a phagocytosis bioassay system.

1.2 Objective of thesis

The main objective of my thesis was to further explore the signaling potential of IpLITR 1.1b with a focus on understanding the molecular details underlying its functional plasticity. The specific aims of my research were: i) to establish a new platform for examining IpLITR 1.1b-mediated integrated control of phagocytosis; ii) to investigate IpLITR-mediated crosstalk during the phagocytic response; and iii) to dissect mechanistic details underlying the inhibitory actions of IpLITR 1.1b on the IpLITR 2.6b-mediated phagocytic activity.

1.3 Outline of thesis

Chapter II is an overview of the literature related to my thesis research. In this chapter, I first provide an overview of characteristics of stimulatory and inhibitory immunoregulatory receptors with an emphasis on IpLITRs in regulating various effector responses. I then discuss functional plasticity of certain IpLITR types that exhibit dual-regulatory properties due to their uncovered signaling versatility. Chapter III provides detailed descriptions of procedures and methods I used throughout my thesis studies. In Chapter IV, I established a new overexpression system and ImageStream flow cytometric-based assay for examining signaling capabilities of IpLITR 1.1b in regulating phagocytosis. Using imaging flow cytometry, my results demonstrated that activation of IpLITR 1.1b in AD293 cells selectively engages intracellular effectors and does not recapitulate the unique phagocytic phenotypes as observed in the previous system. In Chapter V, I examined the crosstalk potential of IpLITR 1.1b and how this crosstalk impacts subsequent effector responses. By stably co-expressing IpLITR 1.1b with a classical activating IpLITR type (i.e. IpLITR 2.6b) that is able to induce phagocytosis using ITAM-dependent pathway, my results demonstrated for the first time that IpLITR 1.1b cross-inhibits phagocytosis likely through down-regulating recruitments of phosphotyrosine molecules to phagocytic cups. This further supports our hypothesis that IpLITR 1.1b has dual-regulatory features to regulate effector responses in a context-dependent manner. In Chapter VI, I further investigated mechanistic details underlying the IpLITR 1.1b -mediated cross-inhibition of phagocytosis. Using a combination of confocal microscopy, imaging flow cytometry and biochemical assays, I showed two signaling modules in the cytoplasmic tail (CYT) of IpLITR 1.1b mediated coordinated recruitments of inhibitory molecules (i.e. Csk and SHP-2) required for sustaining inhibitory effects on phagocytosis. In summary, my research represents the first extensive characterization of immunoregulatory receptor-mediated crosstalk regulation of a vital innate immune cell

effector responses mediated by teleost LITR proteins. Finally, in Chapter VII I summarized my major findings and discuss how these results fit in with our current understanding of dual-regulatory properties that have been observed in several immunoregulatory receptor families. Chapter VIII lists all the references cited in this thesis.

CHAPTER II

LITERATURE REVIEW

2.1 Overview

Innate immune cells use a variety of receptor families to dynamically control the initiation, amplification, as well as termination of effector responses (17,18). In general, immunoregulatory receptors are expressed at the cell surface and communicate extracellular stimuli to sophisticated, yet highly conserved, intracellular signaling networks that control potent antimicrobial functions (17,18). The extracellular domains of each immunoregulatory receptor-type provide the interface for target recognition, whereas the transmembrane (TM) segments and cytoplasmic tail (CYT) regions translate binding events into a range of prototypical immune cell responses; characteristically, through a series of tyrosine-based signaling events (19,20). Receptor-mediated signal transduction responses are vital for host protection from pathogens and, depending on the cell-type(s) activated and specific receptor(s) involved, include: degranulation, phagocytosis, cell-mediated cytotoxicity, and the production of bioactive molecules such as cytokines or various antimicrobial species.

Although it is well established that various teleost immune cell-types can execute the same range of effector responses that are performed by functional counterparts found in mammals, the specific immunoregulatory receptors and their associated signaling networks that control innate cellular defenses in fish remain unknown. For example, teleost immune cells can perform phagocytosis (macrophages and B cells) (21–25), cell-mediated cytotoxicity (Natural killer (NK)-like cells) (3,26), antigen presentation (macrophages) (27,28), and degranulation (mast cells and neutrophils) (29–31). However, the immunoregulatory receptor systems controlling each of these important innate defenses have yet to be characterized in detail. In the

past, these shortcomings were largely due to a lack of identified candidate genes, but the recent cloning and molecular characterization of an assortment of immune-related genes has significantly advanced our understanding of the immunoregulatory receptor families that exist in teleost fishes (32–34).

Many of the identified teleost receptors belong to the immunoglobulin superfamily (IgSF) and some of these share distant phylogenetic relationships and basic structural features with several mammalian immunoregulatory receptor families, including; Fc receptors (FcRs), FcR-like proteins (FcRLs), killer Ig-like receptors (KIRs), and leukocyte Ig-like receptors (LILRs). However, to date the orthologous relationships between the identified teleost genes and the known mammalian receptor sub-types remain to be established. One major factor that precludes defining orthology is the lack of identified ligands for teleost immunoregulatory receptors. Moreover, the discovery and characterization of novel immune-type receptors (NITRs) suggests that teleost immunity may also be in part regulated by unique receptor-types that are exclusive to bony fishes (35). To our knowledge, teleost NITRs are not related to any immunoregulatory receptor families in amphibians, birds, or mammals; but, they do participate in NK cell-mediated allorecognition, implying they are the functional equivalents of mammalian NK receptors (NKRs) (36,37). Further information regarding teleost NITRs can be found in (38–40). Alternatively, teleost leukocyte immune-type receptors (LITRs), which were originally identified in the channel catfish (*Ictalurus punctatus*), do share distant phylogenetic relationships with several families of mammalian IgSF members including FcRs, FcRLs, and various NKRs encoded within the leukocyte receptor complex (LRC) (7). In addition, Table 2.1 presents the results of updated database searches for IpLITR-like proteins in other vertebrates, which further reinforces that these teleost proteins are distantly related to human FcRLs, FcRs, LILRs, KIRs,

sialic acid-binding Ig-type lectins (Siglecs), carcinoembryonic antigen-related cell adhesion molecules (CEACAMs) as well as several IgSF members in rodents, birds, and frogs. It appears likely that the Ig-like domains contained within IpLITRs maintain some basal signatures of an ancestral IgSF that has since diversified throughout vertebrate evolution to become receptors involved in a broad range of vital immunoregulatory functions including antibody-binding, self- and non-self recognition, adhesion, and pathogen detection. Determining which of these important immunoregulatory functions, if any, are controlled by members of the IpLITR family will require further investigations. However, the fact that human immunoregulatory receptor sequences such as FcR/FcRLs, LILRs, and KIRs retrieve IpLITRs as the top matching sequences from basic local alignment search tool (BLAST) analyses indicates that IpLITRs are related to these various mammalian immune proteins. To further broaden the search for human immunoregulatory receptor-like sequences in additional fish species, selected protein sequences from Table 2.1 were also used in BLASTp searches against the teleost databases and representative matches from these searches are listed in Table 2.2. Although some of the human immunoregulatory receptor queries we used for searching the catfish databases did not retrieve any significant matches (i.e., FcγRIIA, FcγRIIB, PIGR, KIR2DL1, Siglec-4, etc.; see Table 2.1) they did identify matches in several other fishes (Table 2.2). However, it remains to be determined whether or not these teleost sequences identified by BLASTp are indeed the functional equivalents of the human immunoregulatory receptor queries. Furthermore, since fish have both teleost-specific receptor families (i.e., NITRs) and those that are distantly related to various mammalian immunoregulatory receptors belonging to the IgSF (i.e., LITRs), it remains a formidable challenge to determine the precise roles of all of these receptor-types in teleost immunity.

Over the past decade, research in our lab has focused on characterizing the biochemistry and functionality of *Ictalurus punctatus* (Ip)LITRs with an emphasis on understanding how putative stimulatory and inhibitory receptor sub-types engage intracellular signaling responses to regulate immune cell actions. These efforts have revealed some expected, as well as unexpected details regarding IpLITR-mediated signaling events and their concomitant regulation of cellular immunity. By designing constructs that allow for the expression of IpLITRs in mammalian cells, we have taken advantage of epitope-tagging technology and commercially-available antibodies (Abs) to easily trigger these receptors in the absence of natural ligands and without developing IpLITR-specific monoclonal (m)Abs. Receptor chimeras that link the CYT regions of IpLITRs with the extracellular domains of mammalian receptors (i.e., KIRs) have also allowed us to promote IpLITR-based signaling events using ligand-expressing target cells (4,11,13,14,16). Both of these strategies have assisted in defining key aspects of the stimulatory and inhibitory actions of IpLITRs as well as defining their unexpected functional versatility. It is important to qualify that our results do rely on heterologous expression of fish immunoregulatory proteins in surrogate, but well-characterized, mammalian cell systems. The interpretations made from the data collected from these types of experiments should always be considerate of this fact. Although this experimental strategy is not adequate for informing the actual in vivo activities of IpLITRs, our work represents the most detailed biochemical and functional examination of teleost immunoregulatory receptors to date. It is clear from our studies that IpLITRs are likely potent effectors of immune cell signaling and that they have the potential to regulate various innate cellular responses including NK cell-mediated killing, phagocytosis, degranulation, and cytokine secretion. In this section, I will review, in detail, the characterization of putative stimulatory and inhibitory IpLITR sub-types and provide frameworks for understanding the

concept of IpLITR functional plasticity; a concept that has also emerged for several mammalian immunregulatory receptor-types.

2.2 Examination of Stimulatory IpLITR-Mediated Responses

2.2.1 Stimulatory Immunoregulatory Receptors

Stimulatory immunoregulatory receptors typically have short CYT regions and positively charged TM segments that facilitate intramolecular association with immunoreceptor tyrosine-based activation motif (ITAM)-containing adaptors (41). For example, the Fc receptor (FcR) common gamma chain (FcRγ) associates with members of the FcR family and is requisite for their surface expression and signaling capacity (42). Engagement of FcRs by binding the Fc region of immunoglobulin induces the activation of Src family kinases (SFKs) that phosphorylate tyrosine residues within the ITAMs of the associated FcRγ (42). Phosphorylation of the ITAM is followed by the rapid recruitment and activation of spleen tyrosine kinase (Syk) (43,44), which then triggers several canonical transduction cascades leading to the induction of effector responses such as phagocytosis, degranulation, and cytokine secretion (45–48). Alternatively, the adaptor protein DAP12 plays a key role in cytotoxicity mediated by natural killer (NK) cells via its association with activating KIRs and other NKRs (49,50). As with FcRγ, formation of KIR-DAP12 complexes is dependent on electrostatic interactions facilitated by the oppositely charged TM segments of the receptor (positively charged) and adaptor (negatively charged) proteins (41). A full complement of ITAM-containing adaptor molecules have been identified in fish, which includes homologues of FcRγ and DAP12 (51). This suggests that the mode of receptor-mediated immune cell activation in teleosts is likely similar to what occurs in mammals.

2.2.2. Stimulatory IpLITRs Demonstrate a Unique Ability to Associate with Intracellular Signaling Adaptors

The characteristic TM segment of IpLITR 2.6b, a representative stimulatory IpLITR-type, contains a positively charged lysine residue and a short CYT region that lacks canonical tyrosine-based signaling motifs (7). Therefore, we predicted that this receptor required an adaptor protein to facilitate its cell surface expression and to stimulate kinase-dependent intracellular signaling networks. We tested this directly using HEK 293T cells co-transfected with hemagglutinin (HA)-tagged IpLITR 2.6b, and demonstrated that this receptor co-immunoprecipitated with the ITAM-containing IpFcRγ, IpFcRγ-L, and IpCD3ζ-L signaling adaptors but not with IpDAP12 (9). In mammals, stimulatory receptor-types that have lysine residues in their TM segments bind DAP12 but not FcRγ (41). A significant increase in the cell surface expression of IpLITR 2.6b in the presence of IpFcRγ or IpFcRγ-L, but not IpCD3ζ-L, was observed; indicating that association with an appropriate adaptor is required for localization of the active signaling complex within the plasma membrane (9,52). These studies also demonstrated that IpLITR 2.6b associated with heterodimeric complexes composed of IpFcRγ-L and IpCD3ζ-L (but not IpDAP12) (9), which has been previously observed for FcRγ-CD3ζ heterodimers during the control of FcR-dependent signal transduction in mammals (53). Mutation of the lysine residue within the TM segment of IpLITR 2.6b to arginine or an uncharged alanine residue had no effect on either surface expression or adaptor recruitment. In addition, the neutralized TM segment of IpLITR 2.6b not only maintained its ability to bind IpFcRγ-L and IpCD3ζ-L, but also acquired the ability to bind IpDAP12, which significantly augmented the cell surface expression of IpLITR 2.6b (9). These observations suggest that, contrary to what has been reported for stimulatory immunoregulatory receptor-adaptor associations in mammals (41), a charged TM segment is not a prerequisite for adaptor

recruitment to IpLITR 2.6b. However, the identity of the residues within the TM segment does appear to define the specificity of IpLITR-adaptor protein interactions. Alternatively, neutralizing the negatively charged TM region of the signaling adaptor IpFcRγ-L completely abrogated assembly with IpLITR 2.6b and inhibited the surface expression of the IpLITR 2.6b-IpFcRγ-L complex (9). These data strongly suggested that the negatively charged TM segment of the channel catfish adaptor molecule was an important requirement for IpLITR-adaptor assembly. Overall, these biochemical studies confirmed that a putative stimulatory IpLITR-type associated with teleost-specific ITAM-containing adaptors and provided interesting new details regarding the specificity of these interactions. Our next objective was to examine the functional implications of IpLITR 2.6b-IpFcRγ-L interactions by testing the ability of this immunoregulatory protein complex to stimulate various innate immune cell activities.

2.2.3 Induction of Intracellular Signaling and Immune Cell Activation by a Stimulatory IpLITR-Adaptor Protein Complex

To directly examine the functional activities of the IpLITR 2.6b-IpFcRγ-L signaling subunit we generated an N-terminal HA-tagged chimeric receptor construct consisting of the extracellular region of IpLITR 2.6b fused with the TM segment and ITAM-containing CYT region of IpFcRγ-L (11). The IpLITR 2.6b/IpFcRγ-L chimera (i.e. IpLITR 2.6b) was then transfected and stably expressed in the rat basophilic leukemia (RBL-2H3) cell line, where it could then be triggered using anti-HA mAbs. Using this approach, we demonstrated that IpLITR 2.6b activated intracellular signaling mediators and that it was a potent stimulator of the RBL-2H3 degranulation response (11). Mutating the IpLITR 2.6b ITAM tyrosine residues to phenylalanine completely blocked functional outputs, reinforcing the ITAM-dependent nature of these cellular responses. Using phospho-specific Abs and Western blotting, we also observed a

unique time-course of extracellular signal-regulated kinase (ERK) 1/2 and protein kinase B (Akt) phosphorylation after IpLITR 2.6b triggering, which did not occur using the ITAM mutated receptor (11). Furthermore, pharmacological inhibitors of SFKs, phosphatidylinositol 3-kinases (PI3Ks), mitogen activated protein kinase (MAPK) kinase (MEK1 and MEK2), and protein kinase Cs (PKC) significantly inhibited IpLITR 2.6b -induced degranulation (11). In comparison, selective inhibitors of the c-Jun N-terminal kinases (JNKs) and p38 MAPK pathways had no effect on stimulated IpLITR 2.6b cellular responses. Overall, these studies provided the first functional information for a putative stimulatory IpLITR-adaptor complex and suggested that the ITAM-dependent signaling activated by IpLITR 2.6b occurs through classical kinase-dependent intracellular cascades (11). A proposed ITAM-dependent signaling mechanism utilized by IpLITR 2.6b was summarized previously in (11).

The functional capacity of IpLITR 2.6b was further examined using a MAPK signaling array as well as cytokine secretion profiling. Anti-HA crosslinking of IpLITR 2.6b increased phosphorylation of several intracellular signaling molecules, including ERK1/2, GSK-3α/β, GSK-3β, RSK1, CREB, JNK (pan), MEK6, MSK2, p38δ, and Akt2 (13). This provided a broader view of the intracellular signaling components phosphorylated downstream of IpLITR 2.6b triggering. These studies also demonstrated that cells activated via IpLITR 2.6b secreted interleukin (IL)-3, IL-4, IL-6, and tumor necrosis factor-α (TNF-α) at levels comparable to what we observed following activation of the cells with phorbol myristate acetate, calcium (Ca^{2+}) ionophore, or stimulation via triggering the endogenous FcεRI (13). This suggested that IpLITR 2.6b/IpFcRγ-L-mediated signaling events coordinately induce both cellular degranulation and cytokine secretion over a comparable temporal scale. Moreover, when the IpLITR 2.6b chimeric construct was triggered with anti-HA mAb opsonized beads, we observed a potent phagocytic

response that was dependent on extracellular Ca^{2+} availability and actin polymerization (13); thus adding another functional dimension to IpLITR 2.6b activation.

In mammals, phagocytic receptors such as FcRs also associate with the ITAM-containing adaptor FcRγ-chain (46,54,55). Phosphorylation of FcRγ-chain ITAMs by SFKs leading to the recruitment of Syk, which then serves as the main effector of FcR-mediated phagocytic signaling by directly binding to and/or phosphorylating specific downstream intracellular components (56,57). Classically, the mediators recruited to FcR-FcRγ complexes include isoforms of PI3Ks, Vav, and Rho family GTPases (4); in particular, Rac1 and Cdc42 dynamically control actin polymerization and are required for phagocytic cup formation as well as pseudopod extension (58,59). Selective pharmacological inhibitors of these mediators were profiled in phagocytic assays in order to obtain detailed information regarding the biochemical pathways that facilitate IpLITR 2.6b/IpFcRγ-mediated phagocytosis and to compare these mechanisms with the classical mammalian FcR phagocytic mode (4). Phagocytic activity was measured using a flow cytometric-based assay and 4.5 μm fluorescent polystyrene microsphere targets. IpLITR 2.6b/IpFcRγ-L-mediated phagocytosis relied on a similar subset of intracellular effectors for target engulfment and was comparable to the ITAM- and SFK-dependent mode of phagocytosis utilized by mammalian FcRs (56,57). Specifically, the IpLITR 2.6b phagocytic response was inhibited using small molecule inhibitors that targeted SFKs, Syk, PI3Ks, Cdc42, Rac1/2/3, phosphoinositide-dependent kinase 1 (PDK1), Akt, PKC, MEK1/2, and F-actin polymerization (4). These data provide further biochemical details describing the phagocytic pathway engaged by a teleost immunoregulatory receptor. The marked similarities observed between IpLITR- and mammalian FcR-mediated phagocytosis indicates that ITAM-dependent stimulatory signaling in

vertebrates may represent a common, and perhaps evolutionarily conserved, signaling mode for active target engulfment.

2.3. Examination of Inhibitory IpLITR-Mediated Responses

2.3.1 Inhibitory Immunoregulatory Receptors

Inhibitory immunoregulatory receptors establish the activation threshold of immune cells and attenuate stimulatory immunoregulatory receptor-induced effector functions. Inhibitory actions are primarily dependent on immunoreceptor tyrosine-based inhibition motifs (ITIMs) within the CYT regions of putative inhibitory receptors (60–62). Following receptor triggering, phosphorylation of the tyrosine residue embedded within ITIMs (S/I/V/LxYxxI/V/L) promotes binding of SH2 domain-containing cytoplasmic phosphatases (SHP-1, SHP-2, and SH2-domain containing inositol 5-phosphatase 1 or 2; SHIP1/2). Activated phosphatases dephosphorylate important proximal signaling proteins and transduction molecules in order to block the transmission of kinase-mediated signaling events and inhibit immune cell effector functions such as phagocytosis, degranulation, and NK cell-mediated killing responses (60,62). Some inhibitory receptors also contain immunoreceptor tyrosine-based switch motifs (ITSMs) in the CYT region that can similarly inhibit cellular activation via phosphatase recruitment, but ITSMs can also alter cellular signaling via phosphatase-independent mechanisms following the selective recruitment of adaptor proteins such as SH2 domain protein 1A (SH2D1A) and Ewing's sarcoma (EWS)-activated transcript 2 (EAT-2) (63). Not surprisingly, many of the identified IpLITRs contain ITIMs and/or ITSMs, and we have investigated the biochemical and functional properties of putative inhibitory IpLITRs, which will be reviewed in this section.

2.3.2. Inhibitory IpLITRs Contain ITIMs and Recruit Protein Tyrosine Phosphatases

We first examined if ITIM-containing IpLITR-types recruited SHP-1 and/or SHP-2 after receptor engagement and phosphorylation of their CYT tyrosines. To do this, expression constructs were generated by fusing the extracellular domain and TM segments of the human NK cell receptor KIR2DL3 to the tyrosine-containing CYT regions of two selected putative inhibitory IpLITR-types, $1.2a^{WT\ CYT}$ and IpLITR 1.1b (10). The extracellular region of KIR2DL3 was used in the fusion constructs since the biological ligand for this receptor is known and readily available (i.e., HLA-Cw3) (60). The KIRED-LITRCYT constructs were originally examined using transient expression experiments in HEK 293T cells (10). Here we demonstrated that following tyrosine phosphorylation, the CYT regions of $1.2a^{WT\ CYT}$ and IpLITR 1.1b recruited SHP-1 and SHP-2 in an ITIM-dependent manner. IpLITR 1.1b also had a unique tyrosine-containing TM proximal region lacking classic inhibitory or stimulatory tyrosine-based signaling motifs that, in our studies, did not bind SHP-1 or SHP-2 (10). After transfection and stable expression of these KIRED-LITRCYT constructs in mammalian NK-like cells, we anticipated that HLA-Cw3-positive target cells would effectively engage the chimeric proteins; allowing us to directly examine IpLITR-mediated inhibitory signaling. This is important since, as outlined above, the natural ligands for IpLITRs are unknown. Using this novel system, we demonstrated that IpLITR-mediated signaling events could influence cytotoxic responses and, as predicted, that IpLITR engagement could abrogate NK cell-mediated killing responses (12). Unexpectedly, we also demonstrated that this inhibitory signaling occurred via both SHP-dependent and -independent mechanisms.

2.3.3. Inhibitory IpLITRs Abrogate the NK Cell Killing Response via Both SHP-1-Dependent and -Independent Signaling Pathways

The inhibitory functions of IpLITRs were examined using a vaccinia virus system to express KIRED-LITR 1.2aCYT and KIRED-LITR 1.1bCYT in mouse spleen-derived cytotoxic lymphocytes (12). Unlike our previous studies, this allowed us to determine the specific effects of IpLITR-induced signaling on lymphocyte cytotoxicity using B cell targets expressing HLA-Cw3 (e.g., 721.221 cells). The main objectives of this study were to examine the inhibitory signaling pathways activated by $1.2a^{WT\ CYT}$ and IpLITR 1.1b as well as to determine if the unique proximal region of the IpLITR 1.1b CYT differentially contributed to the regulation of NK cell-mediated cytotoxicity. We observed that the CYT regions of $1.2a^{WT\ CYT}$ and IpLITR 1.1b both contributed to the inhibition of lymphocyte-mediated target cell killing and determined that for IpLITR 1.2a, this was a SHP-dependent mechanism (12). However, the inhibitory function mediated by the CYT region of IpLITR 1.1b was not affected by co-expression with a catalytically inactive SHP-1 recombinant protein, suggesting that although IpLITR 1.1b binds SHP-1, its inhibitory activity is not dependent on the catalytic activity of this phosphatase (12).

The IpLITR 1.1b CYT region contains six tyrosine residues, evenly distributed between its membrane proximal (Y^{433}, Y^{453}, and Y^{463}) and distal (Y^{477}, Y^{499}, and Y^{503}) regions (10). The distal region contains two ITIMs located at Y^{477} and Y^{499} and one overlapping ITSM (Y^{503}) and when tested as a separate construct, $1.1b^{DISTAL\ CYT}$ displayed potent inhibitory activity that was dependent on SHP-1 (10). We also generated a construct encoding only the CYT proximal region of IpLITR 1.1b and, surprisingly, this receptor variant also blocked NK cell-mediated killing responses despite the fact this construct did not contain any ITIMs or ITSMs and could not recruit SHP-1 or SHP-2 (10,12). This revealed that the SHP-independent inhibitory pathway being activated by IpLITR 1.1b was likely facilitated by one of the tyrosine residues present within its unique proximal CYT region. We then determined that the peptide sequence AVY

^{453}AQV in the 1.1b$^{\text{PROXIMAL CYT}}$ closely matched the consensus-binding motif Y [T/A/S] [K/R/Q/N] [M/I/V/R], which is required for recruiting the C-terminal Src kinase (Csk) (64) .

In mammals, Csk has been identified as a major endogenous inhibitor of SFK-mediated cellular activities and, in general, is an important regulator of intracellular signaling events. However, the ability of Csk to negatively influence cellular immune responses has been recognized (65,66). The inhibitory actions of Csk are dependent on its ability to phosphorylate a conserved tyrosine residue located at the C-terminus of SFKs (i.e., Lyn, Fyn, Hck, etc.), which inhibits SFK catalytic activities (67,68). Kinase-mediated inhibitory signaling opposes the classical phosphatase-driven attenuation of immune cell responses but is likely equally important in terms of the overall regulation of immunity. Using co-immunoprecipitation and site-directed mutagenesis, we confirmed that Y^{453} was indeed required for Csk binding to the IpLITR 1.1b proximal CYT region as well as the inhibitory activity of IpLITR 1.1b (12). Recruitment of Csk to the proximal CYT region of IpLITR 1.1b would appropriately localize this kinase for targeted phosphorylation of SFKs rendering them inactive and thus abrogating the early signaling events required for cellular activation, such as NK cell-mediated killing. These results were the first functional studies reported for an inhibitory ITIM-containing IpLITR and the first to suggest the involvement of Csk as a novel inhibitory signaling mechanism used by a teleost immunoregulatory receptor (12). Furthermore, the unique proximal and distal inhibitory signaling mechanisms mediated by the IpLITR 1.1b CYT reveal marked versatility in the signaling properties within a single LITR. In the subsequent sections, we will review aspects of IpLITR functional plasticity in more detail.

2.4. Examination of IpLITR-Mediated Functional Plasticity

2.4.1. Functional Plasticity and Immunoregulatory Receptors

The classification of immunoregulatory receptors as inhibitory or stimulatory has depended primarily on whether or not they contain key signaling motifs within the CYT region such as ITIMs (inhibitory receptors) or ITAMs (stimulatory receptors). However, the functional outcome of immunoregulatory receptor engagement does not always coincide with the presence of these canonical motifs, as alternative mechanisms of ITIM- or ITAM-dependent signaling events may contribute to functional versatility. For example, there are several reports demonstrating that ITIM-encoding receptors can also stimulate immune cell responses through a wide variety of functionally distinct signaling mechanisms (69–72). In addition, inhibitory actions triggered by phosphorylated ITAMs have also been described (73–75). Functional plasticity in the transduction events controlled by modular protein domains likely serves as an important regulatory mechanism for the fine control of innate immune cell effector functions. Integrated receptor-mediated regulation of signal transduction is also likely to be dependent on many additional factors including the immune cell-type(s) involved as well as the available repertoire of intracellular adaptor and effector molecules. The magnitude and duration of immunoregulatory receptor activation by natural ligands may also play a key role in the type of functional outcomes that occur following receptor engagement. We have already demonstrated that IpLITR 1.1b inhibits NK cell-mediated killing using a classical ITIM- and SHP-dependent mechanism that was regulated by its distal CYT region (12). Interestingly, this receptor also abrogated NK cell responses using an ITIM-independent mechanism that relied on the recruitment of Csk to a tyrosine residue located in the proximal CYT region (12). Although the signaling versatility observed contributed to the same functional outcome, it occurred through two distinct intracellular mechanisms. Moreover, we recently demonstrated that IpLITR 1.1b could potently activate a phagocytic response in RBL-2H3 cells (a representative myeloid cell

type), suggesting that the differential recruitment of signaling mediators in specific immune cell types (i.e., lymphoid vs. myeloid) may facilitate a context-dependent plasticity during the receptor-mediated control of cellular processes (13). Our findings using IpLITRs agree with observations from mammalian models describing alternative mechanisms of immunoregulatory receptor-mediated signaling that extend beyond their putative classifications as strictly inhibitory or stimulatory receptor-types. Overall, alternative stimulatory signaling downstream of IpLITR 1.1b activation provides the basis for the examination of IpLITR functional plasticity as an important immunomodulatory mechanism controlled by these teleost receptors.

2.4.2. Induction of Phagocytosis and Stimulatory Signaling by an Inhibitory IpLITR

In the original description of IpLITR 1.1b functional plasticity, we demonstrated that this receptor stimulated phagocytosis and induced phosphorylation of important signal transduction targets, including ERK1/2 and Akt (13). However, unlike IpLITR 2.6b/IpFcRγ-L, IpLITR 1.1b did not induce the secretion of cytokines and the kinetics of IpLITR 1.1b -induced phosphorylation of ERK1/2 and Akt was significantly different from the ITAM-mediated responses. IpLITR 1.1b stimulatory activities were also independent of any association with an ITAM-containing adaptor protein, and phagocytic activity stimulated by IpLITR 1.1b was insensitive to treatment with the extracellular Ca^{2+} chelator EDTA, which further distinguished IpLITR 1.1b -mediated signaling from the IpLITR 2.6b pathway (13). Finally, without the CYT region, IpLITR 1.1b was still expressed on the cell surface but it no longer stimulated a phagocytic response; indicating that the signal to initiate phagocytosis was due to events promoted by residues contained within the CYT (13). To further understand the requirements for IpLITR 1.1b -mediated phagocytosis, we again considered the unique proximal and distal composition of tyrosine residues within the CYT in an attempt to derive a mechanism that could

be examined in detail using biochemical and functional assays. The first step in this process was to use bioinformatics to predict what intracellular molecules might bind to the IpLITR 1.1b CYT and to hypothesize how these transduction elements would participate in the activation of machinery required for actin polymerization as well as plasma membrane remodeling during target engulfment. Since IpLITR 1.1b does not contain a classical ITAM, or any other recognizable stimulatory motifs that are known to facilitate phagocytosis (10), an alternative mode for the intracellular stimulation of IpLITR 1.1b -mediated phagocytosis was considered. Based on the results described in (13), this mechanism will be explained further below.

One potential mechanism derived from mammalian models hypothesizes that the ITSM-containing distal region of the CYT is primarily responsible for IpLITR 1.1b functional plasticity. For example, ITSMs can bind SHPs that commonly mediate phosphatase-dependent cellular inhibition (76). However, as their name suggests, this motif can also alter conformation to selectively recruit stimulatory adaptor proteins including SH2D1A and EAT-2 that typically activate, rather than inhibit, effector functions in immune cells (77). In particular, ITSMs can facilitate stimulatory signaling through SH2D1A-dependent recruitment and activation of the p85 subunit of class IA PI3Ks (78), which can then induce Akt phosphorylation downstream of phosphatidylinositol 3,4,5-trisphosphate (PI(3,4,5)P3) production as well as directly modulate phagocytosis (63). ITIM- and ITSM-mediated induction of cellular activation has also been shown to involve SHP-2 (79), which instead of abrogating downstream signaling, can serve as a key scaffold for proteins involved in cellular responses. In this scenario, SHP-2 recruitment to ITIMs and/or ITSMs results in phosphorylation at a C-terminal tyrosine that then serves as a binding site for the SH2-containing adaptor molecule growth factor receptor-bound 2 (Grb2) (80). Grb2 associates with members of the Dab/Dos family of scaffolding proteins, known as the

Grb2-associated binders (Gabs). When phosphorylated, Gab2 has been shown to bind and activate class IA PI3Ks, again resulting in the recruitment and phosphorylation of downstream targets that include PDK1 and Akt as well as other components of the phagocytic machinery (81–84). During IpLITR 1.1b -mediated phagocytosis, we predict that Grb2 recruitment to the activated receptor may rely on SHP-2 binding to the ITIMs (Y^{477} and/or Y^{499}), and/or the ITSM (Y^{503}). SHP-2 recruitment would allow for the association of larger protein heteromers, including potential interactions with Gab2 and formation of the SHP-2-Grb2-Gab2 ternary signaling complex that would allow for the subsequent activation of class I PI3Ks (81,85,86). The involvement of SHP-2 as an intracellular scaffold capable of engaging PI(3,4,5)P3-dependent cellular activation pathways provides an explanation for context-dependent functional outcomes contrasting our previously reported SHP-dependent inhibition of NK cell killing induced by IpLITR 1.1b (12). An overall summary schematic of this proposed signaling mechanism is provided in Figure 1.

The stimulatory actions of IpLITR 1.1b are unlikely limited to only the distal CYT region containing the ITIMs and ITSM. As also outlined in Figure 1, Y^{463} matches the known Grb2-binding motif (YxN) that would facilitate direct Grb2 binding to the CYT proximal region of IpLITR 1.1b (64). As already mentioned, Grb2 is an important intracellular scaffold that is also known to associate with guanine nucleotide exchange factors (GEF), such as Son of Sevenless (SoS), which interacts with the SH3 domain of Grb2 via a poly-proline-rich sequence (87). Formation of the Grb2-SoS signaling complex also commonly involves targeting the GEF activity of SoS to the membrane-associated Ras superfamily of small GTPases, subsequently leading to the activation of the Raf-MEK-ERK signaling cassette (88,89). Therefore, direct or indirect (via SHP-2) recruitment of Grb2 to the proximal and/or distal CYT regions of IpLITR

1.1b, respectively, may provide explanations for how this receptor can induce the downstream activation of both ERK1/2 and Akt signaling in RBL-2H3 cells. Alternatively, Grb2 binding directly to phosphorylated Y^{463} (i.e., YxN motif) during phagocytosis could also recruit Gab2 and the class I PI3Ks. Gab2-dependent recruitment and activation of class IA PI3K heterodimers (p85-p110) would increase the local generation of PI(3,4,5)P3, which is required for actin-dependent extension of pseudopods and the engulfment of large extracellular particles (85,90,91). IpLITR 1.1b -induced production of PI(3,4,5)P3 could also attract additional pleckstrin homology (PH) domain-containing adaptors like Vav, another important GEF, that directly bind to plasma membrane PI(3,4,5)P3 (92). Vav activation stimulates Rho family GTPases including Cdc42, Rac1, and RhoA that control local actin polymerization during the formation of lamellipodia required for phagocytosis (93). Control of Rho family GTPase activity by Vav has also been shown to play an important role in FcRγ-, complement receptor-, and CEACAM-mediated phagocytosis (94). It still remains to be seen if Vav-dependent regulation of Rho family GTPases participates in IpLITR-mediated phagocytosis, however, interactions between IpLITR 1.1b and many of the molecules implicated above are the focus of ongoing investigations in our lab.

In addition to Csk, SHP-1, and SHP-2 reported in , we have biochemical evidence for the binding of Grb2, SH2D1A, and the class IA PI3K regulatory subunit p85 to the CYT region of IpLITR 1.1b (12). Overall, our studies using IpLITR 1.1b are the first to demonstrate functional plasticity for an ITIM-containing teleost immunoregulatory receptor. At present, the precise mechanisms of IpLITR 1.1b -induced phagocytosis are unknown, but the events leading to this outcome are clearly distinct from those facilitated by the prototypical ITAM-dependent pathway

used by IpLITR 2.6b and may ultimately represent a novel cellular mode of actin-dependent target engulfment.

2.4.3. IpLITRs Activate Distinct Phagocytic Modes: Further Insights into IpLITR 1.1b -Mediated Functional Plasticity

Details of an alternative ITAM-independent IpLITR-induced phagocytic pathway were revealed in (4). These studies indicated that despite convergence on the control of actin polymerization dynamics, IpLITR 1.1b clearly operates independently of several of the key components of the ITAM-dependent signaling machinery. IpLITR 1.1b -expressing cells also displayed a unique target acquisition and engulfment phenotype that was not observed during IpLITR 2.6b/IpFcRγ-induced phagocytosis. Phagocyte phenotypes were examined by confocal microscopy, which demonstrated that IpLITR 1.1b -expressing cells often formed extended membranous protrusions that captured their targets in phagocytic cup-like structures but failed to completely internalize them. Incomplete target engulfment is indicative of a stalled phagocytic phenotype that was often observed during IpLITR 1.1b -mediated phagocytosis (~44% of cells examined), but was rarely observed for the IpLITR 2.6b/IpFcRγ-L-expressing cells (~3% of cells) that readily internalized extracellular targets (i.e., ~60% of the cells analyzed had completely engulfed two or more beads) (4). Although the capture and partial engulfment phenotype was common during IpLITR 1.1b -mediated phagocytosis, ~30% of the analyzed cells internalized at least one 4.5 μm bead. Surprisingly, while incubations at 22°C inhibited IpLITR 2.6b/IpFcRγ-L, this lower temperature had no effect on the ability of IpLITR 1.1b -expressing cells to capture and partially engulf beads; although the depressed temperature did reduce the ability of IpLITR 1.1b -expressing cells to completely engulf extracellular targets (i.e., from~30% to 10% internalization). Moreover, while small molecule inhibitors of major kinase

and GTPase signaling systems had significant inhibitory effects on the IpLITR 2.6b/IpFcRγ-L-mediated phagocytic pathway (described above), IpLITR 1.1b -induced phagocytosis was insensitive to the majority of these pharmacological inhibitors. For example, IpLITR 1.1b phagocytosis was only significantly blocked by treatment with inhibitors of SFKs, Syk, and F-actin nucleation, whereas inhibition of PDK1, Cdc42, Rac, PI3Ks, and PKCs were ineffective (4). Based on these findings, a distinctive cellular model of phagocytosis for IpLITR 1.1b was proposed that requires a minimal set of intracellular signaling components that directly associate with the actin polymerization machinery (Figure 2). It was also hypothesized that the proximal and distal regions of the IpLITR 1.1b CYT may differentially participate in the recruitment and activation of phagocytic effectors. For IpLITR 1.1b to activate phagocytosis, our recent results suggest that it must stimulate actin polymerization and may require the catalytic activity of the SFK and Syk families of intracellular kinases (4). Therefore, we proposed that CYT proximal region recruits the actin polymerization machinery into the vicinity of a Syk-dependent activation cassette within the distal region of the CYT, which is then triggered following IpLITR 1.1b engagement by extracellular targets (Figure 2).

Recently, co-immunoprecipitation studies further showed that following tyrosine phosphorylation, the differential binding of effector molecules to the CYT region of IpLITR 1.1b occurred (14). For example, the proximal region of IpLITR 1.1b associates with the non-catalytic region of tyrosine kinase adaptor protein 1 (Nck), Grb2, Vav1; whereas the distal region of IpLITR 1.1b recruits Syk, PI3K and SHP-2 (14). Furthermore, WASp family verprolin-homologous protein-2 (WAVE2), which activates nucleation factors (e.g. Arp2/3) was also shown to co-immunoprecipitate with IpLITR 1.1b (Myron Zwozdesky unpublished observations). These novel data add to the growing repertoire of molecules that bind to IpLITR

1.1b and, importantly, link the CYT region of IpLITR 1.1b to endogenously available intracellular proteins that regulate actin-dependent phagocytosis.

Receptor-specific recruitment of Nck, WAVE2, and Syk to IpLITR 1.1b helps to clarify how actin-driven membrane remodeling may be controlled by a putative inhibitory receptor. For example, as described for the human phagocytic receptor CEACAM3 (95), WAVE2 may indirectly associate with IpLITR 1.1b using the adaptor Nck that, based on detailed Src homology 2 (SH2)-domain binding studies (96), could interact with the consensus sequence H-I-Y-D-E-V located around Y^{433} in the proximal region of the IpLITR 1.1b CYT (10). Following or during the recruitment of intracellular effectors responsible for the destabilization of the actin cytoskeleton to the proximal CYT region, Syk may bind the distal CYT region of IpLITR 1.1b by interacting with phosphorylated tyrosines, Y^{477} and Y^{499}, that are positioned in two tandem ITIM motifs capable of accommodating both of the SH2 domains of Syk. This atypical mode of Syk recruitment to tandem ITIMs has already been demonstrated for platelet endothelial cell adhesion molecule-1 (PECAM-1) (97). The tandem ITIMs located within the CYT region of PECAM-1 are spaced such that the tyrosines are separated by twenty-two amino acids. Interestingly, this is also the precise separation between Y^{477} and Y^{499} within IpLITR 1.1b and might explain how Syk also interacts with the distal CYT region (Figure 2). Once recruited to IpLITR 1.1b, we predicted that Syk would bind and activate an intracellular Rho-GEF (i.e., Vav or RhoA) that could then directly regulate one of the many known Rho GTPases that are responsible for controlling rapid actin-driven membrane protrusions through activation of Arp2/3 and the WAVE2 complex (98). Based on our current data, the Rho family GTPases involved are unlikely to be either Cdc42 or Rac1/2/3 (4). Although the precise mechanism underlying IpLITR 1.1b-mediated phagocytic responses still remain to be elucidated, the involvement of Nck and

Syk molecules in facilitating IpLITR 1.1b-mediated target capture and uptake has been further suggested in a recent publication (16). Specifically, live cell imaging demonstrated that IpLITR 1.1b is constitutively associated with Nck within filopodia-like structures under resting conditions; whereas recruitments of Syk only occurs following triggering of IpLITR 1.1b (16). This observation indicates that IpLITR 1.1b is basally phosphorylated at defined tyrosine motifs (e.g. Y^{433}) to allow for the recruitment of Nck molecules. As discussed above, binding of Nck directly couples IpLITR 1.1b to actin polymerization machinery and is likely responsible for the generation of filopodia-like structures in IpLITR 1.1b-expressing cells under resting condition. After encountering phagocytic targets, tyrosine motifs within CYT of IpLITR 1.1b are further phosphorylated as a consequence of receptor clustering, which facilitates recruitment of additional effector molecules (e.g. Syk) to facilitate target uptake (16). Overall, this proposed mechanism provides the framework for exploring a new mode of ITAM-independent phagocytosis and is being investigated further in our lab. It is also worth noting that this revised model for IpLITR 1.1b -mediated phagocytosis does not include the activity of class I PI3Ks, which is in agreement with our pharmacological data. However, as proposed in Figure 1, class I PI3Ks may still participate in other IpLITR 1.1b -dependent functional responses and more work is still required to reconcile the contribution and dynamics of PI3K involvement during IpLITR 1.1b -mediated phagocytosis.

In mammals, FcR-stimulated phagocytosis proceeds through distinctive phases that are dependent on the coordinate activities of several key effector molecules (99). These phases include an early PI3K-independent stimulation of actin polymerization that drives the extension of the phagocytic cup to capture targets, followed by a PI3K-dependent contractile mechanism that subsequently closes phagosomes around targets (99). The size of the extracellular target

directly influences these processes, as the engulfment of larger particles (i.e., >3 μm) requires accessory signaling events to promote the final stages of target internalization (92,100–104). We hypothesize that IpLITR 1.1b activates the early PI3K-independent phases of the phagocytic process over a broad range of temperatures; however, unlike IpLITR 2.6b/IpFcRγ-L, IpLITR 1.1b -expressing cells are not able to effectively stimulate class I PI3K catalytic activity and therefore generally exhibit a stalled phagocytic phenotype. Stalled phagocytosis has been observed in other studies using cells treated with broad-spectrum pharmacological inhibitors of PI3Ks, and this effect was only evident using large beads (i.e., >3 μm) (100,105). All together, these data provide another possible distinction between ITAM-mediated phagocytosis and the alternative PI3K-independent phagocytic mode utilized by IpLITR 1.1b.

2.5. Conclusions

In summary, I have described in this thesis chapter the current knowledge regarding the immunoregulatory potentials of representative IpLITR-types. Stimulatory and inhibitory IpLITR-types are co-expressed by a variety of myeloid and lymphoid cell-types in catfish and, as reviewed here, they regulate cell-mediated cytotoxicity, cytokine secretion, degranulation, and phagocytosis when expressed in representative mammalian immune cell-lines. Although they clearly display potent immunoregulatory potentials, endogenous ligands for IpLITRs are currently unknown and their overall contributions to cellular immunity in teleosts have not yet been established. As it stands, it is possible that members of the IpLITR family may function as teleost FcR-like proteins, regulators of NK cell responses (i.e., NKRs), and as adhesion proteins or pathogen recognition molecules akin to members of the human CEACAM family. However, establishing these functional relationships will depend on further experiments designed to identify IpLITR ligands and explore the precise in vivo functions of individual receptors using

fish immune cells. Although our work to date has relied on heterologous expression of IpLITRs in mammalian cells, this strategy has allowed us to demonstrate important conserved aspects regarding IpLITR-mediated stimulatory and inhibitory immunoregulatory signaling events and revealed some unanticipated aspects regarding IpLITR signaling versatility. In particular, it is now clear that the signaling mechanisms responsible for IpLITR-mediated immune regulation are both cell- and context-specific. The unique activity of IpLITRs in different mammalian immune cell systems also reinforces the role of protein interaction domains during the evolution of immunoregulatory receptor-based signaling networks. The inherent modularity of important signaling motifs within the transduction machinery allows for complex and novel regulatory behaviors to arise from relatively simple genetic events such as recombination, deletion, or insertion (106). As a result, classifications of stimulatory or inhibitory receptors must attempt to match functional outcomes to the presence of canonical immunoregulatory domains such as ITIMs or ITAMs. Alternatively, biochemical studies must be aimed at mapping the relative importance of unique domain organizations within receptor variants in order to better understand receptor-specific contributions to the spatiotemporal activation of transduction molecules within different immune cell types. Studies using these methodologies, including those described here using IpLITRs, already suggest that the heterogeneity observed within the intramolecular interactions between unique immunoregulatory receptors and the diverse complement of intracellular effectors likely facilitates intricate tuning of responses through selective signaling dynamics. The presence of diverse multi-receptor systems throughout immune cell lineages further compound the apparent complexity required for the integrated control of innate immunity. At present, we are only beginning to understand the significance of functional plasticity within individual immunoregulatory receptors, including IpLITRs; however, specific

details regarding the intracellular mechanisms responsible for the signaling versatility observed are only now emerging. Herein, we propose simple context-specific models for IpLITR-mediated immune cell regulation that require a minimal complement of intracellular signaling components. Importantly, these suggested signaling mediators and many others that may participate in the phagocytic process are highly conserved among vertebrates and in particular for our studies they are very similar between mammals and fish (Table 2.1). Therefore, the insights gained from our heterologous studies demonstrate that IpLITR-mediated responses in mammalian cells feature the same signaling components that are likely present in fish immune cells (Table 2.1). Further elucidation of these mechanisms will hopefully reveal insights into how immunoregulatory receptor plasticity has evolved and perhaps continue to uncover novel roles for canonical ITIM- and ITAM-encoding receptors. These foundational studies of IpLITR-mediated signaling events have set the stage for future studies targeted at understanding how the dynamic control of intracellular events controlled by immunoregulatory receptors contribute to the conserved activities of innate immune cells across vertebrates.

Overall, our work has clearly shown that IpLITRs represent an excellent alternative vertebrate model for understanding molecular mechanisms underlying immunoregulatory receptor functions. Furthermore, the unique feature of IpLITR 1.1b to engage both stimulating and inhibitory abilities via selective recruitments of signaling molecules in a context-dependent manner offers an opportunity to expand our knowledge of mechanistic details underlying this dual-regulatory property in regulating effector responses. To further examine the diverse signaling potential of IpLITR 1.1b, my specific research aims were; i) to examine IpLITR 1.1b-mediated integrated control of phagocytic responses using a new flow cytometry-based platform; ii) to investigate the potential IpLITR-mediated receptor crosstalk regulation of the phagocytic

response; and iii) to dissect the molecular details underlying the inhibitory actions of IpLITR 1.1b on IpLITR 2.6b activated phagocytosis. The investigation of IpLITR 1.1b-mediated signaling events in a new system expands our knowledge of signaling potentials of this representative IpLITR member and advances our understanding of dual-regulatory properties of certain immunoregulatory receptors in regulating effector responses.

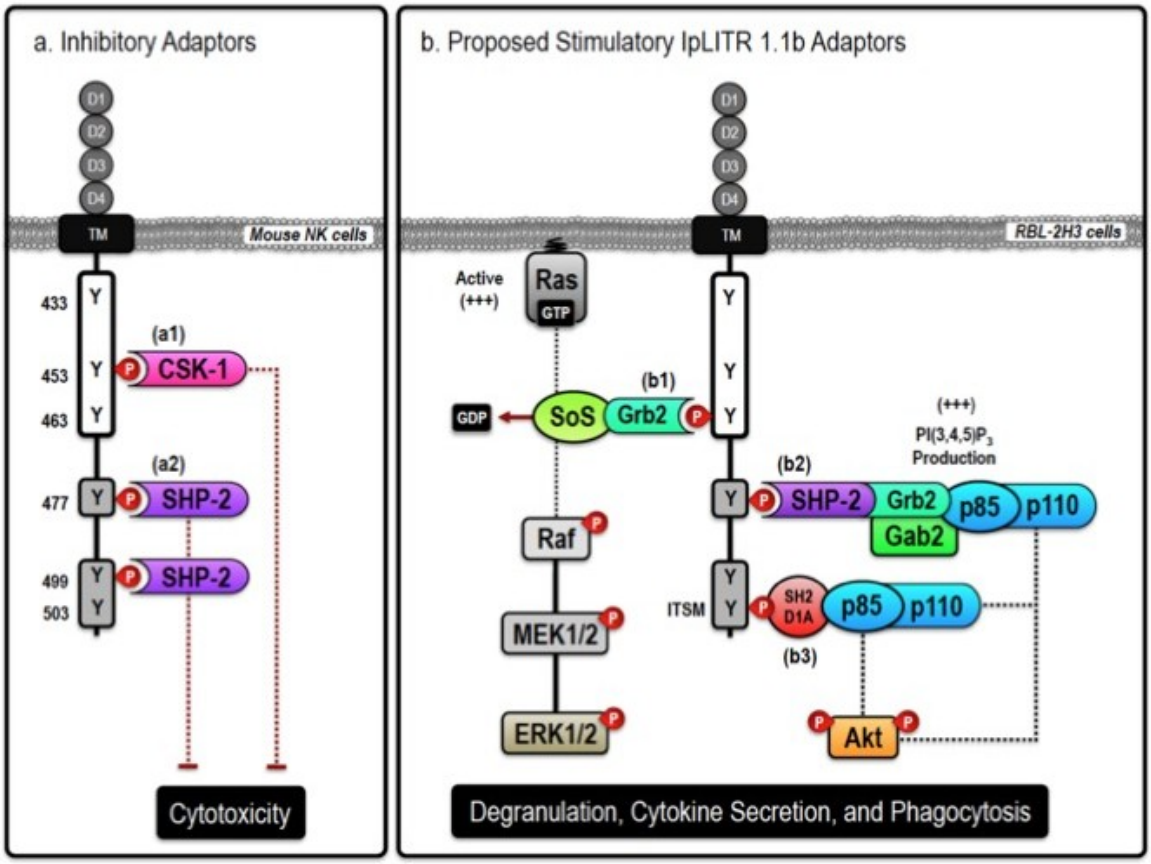

Figure 2.1. Proposed inhibitory and stimulatory (Ictalurus punctatus) leukocyte immune-type receptors (IpLITR) 1.1b-mediated intracellular signaling events. Schematic representation of the proposed inhibitory (**a**) and stimulatory (**b**) signaling events mediated by IpLITR 1.1b in transfected cells. The cytoplasmic tail (CYT) region of IpLITR 1.1b contains six tyrosine residues (Y^{433}, Y^{453}, Y^{463}, Y^{477}, Y^{499}, and Y^{503}) that, when phosphorylated, serve as potential docking sites for various intracellular signaling adaptors. (**a**) In mouse natural killer (NK) cells, we demonstrated that engagement of IpLITR 1.1b caused a potent inhibition of NK cell-mediated cytotoxicity due to the recruitment of Csk-1 at Y^{453} (**a1**) or the binding of SH2 domain-containing cytoplasmic phosphatases (SHP) at Y^{477} and/or Y^{499}, which are in immunoreceptor tyrosine-based inhibition motifs (ITIMs) (**a2**). The immunoreceptor tyrosine-based switch motifs (ITSM) located at Y^{503} may also recruit SHP phosphatases but this has not been examined. (**b**) IpLITR 1.1b engagement also induced phosphorylation of ERK1/2 and Akt as well as promoted phagocytosis in transfected rat basophilic leukemia (RBL)-2H3 cells. These stimulatory effector cell functions could be mediated by the following mechanisms; (**b1**) direct recruitment of growth factor receptor-bound 2 (Grb2) to the YxN motif at Y^{463} may mediate the recruitment, and associated GEF activity, of SoS or the Gab2/class I PI3K (p85/p110) signaling complex. SoS is known to stimulate the accumulation of GTP-loaded Ras that would facilitate the stepwise phosphorylation of the Raf-MEK-ERK cassette. Alternatively, the Gab2 adaptor can localize class I PI3K activation to allow for targeted accumulation of the important signal

transduction molecule phosphatidylinositol 3,4,5-trisphosphate ($PI(3,4,5)P_3$); (**b2**) ITIM-mediated recruitment of SHP-2 at Y^{477} or Y^{499}, could recruit Grb2 and Gab2 allowing for the association of holomeric class I PI3Ks (p85/p110) leading to Akt phosphorylation and induction of phagocytosis. SHP-2-dependent recruitment of class I PI3Ks could also occur at the C-terminal ITSM located at Y^{503}. SHP-2-dependent Grb2 recruitment may also trigger the SoS/Ras/Raf/MEK-dependent activation of ERK1/2; (**b3**) SH2D1A-mediated binding of PI3K (p85/p110) to the ITSM at Y^{503} is also possible. In general, class I PI3K activation can result in Akt phosphorylation or the recruitment of other $PI(3,4,5)P_3$-dependent signaling proteins, including Vav, that are known to regulate phagocytosis. In addition, ITSM-mediated signaling can also recruit the adaptor EAT-2, closely related to SH2D1A, which is not shown here. For clarity, the role of signaling events dependent upon extracellular Ca^{2+}entry or intracellular Ca^{2+} mobilization have also been excluded.

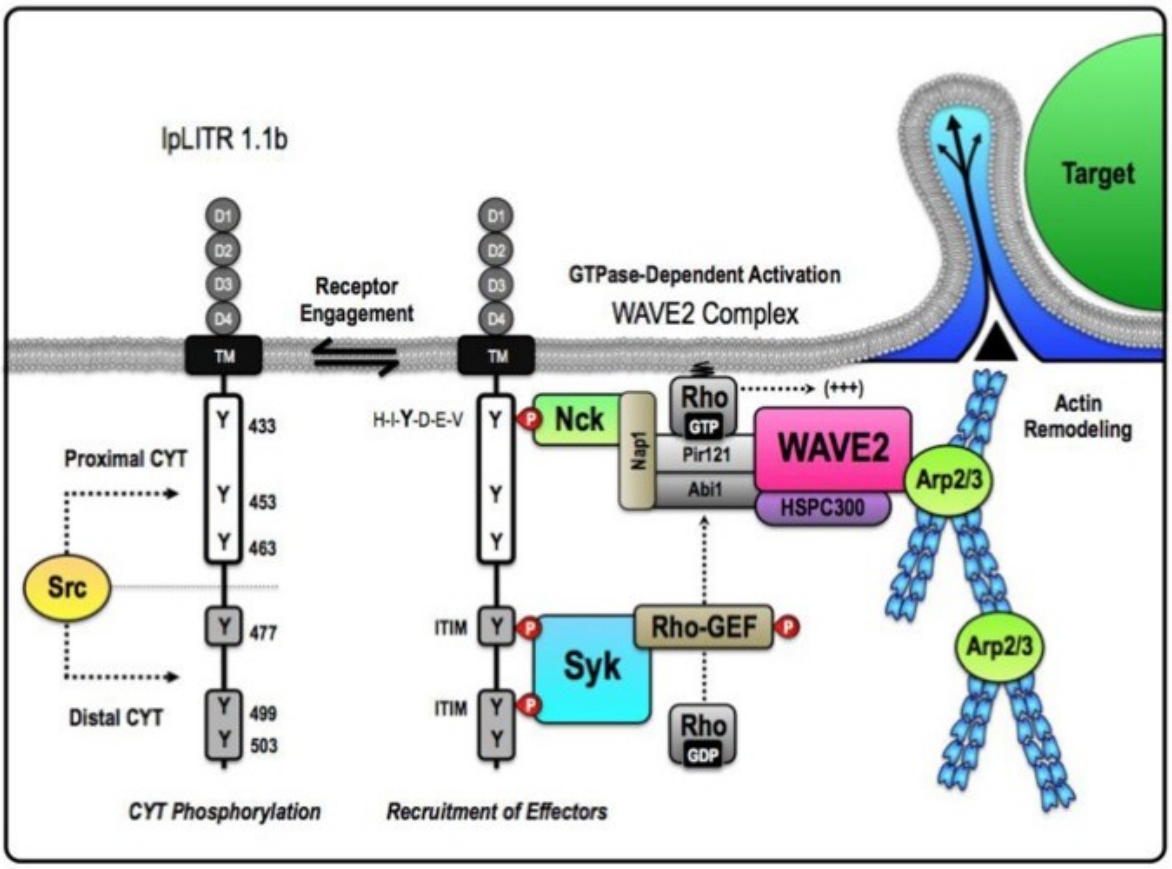

Figure 2.2 Proposed mechanism for an ITAM-independent target acquisition and engulfment pathway facilitated by pLITR 1.1b. The unique short-circuited version of phagocytosis exhibited by IpLITR 1.1b-expressing cells likely requires that the proximal and distal regions of the IpLITR 1.1b CYT differentially participate in the recruitment and activation of select phagocytic effectors. Our results suggest that IpLITR 1.1b-mediated regulation of the actin polymerization machinery is dependent upon the catalytic activity of the Src and spleen tyrosine kinase (Syk) families of intracellular kinases. We hypothesize that Src serves to place IpLITR 1.1b in a primed state that facilitates basal or constitutive coupling of IpLITR 1.1b to the minimal intracellular machinery required for target acquisition and phagocytic cup extension. In this model, the cytosolic adaptor non-catalytic region of tyrosine kinase adaptor protein 1 (Nck) is recruited to the consensus interaction motif H-I-Y-D-E-V located at Y^{433} in the proximal CYT region of IpLITR 1.1b. Nck has been shown to associate with the WAVE2 complex; a highly conserved pentameric heterocomplex that dynamically regulates Arp2/3-dependent actin polymerization. Importantly, in mammalian cells, WAVE2 is expressed ubiquitously and found as a complex with four other proteins: Pir121, Nap1, Abi-1, and HSPC300. The mature WAVE2 complex is basally inactive and directly interacts with the SH3 domain of Nck through Nap1. Activation of the WAVE2 complex requires state-specific phosphorylation as well as

interactions with GTP-bound Rho superfamily proteins, most commonly Rac. As a result, we propose that the assembly of the Nck-WAVE2 complex within the proximal CYT region of IpLITR 1.1b could be coupled to recruitment of a stimulatory Rho-GEF within the distal CYT region. In particular, the spacing of the tyrosines in IpLITR 1.1b suggest that Syk could be recruited to two tandem ITIM motifs at Y^{477} and Y^{499} in the distal CYT region. Based on comparisons with other phagocytic receptors, we suspect that activation of the cytosolic Rho-GEF could be Syk-dependent. Syk activation of the Rho-GEF would provide the necessary catalyst for rapid actin-driven membrane protrusions via the WAVE2 complex. Together, this mechanism would encompass the minimal machinery required for PI3K-independent target capture pathway by IpLITR 1.1b.

Table 2.1 BLASTp searches for vertebrate immunoregulatory receptor-like sequences and intracellular signaling proteins in the Channel catfish (*Ictalurus punctatus*).

Human FcRLs	**Top Matching Catfish Sequences**	**E value**	**Score**	**ID**	**Pos.**	**Cover age**
FcRL6 (XP_005245185)	FcRI (NP_001187150)	4e- 09	55.8	26%	37%	89%
FcRL5 (AAK31327)	LITR TS32.15 L2.1a (ABI23564)	1e -19	165	26%	40%	90%
FcRL4 (NP_112572)	LITR TS32.15 L2.2c (ABI23567)	3e- 11	63.2	25%	38%	89%
FcRL3 (NP_443171)	LITR TS32.15 L1.1a (ABI16036)	1e -18	88.2	25%	39%	90%
FcRL2 (NP_110391)	LITR TS32.17 L2.1a (ABI23578)	6e -06	46.2	24%	39%	79%
FcRL1 (NP_443170)	Hepacam 2 (NP_00118775)	2e -04	40.8	23%	46%	38%
Human FcRs	**Top Matching Catfish Sequences**	**E value**	**Score**	**ID**	**Pos.**	**Cover age**
FcγRI (NP_000557)	FcRI (NP_001187150)	2e- 17	79	26%	40%	96%
	LITR TS32.15 L1.1a (ABI16036)	2e- 11	62.4	26%	40%	50%
FcεRIα (XP_003821022)	LITR TS32.17 L1.1a (ABI16049)	2e- 07	48.5	29%	43%	96%
FcγRIIA (NP_001129691)	−no matches−	–	–	–	–	–

Table 2.1 *Cont.*

FcγRIIIA (NP_001121068)	LITR TS32.15 L2.1a (ABI23564)	1e- 07	49.7	25%	44%	77%
FcγRIIC (NP_963857)	−no matches−	–	–	–	–	–
FcγRIIIB (NP_001231682)	LITR TS32.15 L2.1a (ABI23564)	1e- 05	44.3	25%	44%	66%
FcγRIIB (NP_001002274)	−no matches−	–	–	–	–	–
FcμR (AAP36498)	−no matches−	–	–	–	–	–
PIGR (NP_002635)	−no matches−	–	–	–	–	–
FcαμR (NP_114418)	−no matches−	–	–	–	–	–
Human LRC Proteins	**Top Matching Catfish Sequences**	**E value**	**Score**	**ID**	**Pos.**	**Cover age**
FcαR (NP_001991)	−no matches−	–	–	–	–	–
NKp46 (O76036)	−no matches−	–	–	–	–	–
LAIR1 (NP_001275954)	−no matches−	–	–	–	–	–
LILRB1 (AAC51179)	LITR1 (AAW82352)	6e- 10	98.2	25%	39%	66%

Table 2.1 *Cont.*

LILRB2 (XP_011546934)	LITR TS32.15 L2.2c (ABI23567)	9e- 13	68.6	23%	38%	85%
LILRB3 (O75022)	LITR1 (AAW82352)	4e- 07	50.4	23%	39%	73%
LILRB4 (NP_001265355)	−no matches−	–	–	–	–	–
LILRB5 (NP_006831)	LITR1 (AAW82352)	2e- 10	60.8	24%	38%	66%
LILRA1 (NP_006854)	LITR TS32.15 L2.2c (ABI23567)	2e- 10	61.2	24%	38%	89%
LILRA2 (XP_011545392)	LITR1 (AAW82352)	2e- 13	70.1	24%	38%	66%
LILRA3 (Q8N6C8)	LITR TS32.17 L1.2b (ABII6052)	4e- 09	55.5	24%	40%	53%
LILRA4 (P59901)	LITR1 (AAW82352)	2e -08	54.7	26%	40%	65%
LILRA5 (A6NI73)	−no matches−	–	–	–	–	–
LILRA6 (AGZ61988)	LITR1 (AAW82352)	1e- 09	51.2	23%	38%	68%
KIR3DL1 (ADM64608)	LITR3 (NP_001187136)	7e- 08	52.4	27%	41%	65%
KIR3DS1 (ABX88987)	LITR3 (NP_001187136)	8e- 07	48.9	27%	41%	65%
KIR2DL1 (AAC50335)	−no matches−	–	–	–	–	–

Table 2.1 *Cont.*

KIR2DS1 (XP_011546300)	−no matches−	–	–	–	–	–
KIR2DL4 (ABW73959)	−no matches−	–	–	–	–	–
Human Siglecs	**Top Matching Catfish Sequences**	**E value**	**Score**	**ID**	**Pos.**	**Coverage**
Siglec-1 (Q9BZZ2)	LITR3 (NP_001187136)	2e- 16	137	25%	39%	51%
Siglec-2 (NP_001762)	LITR TS32.15 L1.1a (ABI16036)	7e- 18	170	26%	40%	74%
Siglec-3 (P20138)	−no matches−	–	–	–	–	–
Siglec-4 (NP_002352)	−no matches−	–	–	–	–	–
Siglec-15 (Q6ZMC9)	−no matches−	–	–	–	–	–
Human CEACAMs	**Top Matching Catfish Sequences**	**E value**	**Score**	**ID**	**Pos.**	**Coverage**
Ceacam-1 (NP_001703)	Hepacam 2 (NP_00118775)	4e- 14	144	31%	44%	64%
	LITR3 (NP_001187136)	1e- 09	58.5	24%	43%	65%
Ceacam-3 (NP_291021)	Hepacam 2 (NP_00118775)	9e- 11	59.3	31%	50%	56%

Table 2.1 *Cont.*

Ceacam-4 (NP_001808)	–no matches–	–	–	–	–	–
Ceacam-5 (NP_001295327)	LITR3 (NP_001187136)	1e- 22	166	25%	41%	75%
Ceacam-6 (P40199)	Hepacam 2 (NP_00118775)	4e- 14	71.2	31%	47%	48%
	LITR TS32.17 L2.2b (ABI23581)	3e- 09	56.2	27%	41%	56%
Ceacam-7 (Q14002)	Hepacam 2 (NP_00118775)	2e- 07	49.7	36%	52%	32%
Ceacam-8 (NP_001807)	Hepacam 2 (NP_00118775)	6e- 10	58.5	27%	42%	51%
	LITR TS32.15 L2.3b (ABI23569)	2e- 08	53.1	28%	42%	56%
Mouse PIRs	**Top Matching Catfish Sequences**	**E value**	**Score**	**ID**	**Pos.**	**Cover age**
PIRA (NP_035217)	LITR TS32.15 L1.1a (ABI16036)	1e- 12	61.6	24%	39%	88%
PIRB (AAC53219)	LITR TS32.15 L1.1a (ABI16036)	1e- 11	105	24%	39%	92%
Chicken Receptors	Top Matching Catfish Sequences	E value	Score	ID	Pos.	Cover age
FcRL1-like (XP_015135539)	LITR TS32.17 L2.1a (ABI23578)	2e- 06	46.6	26%	43%	73%

Table 2.1 *Cont.*

FcRL2-like (NP_001090998)	IpFcRI (NP_001187150)	4e- 21	91.3	24%	43%	65%
	LITR3 (NP_001187136)	3e- 11	63.2	25%	41%	69%
CHIR-A (AAG37067)	LITR TS32.17 L2.1a (ABI23578)	5e- 09	53.9	28%	45%	75%
CHIR-B (AAG37068)	LITR1 (AAW82352)	6e- 10	101	27%	42%	83%
CHIR-AB1 (NP_001139613)	LITR TS32.15 L2.2c (ABI23567)	3e- 07	79.7	30%	46%	78%
Xenopus Receptors	**Top Matching Catfish Sequences**	**E value**	**Score**	**ID**	**Pos.**	**Cover age**
FcγRI-L (XP_012809801)	FcRI (NP_001187150)	1e- 18	84	34%	45%	63%
	LITR TS32.15 L2.2c (ABI23567)	1e- 12	67.4	28%	45%	62%
FcR3-L (XP_012824905)	FcRI (NP_001187150)	6e- 17	80.1	22%	46%	43%
	LITR TS32.15 L2.3c (ABI23570)	2e- 15	76.6	25%	43%	61%
FcR4-L (XP_012809008)	FcRI (NP_001187150)	4e- 18	83.2	21%	44%	58%
	LITR TS32.15 L2.2c (ABI23567)	6e- 15	75.5	23%	40%	92%

Table 2.1 *Cont.*

FcR5-L (XP_012825305)	LITR TS32.17 L2.1a (ABI23578)	8e- 19	89.7	25%	44%	41%
ILR-1 (XP_002938564)	LITR TS32.17 L2.2b (ABI23581)	2e- 12	102	28%	44%	67%
ILR-2 (NP_001121201)	LITR TS32.17 L2.1a (ABI23578)	3e- 12	65.1	20%	45%	69%
Human Signaling Proteins	**Top Matching Catfish Sequences**	**E value**	**Score**	**ID**	**Pos.**	**Cover age**
c-Src (P12931)	Lymphocyte PTP (AJW77401)	0	560	59%	77%	82%
SYK (P43405)	SYK (NP_998008)*	0	863	67%	77%	98%
PI3K p85α (NP_852664)	PI3K p85α (AHH41763)	0	864	62%	76%	99%
Csk (NP_004374)	Csk-like (AJW77401)	3e-105	318	40%	58%	95%
GRB2 (CAG467401)	GRB2 (NP_001187313)	3e-151	421	91%	95%	100%
Gab2 (BAA76737)	Gab2 (XP_692935)	0	793	63%	75%	99%
Nck1 (NP_001278928)	Nck1 (NP_001278928)*	0	615	77%	87%	100%
SHP-1 (AAA36610)	SHP-1-like (XP_009290704)*	0	783	66%	78%	95%
SHP-2 (BAA02740)	SHP-2-like (CBX19678)*	0	1076	91%	94%	100%

Table 2.1 *Cont.*

SHIP-1 (AAB49680)	SHIP-1 (AJK26904)	0	1164	56%	67%	99%
SH2D1A (NP_001108409)	SH2D1A (NP_001187495)	2e- 49	155	64%	76%	89%
Vav3 (EAW51251)	Vav3 (XP_009296581)*	0	1173	68%	80%	100%
Rac1 (NP_008839)	Rac1 (AD027935)	4e-136	381	94%	98%	100%
Cdc42 (AAM21109)	Cdc42 (NP_001188177)	2e-134	377	96%	97%	100%
RhoA (P61586)	RhoA-like (NP_001187623)	2e-138	387	95%	98%	100%
Wave2 (P61586)	Wave3 (NP_001074059)*	1e-104	322	44%	53%	100%
	Wave2 (NP_957375)*	2e-104	313	76%	85%	38%
WASp (NP_000368)	WASp (NP_956232)*	1e-106	327	54%	69%	59%
N-WASp (BAA20128)	N-WASp (NP_001076475)*	3e-145	428	75%	85%	53%

(**A**) The amino acid sequences listed in the left column were used as queries to search the non-redundant protein sequence database for catfishes (taxid:7995) by blastp at **http://blast.ncbi.nlm.nih.gov/Blast**; (**B**) Other than the human signaling protein queries, all searches we performed using the predicted extracellular regions of the receptor sequences (*i.e.*, predicted TM segments and CYT regions were excluded from the searches); (**C**) For each search result the Expect (E) value reported provides the overall significance of the match with lower values closer to zero being considered more significant. The score indicates quality of the alignment with a higher score associated with a better alignment. This value is calculated using a formula that considers alignment of similar or identical residues, as wells as gaps in the alignment; (**D**) The top matching Channel catfish sequences are listed in the second column from the left and those marked with an * represent queries that did not retrieve a match using catfishes

(taxid:7995) but did retrieve a match using Danio (taxid:7954); (**E**) Only sequences with scores >40.0 are reported.

Table 2.2 Protein BLAST searches for human immunoregulatory receptor-like sequences in teleost fishes.

Human Receptors	Teleost Matches	E value	Score	ID	Pos.	Coverage
FcRL5 (AAK31327)	Zebrafish **CD22** (XP_009293714)	3e- 46	184	27%	43%	94%
	Salmon **Sialoadhesin-like** (XP_009293614)	3e- 46	184	26%	45%	97%
	Herring **Sialoadhesin-like** (XP_012675080)	8e- 33	316	30%	45%	96%
	Cichlid **CD22-like** (XP_014269289)	1e- 32	276	28%	47%	76%
	Herring **FcRL5** (XP_012678524)	4e- 31	261	25%	40%	94%
FcγRI (NP_000557)	Asian arowana **FcRL5** (KPP56756)	6e- 21	98.2	29%	44%	91%
	Trout **unamed protien** (CDQ78931)	2e- 18	88.6	27%	44%	81%
	Salmon **FcγRI-like** (ACN10126)	4e- 18	88.2	28%	42%	81%
	Catfish **FcRI** (NP_001187150)	3e- 15	79	26%	40%	96%
	Catfish **TS32.15 L1.1a** (ABI16036)	4e- 09	62.4	29%	44%	50%
FcγRIIA (NP_001129691)*	Herring **FcRL5** (XP_012678524)	7e- 10	208	31%	41%	79%
	Yellow Croaker **FcγRII-like** (XP_010752023)	9e- 10	60.5	25%	45%	78%

Table 2.2 *Cont.*

	Tilapia **FcγRIB-like** (XP_013119926)	2e- 09	59.7	37%	54%	41%
	Mexican tetra **CD22** (XP_015459483)	3e- 09	60.8	31%	47%	70%
	Herring **FcRL3** (XP_012675232)	2e- 08	58.9	27%	50%	70%
FcγRIIB (NP_001002274)*	Yellow Croaker **FcγRII-like** (XP_010752023)	1e- 11	65.9	28%	48%	67%
	Killifish **unknown protein** (XP_013889184)	2e- 10	65.1	27%	43%	82%
	Mexican tetra **CD22** (XP_015459483)	4e- 10	63.9	31%	46%	61%
	Herring **FcRL3** (XP_012675232)	2e- 09	62	28%	51%	70%
	Cichlid **FcγRII-like** (XP_006808904)	3e- 08	58.2	28%	42%	76%
FcμR (AAP36498)*	Damselfish **unknown protein** (XP_008286766)	4e- 06	52.8	34%	47%	42%
	Salmon **CMRF35-like** (XP_014058627)	8e- 06	51.2	34%	47%	42%
	Killifish **PIGR-like** (012722396)	2e- 05	50.1	29%	41%	40%
PIGR (NP_002635)*	Tilapia **PIGR-like** (XP_013123119)	4e- 25	115	27%	44%	67%
	Yellow Croaker **PIGR** (KKF27361)	1e- 23	111	25%	39%	81%

Table 2.2 *Cont.*

	Medaka **PIGR** (XP_011484914)	3e- 23	262	28%	44%	72%
	Carp **PIGR** (ADB97624)	1e- 18	92.8	31%	47%	73%
	Zebrafish **PIGR** (NP_001289179)	7e- 18	90.5	30%	47%	68%
FcαR (NP_001991)*	Cichlid **unknown protein** (XP_014265321)	7e- 05	48.5	29%	46%	51%
NKp46 (O76036)*	Atlantic molly **CD276-like** (XP_014823336)	4e- 05	49.7	24%	37%	65%
	Sailfin molly **IgSF 1-like Rc** (XP_014882122)	4e- 04	46.6	24%	38%	69%
LAIR1 (NP_001275954)*	−no matches−	–	–	–	–	–
LILRB1 (AAC51179)	Pike **DSCAM-like** (XP_12987993)	1e- 15	84.3	28%	41%	85%
	Pike **FcRL5** (XP_010867787)	6e- 14	79.7	26%	43%	82%
	Salmon **IgSF 1-like Rc** (XP_01401166)	2e- 11	71.6	27%	41%	83%
	Pike **LILRA4-like** (XP_012988338)	4e- 10	64.3	28%	44%	42%
	Cafish **LITR1** (AAW82352)	2e- 09	65.1	26%	40%	86%
LILRB4 (NP_001265355)*	Cichlid **IgSF 1-like Rc** (XP_014267965)	2e- 11	68.9	27%	47%	78%
	Amazon molly **PEACAM-like** (XP_007571377)	4e- 07	56.2	28%	42%	77%

Table 2.2 *Cont.*

	Atlantic molly **IgSF 1-like Rc** (XP_014827576)	1e- 05	51.6	29%	45%	78%
	Yellow Croaker **LILRA2-like** (KKF09113)	2e- 05	51.2	31%	45%	64%
LILRA2 (XP_011545392)	Trout **unamed protien** (CDQ78931)	1e- 12	75.9	27%	42%	90%
	Pike **DSCAM-like** (XP_12987993)	5e- 12	73.6	27%	42%	82%
	Catfish **LITR1** (AAW82352)	4e- 11	70.1	24%	38%	66%
	Mexican tetra **FcRL5** (XP_015464057)	8e- 11	69.7	28%	41%	72%
	Pike **FcRL5** (XP_010867787)	7e- 10	66.7	27%	42%	77%
LILRA5 (A6NI73)*	Pllatyfish **IgSF 1-like Rc** (XP_005816340)	4e- 06	53.1	28%	40%	72%
	Cichlid **KIR2DL4-like** (XP_005951820)	4e- 05	48.9	35%	48%	40%
	Cichlid **FcγRI-like** (XP_014267764)	6e- 05	48.5	34%	49%	40%
	Cichlid **IgSF 1-like Rc** (XP_014267965)	3e- 04	47	32%	45%	44%
KIR3DL1 (ADM64608)	Asian arowana **FcRL5** (KPP56756)	1e- 11	70.5	25%	42%	63%
	Salmon **KIR3DL1-like** (XP_014042396)	2e- 11	69.7	30%	43%	85%
	Cichlid **IgSF 1-like Rc** (XP_014267965)	9e- 08	70.5	25%	43%	85%

Table 2.2 *Cont.*

	Salmon **KIR3DS1-like** (XP_014043811)	2e- 07	55.5	31%	44%	56%
	Catfish **LITR3** (NP_001187136)	1e- 05	52	27%	41%	65%
KIR2DL1 (AAC50335)*	Salmon **KIR3DS1-like** (XP_014043811)	1e- 05	49.7	28%	40%	78%
	Salmon **KIR3DL1-like** (XP_014042396)	4e- 05	49.3	28%	40%	78%
	Salmon **LILRA4-like** (XP_014037968)	8e- 05	48.5	29%	41%	75%
	Pike **OSCAR-like** (XP_012988534)	1e- 04	47.8	29%	44%	81%
	Pike **DSCAM-like** (XP_12987993)	1e- 04	48.1	26%	43%	81%
Siglec-2 (NP_001762)	Zebrafish **CD22** (XP_009293714)	8e- 71	738	30%	45%	99%
	Cichlid **CD22-like** (XP_005755784)	4e- 64	221	33%	52%	67%
	Tilapia **CD22-like** (XP_013132285)	6e- 61	218	30%	46%	85%
	Trout **unamed protien** (CDQ84455)	2e- 58	212	31%	47%	86%
Siglec-4 (NP_002352)*	Salmon **Siglec-4 (MAG)** (XP_014021122)	4e-154	459	44%	64%	96%
	Pike **Siglec-4 (MAG)** (XP_014021122)	7e-152	454	43%	63%	96%

Table 2.2 *Cont.*

	Black cod **Siglec-4 (MAG)** (XP_010788688)	4e- 151	452	44%	63%	96%
	Tiger puffer **Siglec-4 (MAG)** (NP_001027876)	2e- 149	449	43%	63%	96%
Ceacam-3 (NP_291021)	Herring **Hemicentin-1-like** (XP_012676907)	1e- 18	90.5	34%	52%	65%
	Cichlid **CEACAM 5-like** (XP_014266060)	4e- 16	82.8	33%	53%	82%
	Salmon **CEACAM 1-like** (XP_014038441)	1e- 15	79.3	33%	52%	55%
	Medaka **CEACAM 1-like** (XP_011483887)	5e- 15	77.8	28%	42%	94%
Ceacam-4 (NP_001808)*	−no matches−	–	–	–	–	–
Ceacam-5 (NP_001295327)	Tongue sole **CEACAM 5-like** (XP_008322222)	4e- 80	277	30%	50%	85%
	Yellow Croaker **CEACAM 5** (KKF27703)	4e- 75	918	32%	53%	98%
	Pike **CEACAM 5** (XP_012994902)	4e- 69	570	32%	48%	86%
	Cichlid **Hemicentin-1-like** (XP_004550953)	1e- 65	892	30%	47%	83%
	Salmon **Hemicentin-1-like** (XP_014056825)	3e- 65	1041	30%	46%	86%

(**A**) The human receptor amino acid sequences listed in the left column were used as queries to search the non-redundant protein sequence database for teleost fishes (taxid:32443) by blastp at **http://blast.ncbi.nlm.nih.gov/Blast**; (**B**) Human receptor sequences marked with an * indicate those that did not retrieve matches by blastp searches using catfishes (taxid:7995); see **Table 2.1**; (**C**) All searches we performed using the predicted extracellular regions of the receptor sequences (*i.e.*, predicted TM segments and CYT regions were excluded from the

searches); (**D**) For each search result the Expect (E) value reported provides the overall significance of the match with lower values closer to zero being considered more significant. The score indicates quality of the alignment with a higher score associated with a better alignment. This value is calculated using a formula that considers alignment of similar or identical residues, as wells as gaps in the alignment; **(E**) Representative top-matching teleost protein sequences are listed in the second column from the left; (**F**) Only sequences with scores >40.0 are reported.

CHAPTER III

MATERIALS AND METHODS

3.1 Cells, antibodies and constructs

3.1.1 Cells

Parental AD293 cells (AD293) were cultured in Dulbecco's Modified Eagle's Medium (DMEM; Sigma) supplemented with 10% (v/v) heat-inactivated fetal bovine serum (FBS; GE Healthcare), 100 unit/ml penicillin (Life sciences) and 100mg/ml streptomycin (Life sciences) at 37 °C with 5% CO_2. For routine passaging, cells were grown to ~80% confluency in 6-well tissue culture plates, cell media was aspirated, and cells were washed with 500 µl of sterile PBS and 500 µl of 0.05% trypsin/EDTA (Thermo Fisher Scientific). Cells were then incubated at 37 °C for ~5 min before re-suspending in 1 ml of culturing DMEM and transferred 100 µl of cell suspension to a new 6-well tissue culture plate containing 3 ml of fresh culturing DMEM.

3.1.2 Antibodies

The following antibodies were used for Western blot and confocal microscopy in this thesis: HRP-conjugated mouse αFLAG mAb (Genescript Corp), HRP-conjugated mouse αHA mAb (Genescript Corp), HRP-conjugated goat-α-mouse IgG (H+L) secondary mAb (Bio-rad), HRP-conjugated goat-α-rabbit IgG (H+L) secondary mAb (Bio-rad), rabbit αPhosphotyrosine mAb (Cell Signaling Technologies), FITC-conjugated mouse αphosphotyrosine mAb (Cell Signaling Technologies), rabbit αpSHP-2 mAb (Cell Signaling Technologies), rabbit αCsk mAb (Santa Cruz), rabbit αpErk1/2 (Cell Signaling Technologies), rabbit αErk1/2 (Cell Signaling Technologies), HRP-conjugated bovine-α-goat IgG (H+L) secondary mAb (Santa Cruz), Cy5-conjugate goat-α-mouse IgG (H+L) mAb (Invitrogen), FITC-conjugated goat-α-rabbit IgG

(H+L) secondary mAb (Invitrogen) and AF647-conjugated rabbit-α-mouse IgG (H+L) mAb (Invitrogen).

The following antibodies were used for detecting the surface expression of epitope-tagged IpLITR constructs using flow cytometry: mouse αHA mAb IgG1 (Biolegend), mouse αFLAG mAb IgG1 (Sigma-Aldrich), mouse Isotype IgG1 (Beckman Coulter), PE-conjugated goat-α-mouse IgG (H+L) secondary mAb (Beckman Coulter).

3.1.3 Constructs

The N-terminal hemagglutinin (HA) epitope-tagged pDisplay IpLITR 2.6b/ IpFcγR-L (referred here as $2.6b^{ITAM\ CYT}$ throughout the rest of thesis) and pDisplay IpITR 1.1b (referred here as $1.1b^{WT\ CYT}$ throughout the rest of thesis) were previously generated in our lab (9,11,13). Briefly, $2.6b^{ITAM\ CYT}$ is a chimeric receptor that contains two extracellular Ig-like domains of IpLITR 2.6b (Genbank Accession: ABI23577) fused with the transmembrane (TM) region and cytoplasmic tail (CYT) of the endogenously associated immunoreceptor tyrosine-based activation motif (ITAMs)-containing adaptor IpFcγR-L (Genbank Accession: AF543420). The $1.1b^{WT\ CYT}$ (Genbank Accession: ABI16050) contains four extracellular Ig-like domains, a TM region and a CYT with six tyrosine-based signaling motifs. The pDisplay $1.1b^{WT\ CYT}$ and $2.6b^{ITAM\ CYT}$ were used as templates to generate the $1.1b^{ITAM\ CYT}$ sequence that fuses extracellular Ig-like domains of $1.1b^{WT\ CYT}$ to the TM and CYT region of ITAM-containing IpFcγR-L using splice overlap extension (SOE) polymerase chain reaction (PCR) as describe previously (11,14). The $1.1b^{ITAM\ CYT}$ sequence was further used as template to generate the $1.1b^{ITAM\ CYT\ FF}$ sequence with tyrosines within ITAMs mutated to phenylalanine (F) using mutagenesis primers in Table 3.1 and the QuickChange Lightning Site-directed Mutagenesis Kit (Stratagene) as previously described (9). Both sequences were sub-cloned using SmaI/SalI restriction digest sites into

pDisplay mammalian expression vector (Invitrogen Life Technologies), which adds an N-terminal hemagglutinin (HA) epitope tag to proteins.

pDisplay 1.1b$^{WT\ CYT}$ constructs were also used as templates to generate 1.1b^{CYT} constructs with various combinations of mutated tyrosine motifs in the CYT of 1.1b$^{WT\ CYT}$. Specifically, 1.1b$^{6YF\ CYT}$ is a signaling-incompetent construct with all six tyrosines in the CYT of 1.1b$^{WT\ CYT}$ mutated to F; 1.1b$^{Prox\ CYT}$ has tyrosines in the membrane proximal region (i.e. tyrosine 433/453/463) of CYT of 1.1b$^{WT\ CYT}$ mutated to F; 1.1b$^{Dsital\ CYT}$ has tyrosines in the membrane distal region (i.e. tyrosine 477/499/503) of CYT of 1.1b$^{WT\ CYT}$ mutated to F and 1.1b$^{3F\ CYT}$ has tyrosine 453 (i.e. Csk-binding motif) and two ITIMs (i.e. tyrosine 477 and 499) intact with the rest of three tyrosines mutated to F in the CYT region. All constructs described above were generated using site-directed mutagenesis primers listed in Table 3.1 and the QuickChange Lightning Site-directed Mutagenesis Kit. All construct sequences were sub-cloned using HindIII/BamHI restriction digest sites into pCMV-9 eukaryotic expression vector (Sigma-Aldrich), which adds an N-terminal FLAG epitope tag to the proteins.

3.2 Generation of AD293 cell lines stably expressing IpLITR constructs

To stably express IpLITR constructs in AD293 cells, parental AD293 cells were grown to ~80% confluence in 24-well tissue culture plates and then transfected with pDisplay 1.1b$^{WT\ CYT}$, 1.1b$^{ITAM\ CYT}$ and 1.1b$^{ITAM\ FF\ CYT}$ constructs using 2 µg of TurboFect reagent (Fisher Scientific Company) according to manufacturer's recommended procedures. Transfected cells were incubated for 48 h at 37°C and 5% CO_2 in complete culture medium consisting of DMEM supplemented with 2 mM L-glutamine (Life Technologies), 100 U/ml Penicillin (Life Technologies), 100 µg/ml Streptomycin (Life Technologies), and 10% (v/v) heat-inactivated FBS. Selection of transfectants was then performed by the addition of 800 µg/ml G418 disulfate

salt solution (Sigma–Aldrich) for 1 week and the viable cells were cloned using a serial dilution protocol into round-bottom 96-well tissue culture plates (4,13). Individual clones were then screened for IpLITR surface expression levels. Briefly, clones were harvested using 0.05% trypsin/EDTA and aliquoted (~1×10^5cells) into two 1.5ml Eppendorf tubes for staining. Cells were centrifuged at 500 × g for 2 min and cell pellets were gently disrupted after adding 0.1μg of primary antibody (i.e. αHA mAbs or mouse isotype IgG as an isotype control) diluted in 50μl of FACS buffer (D-PBS, 0.5% bovine serum albumin, 2mM EDTA, 0.05% NaN3). Cells were incubated on ice for 30 min followed by the addition of 1ml ice-cold FACS, centrifuged at 500 × g for 2 min, and then the supernatants were aspirated. Cell pellets were agitated and then 50μl of FACS buffer containing 0.25 μg of goat α-mouse IgG (H+L)-PE was added, and the staining/washing steps repeated as above. Cells were then analyzed for surface staining using flow cytometry (Beckman Coulter) as previously described (4). Positive clones stably expressing respective constructs were referred to throughout this thesis as $1.1b^{WT\ CYT}$, $1.1b^{ITAM\ CYT}$ and $1.1b^{ITAM\ FF\ CYT}$ respectively.

To generate IpLITR co-expression cell lines, AD293 cells stably expressing HA-tagged $2.6b^{ITAM\ CYT}$ was first generated as described above, which was then re-transfected with pCMV-9 FLAG-tagged $1.1b^{CYT}$ constructs. Specifically, $2.6b^{ITAM\ CYT}$-expressing AD293 cells were cultured to ~80% confluency in 24-well tissue culture plates and then re-transfected with 1 μg of CMV-9 plasmid using TurboFect transfection reagent as described above. Transfected cells were then cultured in DMEM supplemented with 10% (v/v) FBS and 800 mg/ml G418 disulfate salt solution at 37 °C with 5% CO2. Cells were harvested after 48h and sorted based using their FLAG epitope staining. The top 15% FLAG-epitope expressing cells were then sorted into round bottom 96-well tissue culture plates as individual clones using a BD FACSAria™ III cell sorter.

Individual clones were grown to confluency, and then screened for co-expression of IpLITR constructs on their surface as described above. Briefly, clones were harvested and aliquoted (~1×10^5cells) into three 1.5ml Eppendorf tubes for staining. Cells were centrifuged at 500 × g for 2 min and cell pellets were gently disrupted after adding 0.1μg of primary antibody (i.e. αHA mAbs, αFLAG mAbs or mouse isotype IgG as an isotype control) diluted in 50μl of FACS buffer (D-PBS, 0.5% bovine serum albumin, 2mM EDTA, 0.05% NaN3). Cells were incubated on ice for 30 min followed by the addition of 1ml ice-cold FACS, centrifuged at 500 × g for 2min, and then the supernatants were aspirated. Cell pellets were agitated and then 50 μl of FACS buffer containing 0.25 μg of goat α-mouse IgG (H+L)-PE was added, and the staining/washing steps repeated as above. Cells were then analyzed for surface staining using flow cytometry (Beckman Coulter) as previously described (4). Stable cell lines co-expressing 2.6b$^{\text{ITAM CYT}}$ with 1.1b$^{\text{WT CYT}}$, 1.1b$^{\text{6YF CYT}}$, 1.1b$^{\text{Prox CYT}}$, 1.1b$^{\text{Distal CYT}}$ and 1.1b$^{\text{3F CYT}}$ were referred to throughout this thesis as 2.6b/1. 1b$^{\text{WT CYT}}$,2.6b/1.1b$^{\text{6YF CYT}}$, 2.6b/1.1b$^{\text{Prox CYT}}$, 2.6b/1.1b$^{\text{Distal CYT}}$ and 2.6b/1.1b$^{\text{3F CYT}}$ respectively.

3.3 Scanning electron microscopy analysis of IpLITR phagocytic responses

To accurately resolve the position of phagocytic targets relative to the plasma membrane, I performed high resolution scanning electron microscopy (SEM) analysis. Specifically, AD293 cell lines expressing 1.1b$^{\text{WT CYT}}$ and 1.1b$^{\text{ITAM CYT}}$ were seeded at 8×10^4 cells/well on poly-L-lysine coated coverslip (Neuvitro) in a 24-well plate and incubate overnight, allowing cells to attach and grow on the coverslip. Next day, culture medium was removed, and cells were washed with PBS before the addition of 1 ml phagocytosis buffer (1:1 mixture of 1X PBS containing 2 mg/ml BSA and 1 X Opti-MEM reduced serum medium; Gibco). 4.5 μm yellow green (YG) beads (2.4×10^5; Polysciences) were used as phagocytic targets and opsonized as

previously described (4). Briefly, YG beads were pre-absorbed with protein A (from *Staphylococcus aureus*; Sigma-Aldrich) and then opsonized with 10 μg/ml of αHA mAbs. After adding YG beads, culture plates were centrifuged at 400 × g for 1 min to synchronize cell-bead interaction and then incubated at 37°C for 60 min. Phagocytosis buffer was then removed and cells were washed with PBS before fixing in 2.5% Glutaraldehyde/2% Paraformaldehyde in a 0.1M phosphate buffer solution. Cells were then dehydrated by the sequential treatments of ethanol and hexamethyldisilazane (HMDS). After dehydration cells were mounted onto SEM studs and sputter coated with an ultrathin layer of gold/plutonium metal. Samples were then imaged using a Philips/FEI XL30 SEM microscope and analysis was performed using the Scandium 5.0 software (Emsis, Germany).

3.4 Standard flow cytometry vs. imaging flow cytometry for differentiating surface-bound from phagocytosed targets during IpLITR-mediated phagocytosis

A bead-based phagocytosis assay was performed as previously described (4,14). Briefly, 4.5 μm YG beads pre-absorbed with protein A were coated with 10 μg/ml of αHA mAb. Then 3 × 10^5 of IpLITR-expressing AD293 cells (i.e. 1.1b$^{WT\ CYT}$ and 1.1b$^{ITAM\ CYT}$) re-suspended in 300 μL phagocytosis buffer were incubated with 9 ×10^5 αHA mAb-coated YG beads for 60 min at 37°C. The bead-cell mixtures were then incubated with 200 μL of phagocytosis buffer containing 2 μg AF 647-conjugated rabbit α-mouse IgG secondary Ab (Invitrogen) on ice for 30 min to stain the extracellularly exposed surface regions of the beads. Samples were then washed with 1 ml of phagocytosis buffer and re-suspended in 200 μL of ice-cold PBS/ EDTA containing 0.05% trypsin (Hyclone) and 1 mM EDTA to remove peripherally (i.e. non-specifically) attached beads. After 15 min incubation on ice, 500 μL ice-cold PBS containing 2 mM EDTA and 0.5% bovine serum albumin was added and cells were centrifuged at 500 × g for 2 min and re-suspended in 100 μL of 1% paraformaldehyde diluted in D-PBS prior to analysis using a BD FACSCanto II

(BD Bioscience) and ImageStreamx Mark II (Amnis Corporation). For each sample, at least 8000 events were collected and for standard flow cytometry, cells were first gated based on FSC-A and SSC-A parameters to exclude cell debris and large aggregates. Doublets were further removed by gating FSC-A versus FSC-H and phagocytosis was gated based on analysis of AF488 (YG beads) versus AF647 (Surface-bound beads). For imaging flow cytometry, data were analyzed using IDEAS® v6.2 software (Amnis Corporation) with connected component masks that allow for the accurate discrimination of phagocytosed vs. surface-bound beads as described elsewhere in detail (107). All analyses were limited to cells associated with up to three beads total as events ≥4 beads per cells could not be accurately discriminated by component masking (107).

3.5 Imaging flow cytometry-based assays

3.5.1 Investigation of impacts of experimental conditions on IpLITR-mediated phagocytosis

To assess if different experimental conditions would affect phagocytic phenotypes, I performed phagocytosis assay under two different conditions (i.e. cells in suspension vs. cells adhered to substrate). Specifically, in the suspension condition, 3×10^5 AD293 cells stably expressing $1.1b^{ITAM\ FF\ CYT}$ were harvested using 0.05% trypsin/EDTA and re-suspended in 300 µl phagocytosis buffer. Then phagocytosis assay was performed as described in section 3.4. For the adherent condition, $1.1b^{WT\ CYT}$, $1.1b^{ITAM\ CYT}$ and $1.1b^{ITAM\ FF\ CYT}$ stable cells (3×10^5) were seeded in 24-well tissue culture plates and allow to attach to plates overnight. On the day of experiments, medium was replaced with 300 µl of phagocytosis buffer before the addition of αHA mAbs-opsonized YG beads (9×10^5). Plates containing cells and targets were centrifuged at 100 × g for 1 min to synchronize cell-bead interactions. After a 60 min incubation at 37°C, cells were rinsed with ice-cold PBS and incubated on ice-cold phagocytosis buffer containing 2µg AF

647-conjugated rabbit α-mouse IgG secondary Abs to differentially stain extracellularly bound beads. After 30 min staining on ice, cells were then rinsed once using ice-cold phagocytosis buffer and then harvested using 0.05% trypsin/EDTA. After re-suspension, harvested cells were washed with ice-cold phagocytosis buffer and fixed in 1% paraformaldehyde (PFA) prior to analysis using an ImageStreamx instrument. For each sample, 5000 events were collected, and data were analyzed using IDEAS® software to resolve two different phagocytic phenotypes as described in section 3.4.

3.5.2 Independent activation of 2.6b$^{ITAM\ CYT}$ and 1.1b $^{WT\ CYT}$ constructs in co-expression AD293 cell lines

To confirm that two IpLITR constructs could be specifically activated in the co-expression AD293 system, I independently activated HA-tagged 2.6b$^{ITAM\ CYT}$ and FLAG-tagged 1.1b$^{WT\ CYT}$ using YG beads opsonized with the respective αHA and αFLAG mAbs and then examined their phagocytic phenotypes using imaging flow cytometry. Specifically, 4.5 μm YG beads pre-absorbed with protein A were opsonized with a range of αHA mAb (i.e. 0.16 μg /ml, 0.32 μg /ml, 0.64 μg /ml and 1.28 μg /ml) and αFLAG mAbs (i.e. 0.32 μg /ml, 0.64 μg /ml, 2.5 μg /ml and 5 μg /ml) respectively. YG beads were also opsonized with 5 μg /ml of the mouse isotype control IgG1. Then AD293 cells co-expressing 2.6b/1.1b$^{WT\ CYT}$ (3×10^5) were seeded in 24-well tissue culture plates one day prior to experiments. The next day, cell media was aspirated, and cells were incubated in phagocytosis buffer containing 9×10^5 of opsonized YG beads as described above and cell-bead interactions were synchronized by 1 min centrifugation at 100 × g. After 15 min and 30 min incubations at 37°C, same staining, fixation and analysis procedures under the adherent condition were followed as described in section 3.5.1.

3.5.3 Binding assays to optimize the concentration of mAbs opsonized on phagocytic targets

To further optimize the concentration of respective mAbs co-opsonized on targets and to prevent disproportionate activation of one IpLITR-type vs. another, a binding assay was performed to select the optimal concentration of respective mAbs required to co-crosslink IpLITR constructs with similar binding avidity. Specifically, 4.5 μm YG beads were opsonized with different dilutions of αHA or αFLAG mAbs as described in section 3.5.2. After selecting the optimal concentration of respective mAbs (i.e. 0.32 μg/ml for αHA mAbs and 2.5 μg/ml for αFLAG mAbs), YG beads were co-opsonized with αHA mAbs (0.32 μg/ml) and isotype IgG1 (2.5 μg/ml) or αFLAG mAbs (2.5 μg/ml) and isotype IgG1(0.32 μg/ml). Mouse isotype IgG1 was included to ensure the same concentration of IgG proteins during bead opsonization. For the binding assay, 2.6b/1.1b$^{\text{WT CYT}}$ and 2.6b/1.1b $^{\text{6YF CYT}}$-expressing AD 293 cells (3×10^5) were seeded in 24-well tissue culture plates. The next day, cell media was aspirated, and the cells were rinsed with ice-cold PBS and then incubated in ice-cold phagocytosis buffer on ice for 15 min before the addition of 9×10^5 opsonized 4.5 μm YG beads. Cell-bead interactions were synchronized by 1 min centrifugation at 100 × g. After a 60 min incubation at 4°C , cells were rinsed with ice-cold phagocytosis buffer and fixed in 1% PFA prior to analysis using an ImageStreamx instrument. For each samples, 5000 events were collected, and data analyzed using IDEAS® software.

3.5.4 Examining the impact of IpLITR-mediated receptor crosstalk on phagocytosis

To investigate the impact of receptor crosstalk on 2.6b$^{\text{ITAM CYT}}$-mediated phagocytosis, AD293 cells co-expressing 2.6b/1.1b$^{\text{WT CYT}}$, 2.6b/1.1b$^{\text{6YF CYT}}$, 2.6b/1.1b$^{\text{Prox CYT}}$, 2.6b/1.1b$^{\text{Distal CYT}}$ and 2.6b/1.1b$^{\text{3F CYT}}$ were seeded in 24-well tissue culture plates (3×10^5 cells/well). The next day, phagocytosis assays under the adherence conditions as described in section 3.5.1 was performed with the exception that cells were given YG beads opsonized with αHA (0.32μg/ml) and αFLAG

mAbs (2.5μg/ml) to co-crosslink 2.6b$^{ITAM\ CYT}$ with the various 1.1b^{CYT} constructs for 15 and 30 min.

3.5.5 Examining the phosphorylation state of intracellular molecules during IpLITR-mediated receptor crosstalk

To determine the phosphorylation status after co-crosslinking of IpLITR constructs, a phospho-flow assay was performed. Briefly, pre-absorbed light yellow (LY, 3.55 μm in diameter; Spherotech Inc) latex beads were opsonized with αHA (0.32 μg/ml) and αFLAG (2.5 μg/ml) to co-crosslink the various IpLITR constructs. To independently crosslink 2.6b$^{ITAM\ CYT}$ and 1.1b^{CYT} constructs, LY beads were also opsonized with αHA (0.32 μg/ml) mAbs and mouse isotype IgG (2.5 μg/ml) or αFLAG (2.5 μg/ml) and mouse isotype IgG (0.32 μg/ml) alone. For the phospho-flow assay, 3×10^5 AD293 stable cells (i.e. 2.6b/1.1b$^{WT\ CYT}$ and 2.6b/1.1b$^{6YF\ CYT}$) seeded in 24-well tissue culture plates were incubated in pre-warmed (37°C) phagocytosis buffer containing 9×10^5 opsonized 3.55-μm LY beads. Cell-bead interactions were then synchronized by 1 min centrifugation at 100 × g. After a 15 min incubation at 37°C, cells were rinsed with ice-cold PBS and fixed in 1% PFA. Cells were then washed with PBS after a 10 min fixation on ice and then permeabilized in 0.1% saponin diluted in PBS for 5 min at room temperature. Cells were then washed with PBS and phospho-tyrosine epitopes were stained by AF488 conjugated α-phosphotyrosine antibodies (1:50 dilution in 5%BSA; Cell Signaling Technology) in the presence of 0.1% saponin. After 1 h staining at room temperature, cells were washed with PBS and re-suspended in 1% PFA prior to analysis using an ImageStreamx instrument. For each sample, 3000 events were collected and phosphotyrosine signals were identified and calculated using the intensity mask and feature in IDEAS® software as described in (107).

3.6 Confocal microscopic examination of the recruitment of intracellular molecules during IpLITR-mediated crosstalk regulation of phagocytosis

3.6.1 Examining the recruitment of phosphotyrosine molecules at phagocytic cups

To investigate the recruitment of phosphotyrosine molecules to phagocytic cups during IpLITR-mediated regulation of phagocytosis, I performed a confocal microscopy-based phagocytosis assay using a variety of staining procedures. Specifically, 4.5 μm non-fluorescent (NF) latex beads (Polysciences, Inc) were used as phagocytic targets in this assay. NF beads were opsonized with αHA (0.32 μg/ml) and αFLAG (2.5 μg/ml) to co-crosslink IpLITR constructs. As controls to independently crosslink 2.6b$^{ITAM\ CYT}$ and 1.1b^{CYT} constructs, LY beads were also opsonized with αHA (0.32 μg/ml) mAbs and mouse isotype IgG (2.5 μg/ml) or αFLAG (2.5 μg/ml) and mouse isotype IgG (0.32 μg/ml) alone. For the confocal microscopy-based phagocytosis assay, 2.6b/1.1b$^{WT\ CYT}$ cells (2×10^5) were grown seeded onto glass coverslips in a 24-well tissue culture plate and then allowed to adhere overnight. Coverslips were then washed with PBS and given 500 μl of phagocytosis buffer containing 6×10^5 opsonized NF beads, and then centrifuged at 100 × g for 1 min. After 8 min incubation, cells were fixed with 4% PFA for 10 min and then beads were stained for inside-outside discrimination as previously described (4,108). Briefly, coverslips were placed cell-side down onto parafilm strips containing a droplet (~50 μl) 0.5 μg/ml of AF647 conjugated goat-α-mouse secondary mAbs (Thermo Fisher Scientific) to stain exposed areas of NF beads. After 30 min incubation at 4 °C, coverslips were washed with antibody staining buffer (ASB; 0.05% sodium azide; Sigma, 1% BSA in PBS) and then given 1 X permeabilization buffer (Biolegend) for 15 min at room temperature. Once permeabilized, coverslips were then placed onto parafilm containing 1:100 v/v dilution of primary rabbit α-phosphotyrosine antibody (Cell Signaling Technologies) in cell staining buffer

(CSB; Biolegend). After staining for 30 min at room temperature, cells were washed with CSB and then stained on parafilm strip with 2 μg/ml of goat-α-rabbit AF488 secondary antibody in CSB for 30 min at room temperature. Lastly, coverslips were washed in CSB and mounted onto microscope slides containing a small droplet of Prolong® Gold antifade mounting media and allowed to cure overnight at room temperature. Imaging was performed as previously described (4,108) using a Laser Scanning Confocal Microscope (LSCM; Zeiss LSM 710, objective 60X 1.3 oil plan-Apochromat). All images were collected and analyzed using Zen 2011 software and ImageJ for calculating fluorescent intensities. Individual cellular events were then isolated from the various z-stack images and the mean fluorescence intensities (MFIs) for both bead staining as well as for the intracellular molecules being studied (i.e phosphotyrosine molecules) were recorded. MFIs were obtained using an 'analysis line' which was placed onto a chosen z-stack image. This analysis line collects the MFIs for all intensities that are present along the line. To calculate integrated fluorescent intensities within phagocytic cups, a region of interest (ROI) was drawn and set consistency throughout analyses. This ROI includes phagocytic cups within which the integrated fluorescent intensities were measured using the ImageJ analysis software.

3.6.2 Examining selective recruitments of Csk and pSHP-2 to the CYT region of 1.1b$^{WT\ CYT}$ during IpLITR-mediated receptor crosstalk regulation of phagocytosis

To further investigate selective recruitments of potential effector molecules (i.e. Csk and pSHP-2) to distinct CYT region of 1.1b$^{WT\ CYT}$, I performed confocal microscopy-based phagocytosis assay detailed in section 3.6.1 on various co-expression AD293 cell lines. Briefly, 2.6b/1.1b$^{WT\ CYT}$, 2.6b/1.1b$^{6YF\ CYT}$, 2.6b/1.1b$^{Prox\ CYT}$, 2.6b/1.1b$^{Distal\ CYT}$ and 2.6b/1.1b$^{3F\ CYT}$ expressing cells were grown on coverslips at the density of 2×10^5 in a 24-well tissue culture plate and allow to adhere overnight. The following day, coverslips were washed with PBS and then

given 500 µl of phagocytosis buffer containing 6×10^5 co-opsonized NF beads to co-crosslink 2.6b$^{ITAM\ CYT}$ and various 1.1b^{CYT} constructs. As controls, 2.6b/1.1b$^{WT\ CYT}$ cells were also given NF beads opsonized with αHA or αFLAG mAbs alone as described in section 3.6.1 to activate the 2.6b$^{ITAM\ CYT}$ and 1.1b$^{WT\ CYT}$ constructs, respectively. Cell-bead interactions were synchronized by 1 min centrifugation at 100 × g. After 8 min incubations, cells were fixed with 4% PFA for 10 min and then the beads were stained for inside-outside discrimination as previously described (4,108). Briefly, coverslips were placed cell-side down onto parafilm strips containing a droplet (~50 µl) 0.5 µg/ml of AF647 conjugated goat-α-mouse secondary mAbs to stain exposed areas of NF beads. After 30 min incubation at 4 °C, coverslips were washed with ASB and then given 1 X permeabilization buffer for 15 min at room temperature. Once permeabilized, coverslips were then place onto parafilm containing either 1:100 or 1:200 v/v dilution of primary rabbit mAbs in CSB for each respective intracellular protein examined using the manufacturer's recommended concentrations (i.e. 1:100 for pSHP-2; 1:200 for Csk). After staining for 30 min at room temperature, cells were washed with CSB and then stained on parafilm strips with 2 µg/ml of goat-α-rabbit AF488 secondary antibody in CSB for 30 min at room temperature. Lastly, coverslips were washed with CSB and mounted onto microscope slides containing a small droplet of Prolong® Gold antifade mounting media and allowed to cure overnight at room temperature. For each sample, at least 50 phagocytic cups were analyzed for staining intensities as detailed in section 3.6.1.

3.7 Magnetic beads-based co-immunoprecipitation assays

To investigate the identity of potential inhibitory molecules recruited to 1.1b$^{WT\ CYT}$ during receptor crosstalk, a co-immunoprecipitation assay was performed using magnetic beads as described in (109). Specifically, AD293 cells (i.e. 2.6b/1.1b$^{WT\ CYT}$, 2.6b/1.1b$^{6YF\ CYT}$, 2.6b/1.1b^{Prox}

^{CYT}, 2.6b/1.1b$^{Distal\ CYT}$ and 2.6b/1.1b$^{3F\ CYT}$) were seeded at the density of 3×10^5 in 24-well tissue culture plates and allowed to adhere overnight. The next day, cell media was aspirated and the cells were given 500 µl of phagocytosis buffer containing 3×10^6 magnetic beads (Thermo Fisher Scientific) that were co-opsonized with αHA (0.32 µg/ml) and αFLAG (2.5 µg/ml) mAbs to co-crosslink 2.6b$^{ITAM\ CYT}$ with the various 1.1b^{CYT} constructs. To independently crosslink IpLITR constructs, 2.6b/1.1b$^{WT\ CYT}$ cells were also incubated with magnetic beads opsonized with αHA (0.32 µg/ml) and isotype IgG1 (2.5 µg/ml) or αFLAG (2.5 µg/ml) and isotype IgG1(0.32 µg/ml) alone. Furthermore, 2.6b/1.1b$^{WT\ CYT}$ cells were also given magnetic beads opsonized with isotype IgG1 (2.82 µg/ml) as a control. After incubating the cells with the magnetic beads in phagocytosis buffer, cell-bead interactions were synchronized by a 1 min centrifugation at 200 ×g. After 8 min incubation at 37°C, cells were washed with ice-cold PBS and then immediately lysed in 300 µl of pre-chilled lysis buffer (50mM Tris-HCL, 150mM NaCl, 1% Triton X-100, protease inhibitor cocktail (Roche), phosphatase inhibitor cocktail (Sigma-Aldrich), pH=8.0) on ice for 20 min and then magnetic beads were isolated using magnetic particle separator (Stemcell^{TM} Technologies). Isolated magnetic beads were washed in 500 µl of ice-cold lysis buffer twice before being re-suspended in 40 µl of 1 X reducing buffer (Bio-Rad) containing 5% β-mercaptoethanol (Bio-Rad). Magnetic beads were then boiled at 95°C for 10 min to elute the proteins. Proteins were then separated via 10% SDS-PAGE gel and transferred to nitrocellulose membranes (Bio-Rad) that were probed with HRP-conjugated αHA (1:1000) mAbs and HRP-conjugated αFLAG mAbs (1:1000) at 4°C overnight to examine successful pull-down of the various epitope-tagged IpLITR constructs. In addition, membranes were further blocked in 5% BSA and also probed with αCsk (1:500), αpSHP-2 (1:1000), αPTEN (1:1000) and αSHIP-2 (1:1000) mAbs at 4 °C overnight, followed by the incubation with HRP-conjugated goat- α-

rabbit IgG (H+L) secondary mAbs (1:2000) at room temperature for 2h. Immunoreactive bands were detected using SuperSignal^{TM} West Pico PLUS Chemiluminescent Substrate kits (Thermo Fisher Scientific) and imaged on ChemiDoc imaging system (Bio-Rad).

3.8 Time course examination of intracellular signaling molecule activation following the co-crosslinking of 2.6b$^{ITAM\ CYT}$ with various 1.1b^{CYT} constructs

To investigate the phosphorylation status of intracellular signaling molecules following co-crosslinking of 2.6b$^{ITAM\ CYT}$ and various 1.1b^{CYT} constructs, AD293 cells (i.e. 2.6b/1.1b$^{WT\ CYT}$, 2.6b/1.1b$^{6YF\ CYT}$, 2.6b/1.1b$^{Prox\ CYT}$, 2.6b/1.1b$^{Distal\ CYT}$ and 2.6b/1.1b$^{3F\ CYT}$) were seeded at the density of 3×10^5 in 24-well tissue culture plates and allowed to adhere overnight. The next day, cell media was aspirated, and the cells were given 500 µl of phagocytosis buffer containing 9×10^5 YG beads that were co-opsonized with αHA (0.32 µg/ml) and αFLAG (2.5 µg/ml) mAbs. As controls, 2.6b/1.1b$^{WT\ CYT}$ cells were also incubated with YG beads that were opsonized with αHA mAbs (0.32 µg/ml) and isotype IgG1 (2.5 µg/ml) or αFLAG mAbs (2.5 µg/ml) and Isotype IgG1(0.32 µg/ml) alone. After incubating the cells with the YG beads in phagocytosis buffer, cell-bead interaction was synchronized by a 1 min centrifugation at 100 × g and then cells were stimulated at 37°C for 2, 8, 15 and 30 min respectively. After stimulation, cells were immediately lysed in 150 µl of pre-chilled lysis buffer on ice for 20 min and then lysates were collected and subjected to two rounds of sonication (50kHz, 3s/round). After sonication, lysates were centrifuged at 13200 × g for 10 min and then the supernatant fraction was collected and a 12.5 µl sample of supernatant was mixed with 50 ul of 4 X reducing buffer containing 5% β-mercaptoethanol. SDS-PAGE and Western blot were performed as described in section 3.7. Membranes were first probed with αpErk1/2 (1:1000) and after incubating in the stripping buffer (3.47mM SDS, 0.2M glycine, 1% Tween-20, pH=2.0), the membranes were re-probed with αErk1/2 (1:1000) mAbs.

3.9 Statistical analysis

Means were first compared by ANOVA to determine if any one mean differed significantly from the rest. If a difference was found, individual means were tested against one another using a post-hoc Tukey analysis. Significantly different means were denoted with alphabetically assigned letters or asterisk as described in figure captions.

Table 3.1. Primers used in this thesis

Primer Name	Primer Sequence 5' to 3'
[a]1.1b$^{WT\ CYT}$ Y433F Fwd	CACATTTTTGACACTGTGGAGAACGC
[a]1.1b$^{WT\ CYT}$ Y433F Rvs	GCGTTCTCCACAGTGTCAAAAATGTG
[a]1.1b$^{WT\ CYT}$ Y453F Fwd	GCCGTTTTTGCACAGGTCATGAAG
[a]1.1b$^{WT\ CYT}$ Y453F Rvs	CTTCATGACCTGTGCAAAAACGGC
[a]1.1b$^{WT\ CYT}$ Y463F Fwd	GAGTCATTCAAGAATAAAGATGATG
[a]1.1b$^{WT\ CYT}$ Y463F Rvs	CATCATCTTTATTCTTGAATGACTC
[a]1.1b$^{WT\ CYT}$ Y477F Fwd	TGATTTTCACTGAGCTTGAAATCAAG
[a]1.1b$^{WT\ CYT}$ Y477F Rvs	CTTGATTTCAAGCTCAGTGAAAATCA
[a]1.1b$^{WT\ CYT}$ Y499F Fwd	GAAGGCCAGTGTAGAGTTTGAAAC
[a]1.1b$^{WT\ CYT}$ Y499F Rvs	GTTTCAAACTCTACACTGGCCTTC
[a]1.1b$^{WT\ CYT}$ Y503F Fwd	ACTATTTTTTCACAGCTGAAGCAG
[a]1.1b$^{WT\ CYT}$ Y503F Rvs	CTGCTTCAGCTGTGAAAAAATAGT
[b]1.1b$^{WT\ CYT}$ Fwd	AAGCTTGTTCTGTCTGTGGAGCCGAATTC
[b]1.1b$^{WT\ CYT}$ Rvs	GGATCCCTATGTGTTCTGCTTCAGCTGTG
[c]1.1b$^{ITAM\ CYT}$ Y218F Fwd	AGAATCCAGATGGCATCTTCCAGGGTTTGAA
[c]1.1b$^{ITAM\ CYT}$ Y218F Rvs	TTCAAACCCTGGAAGATGCCATCTGGATTCT
[c]1.1b$^{ITAM\ CYT}$ Y229F Fwd	GAATCAGGACACCTTTGAGACACTCCATGTGA
[c]1.1b$^{ITAM\ CYT}$ Y229F Rvs	TCACATGGAGTGTCTCAAAGGTGTCCTGATTC

Table 3.1. [a]Primers used for mutating specific tyrosines within CYT region of the 1.1b$^{WT\ CYT}$ sequence. [b]Amplification of respective 1.1b sequences from pDisplay plasmids and sub-cloned into pCMV-9 plasmids. [c]Primers used for mutating specific tyrosines within ITAMs in the CYT region of 1.1b$^{ITAM\ CYT}$ sequence.

CHAPTER IV

CONNECTED COMPONENT MASKING ACCURATELY IDENTIFIES THE RATIO OF PHAGOCYTOSED AND SURFACE-BOUND PARTICLES IN INDIVIDUAL CELLS BY IMAGING FLOW CYTOMETRY

4.1 Introduction

Phagocytosis is a biological process by which specialized cells called phagocytes ingest large particles ranging in size from ~0.5 μm to 8 μm. Phagocytosis is initiated by the ligation of cell surface receptors (110), which leads to induction of signalling cascades, actin polymerization, membrane remodelling, and subsequent internalization of the particle (111). Phagocytosis can be performed by unicellular organisms for nutrient acquisition and by complex multicellular organisms for innate immune defense, as well as for the maintenance of tissue homeostasis through the clearance of damaged and dying host cells (112). Several distinct phagocytic mechanisms have been identified that rely on specific signalling components (113,114). Understanding the dynamic regulation of phagocytosis and the intracellular signalling events that occur during this process can provide key insights into the immunoregulatory receptor-mediated control of actin polymerization and membrane remodelling events.

Classically, phagocytosis has been studied by light microscopy, fluorescence microscopy, and flow cytometry, which allows for the examination of this process with varying levels of specificity. However, each technique has caveats that limit precise quantification of the phagocytic process (e.g. amount of time needed to collect experimental data by imaging, poor reproducibility in quenching fluorescence from surface-bound particles, lack of spatial resolution, etc.) (115). Recently, imaging flow cytometry has proven to be a powerful technique to study phagocytosis as it combines the spatial resolution gained from microscopy with the statistical robustness of flow cytometry. Imaging flow cytometry has been successfully used to

study phagocytosis in a number of systems (42,115–119). These studies have used various masking strategies to discriminate particles that were phagocytosed vs. those that were surface bound. For example, fluorescent events captured within the "cell mask" were considered phagocytosed while fluorescence detected at the periphery were evaluated as surface-bound and generally eliminated from subsequent analyses. This method, however, poorly discriminates surface-bound particles, often counting them in the phagocytosed gate. To overcome the limitation of accurately discriminating surface-bound from engulfed particles, an updated protocol added a staining step to detect particles that had not been fully internalized (120). Specifically, following phagocytosis of CFSE-labeled *N. gonorrhoeae,* cells were stained with an anti-*N. gonorrhoeae* DL650 antibody to determine if cells had any bacteria remaining on the cell surface. The addition of this staining step allowed for more sensitive detection of surface-bound events than relying on the "cell mask" alone does. However, the masks employed in both these methods only allow analysis of the parameter of which they were created to analyse. That being said, they are not able to analyze multiple features (e.g. two types of fluorescence present on particles) within a mask and thus, incapable of further resolving the position of particles (i.e. whether particles are double positive or only CFSE-positive) within individual cells. Therefore, this method only provides information regarding % of surface-bound and internalized particles in a cell population, while sacrificing the phenotype of individual cells (% of cells having internalized particles vs. % of cells only have surface-bound particles are unknown). In this chapter, I utilize a newly developed masking strategy, termed connected component masking, to accurately analyze multiple features within a mask during IpLITR-mediated phagocytosis.

The connected component mask is a new masking feature within the IDEAS® software. This mask allows you to break down a mask that has multiple pieces (or components) thereby

allowing you to analyze those pieces individually (the connected pixels). Each component can be ranked in every image by any analysis feature available in the software= size (area), intensity, aspect ratio, circularity, etc. New features can be created based on each component, allowing you to analyze the components separately or against one, another depending on the features created and the application. For my purposes, this allowed me to first identify the particles of interest (YG bead) and analyze both the fluorescence intensity of green and red within this mask, rather than in previous strategies where green and red fluorescence would have to be analyzed in separate masks.

Our lab is focused on understanding the conserved and divergent aspects of the phagocytic process across vertebrates and, specifically, we have characterized the role of two functionally distinct channel catfish (*Ictalurus punctatus*) leukocyte immune-type receptors (IpLITRs) during phagocytosis (4,9,11,13,15). In particular, 2.6b$^{\text{ITAM CYT}}$ represents a stimulatory teleost receptor-type that mediates an immune tyrosine-based activation motif (ITAM)-dependent mode of phagocytosis akin to classical stimulatory mammalian Fc receptors (4,9,11). This process controls the rapid engulfment of extracellular targets via a Syk-dependent intracellular signalling network that culminates in the activation of F-actin polymerization. Alternatively, 1.1b$^{\text{WT CYT}}$ facilitates a unique ITAM-independent phagocytic pathway as cells expressing this receptor were shown to effectively capture beads and form phagocytic cup-like structures but many of the beads were not fully phagocytosed (4,13,15,16). This represents a unique, and yet to be fully characterized mechanism, which does not require many of the signalling components used during ITAM-mediated phagocytosis.

In our studies, we have studied phagocytosis using standard flow cytometry with 4.5 μm yellow-green (YG) beads opsonized with αHA antibodies as the target particles; these antibody-

opsonized beads specifically trigger the N-terminal HA-tagged IpLITR constructs (4,14). IpLITR-expressing cells that associated with target beads were detected in the green fluorescent gate due to the YG bead fluorescence, but accurate position of the beads relative to the plasma membrane could not be precisely determined. Consequently, confocal microscopy combined with 3-D rendering was used to accurately identify fully engulfed beads and those that were partially engulfed and or simply attached to the cell surface (4). Although this imaging-based technique provides detailed information regarding cell-target interactions, the amount of time consumed to collect enough events for statistical analysis hinders its application in studies where many samples are tested, and quantitative analyses are required. This prompts the development of a high throughput method that can accurately differentiate surface-bound from phagocytosed targets.

The main research objectives of this thesis chapter were to develop a high throughput phagocytic assay for discriminating surface-bound vs. internalized particles and using this to establish the phagocytic phenotype of IpLITR-expressing AD 293 cells. My results show that by using an αIgG-AF647 polyclonal antibody and new analysis features within IDEAS®, accurate detection and discrimination of surface-bound and phagocytosed beads can be achieved using ImageStream flow cytometry alone. The use of connected component masking allows for detection of both red and green fluorescence for each individual particle in the cell and determines the various combinations of red and green fluorescence, as well as their relative brightness. Successful development of this imaging flow cytometry-based assay allows me to re-examine phagocytic responses using AD 293 cells expressing IpLITR constructs as a platform for rapidly establishing the phagocytic phenotypes of these receptors. My results show that a $1.1b^{ITAM\ CYT}$ construct predictably triggers robust phagocytic activity, with most cells completely

internalizing one or more targets. In comparison, 1.1b$^{WT\ CYT}$ was shown to effectively bind but not phagocytose bead targets. Collectively, the data presented in this chapter demonstrate that imaging flow cytometry can be used to accurately discriminate surface-bound from internalized targets and is a valuable tool for studying IpLITR-mediated phagocytic phenotypes. Furthermore, my data shown that 1.1b$^{WT\ CYT}$ is not a *bona fide* phagocytic receptor when expressed in the non-immune AD 293 cell line.

4.2 Results

4.2.1 Generation of IpLITRs-expressing AD 293 cell lines

To examine IpLITR-mediated phagocytosis, I first expressed N-terminal HA epitope-tagged 1.1b$^{ITAM\ CYT}$, 1.1b$^{ITAM\ FF\ CYT}$ and 1.1b$^{WT\ CYT}$ in AD 293 cells. 1.1b$^{ITAM\ CYT}$ is a chimeric construct combining the extracellular domains and transmembrane region of 1.1b$^{WT\ CYT}$ with the CYT region of the channel catfish ITAM-containing adaptor protein IpFcRγ-L. 1.1b$^{ITAM\ FF\ CYT}$ is the same as the 1.1b$^{ITAM\ CYT}$ construct but with two tyrosines within ITAMs mutated to phenylalanine. The design of these constructs ensures any differences in subsequent effector responses (i.e. phagocytosis) are due to the possession of different CYT regions, thus ruling out the impact of other factors (e.g. difference in extracellular domains or transmembrane regions) that may complicate the interpretation of results. After stable transfection, surface expression of IpLITR proteins was then monitored using αHA mAbs followed by PE-conjugated secondary mAbs staining (Fig. 4.1). This epitope-tagging technique allows me to specifically activate IpLITR proteins without knowing their endogenous ligand(s) or developing specific antibodies against IpLITR proteins. Successful development of this heterologous expression system will also serve as a platform to examine phagocytic activities induced by additional constructs tested throughout this thesis.

4.2.2 Standard flow cytometry lacks the resolution to discriminate cells in double positive population

By confocal microscopy, we have previously visualized three distinct phagocytic phenotypes in IpLITR-expressing cells: cells with surface-bound only beads, cells with phagocytosed beads, and cells with a combination of phagocytosed and surface-bound beads. In my thesis study, I wanted to further elucidate the roles of immunoregulatory receptors in mediating actin-dependent membrane remodeling events after target acquisition, especially differentiating cells with surface-bound only beads from those that have internalized particles (representative EM image shown in Fig. 4.2). The flow cytometry-based phagocytosis assay in our lab (12,13) was modified by adding an extra staining step to differentially stain surface-bound targets (Fig. 4.3). Using this modified phagocytosis assay, ITAM-dependent and -independent IpLITR-mediated phagocytic events were further examined by comparing the phagocytic activities of $1.1b^{ITAM\ CYT}$ (as a model of canonical ITAM-dependent phagocytosis) with $1.1b^{WT\ CYT}$ (as a model of ITAM-independent phagocytosis) -expressing AD 293 cells using standard flow cytometry (Fig. 4.4). I observed that $1.1b^{ITAM\ CYT}$ had an increase in the percentage of cells with phagocytosed particles compared to $1.1b^{WT\ CYT}$ (cells with green only fluorescence), similar to what we had previously found when comparing phagocytic rates of cells expressing $2.6b^{ITAM\ CYT}$ (ITAM-dependent mode of phagocytosis) and $1.1b^{WT\ CYT}$ (ITAM-independent phagocytosis) (4). However, by standard flow cytometry, I lacked the resolution to separate out the events within the double positive population (i.e. in Q2, I could not determine whether this quadrant contained cells with only surface bound beads or cells with a mixture of surface bound and internalized beads, as both these possibilities would display a double positive (AF647 and YG) phenotype). Consequently, an underestimation of the phagocytic activity of these cells

could occur, as any cells that were AF647 positive were marked as surface positive for beads although some of these cells may also have internalized YG beads.

4.2.3 Connected component masking accurately discriminate surface-bound from internalized beads within individual cells

The ImageStream flow cytometer is a powerful tool to study surface binding and internalization events (117–121). Detection of surface-bound vs. internalized events is accomplished by the use of masks to identify the cell and the particle, and to examine their relative relation to each other. To analyze phagocytosis using connected component masks, a series of masks were created to identify the beads (Appendix Figure A1). The connected component masks were then set up to identify individual beads within the cells, based on ascending size of the pixel area of the beads– Component 1 had the smallest YG pixel area and Component 3 had the largest YG pixel area. Similar to previous reports (120), above the threshold of 3 beads/cell the masking strategies were less efficient at discriminating between individual beads so all analyses in our study were limited to cells with 1-3 beads total. After gating on cells with 1-3 beads, I was able to use these masks marking the YG fluorescence to examine for the presence of AF647 fluorescence in the same pixel area. This approach allowed us to accurately detect cells with surface-bound beads and cells with a least 1 phagocytosed bead (with or without surface bound beads) (Fig. 4.5). The connected component masks detect both red (e.g. AF647 positive) and green (e.g. YG bead positive) fluorescence on each individual particle in the cell, can determine the various combinations of red and green fluorescence, and can detect how bright the green and red fluorescence is. As a gating control I used cells expressing $1.1b^{WT\ CYT}$ that were held at $4^{o}C$ for the phagocytosis incubation period. This provides a blockade of particle internalization, leaving all particles surface-bound and allowing

us to accurately set the SBa and SBb gates. Phag+SB (internalized and surface bound) events were gated based on fluorescence intensity and remaining events.

4.2.4 Quantitative examination of IpLITR-mediated phagocytosis using imaging flow cytometry-based method

The development of a connected component masking strategy allows for the quantitative examination of IpLITR-mediated phagocytosis process in a high throughput manner. Applying these masks to my samples, I was able to analyze the IpLITR-mediated phagocytosis in greater detail. To do this, I chose to create two populations: a population that contained cell with only surface bound particles (Surface-bound) and a population that contained at least one phagocytosed particle (Phagocytosis). After incubating cells with YG beads at 37 °C, $1.1b^{ITAM\ CYT}$ -expressing AD 293 cells exhibited robust phagocytic activity with ~71% cells internalizing at least one bead; comparatively, ~ 73% $1.1b^{WT\ CYT}$ -expressing AD 293 cells had only surface-bound beads and the % of cells exhibiting phagocytic activity was ~27% (Fig 4.6). Data presented here automatically combine the various cell-bead interaction profiles to show the total % of surface-bound events vs. % of phagocytosis of each construct. However, with images associated with each event, I can further manually break down profiles of cell-bead interaction within two cell populations. The distributions of the surface bound phenotypes (i.e. 1, 2 or 3 surface bound beads only) and the phagocytic phenotypes (i.e. 1 or 2 phagocytosed beads with 1 or 2 surface bound beads or 1, 2, or 3 phagocytosed beads only) were also summarised for each construct tested (Fig 4.6). Overall, the most common cell-bead interactions involved one bead (surface bound or phagocytosed) and the least common profiles are cells with three beads, especially the profiles with both surface-bound and phagocytosed beads. This data provides a more accurate quantification of completely phagocytosed targets relative to those that are

partially engulfed or peripherally associated with the plasma membrane and could potentially provide further understanding of the phagocytic processes in individual cells.

To further validate that the low level of phagocytic activities observed in $1.1b^{WT\ CYT}$-expressing cells was signaling-dependent, I further performed the same experiment using AD 293 cells expressing $1.1b^{ITAM\ FFCYT}$. This construct lacks functional tyrosines within ITAMs and thus, is unable to trigger ITAM-dependent phagocytosis. The % of cells showing phagocytic activity can be viewed as the background activity of this heterologous expression system. After engaging $1.1b^{ITAM\ FF\ CYT}$, the level of phagocytic activities (~33%) observed was similar to that of $1.1b^{WT\ CYT}$ (Fig. 4.7).

To test the possibilities that experimental conditions might lead to false positive results and explain the observed phagocytic activity after activating $1.1b^{ITAM\ FF\ CYT}$ construct, I modified the phagocytosis assay and synchronized cell-bead interaction through centrifugation while cells were still adherent to the plate. As shown in Fig. 4.7, $1.1b^{ITAM\ CYT}$-expressing cells still exhibited robust phagocytic activity with ~88% of cells internalizing at least one bead; whereas the % of phagocytosis was significantly dropped to basal level (~15%) in cells expressing $1.1b^{ITAM\ FF\ CYT}$. However, the % of phagocytosis was also reduced to basal level (~10%) in $1.1b^{WT\ CYT}$-expressing cells.

4.3 Discussion

Phagocytosis is a tightly regulated, complex process by which particles are recognized, bound, and subsequently internalized by cells. The ability to study the cellular activities and signalling processes occurring at each stage will provide important information regarding phagocytic processes. My major objective in this thesis chapter was to utilize the updated

connected components mask within IDEAS® software and customize this masking strategy to discriminate cells with only surface-bound targets from cells that phagocytosed at least one target. To differentiate between different modes of phagocytosis, I used cells expressing different immunoregulatory receptor-types that we have previously characterized: 1.1b$^{ITAM\ CYT}$ displays a canonical ITAM-dependent mode of phagocytosis that is akin to the well-studied FcR-mediated phagocytic pathway in mammals. This process controls the rapid engulfment of extracellular targets via a Syk-dependent intracellular signalling network that culminates in the activation of F-actin polymerization. Comparatively, 1.1b$^{WT\ CYT}$ displays a unique ITAM-independent phagocytosis that results in target capture and often an overall stalled phagocytic phenotype. Despite convergence on the control of actin polymerization dynamics, 1.1b$^{WT\ CYT}$ clearly operates independently of several of the key components of the ITAM-dependent signalling machinery. It appears that 1.1b$^{WT\ CYT}$ may differentially participate in the recruitment and activation of distinct phagocytic effectors culminating in a short-circuited mode of phagocytic signalling. Understanding alternative modes of phagocytosis will significantly augment our understanding of how immunoregulatory receptors can network extracellular target binding into actin-dependent plasma membrane remodeling. The biological significance of novel phagocytic pathways has yet to be understood but exploration of this will be augmented with my recently developed imaging flow cytometry-based phagocytic assay.

I show that connected component masks accurately discriminate IpLITR phagocytic phenotypes by allowing for analysis of cells with various combinations of internalized and bound beads. While the connected component masks can be built for as many components as needed, I limited my study to three components. When cells had internalized more than three beads, I found that bead masks started to overlap, and I could no longer accurately identify all beads

individually. However, in general the proportion of cells with more than three beads was less than 10%, and as detection resolution increases, this number could potentially be increased in the future. Furthermore, connected component masking has the potential to impact image analysis in many applications. Its utility has recently been published in analysis of the cytokinesis-block micronucleus assay, allowing for analysis of micronuclei in a bi-nucleated cell (122). One can also imagine a utility for the masking strategy in other applications analyzing subcellular processes.

In addition to being able to accurately identify phagocytosed and surface-bound beads, I was also able to analyze for the first time the ratio of internalized and surface-bound beads within a single cell. As I show here, I can break down phagocytic populations to cells with 1 bead internalized (1+) versus 1 bead surface-bound (1−) versus 1 bead internalized and 1 bead surface-bound (1+/1–), and so forth, and specifically analyze all the various combinations. This analysis could be used in combination with downstream staining of signalling pathways and the ability to analyze these sub-populations could provide further insights into the signalling that occurs during the various stages of target engulfment at a single cell level. Overall, this imaging flow cytometry-based technique will also serve as a platform to examine phagocytic activities induced by additional stable cell lines tested throughout this thesis.

The re-examination of IpLITR-mediated phagocytosis was performed by heterologous expression of IpLITR proteins in a mammalian fibroblast cell line, AD 293 cells. Although these fibroblast cells possess signalling components to control dynamic actin polymerization and membrane polarization, they do not express the classical phagocytic receptors that are capable of transducing sub-membrane signaling events into internalization of foreign targets. This makes fibroblast cells useful tools to identify *bona fide* phagocytic receptors, a strategy that has been

successfully used to functionally characterize phagocytosis in a number of systems (123). This reductionist approach mitigates the interference from unwanted activation of other phagocytic receptors expressed on immune cells and isolate signaling events specifically downstream of receptors of interest. After activating $1.1b^{ITAM\ CYT}$ on AD 293 cells, I was able to recapitulate the robust phagocytic phenotype observed in RBL-2H3 cells and this phagocytic activity was not observed in mock transfection cells or stable cells incubated with isotype IgG-opsonized beads (14). This observation further proves that AD 293 cells are not endogenously phagocytic but can induce phagocytosis by the heterologous expression of *bona fide* phagocytic receptors. Comparatively, only modest level of phagocytosis (~25%) was observed in $1.1b^{WT\ CYT}$ -expressing AD 293 cells with most cells only having surface-bound targets. This is similar to previous findings in $1.1b^{WT\ CYT}$ -expressing RBLs (4). However, similar level of phagocytosis was also observed in cells expressing a mutant construct (i.e. $1.1b^{ITAM\ FF\ CYT}$) that is competent for binding but not able to induce any signaling events for target internalization. This observation challenges my original hypothesis that $1.1b^{WT\ CYT}$ is a *bona fide* phagocytic receptor that is able to induce a distinct mode of phagocytosis after receptor activation; instead, the phagocytic activity observed here might be through a different mechanism. For example, a "tethering and tickling" model has been described for the removal of dead cells. This two-step process involves binding of apoptotic cells to plasma membrane through tethering receptors and followed by the recognition of phosphatidylserine (i.e. "eat-me" signals) that "tickles" the cell to internalize targets (124). However, this is unlikely the scenario responsible for the modest level of phagocytic activity observed in $1.1b^{ITAM\ FF\ CYT}$ -expressing AD 293 cells. Although $1.1b^{ITAM\ FF\ CYT}$ can initiate binding events, no *bona fide* phagocytic receptor was expressed on AD 293 cells to further induce targets internalization. Alternatively, phagocytosis observed here is likely due

to the background activity under specific experimental condition. In my phagocytosis assay, cells were first detached from the plate using the trypsin and then cell-bead interactions occurred in the suspension condition. Of note, trypsin is a type of serine protease and cleavage of adhesion molecules and breakdown of extracellular matrix on cell membrane may change the biology of AD 293 cells and consequently, resulting in the high background activity. In addition, cells can behave differently in response to various physical and mechanical cues. It has been reported that changes in the rigidity of substrate can affect the efficiency of phagocytosis in macrophages (125). Therefore, it is possible that experimental conditions (cells in suspension vs. cells adherent to the plate) under which the phagocytosis assay was performed can impact the results. Indeed, the % of phagocytosis was reduced to the basal level when $1.1b^{ITAM\ FF\ CYT}$ -expressing AD 293 cells still adherent to the plate during phagocytosis. Similar % of phagocytosis was also observed in AD 293 cells expressing $1.1b^{WT\ CYT}$ under this adherent condition. Comparatively, cells expressing *bona fide* phagocytic receptor $1.1b^{ITAM\ CYT}$ was still able to induce robust phagocytic activities and even with slight increase in % of phagocytosis. These observations strongly suggested that the background phagocytic activity varies under different experimental conditions and $1.1b^{WT\ CYT}$ is not able to induce distinct mode of phagocytosis in AD 293 cells. Detailed mechanisms regarding different background phagocytic activities of AD 293 cells under different conditions (i.e. adherence vs. suspension) is beyond the scope of my thesis study and can be an interesting avenue for future studies.

Overall, the data presented in this chapter outline the establishment of an imaging flow cytometry-based method that is able to accurately discriminate surface-bound from internalized targets within individual cells. Using this new method, I further examined IpLITR-mediated phagocytic responses and my results suggest that $1.1b^{WT\ CYT}$ can only facilitate target binding

activities but is unable to induce phagocytosis in AD 293 cells. This observation challenges our original hypothesis and prompts questions regarding the function of $1.1b^{WT\ CYT}$ in regulating phagocytosis, which will be the focus of Chapter V.

A.

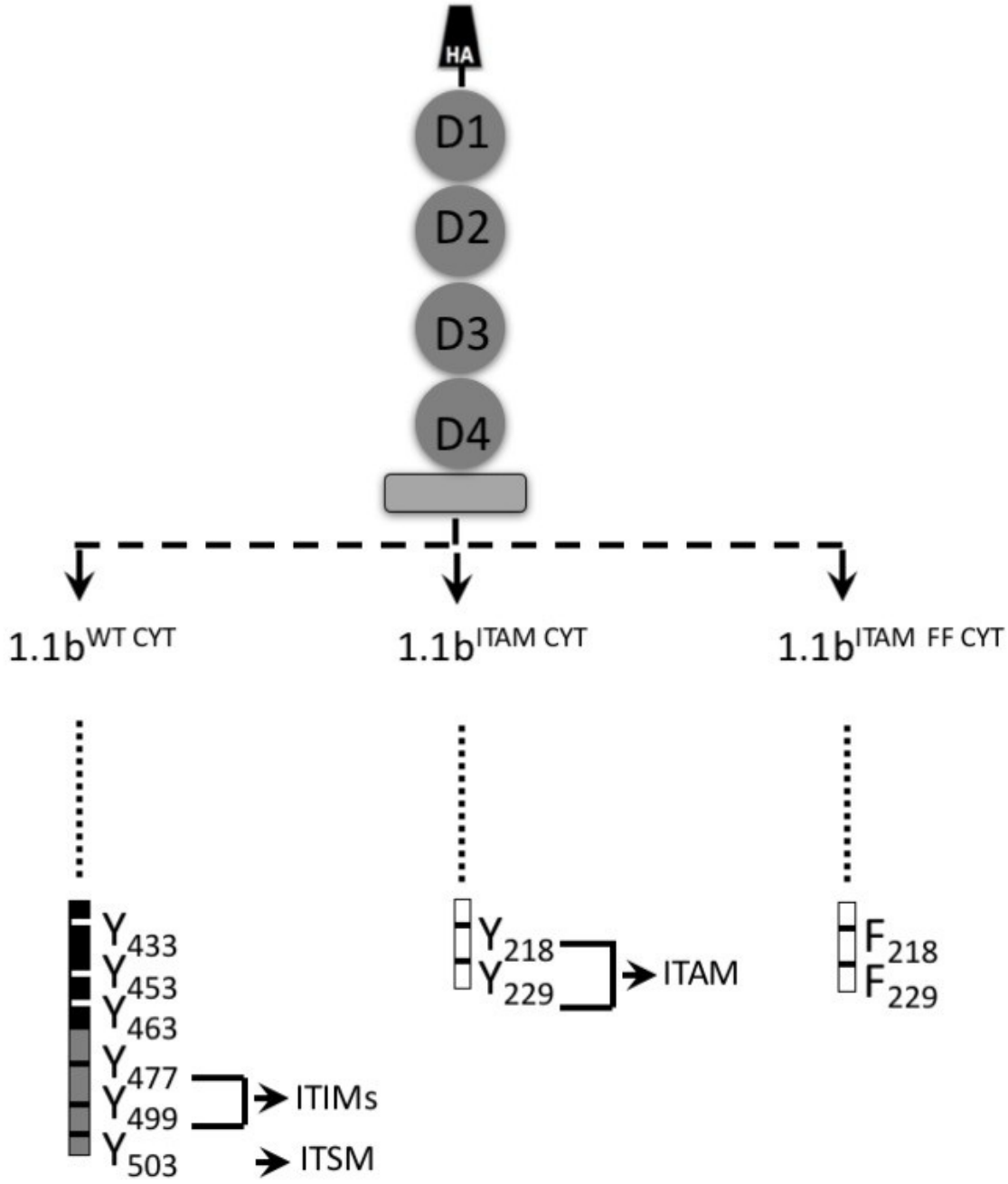
HA
D1
D2
D3
D4
1.1b WT CYT
1.1b ITAM CYT
1.1b ITAM FF CYT
Y433
Y453
Y463
Y477
Y499
Y503
ITIMs
ITSM
Y218
Y229
ITAM
F218
F229

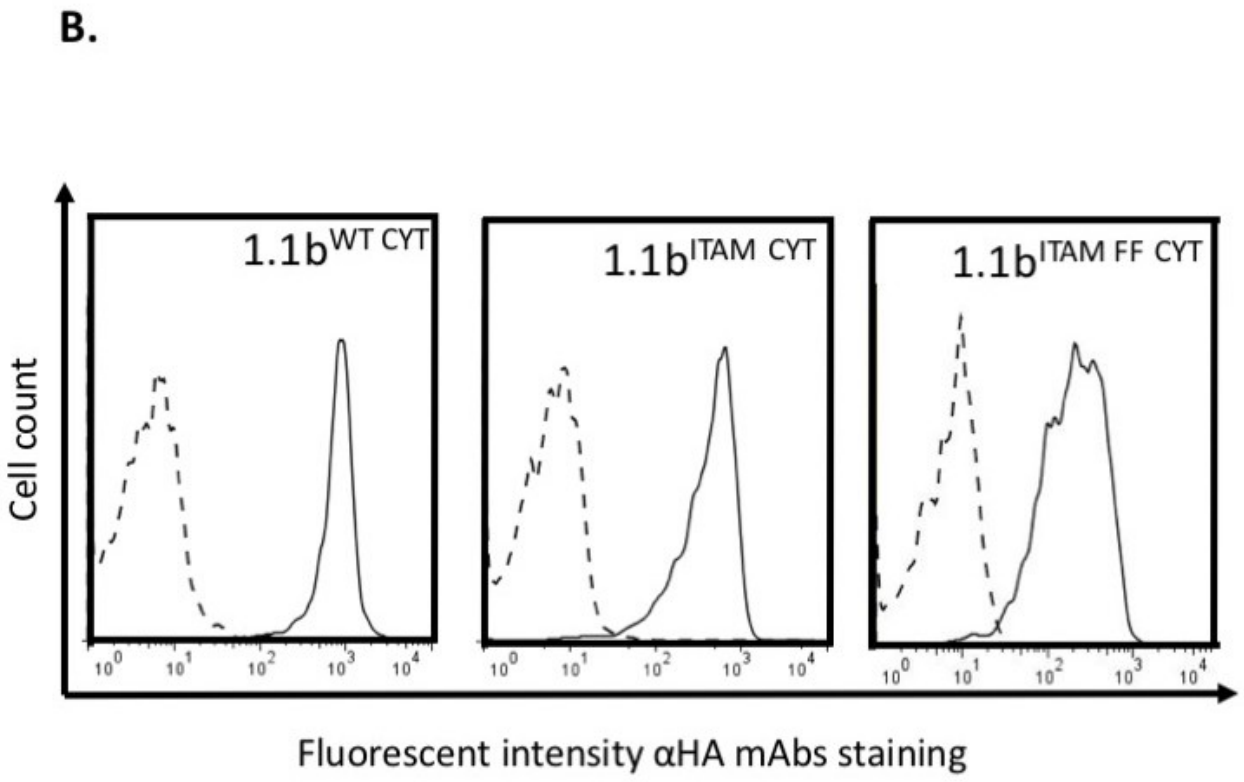

Figure 4.1. Generation, transfection and stable expression of N-terminal HA-tagged IpLITR 1.1b CYT region expression constructs in AD 293 cells. (A) A schematic representation of constructs used in this chapter are shown. $1.1b^{WT\ CYT}$ was previously generated in our lab (13,14) and contains six tyrosines in the CYT region, including two ITIMs and one ITSM. In addition, $1.1b^{ITAM\ CYT}$ is a chimeric construct that combines the extracellular domains and transmembrane region of $1.1b^{WT\ CYT}$ with CYT segments of channel catfish IpFcRγ-L (ITAM). $1.1b^{ITAM\ FF\ CYT}$ is the same as $1.1b^{ITAM\ CYT}$ with the exception that tyrosines within ITAMs mutated to phenylalanine. (B) Surface expression levels of the 1.1b CYT region constructs were detected by flow cytometry after staining the AD 293 cells with the αHA mAb HA.C5 (solid line) or the mouse IgG3 as an isotype control (dotted line), followed by the addition of a PE- conjugated goat αmouse IgG (H + L) polyclonal secondary Ab.

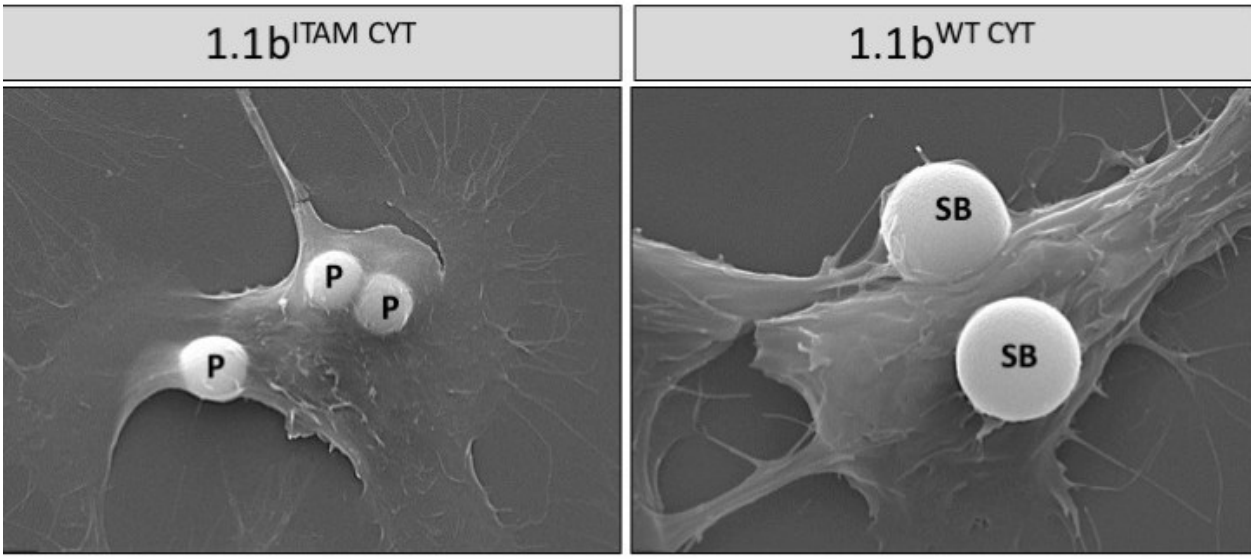

Figure 4.2. SEM analysis of IpLITR-mediated phagocytic responses in AD 293 cells. AD 293 cells stably expressing the N-terminal HA-tagged 1.1b$^{ITAM\ CYT}$ construct (left panel) and 1.1b$^{WT\ CYT}$ (right panel) were incubated with anti-HA mAb opsonized YG beads for 60 min at 37°C. After sample preparation and SEM imaging, representative images demonstrating the various bead-cell associations are shown. In 1.1b$^{ITAM\ CYT}$ -expressing AD 293 cells, three beads (indicated as "P") are fully internalized by the plasma membrane. Comparatively, two surface-bound beads (indicated as "SB") that are attached to the cell membrane but not surrounded by plasma membrane are observed in 1.1b$^{WT\ CYT}$-expressing AD 293 cells.

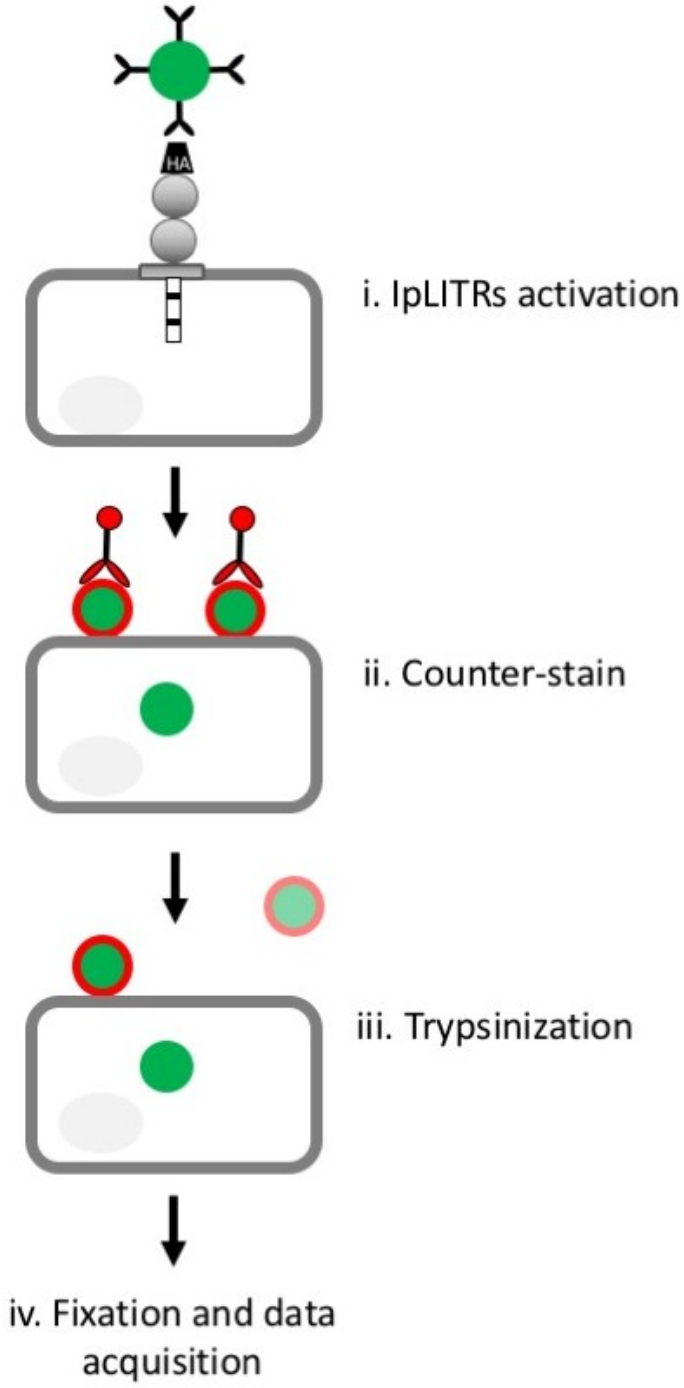

Figure 4.3. Schematic representation of the phagocytic assay. (i) HA-tagged IpLITR constructs were activated by incubating with 4.5 µm YG beads opsonized with αHA mAbs. (ii) After incubating at 37 ℃ for indicated time, surface-bound YG beads were differentiated from internalized YG beads by an additional staining step using AF647-conjugated rabbit-α-mouse secondary mAbs. (iii) Non-specific bound YG beads were removed from cell surface by 10 min trypsinization at 4 ℃. (iv) Cells were fixed in 1% PFA prior to analysis.

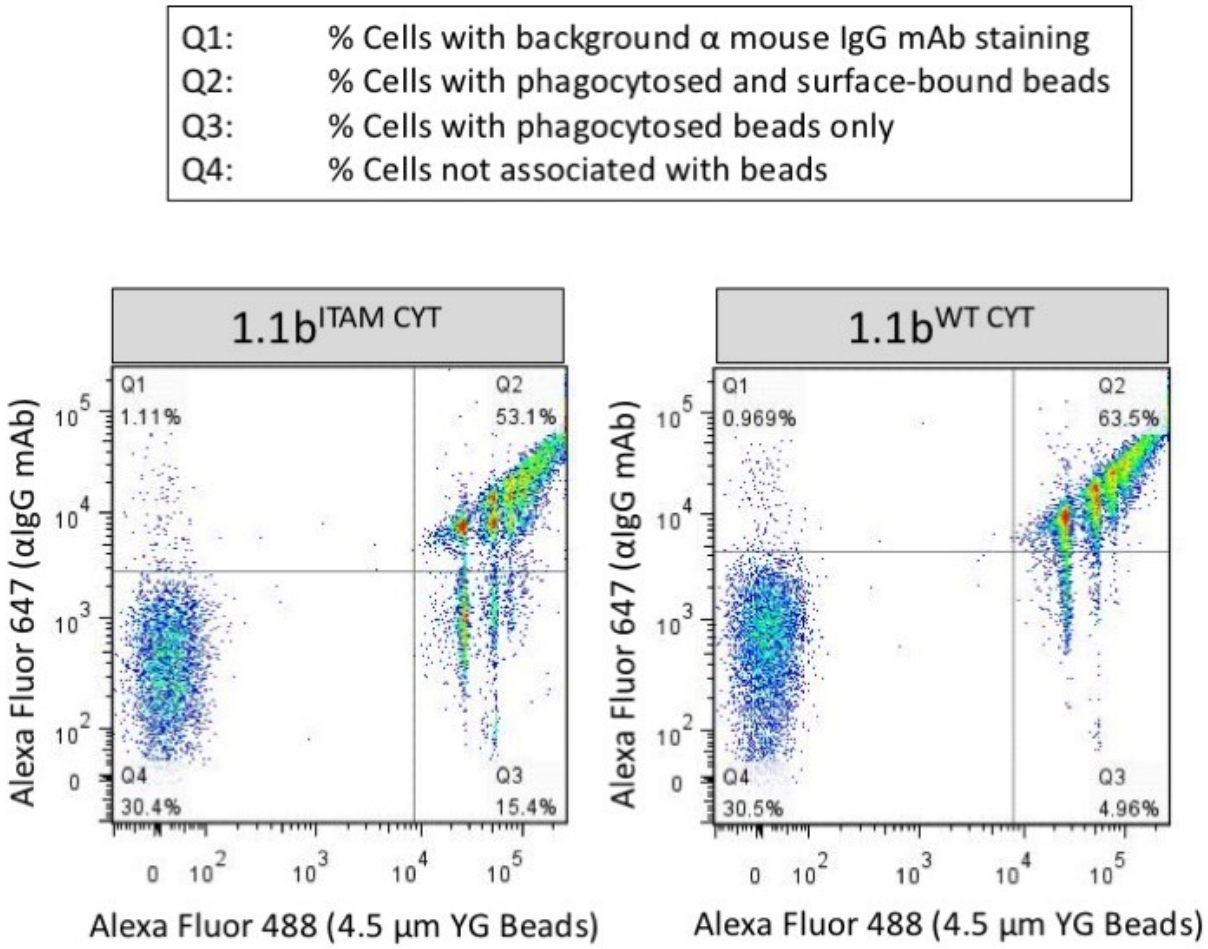

Figure 4.4. Standard flow cytometry lacks the resolution to discriminate cells of different phenotypes in the double positive population. AD 293 cells stably expressing the N-terminal HA-tagged 1.1b$^{ITAM\ CYT}$ construct (left panel) and 1.1b$^{WT\ CYT}$ (right panel) were incubated with anti-HA mAb opsonized YG beads. After 60 min incubation at 37°C, surface-bound beads were discriminated by the addition of AF647-conjugated rabbit-α-mouse secondary mAbs prior to the analysis using a BD FACSCanto II. Cells with only phagocytosed beads (Q3) could be detected. Cells with surface-bound or a combination of surface-bound+ phagocytosed beads (Q2) could not be differentiated.

A.

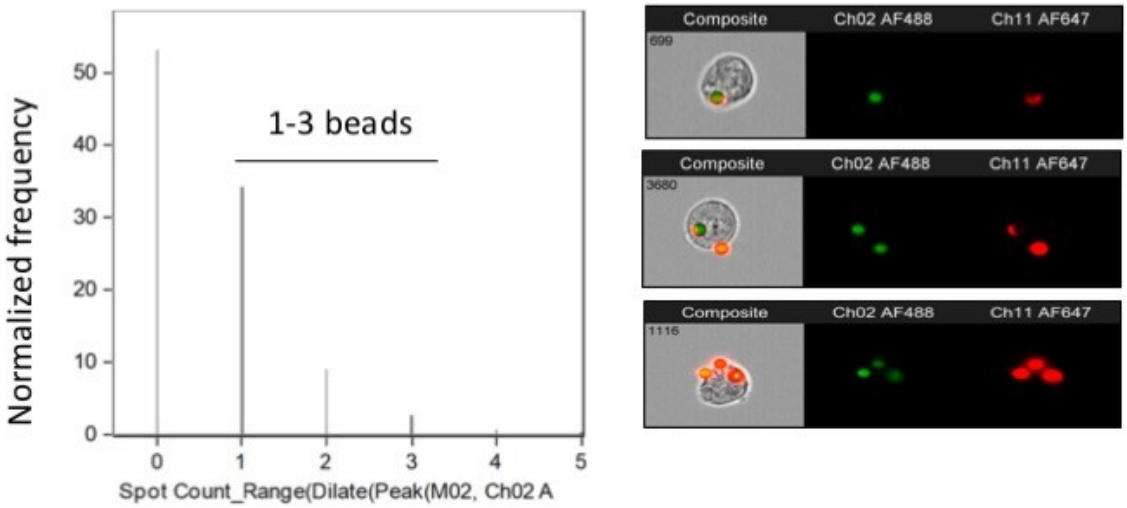
Normalized frequency
50
40
30
20
10
0
1-3 beads
0
1
2
3
4
5
Spot Count_Range(Dilate(Peak(M02, Ch02 A
Composite
Ch02 AF488
Ch11 AF647
699
Composite
Ch02 AF488
Ch11 AF647
3880
Composite
Ch02 AF488
Ch11 AF647
1116

B.

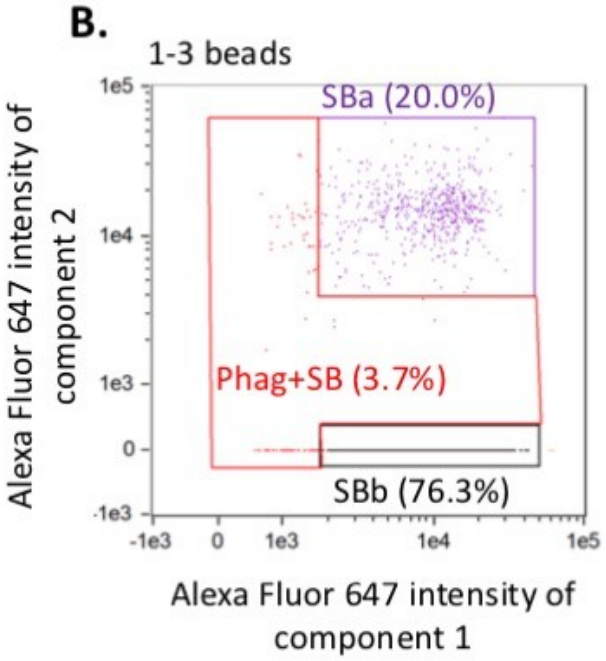
1-3 beads
SBa (20.0%)
Phag+SB (3.7%)
SBb (76.3%)
Alexa Fluor 647 intensity of component 2
1e5
1e4
1e3
0
-1e3
-1e3
0
1e3
1e4
1e5
Alexa Fluor 647 intensity of component 1

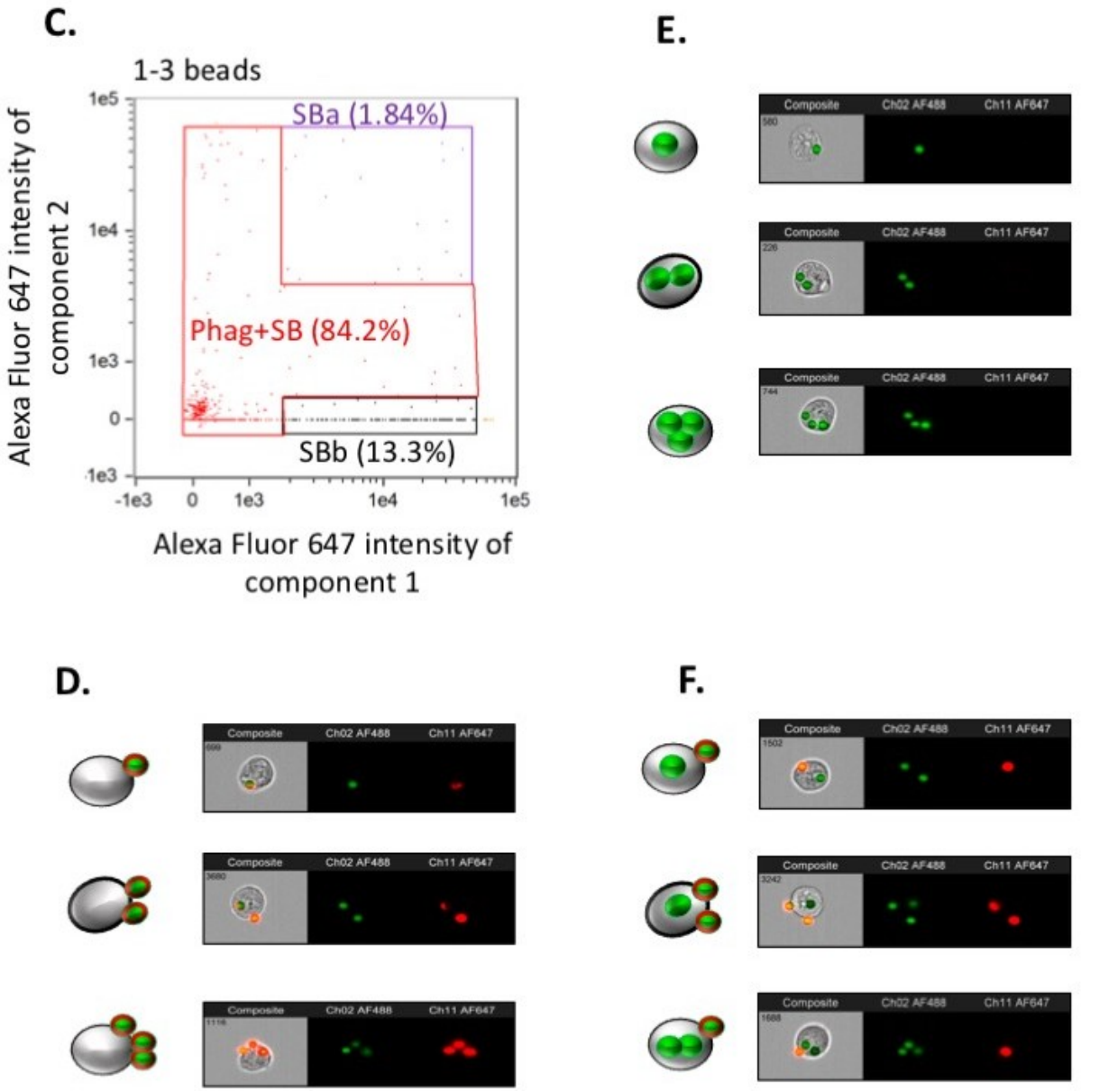

Figure 4.5. Imaging flow cytometry allows analysis of cells with bound and phagocytosed beads. (A) Spot count masks were created to identify beads within cells (representative images of Ch2). Spot Count_Ch2 was plotted and cells with 1–3 spots were gated. (B) Gating strategy for surface bound events. Cells expressing $1.1b^{WT\ CYT}$ were incubated with beads at 4°C to prevent internalization of beads. This identified two populations were cells with surface bound beads = SBa and SBb. The difference was the presence of red fluorescence in the second component. Representative plot shows gate percentages. (C) Connected component masks were used to analyze bead location. Cells were gated based on cells with surface-bound beads ("SBa" and "SBb") and cells with a combination of phagocytosed and surface-bound beads ("Ph + SB"). Representative plot shows gate percentages (D) Representative images of cells with surface-bound beads. (E) Representative images of cells with phagocytosed beads. (F) Representative images of cells with both phagocytosed and surface-bound beads.

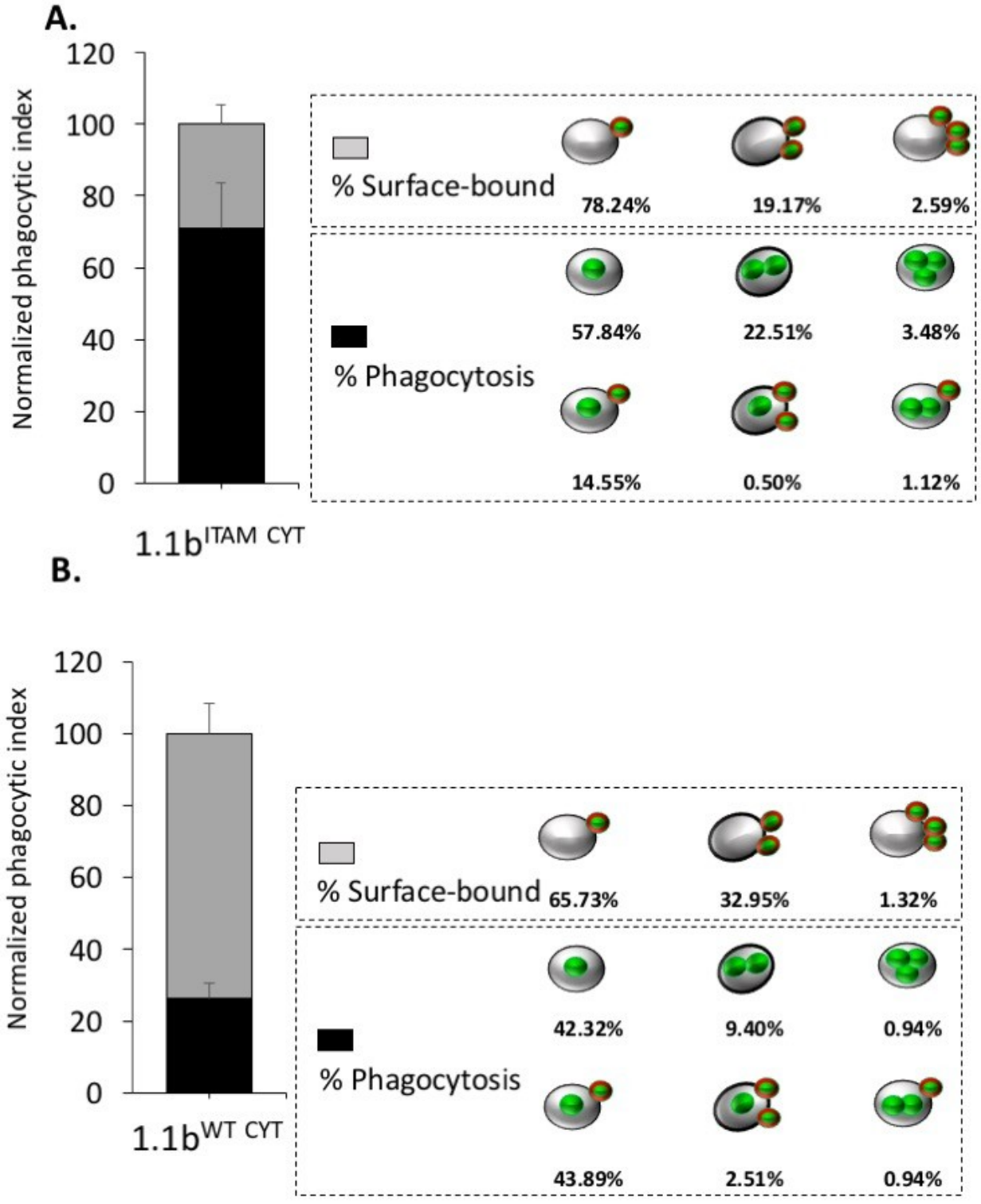
A.
120
100
80
60
40
20
0
Normalized phagocytic index
1.1b ITAM CYT
% Surface-bound
78.24%
19.17%
2.59%
% Phagocytosis
57.84%
22.51%
3.48%
14.55%
0.50%
1.12%
B.
120
100
80
60
40
20
0
Normalized phagocytic index
1.1b WT CYT
% Surface-bound
65.73%
32.95%
1.32%
% Phagocytosis
42.32%
9.40%
0.94%
43.89%
2.51%
0.94%

Figure 4.6. Phagocytic analysis of 1.1b$^{ITAM\ CYT}$ and 1.1b$^{WT\ CYT}$ using imaging flow cytometry-based method. AD 293 cells stably expressing the N-terminal HA-tagged 1.1b$^{ITAM\ CYT}$ construct (A) and 1.1b$^{WT\ CYT}$ (B) were incubated with anti-HA mAb opsonized YG beads. After 60 min incubation at 37°C, surface-bound beads were discriminated by the addition of AF647-conjugated rabbit-α-mouse secondary mAbs prior to the analysis using imaging flow cytometry. Raw data were subjected to component masking analysis using IDEAS® v6.2 software as previously described. Grey bar represents normalized % of cells containing surface-bound beads only (i.e. non-phagocytic cells) and black bar represents normalized % of cells with at least one phagocytosed bead. With images associated with each event, I was able to further break down the profiles of cell-bead interactions within each population. Results are representative of the mean ± SEM of three independent experiments. Normalized % was calculated as: % surface-bound or % phagocytosis cells / % total bead-associated cells.

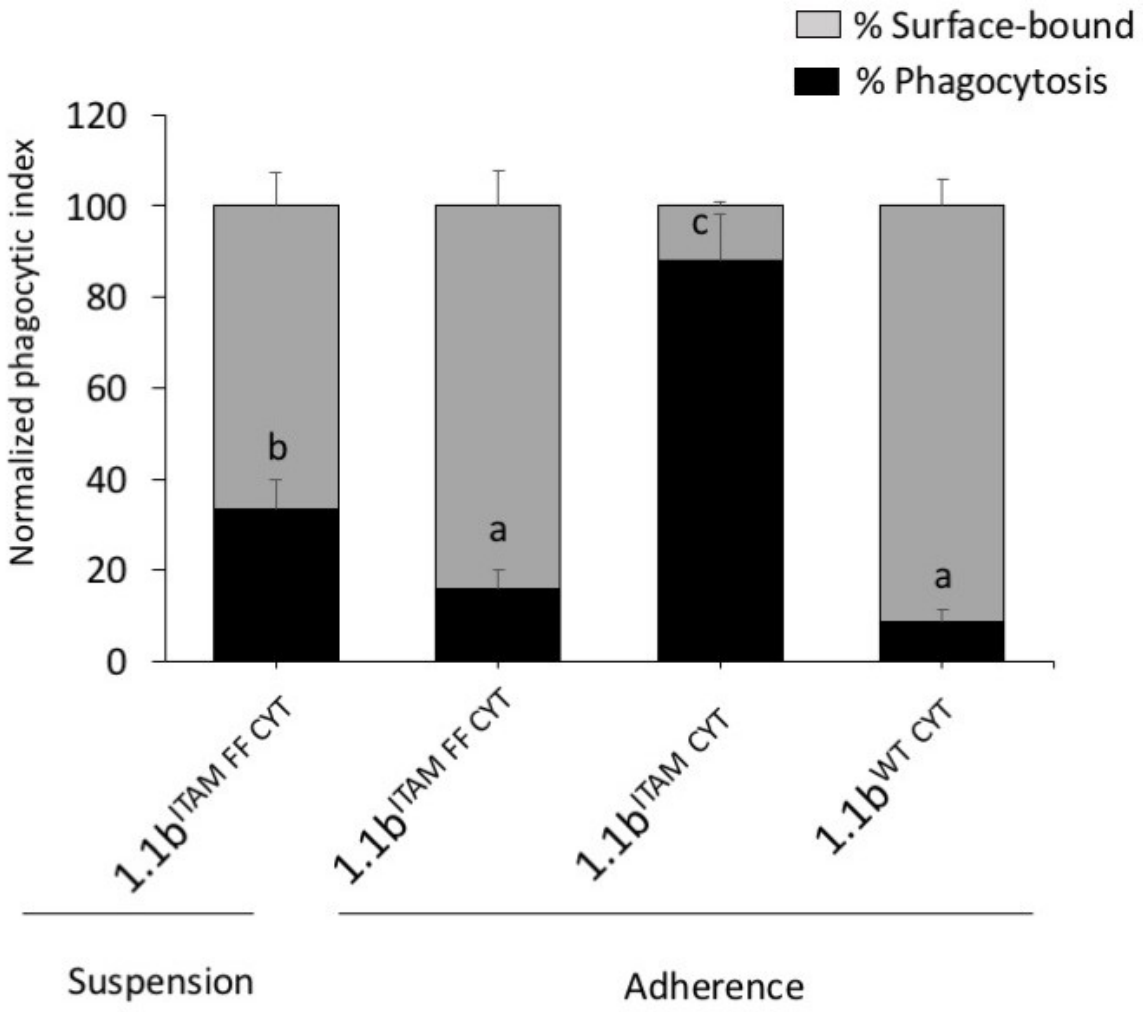

Figure 4.7. Experimental conditions affect phagocytic activities in AD 293 heterologous expression system. Phagocytosis assay was performed under two conditions. In the suspending condition, AD 293 cells expressing 1.1b$^{\text{ITAM FF CYT}}$ were harvested from plate using 0.05% trypsin before the addition of YG beads opsonized with αHA mAbs. In the adherent condition, opsonized YG beads were added to the plate while AD 293 cells expressing various IpLITR constructs were still adherent to the poly-lysine-coated well. Cell-bead interactions were synchronized by 1 min centrifugation at 100 x g. Steps after activating IpLITR constructs for both conditions were the same, including count-staining surface-bound targets prior to analysis on the imaging flow cytometry. Raw data were subjected to component masking analysis using IDEAS® v6.2 software as previously described. Grey bar represents normalized % of cells containing surface-bound beads only (i.e. non-phagocytic cells) and black bar represents normalized % of cells with at least one phagocytosed bead. Normalized % was calculated as: % surface-bound or % phagocytosis cells / % total bead-associated cells. Results are representative of the mean ± SEM of three independent experiments. Letters indicate statistical significance ($P \leq 0.05$) when comparing % of phagocytosis.

CHAPTER V

EXAMINATION OF THE POTENTIAL RECEPTOR CROSSTALK BETWEEN TWO IpLITR-TYPES IN THE CONTROL OF THE PHAGOCYTIC RESPONSE

5.1 INTRODUCTION

Phagocytosis is an ancient component of innate immunity and utilized by all multicellular organisms across evolution as a host-defence mechanism to combat infections and maintain homeostasis (110). Professional phagocytes often encounter targets bearing multiple types of ligands leading to coincident engagement of cognate receptors. Integration of multiple sub-membrane proximal signaling events from different receptors is termed crosstalk and this provides information regarding the chemical constitute and physical characteristic of targets, which helps regulate subsequent cellular responses (112,126). For instance, the simultaneous engagement of toll-like receptors (TLRs) and FcRs synergizes secretion of pro-inflammatory cytokines, which are not or only minimally produced when either of these receptors are activated alone (127,128). However, excessive production of pro-inflammatory cytokines as well as tissue-damaging products during phagocytosis is detrimental to self-tissues thus it is no surprise that this dynamic process is tightly regulated to prevent unnecessary collateral damage to host tissues.

One of regulatory mechanisms controlling phagocytosis is through antagonistic receptor crosstalk, in which activating receptors (e.g. FcγRIIa) are co-crosslinked with inhibitory counterparts (e.g. FcγRIIb). This results in the recruitment of inhibitory signaling molecules (e.g. phosphatases) to the phagocytic synapse that down-regulate phagocytosis and help regulate the secretion of bioactive molecules such as cytokines (129–131). Loss of inhibitory FcγRs in knock-out animal models is often associated with autoimmune diseases as a consequence of unregulated secretion of pro-inflammatory cytokines and enhanced phagocytic activity, further reinforcing the importance of antagonistic receptor crosstalk during immune cell effector

responses (132). Collectively, the simultaneous activation of multiple receptors and the integration of various signaling events is an important regulatory mechanism for modulating the magnitude of innate immune cell antimicrobial activities. However, the overall mechanistic details responsible for regulating antimicrobial responses such as phagocytosis are not fully understood and studies using alternative vertebrate models can provide new insights into the conserved and divergent aspects of receptor crosstalk in regulating this dynamic process.

Our lab has mainly focused on the functional characterization of two teleost immunoregulatory proteins from a multi-gene family called channel catfish (*Ictalurus punctatus*) leukocyte immune-type receptors (IpLITRs). Specifically, a stimulatory construct (i.e. $2.6b^{ITAM\ CYT}$) promotes canonical ITAM-dependent intracellular signaling that triggers degranulation, cytokine secretion, and phagocytosis in a manner similar to mammalian FcγRs (4,9,11). In comparison, $1.1b^{WT\ CYT}$ is a putative inhibitory receptor-type capable of inhibiting NK cell killing through selective recruitment of inhibitory molecules. Interestingly, $1.1b^{WT\ CYT}$ also activates the phagocytic response when stably transfected in the rat basophilic leukemia (RBL)-2H3 myeloid cell line (4,13). Detailed examination of $1.1b^{WT\ CYT}$-mediated phagocytosis revealed a distinct phagocytic phenotype controlled by this protein, in which finger-like protrusions (i.e. filopodia) extended out from the plasma membrane to reach-out and then pull extracellular targets back towards the cell surface in what appeared to be an active capturing phenotype (4). This observation agrees with recent hypotheses that professional phagocytes are actively generating filopodia to increase the likelihood of encountering targets. After capturing and securing targets on plasma membrane, uptake of targets then occurs when phagocytic receptors are co-crosslinked with tethering receptors (124). This step-wise capture and engulfment process has been shown to be responsible for the elimination of apoptotic cells (124).

In the previous chapter, I demonstrated that 1.1b$^{WT\ CYT}$ did not induce a distinct mode of phagocytosis but only showed target binding activity when expressed in AD 293 cells. This raises the question regarding the contribution of 1.1b$^{WT\ CYT}$-mediated signaling events during the phagocytic process. One hypothesis is that the expression of 1.1b$^{WT\ CYT}$ triggers the generation of filopodia-like structures in AD 293 cells. These dynamic actin-rich protrusions help bringing targets into close proximity to the plasma membrane and allow the engagement of classical phagocytic receptors to then initiate targets uptake (124). In addition, 1.1b$^{WT\ CYT}$-mediated signaling events can potentially result in the de-stabilization of cytoskeletal networks beneath contacted sites and thus, increasing the mobility of membrane-anchored receptors and enabling lateral clustering of phagocytic receptors to the phagocytic synapse to initiate target internalization (110,112). This may explain this "stalled" phagocytic phenotype observed in 1.1b$^{WT\ CYT}$-expressing cells showing that although targets were tethered on the plasma membrane, no classical phagocytic receptor is expressed to induce the uptake of targets in AD 293 cells. Alternatively, like other ITIM-containing immunoregulatory receptors that are often co-expressed with their stimulating counterparts, these "paired receptors" often share similar extracellular domains but deliver opposite signals (e.g. ITAM vs. ITIM-dependent signaling) (132–134). Consequently, co-crosslinking of stimulating receptors with their inhibitory counterparts results in antagonistic receptor crosstalk to diminish or inhibit various effector responses (133). Indeed, transcripts of stimulating and inhibitory IpLITRs were shown to be co-expressed in channel catfish immune cells, and early work demonstrated they can also form homo/heterodimers (8,9). Furthermore, the membrane distal immunoglobulin domains (i.e. D1 and D2) of 2.6b$^{ITAM\ CYT}$ and 1.1b$^{WT\ CYT}$, which are predicted to be involved in ligand binding are highly similar, indicating that these two IpLITR types might be co-crosslinked in response to

similar ligands to regulate subsequent effector responses (e.g. phagocytosis) through receptor crosstalk.

The main research objective of this thesis chapter was to test the hypothesis that teleost immunoregulatory proteins fine-tune innate cellular responses through receptor crosstalk. This required the establishment of a cell-based system to allow for the specific examination of the contribution of IpLITR-mediated crosstalk on the phagocytic response. My results show that after co-crosslinking of IpLITR-types in AD 293 cells, $2.6^{ITAM\ CYT}$-mediated phagocytosis was cross-inhibited by$1.1b^{WT\ CYT}$ engagements. This inhibition is accompanied by a reduced phosphotyrosine signal at the phagocytic cups. Examination of IpLITR-mediated receptor crosstalk provides new information regarding regulatory mechanisms in the control of phagocytosis. Furthermore, this work sets the stage for exploring mechanistic details regarding $1.1b^{WT\ CYT}$-mediated inhibition of phagocytosis, which is the focus of Chapter VI.

5.2 RESULTS

5.2.1 Co-expression of different IpLITR-types in AD 293 cell lines for the examination of potential receptor crosstalk

I generated AD 293 stable lines co-expressing N-terminal HA-tagged $2.6b^{ITAM\ CYT}$ and FLAG-tagged $1.1b^{WT\ CYT}$ constructs (referred to here as $2.6b/1.1b^{WT\ CYT}$). This allows for independent IpLITR triggering or co-crosslinking of the constructs using αHA/FLAG mAb-coated beads. As a control, the $1.1b^{6YF\ CYT}$ construct was also co-expressed with $2.6b^{ITAM\ CYT}$ (referred to here as $2.6b/1.1b^{6YF\ CYT}$). The surface expression levels of the IpLITR constructs were confirmed by αHA mAb and αFLAG mAb staining (Fig. 5.1)

To verify that two IpLITR constructs could be specifically activated in this co-expression system, 4.5 μm YG beads were opsonized with a range of αHA mAb concentrations (i.e. 0.16 μg

/ml, 0.32 μg /ml, 0.64 μg /ml and 1.28 μg /ml) and αFLAG mAbs (i.e. 0.32 μg /ml, 0.64 μg /ml, 2.5 μg /ml and 5 μg /ml) respectively. YG beads were also opsonized with 5 μg /ml of the mouse isotype control IgG1. AD 293 cells expressing 2.6b/1.1b$^{WT\ CYT}$, were then incubated with the various mAb opsonized YG beads at 37°C for 15 or 30 min respectively. Then, using the imaging flow cytometry-based method developed in previous chapter, their phagocytic activities were examined. When activating the 2.6b$^{ITAM\ CYT}$ construct, robust phagocytic activities were observed. Specifically, 12.6% cells showed phagocytic activity (i.e. cells having at least one internalized bead) after incubating with 0.16 μg/ml of αHA mAb-opsonized YG beads. This value increased to 33.29%, 44.7% and 41.95%. respectively, when the cells were incubated with YG beads opsonized with higher concentrations of αHA mAbs at 15 min (Fig. 5.2A). However, in all cases, ~12% cells had beads bound to their membranes (i.e. % surface-bound). In comparison, significant target binding activity was observed after activating 1.1b$^{WT\ CYT}$ with only background levels of phagocytosis observed (i.e. ranging from 0.16-6.33%). Specifically, ~40% of the AD 293 cells expressing 1.1b$^{WT\ CYT}$ captured targets but did not engulf them when incubated with 2.5 μg/ml or 5 μg/ml of αFLAG mAb-coated beads (Fig. 5.2A). In comparison, the percentage of surface-bound beads was decreased to 11.25% and 5.19% when the concentrations of αFLAG mAbs on beads was reduced to 0.64 μg/ml and 0.32 μg/ml, respectively. Similar trends were also observed when cells were incubated for 30 min with the various target beads (Fig. 5.2B). For example, cells incubated with αHA mAbs-opsonized beads exhibited robust phagocytic phenotypes, representing an ~1.5-fold increase in % of phagocytosis when compared to the 15 min incubations. In comparison, the % surface-binding activity observed using the αFLAG mAbs-opsonized beads were similar to the 15 min incubation but with a slight increase to 8.1%, 14.41%, 50.04% and 43.24% respectively (Fig. 5.2B).

To further optimize the concentration of respective mAbs co-opsonized on targets and to prevent disproportionate activation of one IpLITR-type vs. another, a binding assay using 4.5 μm YG beads opsonized with different dilutions of αHA or αFLAG mAbs described above was also performed to select the optimal concentration of respective mAbs required to co-crosslink IpLITR constructs with similar binding avidity. Specifically, 2.6b/1.1b$^{WT\ CYT}$ and 2.6b/1.1b$^{6YF\ CYT}$-expressing AD 293 cells, were incubated with opsonized YG beads for 60 min at 4°C. After incubation, ~22.76% binding was observed when 2.6b/1.1b$^{WT\ CYT}$ cells were incubated with 0.16 μg/ml of αHA mAb-opsonized YG beads; this value gradually increases to 37.39%, 44.29% and 49.89%, respectively, along with the increase in the concentration of αHA mAbs opsonized on YG beads (Fig. 5.3A). In comparison, crosslinking of 1.1b$^{WT\ CYT}$ with different dilutions of αFLAG mAb-opsonized YG beads showed similar binding profiles and % of binding ranged from 8.21-38.33% (Fig. 5.3A). When 2.6b/1.1b $^{6YF\ CYT}$ cells were incubated with various opsonized YG beads, similar trends were observed as the binding profile described above. For example, cells incubated with αHA mAb-opsonized beads displayed 14.24%, 35.16%, 40.77% and 44.35% of binding, respectively. Comparatively, slight increase in these values (~10%) were observed when 1.1b$^{6YF\ CYT}$ was crosslinked by αFLAG mAb-opsonized YG beads in comparison to values from crosslinking 1.1b$^{WT\ CYT}$ (Fig. 5.3B). The binding profiles described above allows me to select the concentrations of αHA and αFLAG mAbs to co-opsonize YG beads in order to co-crosslink 2.6b$^{ITAM\ CYT}$ and 1.1b^{CYT} constructs (i.e. 1.1b$^{WT\ CYT}$ and 1.1b$^{6YF\ CYT}$) with similar binding avidity. Based on these results, specific concentration of αHA (0.32 μg/ml) and αFLAG (2.5 μg/ml) mAbs were selected for further test based on similar % of binding activity (~35%) after engaging cognate IpLITR constructs.

To further validate that the selected concentrations of αHA (0.32 μg/ml) and αFLAG (2.5 μg/ml) mAbs can crosslink 2.6b$^{ITAM\ CYT}$ and 1.1b^{CYT} constructs with similar binding profile, YG beads were opsonized with 0.32 μg/ml of αHA mAbs and 2.5 μg/ml of isotype IgG or 2.5 μg/ml of αFLAG mAbs and 0.32 μg/ml of isotype IgG. The addition of isotype IgG ensures that the same overall concentrations of IgG proteins are present on the different beads used to activate the receptors. After 60 min incubation at 4°C, crosslinking of 2.6b$^{ITAM\ CYT}$ and 1.1b^{CYT} constructs displayed similar binding profile (Fig. 5.3C). For example, 30.31% and 27.25% of binding activity was observed when 2.6b$^{ITAM\ CYT}$ and 1.1b$^{WT\ CYT}$ were crosslinked respectively; these values slightly increased to 31.19% and 37.54% after crosslinking 2.6b$^{ITAM\ CYT}$ and 1.1b $^{6YF\ CYT}$. No significant difference was observed between these values (i.e. 30.31% vs. 27.25%; 31.19% vs. 37.54%).

5.2.2 Cross-inhibition of 2.6b$^{ITAM\ CYT}$ -mediated phagocytosis by 1.1b$^{WT\ CYT}$

To investigate potential receptor crosstalk, I co-crosslinked 2.6b$^{ITAM\ CYT}$ and 1.1b^{CYT} constructs using 4.5 μm YG beads opsonized with both αHA mAb (0.32 μg/ml) and αFLAG (2.5 μg/ml) mAbs, respectively (Fig. 5.4). Of note, obtained % of association values across constructs range from ~55% to 65%. To simplify the visualization of the dataset, only cells associated with YG beads (% of association) were gated; % of phagocytosis and % of surface-bound were then normalized to % of association. Specifically, after co-crosslinking 2.6b$^{ITAM\ CYT}$ with 1.1b $^{6YF\ CYT}$, robust phagocytic activities were observed with ~80% cells internalizing at least one bead after 15 and 30 min incubations (Fig. 5.5). This observation shows that co-crosslinking 2.6b$^{ITAM\ CYT}$ with 1.1b$^{6YF\ CYT}$ mutant construct devoid of CYT region tyrosine residues does not disrupt 2.6b$^{ITAM\ CYT}$ -mediated phagocytosis. Comparatively, a significant reduction (~50%) in % of

phagocytosis was observed after co-crosslinking 2.6b $^{ITAM\ CYT}$ with 1.1b $^{WT\ CYT}$ for 15 min and 30 min respectively (Fig. 5.5).

5.2.3 Co-crosslinking of 2.6b $^{ITAM\ CYT}$ with 1.1b $^{WT\ CYT}$ down-regulates 2.6b $^{ITAM\ CYT}$-induced phosphotyrosine signaling.

To determine if 1.1b $^{WT\ CYT}$-mediated inhibition of 2.6b $^{ITAM\ CYT}$ phagocytic activity could be examined by monitoring intracellular signaling events, I developed an imaging flow cytometry-based phospho-flow assay. Specifically, 2.6b/1.1b$^{WT\ CYT}$ cells were first incubated with light yellow (LY) beads co-opsonized with 0.32 μg/ml αHA mAb and 2.5 μg/ml isotype IgG. After 15 min activation of 2.6b $^{ITAM\ CYT}$ constructs at 37°C, cells were immediately fixed, permeabilized and intracellularly stained using an AF488-conjugated α-phosphotyrosine mAb. Two cell populations (i.e. cells associating or not with LY beads) were then gated based on their light-yellow fluorescence signal and then subsequently analyzed for their phosphotyrosine staining intensities (Fig. 5.6A). To measure the intensity of phosphotyrosine signals within individual cells, an intensity mask that identified signals with fluorescent intensity value above 72 MFI was first created to eliminate background signals (i.e. signals with fluorescent intensity value below 72 MFI was considered as background staining and excluded from subsequent analysis) (Fig. 5.6B). After applying this mask to cell populations of interest, cells with no target associations showed basal levels of phosphotyrosine signals (MFI=143) and predictably, an induction of signal intensity (MFI=2781) was observed when the IpLITR-expressing cells bound αHA mAbs-opsonized LY beads (Fig. 5.6C). This phospho-flow assay can detect changes in phosphotyrosine signals after receptor activation and serves as a platform to investigate the impact of IpLITR crosstalk on phosphotyrosine intensity at the whole cell populational level. Next, 2.6b $^{ITAM\ CYT}$ and 1.1b^{CYT} constructs were co-crosslinked using LY beads opsonized with

both 0.32 μg/ml αHA and 2.5 μg/ml αFLAG mAbs. As controls, 2.6b $^{ITAM\ CYT}$ and 1.1b^{CYT} constructs were also individually crosslinked by LY beads opsonized with αHA (0.32 μg/ml) and isotype IgG (2.5 μg/ml) or αFLAG mAbs (2.5 μg/ml) and isotype IgG (0.32 μg/ml). Using 2.6b/1.1b$^{6YF\ CYT}$ cells, crosslinking of 1.1b $^{6YF\ CYT}$ alone demonstrated basal level of phosphotyrosine signals, with an MFI value of 177.67±49.23 (Fig. 5.7A). However, a clear induction of tyrosine phosphorylation (MFI=2231.54±252.84) occurred when 2.6b $^{ITAM\ CYT}$ was activated (Fig. 5.7A). Although the MFI reduced to 1832.99±478.53 when 2.6b $^{ITAM\ CYT}$ was co-crosslinked with 1.1b $^{6YF\ CYT}$, this was not a statistically significant reduction in phosphotryosine staining (Fig. 5.7A). Crosslinking of 1.1b $^{WT\ CYT}$ induced an MFI value of 184.88±45.61, and a significantly higher MFI of 2897.34±385.29 occurred when 2.6b $^{ITAM\ CYT}$ was triggered. Finally, when 2.6b $^{ITAM\ CYT}$ was co-crosslinked with 1.1b$^{WT\ CYT}$, a significant reduction in phosphotyrosine staining was observed (e.g. MFI=930.83±385.29) when compared to the value for 2.6b $^{ITAM\ CYT}$ activation alone (MFI=2897.34±385.29; Fig. 5.7B).

This phospho-flow assay allowed me to examine the change of phosphotyrosine signals following co-crosslinking of IpLITR constructs in a high-throughput manner. However, it lacks the resolution for examining what occurs at the phagocytic synapse during cell-target interactions that occur during the phagocytic process. Therefore, I was unable to monitor the change of signal intensities within this specific structure using the whole cells assay. To achieve higher resolution, a confocal microscopy-based phagocytosis assay was performed as previously described (4,108). Specifically, αHA mAb-opsonized beads were incubated with 2.6b/1.1b$^{WT\ CYT}$-expressing AD 293 cells that were subsequently stained for intracellular phosphotyrosine molecules using an α-phosphotyrosine rabbit mAb conjugated with FITC (green). These cells were also co-stained with an α-mouse IgG mAb conjugated with Cy5 (red) to detect surface exposed areas of the non-

fluorescent (NF) target beads. Cell-bead contact sites (i.e. phagocytic synapses) are protected by plasma membrane and thus are not accessible to antibody staining. Consequently, surface areas of beads, that are not enclosed by plasma membrane, are stained red. A representative image of a cell with three partially internalized NF beads and intracellular phosphotyrosine molecules staining is shown in Fig. 5.8A. A staining intensity histograms (Fig. 5.8B) complete with MFI for phosphotyrosine molecules (green) and the extracellular exposed areas of the selected beads (red) are also shown. An arrowed line was then drawn across the selected bead (indicated by *) to show the areas of the image that were selected for MFI analysis, with the direction of the arrow correlating with the distance in μm (starting at 0 μm) of the x-axis. As shown in Fig. 5.8B, the selected bead is partially internalized with the red staining in the exposed area, which correlates with relatively high MFI values (~160 MFI) in the red channel calculated along the arrowed line. Comparatively, at the cell-bead contact site, the phosphotyrosine molecules staining is clearly visible as a thin green line outlining the phagocytic synapse. The calculated MFI for the bead (red histogram line) at this site is reduced to the basal level whereas MFI values of phosphotyrosine molecules (green histogram line) increase to ~113, indicating the enrichment of phosphorylated proteins localized at the phagocytic synapse. To further quantify the signal intensity of phosphotyrosine molecules recruited to phagocytic cups under different activation conditions (i.e. co-crosslinking of $2.6b^{ITAM\ CYT}$ and $1.1b^{WT\ CYT}$ vs. independent crosslinking of respective IpLITR type), a region of interest (ROI) was drawn to include phagocytic synapses for calculating integrated signal intensity in this specific region (dashed circle in Fig. 5.8C). For consistency, the size of the ROI is set to the same throughout the analysis for calculating signal intensity. As summarized in Fig. 5.8D, crosslinking of $1.1b^{WT\ CYT}$ only showed basal level of phosphotyrosine signal intensity (19103.82±2076.75) whereas a significantly higher value of

112488.42±6717.49 occurred when 2.6b$^{ITAM\ CYT}$ was crosslinked. Finally, when 2.6b$^{ITAM\ CYT}$ was co-crosslinked with 1.1b$^{WT\ CYT}$, a significant reduction in phosphotyrosine staining was observed (e.g. 57427.37±3350.71) when compared to the value for 2.6b$^{ITAM\ CYT}$ crosslinking (112488.42±6717.49). Overall, this confocal microscopy-based method allowed me to identify phagocytic cups and to specifically measure the phosphotyrosine signal intensity at this site as a proxy for activated signaling molecules recruited to the phagocytic synapses.

5.3 DISCUSSION

The main objective of this thesis chapter was to examine the effect of IpLITR-mediated crosstalk on the phagocytic response. Specifically, I showed that the heterologous co-expression of IpLITR constructs in AD 293 cells is a valuable tool for functionally characterizing receptor crosstalk, revealing a new regulatory role of 1.1b$^{WT\ CYT}$ as a potent inhibitor of the 2.6b$^{ITAM\ CYT}$-mediated phagocytic response. This inhibition on likely occurs via down-regulation of the phosphorylation status of intracellular signaling molecules recruited to the phagocytic cups. Taken together, these observations indicate that receptor crosstalk is an important regulatory mechanism utilized by teleost proteins to fine-tune phagocytosis, an essential and evolutionary conserved innate immune response.

Cross-inhibition of phagocytosis through receptor crosstalk was first demonstrated in the functional characterization of human FcγRIIs. For example, a chimeric FcγRIIA receptor containing the extracellular domain of FcγRI and the transmembrane and cytoplasmic region of FcγRIIA were co-expressed with FcγRIIB in COS cells to investigate signaling crosstalk due to technical difficulties associated with the fact that several different FcγR classes may be expressed in hematopoietic cells and also due to the lack of specific mAbs targeting individual FcγR isoforms (131). Therefore, co-expression of two FcγRII isoforms of interest in a

heterologous system can take out unknown confounding factors (e.g. activating other isoforms of FcγR classes) from the equation and allowing for the specific investigation of the effects of potential crosstalk interactions between two human FcγR-types during phagocytosis. These studies provided valuable information regarding the inhibitory functions of FcγRIIB and set the stage for understanding how FcγRIIB regulates various immune responses both *in vitro* and *in vivo* (135,136). My study used similar approaches whereby 2.6b$^{ITAM\ CYT}$ and 1.1b^{CYT} constructs were first differentially tagged with HA and FLAG epitopes and then stably co-expressed in AD 293 cells to examine potential crosstalk between these IpLITR types. This heterologous co-expression system allowed me to specifically activate IpLITR constructs using commercially available mAbs. To validate the specificity of this system, IpLITR co-expressing AD 293 cells were incubated with phagocytic targets with calibrated opsonizations using αHA or αFLAG-specific mAbs. My results showed that crosslinking of 2.6b$^{ITAM\ CYT}$ caused a robust phagocytic response whereas only binding activity was observed following 1.1b$^{WT\ CYT}$-triggering. This is consistent with phenotypes observed in AD 293 cells solely expressing 1.1b $^{ITAM\ CYT}$ and 1.1b$^{WT\ CYT}$ and rules out the possibility of cross-reactivity between αHA and αFLAG mAbs and also suggests that I was able to induce expected responses in co-expression AD 293 cells after triggering the distinct IpLITR-types.

After validating the specificity of this co-expression system, I further optimized the concentration of respective mAbs co-opsonized on targets to co-crosslink two IpLITR types with similar binding avidity. Binding avidity is influenced by both the affinity of receptors and their cognate ligands and also by the number of receptors engaged; higher-avidity interactions often result in stronger downstream signals and thus, influencing the nature and magnitude of ensuing effector responses (137). For example, disproportionate activation of stimulating receptors due to

higher binding avidity to their cognate ligands is likely overriding inhibitory signals and vice versa (138,139). Therefore, it is necessary to optimize concentration of mAbs co-opsonized on targets in the study of IpLITR-mediated crosstalk to rule out artifacts from disproportionate activation of one IpLITR-type vs. another. The concentration of respective mAbs co-opsonized on targets was optimized by incubating cells with targets on ice (i.e. 4°C). At this decreased temperature, signal transduction following receptor-ligand interaction is largely abrogated and thus % of binding is positively correlated with the binding avidity. At the concentration of 0.32 μg/ml of αHA and 2.5 μg/ml of αFLAG mAbs, crosslinking of $2.6b^{ITAM\ CYT}$ and $1.1b^{CYT}$ constructs generated similar binding profiles. Overall, these results suggest that I can specifically activate IpLITRs and also control the magnitude of activation through manipulating the concentration of mAbs opsonized on targets. Therefore, this heterologous co-expression system represents a valuable tool for examining potential IpLITR-mediated crosstalk in a well-controlled manner.

With the establishment of this co-expression cell system, potential IpLITR-mediated crosstalk was further examined using YG beads opsonized with αHA and αFLAG mAbs. After co-crosslinking, I shown that $1.1b^{WT\ CYT}$ cross-inhibited $2.6b^{ITAM\ CYT}$-mediated phagocytosis and this inhibitory effect is likely dependent on signaling events downstream of $1.1b^{WT\ CYT}$ activation. This observation does not agree with the reported functional roles of $1.1b^{WT\ CYT}$ in RBL-2H3 cells and is contrary to my original hypothesis that $1.1b^{WT\ CYT}$ might cooperate with classical phagocytic receptors (e.g. $2.6b^{ITAM\ CYT}$) and function as a tethering receptor to actively capture and secure targets on the plasma membrane to facilitate an efficient uptake of targets. This functional plasticity of $1.1b^{WT\ CYT}$ observed here likely lies in the difference of cell types (i.e. epithelioid cells and myeloid cells) used to study $1.1b^{WT\ CYT}$; expression level and profile of

signaling molecules vary between different cell types and thus, crosslinking of 1.1b$^{WT\ CYT}$ may trigger cell type-specific signaling pathways that eventually leads to different effector responses. Indeed, changes in the expression level of endogenous signaling molecules can result in opposite functional outcomes even though the same receptors are activated. For example, 2B4 (CD244) receptors are primarily expressed on lymphoid lineage cells and activation of this receptor is capable of inducing cytotoxicity in mature NK cells through recruitment of signaling lymphocyte activation molecular-associated protein (SAP) (140). However, no functional SAP is present in developing NK cells and crosslinking of 2B4 receptors recruit phosphatases (e.g. SHP-1/2 and SHIP) and Csk instead, thereby exhibiting inhibitory functions in this context, which is necessary for the self-tolerance of developing NK cells (141–143). Therefore, it is likely that 1.1b$^{WT\ CYT}$ is also capable of networking to different signaling pathways in a context-dependent manner and this functional plasticity of 1.1b$^{WT\ CYT}$ further proves that IpLITRs are a valuable alternative vertebrate model to study signaling versatility in the regulation of innate cell effector responses.

The initiation of phagocytosis is often associated with increased tyrosine phosphorylation of intracellular signaling proteins. Disruption of phosphotyrosine signaling events by phosphatases (e.g SHPs) specifically targets kinases (e.g Syk) and adaptor molecules (e.g Grb2) to inhibit phagocytosis (56,85,144). My results show that inhibition of 2.6b$^{ITAM\ CYT}$-mediated phagocytosis is also associated with a significant reduction in phosphotyrosine signals after co-crosslinking with 1.1b $^{WT\ CYT}$. Interestingly, this value is still significantly higher than the basal level of tyrosine phosphorylation observed when 1.1b$^{WT\ CYT}$ is independently crosslinked, indicating that low level of intracellular tyrosine phosphorylation is still occurring. It is possible that 2.6b$^{ITAM\ CYT}$-dependent activating signals are not completely counterbalanced by phosphatases recruited to 1.1b$^{WT\ CYT}$ and this may account for the residual phagocytic activity

observed after co-crosslinking 2.6b$^{ITAM\ CYT}$ with 1.1b$^{WT\ CYT}$ (Fig. 5.5). Furthermore, inhibitory molecules recruited to 1.1b$^{WT\ CYT}$ during receptor crosstalk can also be phosphorylated and this modification on regulatory tyrosine(s) has been reported to increase enzymatic activity of phosphatases, such as SHP1/2 and SHIP (145–151). Collectively, recruitments of inhibitory molecules during receptor crosstalk are the key step to down-regulate phosphorylation of tyrosine molecules and this further raises the question of how 1.1b $^{WT\ CYT}$ activation was initiated. Of note, independent engagement of 1.1b$^{WT\ CYT}$ constructs only showed basal level of phosphorylation status similar to cells associating with no target, indicating that crosslinking 1.1b$^{WT\ CYT}$ alone is not sufficient to phosphorylate tyrosine motifs in its CYT that lead to subsequent recruitments of phosphatases. Therefore, co-crosslinking of 1.1b$^{WT\ CYT}$ with 2.6b$^{ITAM\ CYT}$ is likely required for activation of 1.1b$^{WT\ CYT}$. Such a *tran*-phosphorylation mechanism that requires co-crosslinking of inhibitory and stimulating receptors to produce inhibition has been seen in the control of mast cell activation and represents a built-in regulatory mechanism to fine-tune the magnitude of activation and also to prevent over-stimulation of cells (152). Overall, the data presented here demonstrated that following co-crosslinking, tyrosine motifs in the CYT of 1.1b$^{WT\ CYT}$ were likely phosphorylated by proximal signaling events downstream of 2.6b$^{ITAM\ CYT}$ activation and in turn result in the production of inhibitory signals. Mechanistic details regarding 1.1b$^{WT\ CYT}$ activation is far from understood and the identity of signaling molecules participating in IpLITR-mediated crosstalk also remain to be examined since the αphosphotyrosine mAbs used in the assay will recognize a broad range of tyrosine-phosphorylated proteins, which will be further explored and discussed in the next chapter.

Phagocytosis is a multi-step process that can be conceptually separated into three distinct stages; i) binding of target particles by cognate receptors, ii) clustering of receptors leading to

consequent signaling, and iii) engulfment of particles through actin filament-dependent polymerization and de-polymerization events (112). For example, constant actin polymerization occurs at the leading edge of advancing pseudopods that direct the movement of plasma membrane to surround target particle's; whereas actin near the sites where particles were initially contacted start to dismantle, clearing path for particle internalization (110,112). This coordinated polymerization and de-polymerization of actin filaments is tightly regulated through spatiotemporal recruitment of various effector molecules to the interface of cell-target engagement, known as the phagocytic synapse or cup that brings engaged receptors and recruited signaling molecules into close proximity, creating a microenvironment where signal transduction occurs (153,154). This makes the phagocytic synapse an interesting structure for elucidating molecular aspects of phagocytosis. Although flow cytometry-based assays (e.g. phospho-flow) represent a high throughput platform to examine the activation of signaling molecules during phagocytosis, this technique is only able to resolve effector molecules that require posttranslational modifications (e.g. tyrosine phosphorylation) for activity by using specific antibodies that are able to discriminate the molecules after post-translational modifications. However, some signaling molecules (e.g. SHIPs and Csk) does not require posttranslational modifications for activation; instead, these molecules are constitutively active and simply translocate to the site where substrates are resident (e.g. from the cytosol to the plasma membrane) to exert their enzymatic activities (155,156). This phenomenon poses technical challenges for flow cytometry-based assays to differentiate activation status of these signaling molecules and thus other techniques that are able to specify the area of interest (e.g. phagocytic synapse) are required to specifically monitor various signaling molecules at different sites. Confocal microscopy provides high resolution of cell-target interactions and with an additional

staining step, I was able to also locate phagocytic synapses and further examine the recruitment of phosphotyrosine molecules during phagocytosis. Overall, similar trends were observed as in the phospho-flow assay described above. Furthermore, this confocal microscopy-based technique now allows me to examine the recruitment of specific candidate molecules of interest to the site during IpLITR-mediated receptor crosstalk, representing a valuable tool to elucidate molecular details responsible for 1.1b$^{WT\ CYT}$-mediated cross-inhibition of phagocytosis.

Overall, as reported in this chapter, I successfully established a heterologous co-expression system that allows me to study IpLITR-mediated receptor crosstalk. For the first time I have also shown that teleost LITRs are capable of fine-tuning phagocytosis through receptor crosstalk. The inhibition of 2.6b$^{ITAM\ CYT}$ -mediated phagocytosis is likely due to the reduced phosphorylation of effector molecules in the phagocytic signaling pathway after co-crosslinking with 1.1b $^{WT\ CYT}$ construct. This agrees with our previous functional studies of 1.1b $^{WT\ CYT}$ in NK cells that showed the selective recruitment of inhibitory molecules (i.e. Csk and SHPs) to different regions in the CYT of 1.1b $^{WT\ CYT}$ can independently abrogate NK cell killing responses (10,12). Of note, both effector responses require the formation of synaptic structures (i.e. phagocytic and immunological synapse) and share a very close series of signaling molecules to regulate actin and microtubule dynamics (157). These observations may account for inhibitory roles of 1.1b $^{WT\ CYT}$ in regulating two distinct effector responses and also provide a model system to draw comparisons between 1.1b$^{WT\ CYT}$-mediated inhibition of cytotoxicity and phagocytosis. The establishment of the AD 293 heterologous co-expression system now allows me to determine if 1.1b $^{WT\ CYT}$ utilizes the same mechanisms to cross-inhibit phagocytosis as was demonstrated for its inhibitory effects on NK cell-mediated cytotoxicity. I can also determine what inhibitory molecules are specifically recruited by 1.1b$^{WT\ CYT}$ during cross-inhibition of

phagocytosis and what effector molecules are targeted. These questions will be addressed by co-expressing 1.1b ^{CYT} constructs that have various combinations of mutated tyrosine motifs with 2.6b$^{ITAM\ CYT}$ and the mechanistic details responsible for 1.1b$^{WT\ CYT}$-mediated inhibition of phagocytosis will be the focus of Chapter VI.

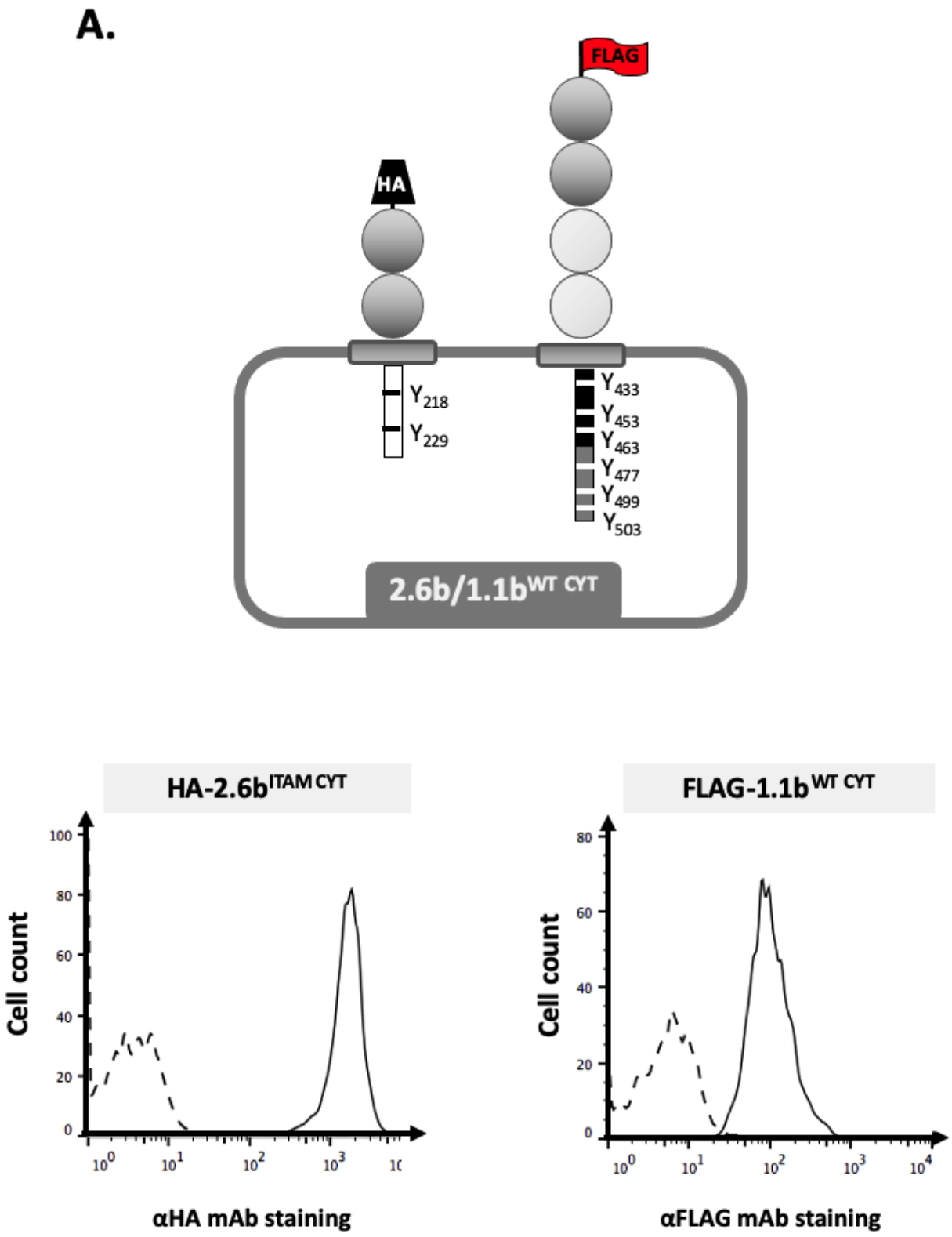
A.
FLAG
HA
Y218
Y229
Y433
Y453
Y463
Y477
Y499
Y503
2.6b/1.1bWT CYT
HA-2.6bITAM CYT
Cell count
αHA mAb staining
FLAG-1.1bWT CYT
Cell count
αFLAG mAb staining

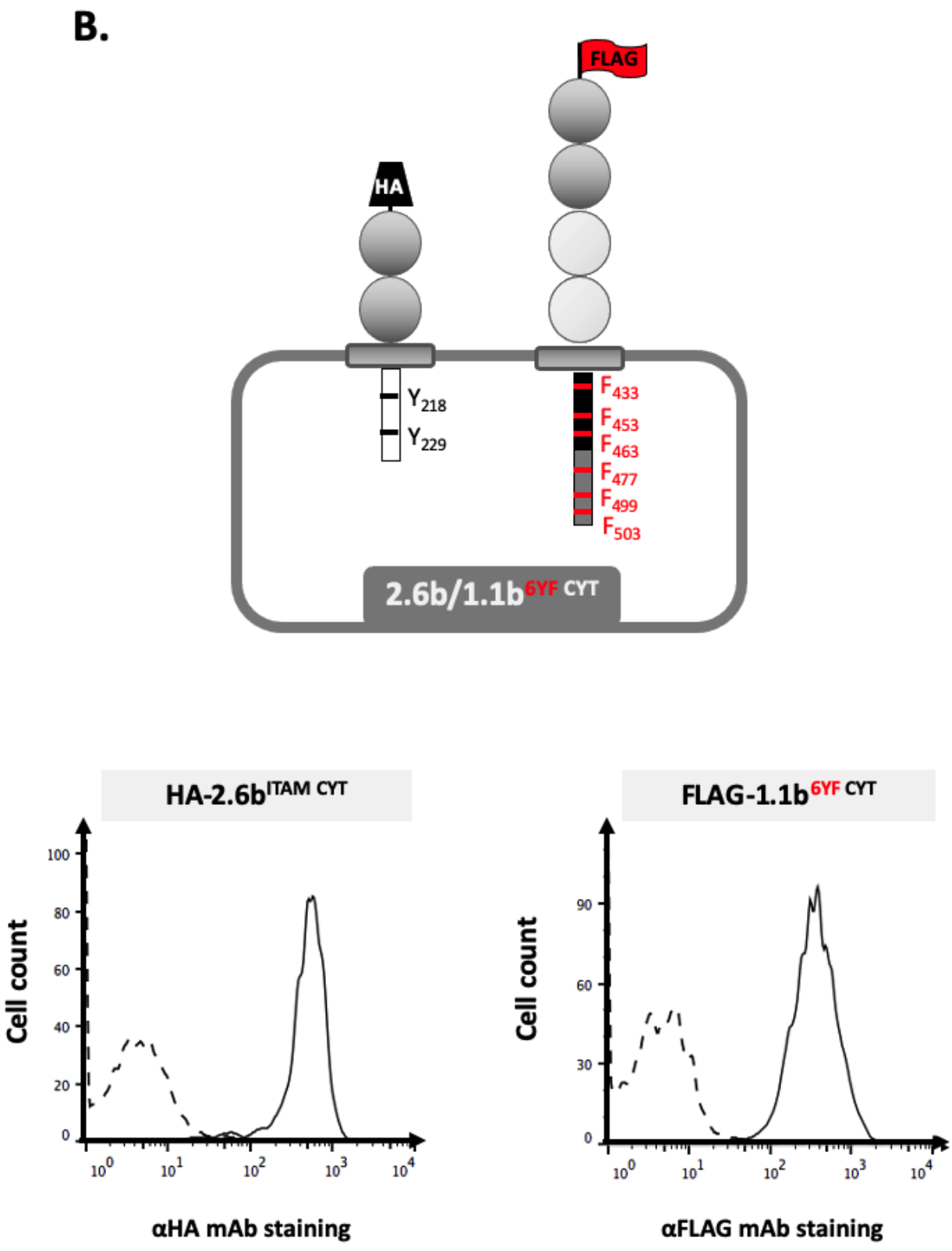
B.
FLAG
HA
Y218
Y229
F433
F453
F463
F477
F499
F503
2.6b/1.1b6YF CYT
HA-2.6bITAM CYT
Cell count
αHA mAb staining
FLAG-1.1b6YF CYT
Cell count
αFLAG mAb staining

Figure 5.1. Generation and stable co-expression of N-terminal HA and FLAG epitope-tagged IpLITR constructs in AD293 cells. Detection of the cell surface co-expression of 2.6b$^{ITAM\ CYT}$ with 1.1b$^{WT\ CYT}$ (referred to here as 2.6b/1.1b $^{WT\ CYT}$, (A)) or 1.1b$^{6YF\ CYT}$ (referred to here as 2.6b/1.1b $^{6YF\ CYT}$ (B)) in transfected, selected and sorted AD 293 cells. Co-expression stable cells were stained by incubation with an αHA mAb (2.6b$^{ITAM\ CYT}$ staining, solid line, left panel), αFLAG mAb (1.1b^{CYT} constructs staining, solid line, right panel) or mouse IgG1 (isotype control, dash line) followed by staining with goat αmouse IgG pAb coupled to PE. Surface expression was then determined as an increase in fluorescence intensity in comparison with IgG1-stained cells. Shown are representative stains for each stable cell line.

A.

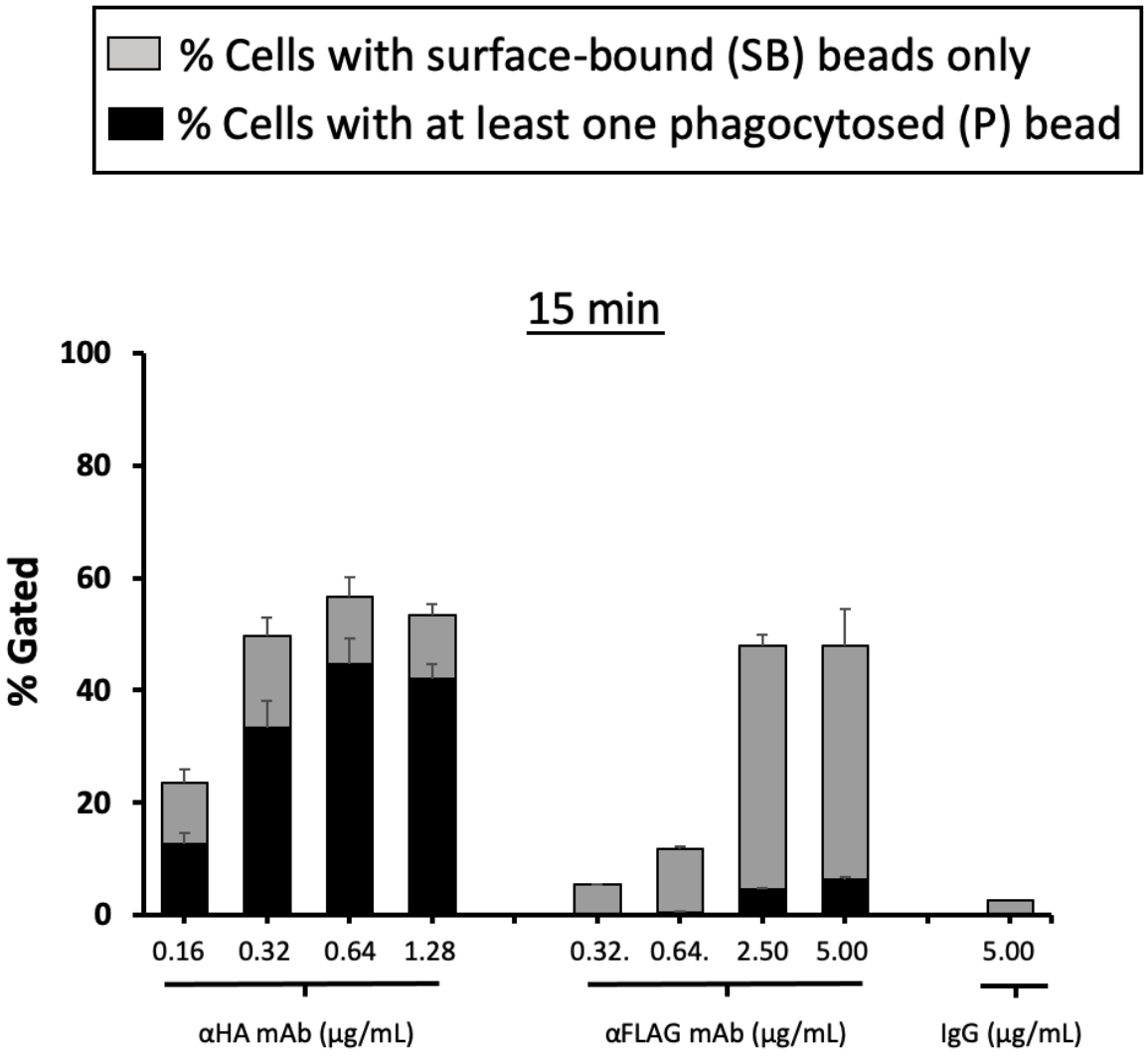
% Cells with surface-bound (SB) beads only
% Cells with at least one phagocytosed (P) bead
15 min
% Gated
100
80
60
40
20
0
0.16
0.32
0.64
1.28
0.32.
0.64.
2.50
5.00
5.00
αHA mAb (µg/mL)
αFLAG mAb (µg/mL)
IgG (µg/mL)

B.

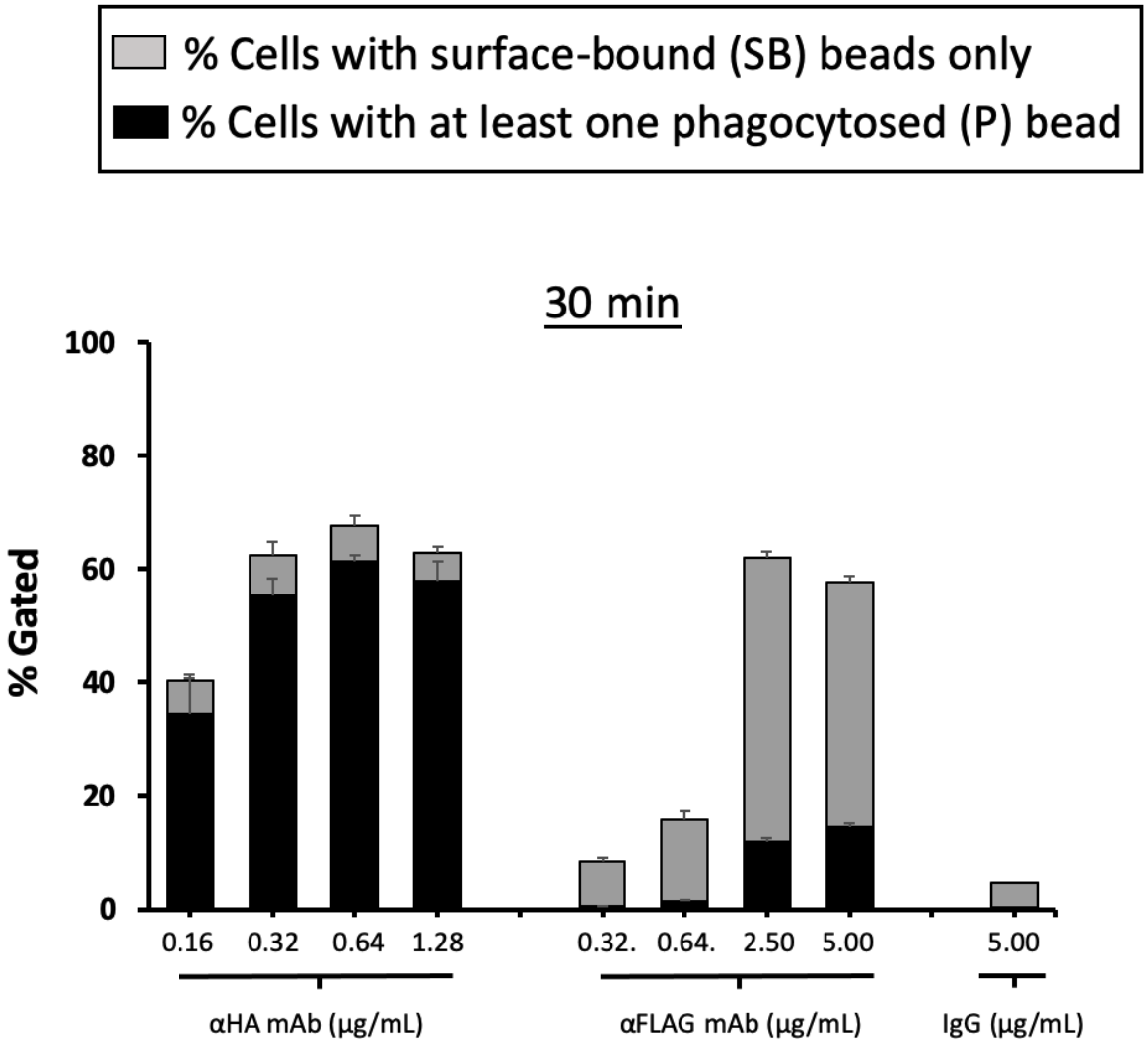

Figure 5.2. Specific activation of 1.1b$^{WT\ CYT}$ and 2.6b$^{ITAM\ CYT}$ in co-expressing AD 293 cells. 2.6b/1.1b $^{WT\ CYT}$–expressing AD 293 cells (2×10^5) were incubated with 4.5 µm YG beads (6×10^5) opsonized with different dilution of αHA, αFLAG mAbs and mouse IgG (isotype control) for 15 (A) and 30min (B) at 37 ℃ prior to analysis of samples using the ImageStream^x Mark II instrument. Two phenotypes (i.e. % of surface-bound and % of phagocytosis) were discriminated using previously described connected component masking (#). The percentage of gated cells only contains surface-bound beads are shown in grey bar and percentage of gated cells contains at least one phagocytosed beads are shown in black bar. Each bar represents the mean ± SEM of three independent experiments.

A.

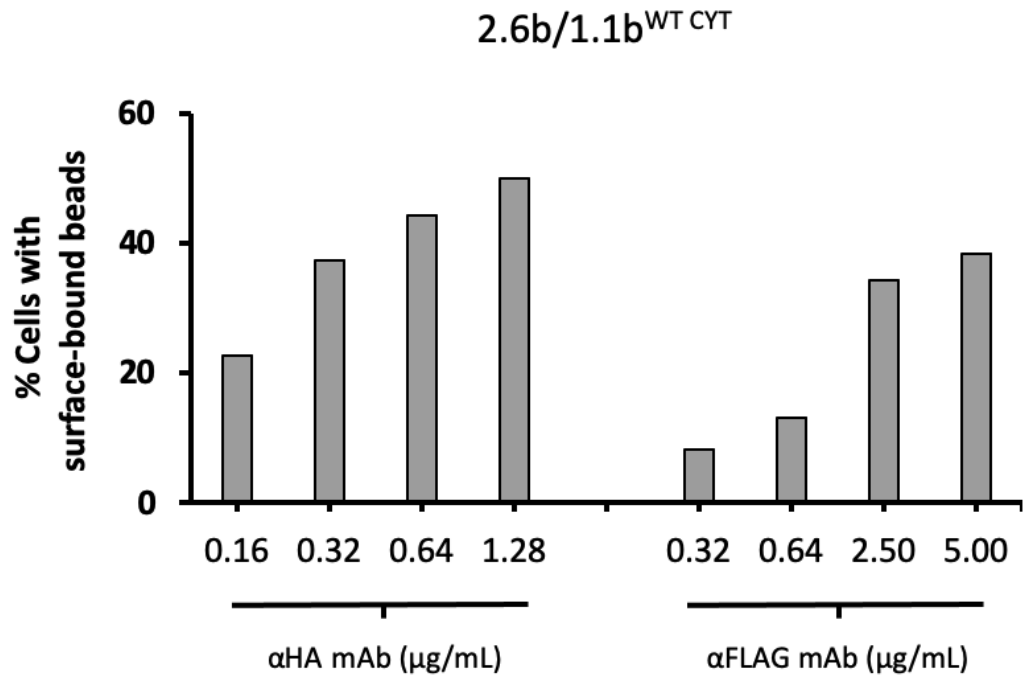
2.6b/1.1b WT CYT
% Cells with surface-bound beads
60
40
20
0
0.16 0.32 0.64 1.28
0.32 0.64 2.50 5.00
αHA mAb (μg/mL)
αFLAG mAb (μg/mL)

B.

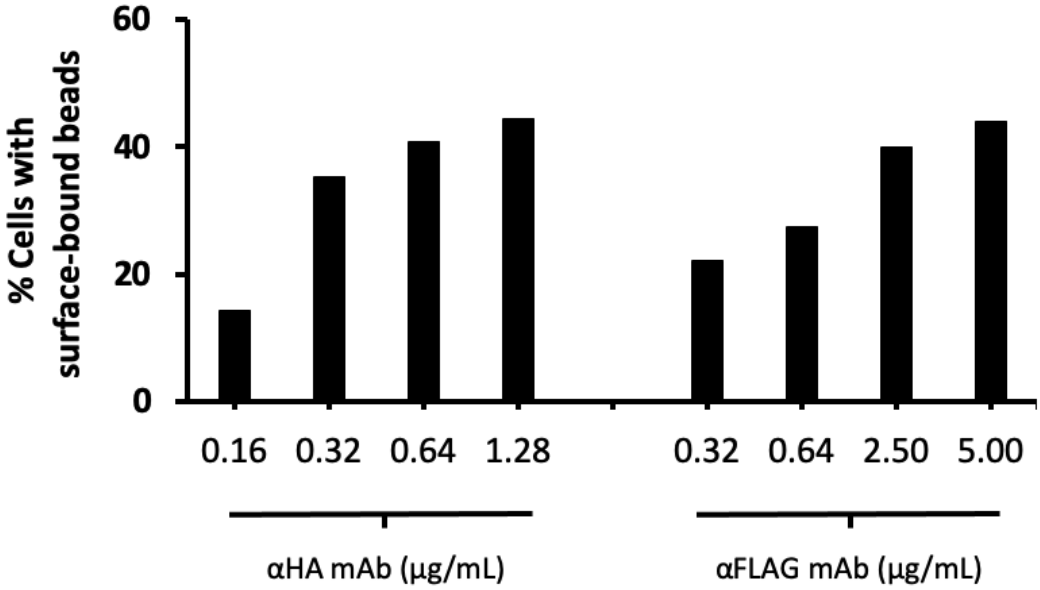
2.6b/1.1b 6YF CYT
% Cells with surface-bound beads
60
40
20
0
0.16 0.32 0.64 1.28
0.32 0.64 2.50 5.00
αHA mAb (μg/mL)
αFLAG mAb (μg/mL)

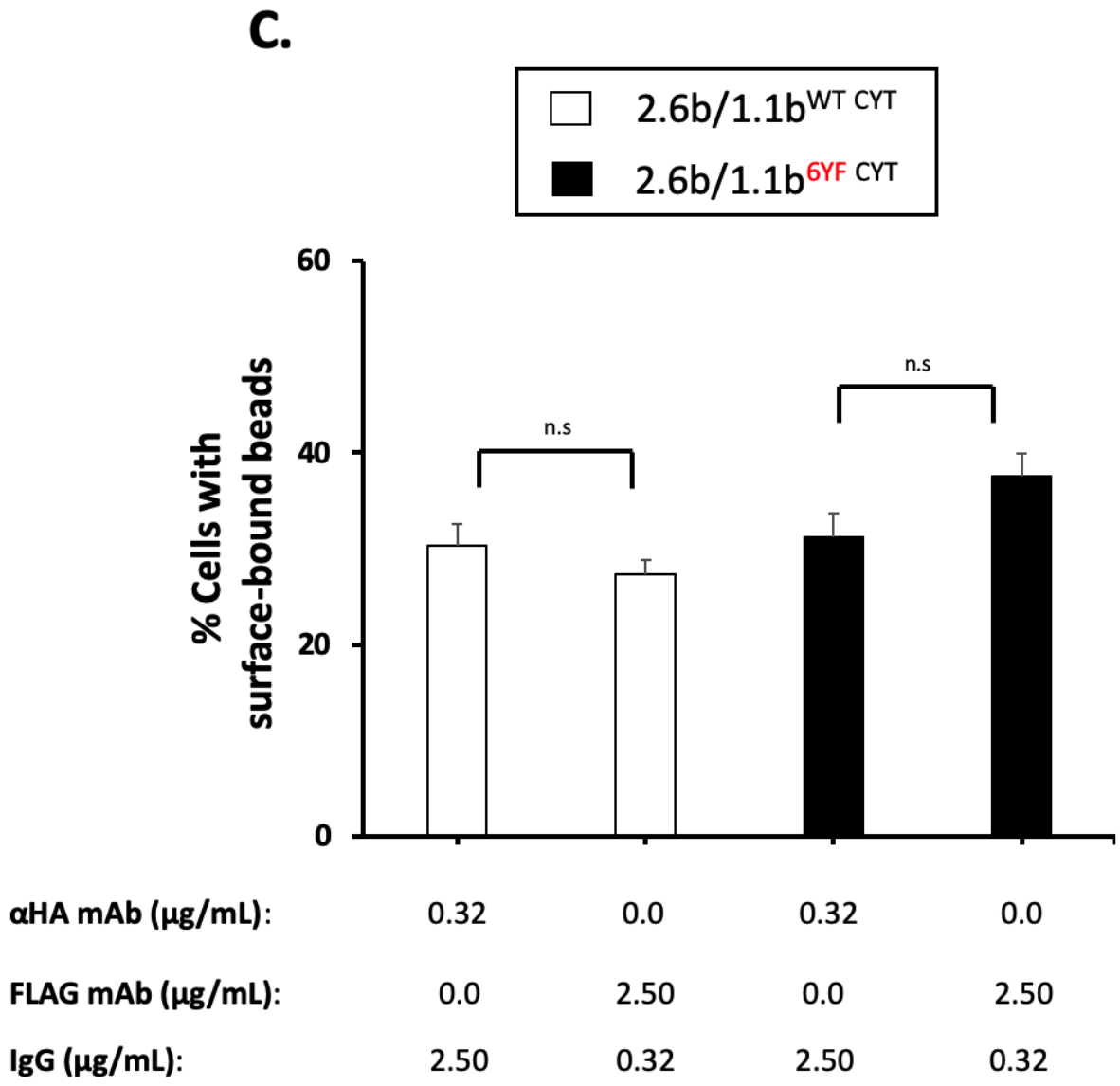

Figure 5.3. Optimal concentration of αHA and αFLAG mAbs opsonized on phagocytic targets to crosslink 2.6b$^{ITAM\ CYT}$ and 1.1b^{CYT} constructs with similar binding avidity. (A) Co-expression stable cells (2×10^5), 2.6b/1.1b$^{WT\ CYT}$ (A) and 2.6b/1.1b$^{6YF\ CYT}$ (B) were pre-chilled on ice for 15 min before adding 4.5 μm YG beads (6×10^5) opsonized with indicated dilution of αHA and αFLAG mAbs. Binding was allowed to proceed on ice for 60 min prior to analysis of samples using the ImageStreamx Mark II instrument. Results shown here are from two independent experiments. (C) 4.5μm YG beads were opsonized with selected concentration of αHA (0.32μg/ml) or αFLAG (2.5μg/ml) mAbs. Mouse isotype IgG1 was also included to ensure the equal concentration of mAbs during beads opsonization. Same binding assay was performed, and each bar represents the mean ± SEM of three independent experiments.

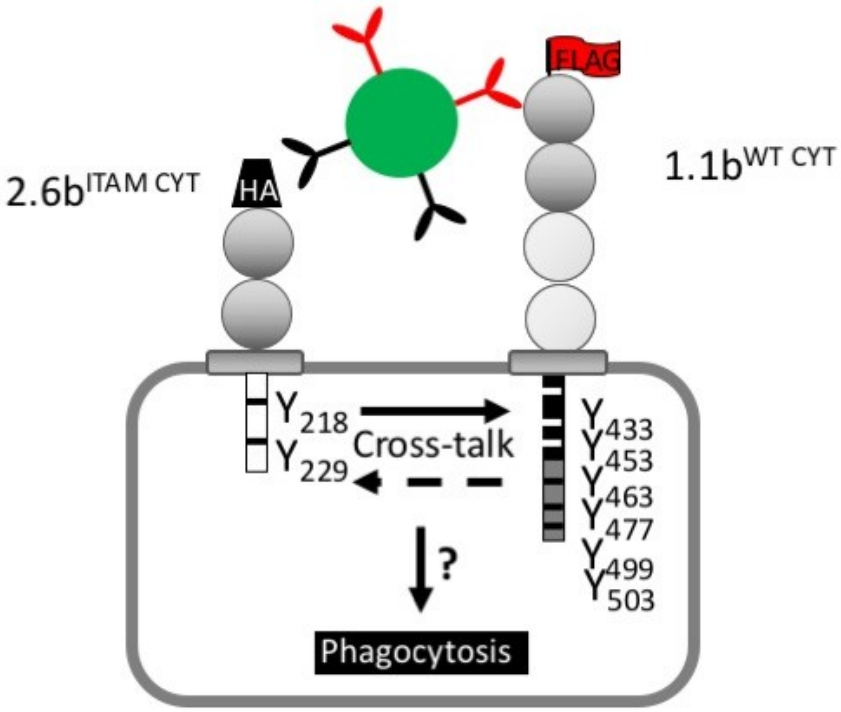

Figure 5.4. Schematics of examining potential IpLITRs-mediated crosstalk. 2.6b$^{ITAM\ CYT}$ and 1.1b$^{WT\ CYT}$ constructs differentially tagged with HA and FLAG epitopes were stably co-expressed on AD 293 cells. 4.5µm YG beads co-opsonized with αHA (0.32µg/ml) and αFLAG (2.5µg/ml) were used as phagocytic targets to co-crosslink two IpLITR types and potential receptor crosstalk on 2.6b$^{ITAM\ CYT}$-mediated phagocytosis can then be examined using phagocytosis assay described in Figure 4.3.

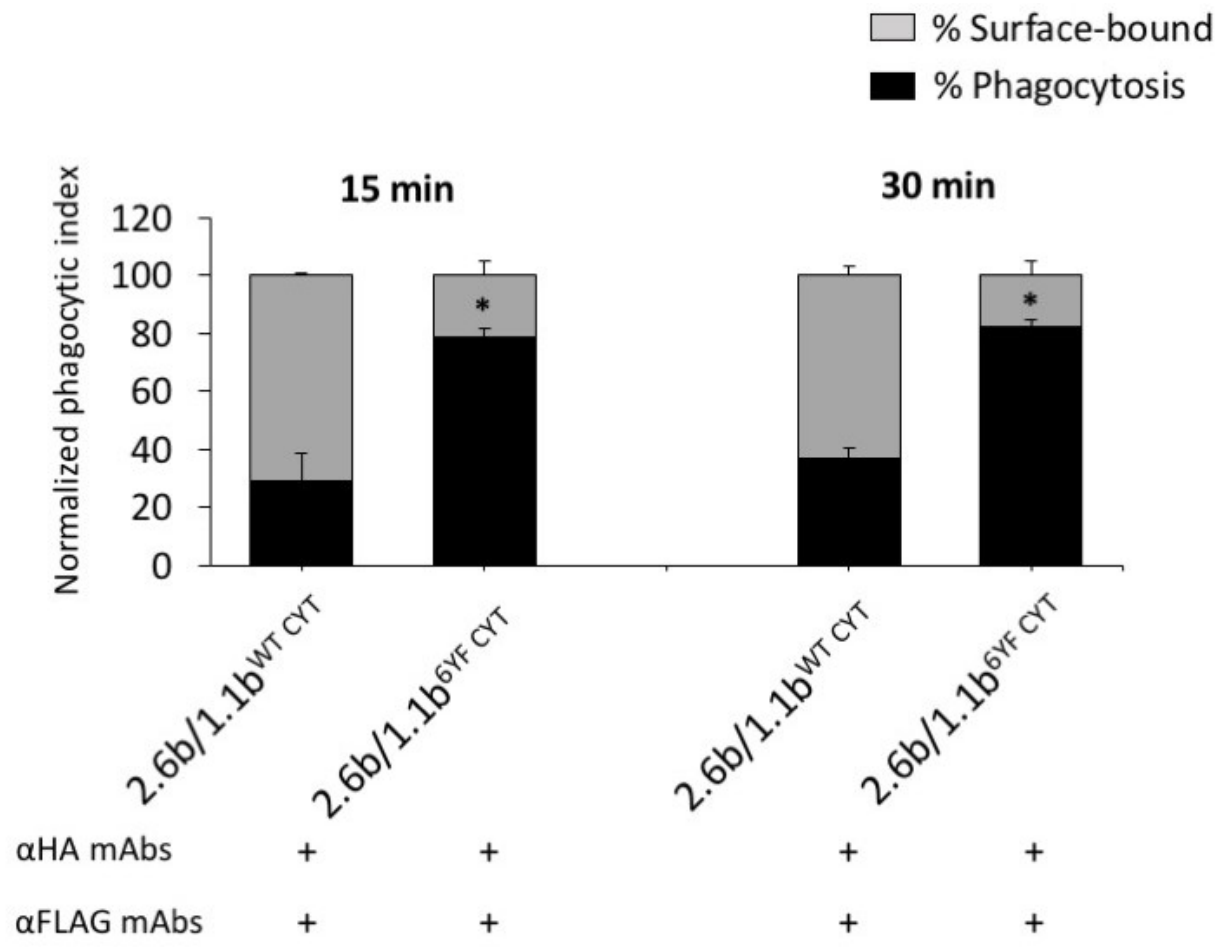

Figure 5.5. Inhibition of 2.6b$^{ITAM\ CYT}$-mediated phagocytosis following co-crosslinking with 1.1b$^{WT\ CYT}$. Co-expression stable cells (2×10^5), 2.6b/1.1b$^{WT\ CYT}$ and 2.6b/1.1b$^{6YF\ CYT}$ were incubated with co-opsonized (αHA and αFLAG mAbs) 4.5 μm YG beads for 15 and 30 min at 37 ℃ prior to analysis of samples using the ImageStreamx Mark II instrument. Percentage of cells exhibit two phenotypes is normalized and calculated as: % phagocytosis or surface-bound cells / % total bead-associated cells. Grey bars represent the percentage of cells with only surface-bound targets (i.e. no internalization) and black bars represent the percentage of cells with ≥1 fully internalized bead. Each bar represents the mean ± SEM of three independent experiments. $^{*}P \leq 0.05$ when comparing the % phagocytosis of co-crosslinking 2.6b$^{ITAM\ CYT}$ with 1.1b $^{WT\ CYT}$ vs. 1.1b $^{6YF\ CYT}$ at each time point.

A.

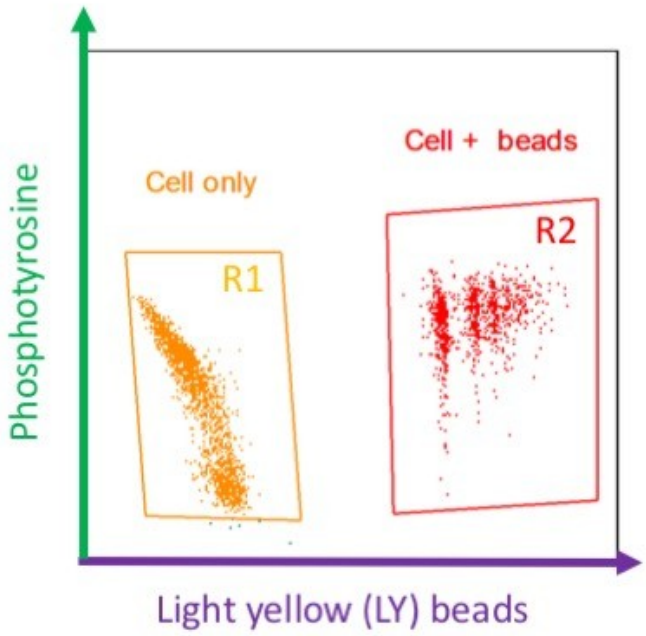

B.

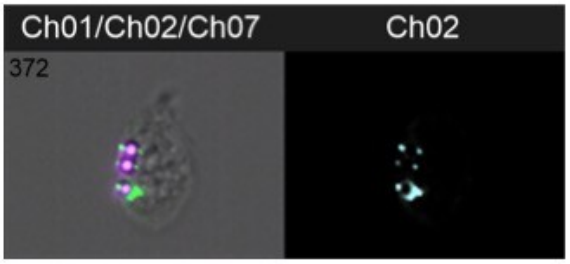

Mask	Description
Intensity (M02, 72-4025)	Intensity mask used to identify phospho-tyrosine signals above background in channel 2

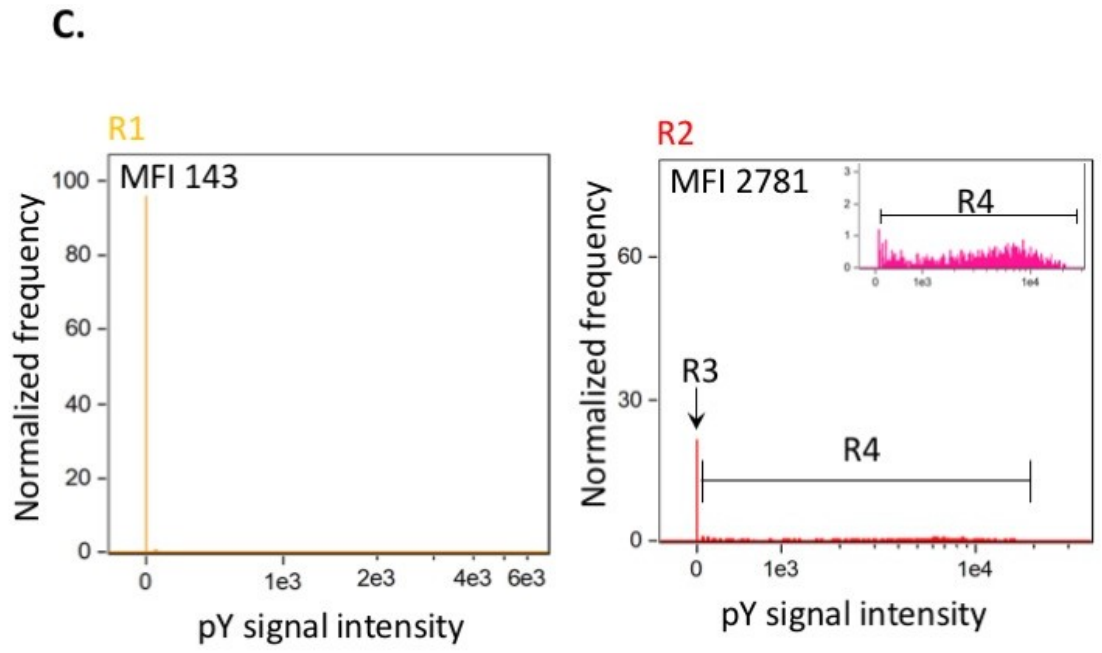

Figure 5.6. Examination of phosphotyrosine signaling events using imaging flow cytometry. (A) Gating strategy to discriminate cells associating with beads from cells alone. 2.6b/1.1b$^{WT\ CYT}$ cell lines were incubated with αHA Abs-opsonized light yellow (LY) beads to crosslink 2.6b$^{ITAM\ CYT}$ and allow phagocytosis to proceed for 15 min at 37 ℃ before cells were permeabilized and intracellularly stained with AF488-conjugated αphosphotyrosine antibodies. Two cell populations (cells alone (R1) or with targets (R2)) were gated based on the fluorescence intensity of LY beads. (B) Intensity mask in the IDEAS® software was used to identify positive phospho-tyrosine signals within individual events. Phospho-tyrosine signals and LY beads were detected in channel 2 and 7 respectively. An intensity mask was created and then applied to identify phospho-tyrosine signals with intensity value from 72 to 4025 MFI (cyan-coloured spots) and signals below 72 MFI (background staining) will be excluded from further analysis. (C) Phospho-tyrosine profile of R1 and R2. Fluorescent intensity of cells in R1 and R2 gate was then calculated after application of the intensity mask; cells associating with no LY target (left panel) only exhibit basal level of phosphotyrosine signal (MFI 143). In comparison, an increase in phosphotyrosine signal intensity (MFI 2781) was observed when cells associate with LY beads (R2) and two cell populations (R3 and R4) were revealed based on fluorescent intensity. Specifically, Cells in R3 had no phosphotyrosine signal (<72) while cells in R4 had phospho-tyrosine signals of various intensity. The inset shown cells in R4 alone.

A.

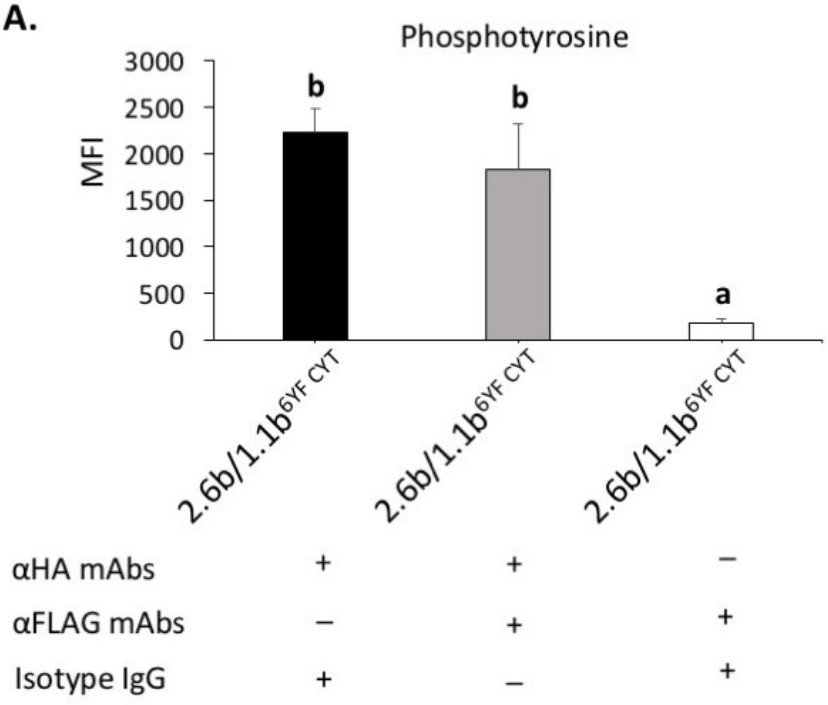
Phosphotyrosine
MFI
3000
2500
2000
1500
1000
500
0
b
b
a
2.6b/1.1b6YF CYT
2.6b/1.1b6YF CYT
2.6b/1.1b6YF CYT
αHA mAbs + + –
αFLAG mAbs – + +
Isotype IgG + – +

B.

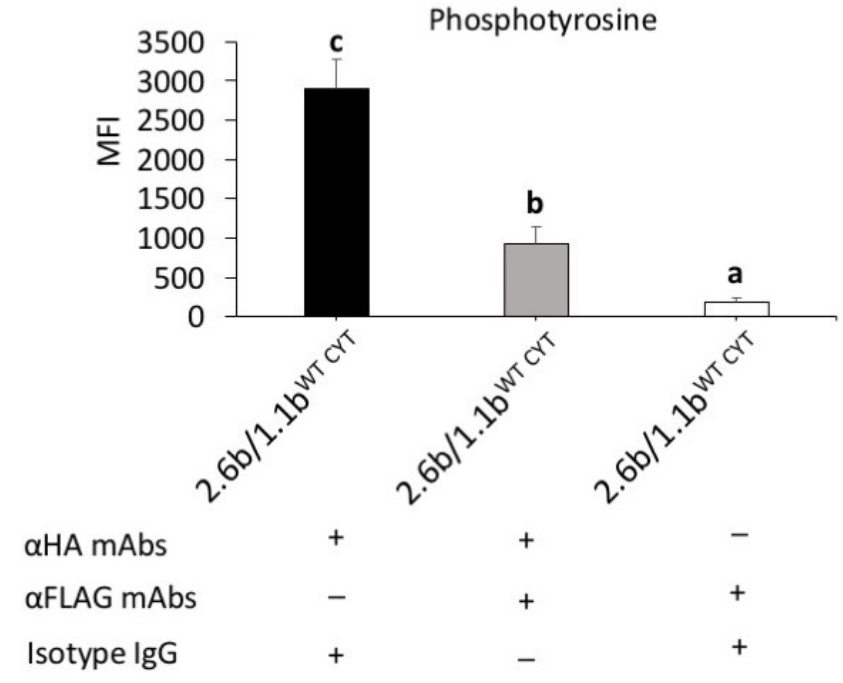
Phosphotyrosine
MFI
3500
3000
2500
2000
1500
1000
500
0
c
b
a
2.6b/1.1bWT CYT
2.6b/1.1bWT CYT
2.6b/1.1bWT CYT
αHA mAbs + + –
αFLAG mAbs – + +
Isotype IgG + – +

Figure 5.7. Down-regulation of 2.6b$^{ITAM\ CYT}$-mediated phosphotyrosine signaling following co-crosslinking with 1.1b$^{WT\ CYT}$. Co-expression stable cell lines (2×10^5), 2.6b/1.1b$^{6YF\ CYT}$ (A) and 2.6b/1.1b$^{WT\ CYT}$ (B) were incubated with LY beads (6×10^5) at 37 ℃. LY beads were opsonized with αHA and αFLAG to co-crosslink 2.6b$^{ITAM\ CYT}$ and 1.1b^{CYT} constructs. To independently crosslink 2.6b$^{ITAM\ CYT}$ and 1.1b^{CYT} constructs, LY beads were opsonized with αHA or αFLGA mAbs along with mouse isotype IgG. The isotype IgG was always included during beads opsonization when independently activate IpLITR constructs to ensure the overall concentration of IgG was the same. After 15 min incubation, cells were permeabilized and intracellularly stained with AF488-conjugated αphosphotyrosine mAbs prior to analysis of samples using the ImageStreamx Mark II instrument. Fluorescent intensity of cells associated with LY beads was then calculated and represented as mean fluorescent intensity (MFI). Each bar represents the mean ± SEM of four independent experiments. Letters indicate statistical significance ($P \leq 0.05$) between the means.

A.

2.6b/1.1b$^{WT\ CYT}$+αHA mAbs-opsonized beads

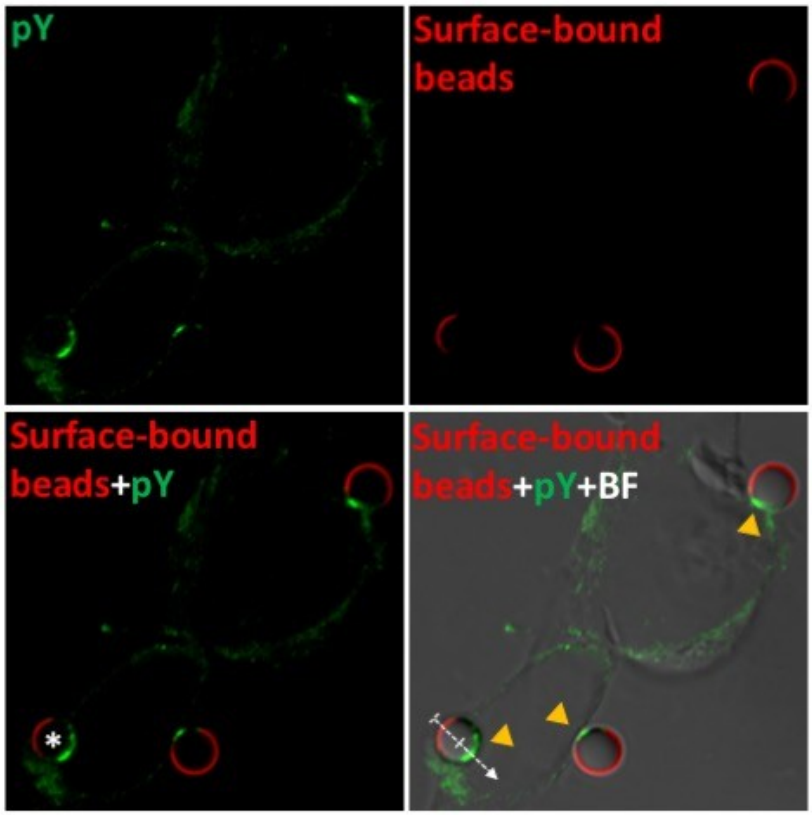

B.

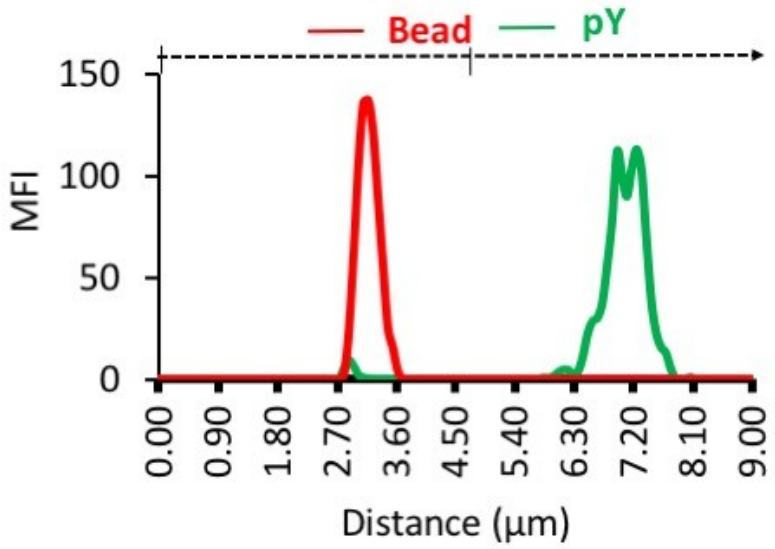

C.

2.6b/1.1b$^{WT\ CYT}$

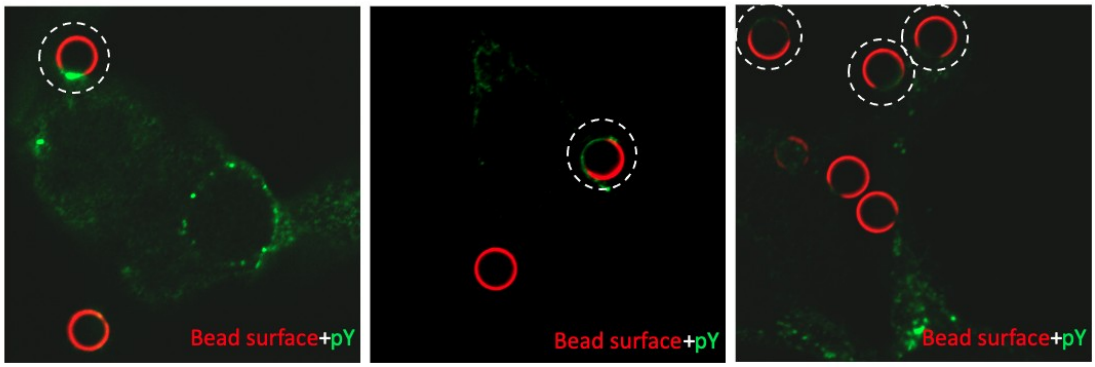

αHA mAb:	+	+	-
αFLAG mAb:	-	+	+
Isotype IgG:	+	-	+

D.

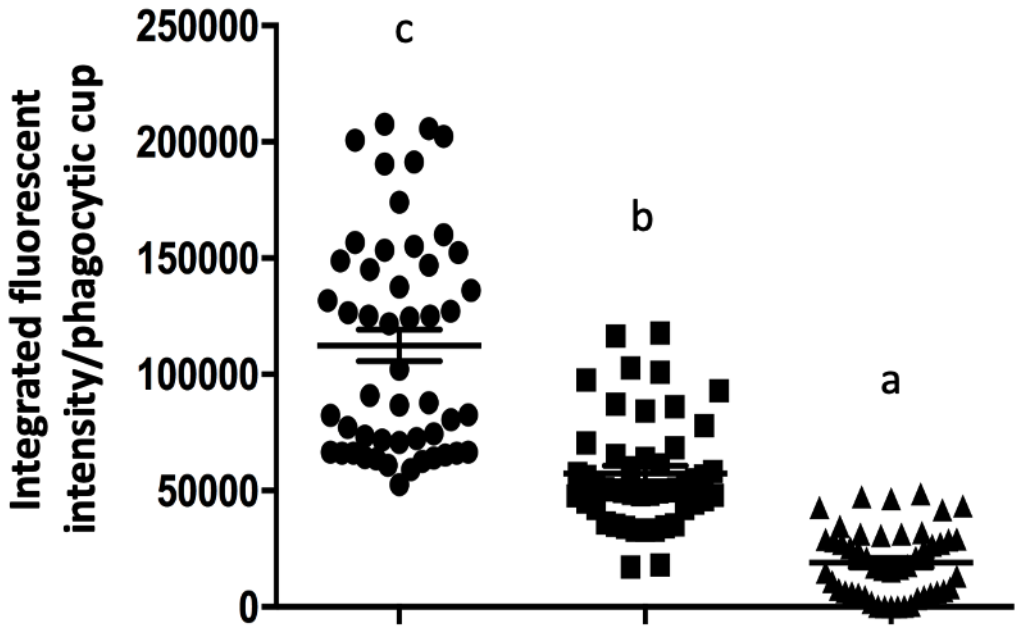

αHA mAb:	+	+	-
αFLAG mAb:	-	+	+
Isotype IgG:	+	-	+

Figure 5.8. Confocal microscopy analysis of signaling molecules recruited to phagocytic cups. (A) 2.6b/1.1b$^{WT\ CYT}$-expressing AD 293 cells (2×10^5), were grown on coverslips and incubated with 4.5 μm non-fluorescent (NF) beads opsonized with αHA mAb and mouse isotype IgG at 37 ℃. After 8 min incubation, cells were fixed with 4% PFA for 10 min and partially internalized beads were then stained using Cy5-conjugated goat-anti-mouse secondary mAbs. After beads staining, cells were permeabilized and stained for intracellular phosphotyrosine molecules via first incubating with a rabbit anti-pY mAb and then a secondary goat-anti-rabbit mAbs conjugated to FITC. Z-stack images were then obtained at a magnification of 63× using a Zeiss LSM 710 scanning confocal microscope. Representative images from z-stack acquisitions are shown as images showing phosphotyrosine molecules (green) staining alone, surface-bound beads (red) staining alone, merged-fluorescence images or brightfield-fluorescence merged images using the Zen 2009 imaging software. Yellow arrowheads indicate phagocytic cups and the target bead of interest is indicated by an asterisk (*). Qualitative analysis of bead and phosphotyrosine molecules staining intensities was performed using Fiji software (B) by calculating the MFI (y-axis) of the bead (red line) and phosphotyrosine molecules staining (green line) across the dash arrowed line. (C) To further quantify phosphotyrosine molecules recruited to phagocytic cups under different activation conditions, 2.6b/1.1b$^{WT\ CYT}$-expressing cells were incubated with NF beads opsonized with indicated mAbs. Same experiments as described above were performed. For analyses, a region of interest (ROI, indicated by dashed circles) was first drawn that includes phagocytic cups so phosphotyrosine signal intensities in this area can then be calculated and as summarized in (D), at least 50 phagocytic cups from three independent experiments were pooled and represented as mean integrated fluorescent intensity ± SEM. Letters indicate statistical significance ($P \leq 0.05$) between the means.

CHAPTER VI

CROSS-INHIBITION OF ITAM-DRIVEN PHAGOCYTOSIS THROUGH COORDINATE RECRUITMENTS OF CSK AND SHP-2 TO 1.1B$^{WT\ CYT}$ DURING RECEPTOR CROSSTALK

6.1 Introduction

In the previous chapter, I established a heterologous expression system in which differentially-tagged 1.1b$^{WT\ CYT}$ and 2.6b$^{ITAM\ CYT}$ constructs are co-expressed in AD 293 cells. This allows for the co-crosslinking of two IpLITR-types and examination of the subsequent effects of potential receptor cross-during the control of the phagocytic response. A significant reduction in phagocytosis was observed after co-crosslinking 2.6b$^{ITAM\ CYT}$ with 1.1b$^{WT\ CYT}$ but not with the signaling-incompetent mutant 1.1b$^{6YF\ CYT}$ construct. This observation suggests that 1.1b$^{WT\ CYT}$ plays an inhibitory role in the control of phagocytosis and inhibitory signals downstream of 1.1b$^{WT\ CYT}$ disrupt critical signaling components that are required for ITAM-driven phagocytosis.

Internalization of IgG-opsonized particles by FcγRs is by far the best-understood model of ITAM-mediated phagocytosis. This process requires spatiotemporal activation of various effector molecules that regulate: i) tyrosine phosphorylation; ii) phospholipid metabolism, and; iii) dynamic cytoskeletal rearrangement by virtue of actin nucleation factors (110,112,153). Although multiple signaling pathways are activated during phagocytosis, the initiation of this dynamic process is mediated by conserved proximal signaling events that are also responsible for activating other immune responses, such as cytotoxicity, and degranulation (158,159). In the context of phagocytosis, engagement of activating receptors (e.g. FcγRIIA) with their IgG-coated targets triggers phosphorylation of tyrosines within ITAMs by Src family kinases, which provide docking sites for the binding of Syk molecules (110,144). Syk is recruited to the site of the

activated receptor where it serves as a critical signaling effector molecule that can activate downstream effector molecules. Selected examples include phospholipase C, PI3K, Akt, Rho-family small GTPases, and the extracellular signal-regulated (Erk) mitogen-activated protein kinase (MAPK) (93,160–163). These effector molecules further amplify signaling cascades to regulate cytoskeletal reorganization, transcription of immune-related genes and the synthesis and secretion of inflammatory mediators such as cytokines. For many years, studies on FcγR-mediated phagocytosis have been dedicated to investigating molecular events leading to the activation of this process. Only recently has evidence revealed that phagocytosis is also subjected to tight regulations by the action of certain inhibitory receptors and enzymes that work alongside activating signals to temper the response (164). Since then, various inhibitory molecules that target substrates at different levels of signaling pathways have been identified and these provide new insights into molecular details during the control of phagocytosis. For example, the non-receptor tyrosine kinase, C-terminal src kinase (Csk), is ubiquitously expressed and specifically targets proximal signaling events by phosphorylating a conserved inhibitory tyrosine residue on Src family kinases, thus rendering them in an auto-inhibitory conformation (165,166). Overexpression of Csk molecules reduces phagocytic efficiency in macrophages (167). Alternatively, tyrosine phosphatases, like SHP-1, are restrictively expressed in hematopoietic cell lineages overexpression of this inhibitory molecule in a fibroblast cell line suppresses the activation of Rho-family small GTPases (i.e. Rac) and inhibits FcγRIIA-mediated phagocytosis (168). Other inhibitory molecules, such as SHIPs exert their inhibitory effects on phagocytosis by converting PIP3, which is generated by PI3K, back to PIP2 and thus prevents translocation of pleckstrin homology (PH) domain-containing molecules (e.g. Akt and PLCγ) to the plasma membrane during phagocytosis (169,170).

Previous pharmacological studies in our lab have shown that inhibition of Src family tyrosine kinases, Syk, PI3K and Akt molecules largely reduced phagocytosis in 2.6b$^{ITAM\ CYT}$-expressing cells (4). This observation indicates that crosslinking of 2.6b$^{ITAM\ CYT}$ constructs engage classical ITAM-dependent signaling pathways to mediate phagocytosis. Consequently, impairment of 2.6b$^{ITAM\ CYT}$-mediated phagocytosis following co-crosslinking with 1.1b$^{WT\ CYT}$ may also be regulated by a similar repertoire of aforementioned inhibitory molecules. Indeed, binding of Csk and SHP-1/2 to membrane proximal and distal CYT regions of 1.1b$^{WT\ CYT}$ has been observed in previous *in vitro* biochemical assays (14). Functional studies further showed that these two CYT regions of 1.1b$^{WT\ CYT}$ independently exert inhibitory effects on cytotoxicity when 1.1b$^{WT\ CYT}$ was expressed inn NK cells (10,12). Since similar synaptic structures are formed and a shared pool of effector molecules are involved in regulating phagocytosis and cytotoxicity, a possible evolutionary link between these two processes has been suggested (157), and this may account for the regulatory role of 1.1b$^{WT\ CYT}$ in controlling these innate effector responses. Understanding the molecular details underlining 1.1b$^{WT\ CYT}$-mediated cross-inhibition of phagocytosis will expand our knowledge on the functional capabilities of 1.1b$^{WT\ CYT}$ in regulating effector responses through networking with various signaling pathways.

The main research objective of this thesis chapter was to further investigate mechanistic details regarding the inhibitory effects of 1.1b$^{WT\ CYT}$ on 2.6b$^{ITAM\ CYT}$-driven phagocytosis. Specifically, I tested the hypothesis whether membrane proximal and distal CYT regions of 1.1b$^{WT\ CYT}$ independently cross-inhibit phagocytosis. Secondly, I further explored the recruitment of endogenous inhibitory molecules to 1.1b$^{WT\ CYT}$ constructs that may be involved in the cross-inhibition of phagocytosis. Finally, I examined the phosphorylation state of representative signaling components that are often activated during phagocytosis following receptor crosstalk.

My results show that two distinct CYT regions of 1.1b$^{WT\ CYT}$ are both required for coordinated recruitments of endogenous Csk and SHP-2 molecules to disrupt Erk1/2 signaling pathways and thus sustain inhibitory effects on ITAM-driven phagocytosis. This represents a novel regulatory mechanism for the cross-inhibition of phagocytosis and provides additional information regarding the immunoregulatory role of 1.1b$^{WT\ CYT}$ in controlling innate cellular responses.

6.2 Results

6.2.1 Generation of stable AD 293 cells co-expressing 2.6b $^{ITAM\ CYT}$ with various 1.1b ^{CYT} tyrosine mutant constructs

To further investigate the tyrosine motifs in the CYT of 1.1b $^{WT\ CYT}$ that are critical for cross-inhibition of 2.6b$^{ITAM\ CYT}$-mediated phagocytosis, three new FLAG-tagged constructs were generated: i) 1.1b$^{Prox\ CYT}$ (tyrosines 433/453/463, including the Csk-binding motif Y453, in the proximal region of the CYT of 1.1b $^{WT\ CYT}$ were mutated to phenylalanine), ii) 1.1b$^{Distal\ CYT}$ (two ITIMs (tyrosine 477 and 499) and one ITSM (tyrosine 503) in the distal region of the CYT of 1.1b $^{WT\ CYT}$ were mutated to phenylalanine) and iii) 1.1b $^{3F\ CYT}$ (tyrosine 433/463/503 mutated to phenylalanine). These constructs were co-transfected with HA-tagged 2.6b $^{ITAM\ CYT}$ to generate co-expressing AD 293 cell lines (referred to here as 2.6b/1.1b$^{Prox\ CYT}$, 2.6b/1.1b $^{Distal\ CYT}$ and 2.6b/1.1b $^{3F\ CYT}$ respectively). The surface expression levels of the IpLITR constructs were confirmed by αHA mAb and αFLAG mAb staining (Fig. 6.1)

6.2.2 Tyrosine 453 and ITIMs in the CYT of 1.1b$^{WT\ CYT}$ are minimally required for sustaining the inhibitory effects on 2.6b$^{ITAM\ CYT}$-mediated phagocytosis

To identify 1.1b$^{WT\ CYT}$ CYT region tyrosine residues that are required for cross-inhibiting 2.6b$^{ITAM\ CYT}$ -mediated phagocytosis, I generated new constructs with combinations of CYT tyrosine mutations and then co-expressed these with 2.6b$^{ITAM\ CYT}$ in AD 293 cells. After co-

crosslinking 2.6b$^{ITAM\ CYT}$ with various 1.1b^{CYT} tyrosine mutant constructs (i.e. 1.1b$^{Prox\ CYT}$, 1.1b $^{Distal\ CYT}$ and 1.1b $^{3F\ CYT}$) for 15 min and 30 min, the dataset was first normalized as described in chapter V and then the % of phagocytosis was compared to the value obtained from co-crosslinking with 1.1b$^{WT\ CYT}$ (maximum inhibition on 2.6b$^{ITAM\ CYT}$-phagocytosis) and 1.1b$^{6YF\ CYT}$ (minimal inhibition on 2.6b$^{ITAM\ CYT}$-phagocytosis) respectively. As shown in Figure 6.2A-B, 1.1b $^{Distal\ CYT}$ fails to cross-inhibit 2.6b$^{ITAM\ CYT}$-mediated phagocytosis. However, a significant cross-inhibition on phagocytosis was observed after co-crosslinking IpLITR constructs in the 2.6b/1.1b $^{3F\ CYT}$ cell line (44.2% and 46.9% at 15 and 30min respectively). Although ~10% increase in the % of phagocytosis was observed compared to the value from co-crosslinking with 1.1b $^{WT\ CYT}$ (~28% and ~36%, respectively), there is no significant difference at both time points. Interestingly, the lowest % of phagocytosis (~33%) among all 1.1b^{CYT} tyrosine mutant constructs tested was observed after co-crosslinking 2.6b$^{ITAM\ CYT}$ with 1.1b$^{Prox\ CYT}$ at 15 min but the value significantly increased to ~74% after 30 min (i.e. it failed to maintain the inhibition of phagocytosis at 30 min). A summary of the relative % inhibition of 2.6b$^{ITAM\ CYT}$ -mediated phagocytosis by the various 1.1b^{CYT} constructs are shown in Figure 6.2C. For example, at 15 min, co-crosslinking of 1.1b$^{WT\ CYT}$ reduced phagocytosis most efficiently (~64% inhibition). A moderate inhibitory effect on 2.6b$^{ITAM\ CYT}$-mediated phagocytosis was observed after co-crosslinking with 1.1b$^{Prox\ CYT}$ or 1.1b$^{3F\ CYT}$, representing a ~58% and ~44% inhibition, respectively. These values were further reduced to ~10% after co-crosslinking with 1.1b $^{Distal\ CYT}$. Similar trends were observed after co-crosslinking 2.6b$^{ITAM\ CYT}$ with various 1.1b constructs for 30 min with slight fluctuations in the value (±~8%). However, after co-crosslinking with the 1.1b$^{Prox\ CYT}$ construct, this value was dramatically decreased from ~58% at 15 min to ~10% at 30 min. Overall, the 1.1b$^{3F\ CYT}$ constructs are most effective at sustaining an inhibitory effect on

ITAM-driven phagocytosis among all the tested tyrosine mutant constructs. This strongly suggests that tyrosine motifs found in the membrane proximal and distal CYT segments of 1.1b$^{WT\ CYT}$ are required to coordinately cross-inhibit 2.6b$^{ITAM\ CYT}$-mediated phagocytosis.

6.2.3 Coordinated recruitment of pSHP-2 and Csk molecules to the CYT of 1.1b $^{WT\ CYT}$ during crosstalk inhibition of the phagocytic response.

To further investigate the identity of recruited effector molecules during receptor crosstalk, a co-immunoprecipitation assay was performed. In these experiments, 2.6b $^{ITAM\ CYT}$ and 1.1b ^{CYT} constructs (i.e. 1.1b$^{WT\ CYT}$, 1.1b$^{6YF\ CYT}$, 1.1b$^{Prox\ CYT}$, 1.1b$^{Distal\ CYT}$ and 1.1b$^{3F\ CYT}$) were co-crosslinked using protein A-coated magnetic beads co-opsonized with αHA/FLAG mAbs. As controls, 2.6b/1.1b $^{WT\ CYT}$ -expressing AD 293 cells, were incubated with magnetic beads opsonized with αHA, αFLAG and isotype IgG1, respectively. After incubation with various antibody-coated beads, cells were lysed, and magnetic beads were isolated using a magnetic separator. Immunoprecipitated proteins (i.e. targeted IpLITR constructs along with any recruited effector molecules) that bound to the magnetic beads were then identified by immunoblotting. Nitrocellulose membrane was first probed with αHA and αFLAG mAbs as an indicator of the successful pull-down of the various N-terminal HA or FLAG-tagged IpLITR constructs. Specifically, immunoreactive bands corresponding to 2.6b$^{ITAM\ CYT}$ and 1.1b ^{CYT} constructs were both present upon co-crosslinking of two IpLITR-types using co-opsonized magnetic beads, whereas only 2.6b $^{ITAM\ CYT}$ or 1.1b ^{CYT} constructs were present when magnetic beads opsonized with αHA or αFLAG mAbs, respectively, were used (Fig. 6.3A-B). Notably, no band was observed when cells were incubated with isotype IgG1-opsonized magnetic beads. To further validate selective recruitments of Csk and SHP-2 molecules to the CYT of 1.1b $^{WT\ CYT}$ in previous biochemical assays, the nitrocellulose membrane was probed using mAbs specific for

Csk and pSHP2. Immunoreactive bands corresponding to Csk were only detected upon co-crosslinking of 2.6b$^{ITAM\ CYT}$ and 1.1b^{CYT} constructs that contain tyrosine 453 in their CYTs (i.e. 1.1b$^{WT\ CYT}$, 1.1b$^{Distal\ CYT}$ and 1.1b$^{3F\ CYT}$; Fig. 6.3C). Comparatively, pSHP-2 bands were observed after co-crosslinking with 1.1b^{CYT} constructs with ITIMs in CYTs (i.e. 1.1b$^{WT\ CYT}$, 1.1b$^{Prox\ CYT}$ and 1.1b$^{3F\ CYT}$; Fig. 6.3D). Of note, independent IpLITR triggering or co-crosslinking of 2.6b$^{ITAM\ CYT}$ and 1.1b$^{6YF\ CYT}$ only, results in the precipitation of respective IpLITR constructs with no associated Csk or pSHP-2 molecules (Fig. 6.3C-D). Potential recruitments of other inhibitory effector molecules involved in lipid signaling upon co-crosslinking of IpLITR-types were also examined; however, no immunoreactive bands corresponding to phosphatase and tensin homolog (PTEN) and SHIP-2 were detected even though these signaling molecules were present in the whole cell lysates (Fig. 6.3E-F).

To further confirm and quantify selective recruitments of Csk and pSHP2 to different CYTs of 1.1b^{CYT} constructs, a confocal microscopy-based assay was performed as described in Chapter V. Briefly, 2.6b/1.1b^{CYT}-expressing AD 293 cells were incubated with co-opsonized NF beads to co-crosslink two IpLITR-types. As controls, 2.6b/1.1b$^{WT\ CYT}$-expressing cells were incubated with αHA or αFLAG mAb-opsonized NF beads that result in the independent activation of the IpLITR constructs. After incubation, exposed areas of surface-bound NF beads and intracellular effector molecules of interest (i.e. Csk and pSHP-2) were differentially stained red and green, respectively. Consistent with the co-immunoprecipitation results, the recruitment of Csk molecules to the phagocytic synapses were only observed upon co-crosslinking of 2.6b$^{ITAM\ CYT}$ and 1.1b^{CYT} constructs containing tyrosine 453 (Fig. 6.4A-B). This observation was further confirmed by quantitative analysis of fluorescent signal intensities within phagocytic synapses. Specifically, independent engagement of 2.6b$^{ITAM\ CYT}$ and 1.1b$^{WT\ CYT}$ only showed

basal level of fluorescent intensities at the phagocytic synapses, with values of 44800.59-±2912.57 and 38695.77±2384.51, respectively. Although signal intensities were slightly increased to 51008.21±2461.30 and 49154.21±2762.76 following co-crosslinking of 2.6b$^{ITAM\ CYT}$ with 1.1b$^{6YF\ CYT}$ and 1.1b$^{Prox\ CY}$ constructs, respectively, these changes did not represent statistically significant increases in Csk recruitments to phagocytic synapses. However, significant increases of signal intensities were observed after co-crosslinking 2.6b$^{ITAM\ CYT}$ with 1.1b ^{CYT} constructs containing tyrosine 453 (i.e. 1.1b$^{WT\ CYT}$, 1.1b$^{Distal\ CYT}$ and 1.1b$^{3F\ CYT}$), with values of 113829.37±6773.95, 108223.91±5162.79 and 119418.42±4273.65. respectively (Fig. 6.4C). Comparatively, enrichment of pSHP2 molecules at the phagocytic synapses were only seen after co-crosslinking 2.6b$^{ITAM\ CYT}$ with 1.1b^{CYT} that contained functional ITIMs in their CYT regions (Fig. 6.5A-B). Similarly, basal levels of pSHP-2 signals (signal intensities of ~30000) was observed after independent engagement of 2.6b$^{ITAM\ CYT}$ and 1.1b$^{WT\ CYT}$ constructs or co-crosslinking of 2.6b$^{ITAM\ CYT}$ with 1.1b^{CYT} constructs with mutated ITIMs (i.e. 1.1b$^{6YF\ CYT}$ and 1.1b$^{Distal\ CYT}$). A significant increase of pSHP-2 signals was seen after co-crosslinking 2.6b$^{ITAM\ CYT}$ with 1.1b^{CYT} constructs that have intact ITIMs (i.e. 1.1b$^{WT\ CYT}$, 1.1b$^{Prox\ CYT}$ and 1.1b$^{3F\ CYT}$), represented by staining intensity values of 41380.35±2391.50, 44447.96±3741.96 and 45666.20±2484.31, respectively (Fig. 6.5C).

6.2.4 Reduction in phosphorylation of Erk1/2 but not Akt during crosstalk inhibition of the phagocytic response.

Having established that 1.1b$^{WT\ CYT}$ -mediated cross-inhibition of phagocytosis is likely through selective recruitments of Csk and pSHP-2 molecules, I next examined the potential candidates of downstream effector molecules that are targeted during of IpLITR crosstalk inhibition of the phagocytic response. Stable AD 293 cells were incubated with co-opsonized YG

beads to co-crosslink 2.6b$^{ITAM\ CYT}$ and 1.1b^{CYT} constructs. As controls, 2.6b$^{ITAM\ CYT}$ and 1.1b$^{WT\ CYT}$ constructs were independently engaged following incubation of 2.6b/1.1b$^{WT\ CYT}$-expressing AD 293 cells with YG beads opsonized with αHA and αFLAG mAbs, respectively. After stimulating the receptors for indicated time points, cells were immediately lysed, sonicated and centrifuged to eliminate debris and then supernatant fractions were collected for subsequent immunoblotting analysis. In my studies, I focused on the two effector molecules ERK1/2 and Akt, which are known to be activated during phagocytic responses (163,171). Specifically, I examined the phosphorylation status of these two molecules as indications of which signalling pathways may be disrupted during 1.1b$^{WT\ CYT}$-mediated cross-inhibition events. After independent engagement of 1.1b$^{WT\ CYT}$ for 2, 8, 15 and 30 min, no Erk1/2 phosphorylation was induced with only background signals similar to resting cells observed (i.e. 0 min group; Fig. 6.6A). In contrast, independent activation of 2.6b$^{ITAM\ CYT}$ or co-crosslinking with 1.1b$^{6YF\ CYT}$ constructs induced Erk1/2 phosphorylation at 2 min (~10 fold increase relative to 0 min) that peaked at 15 min (~30 fold increase) and subsided by 30 min (~10 fold increase) post-stimulation (Fig. 6.6B and Fig. 6.6D). A clear reduction of Erk1/2 phosphorylation was observed after co-crosslinking 2.6b$^{ITAM\ CYT}$ with 1.1b$^{WT\ CYT}$, representing ~4 fold increase in relative to 0 min over time (Fig. 6.6C). To further investigate the contribution of tyrosine motifs in the CYT of 1.1b$^{WT\ CYT}$ required to down-regulate Erk1/2 phosphorylation, the phosphorylation state of Erk1/2 was examined after co-crosslinking 2.6b$^{ITAM\ CYT}$ with various tyrosine mutant 1.1b^{CYT} constructs. A similar induction profile of Erk1/2 phosphorylation was observed following co-crosslinking 2.6b$^{ITAM\ CYT}$ with 1.1b$^{Prox\ CYT}$ or 1.1b$^{Distal\ CYT}$ but with reduced magnitude at each time point (Fig. 6.6E-F). Comparatively, after co-crosslinking 2.6b$^{ITAM\ CYT}$ with 1.1b$^{3F\ CYT}$, Erk1/2 phosphorylation was largely reduced and similar to the levels observed when 2.6b$^{ITAM\ CYT}$

was co-crosslinking with the functionally intact 1.1b$^{WT\ CYT}$ (Fig. 6.6G).

With respect to the phosphorylation state of Akt molecules, independent engagements of 1.1b$^{WT\ CYT}$ for various time points results in no induction of Akt phosphorylation with only basal levels of pAkt signals observed (data not shown). Comparatively, crosslinking of 2.6b$^{ITAM\ CYT}$ lead to a rapid and sustained phosphorylation of Akt and pAkt levels were maintained for up to 30 min (data not shown). Similar trends were also observed following co-crosslinking 2.6b$^{ITAM\ CYT}$ with various 1.1b^{CYT} constructs (data not shown). These observations suggest that pAkt signaling events were not affected as a result of IpLITR crosstalk.

6.3 DISCUSSION

Having established in the previous chapter that IpLITR crosstalk is an important regulatory mechanism controlling phagocytosis, the objectives of this chapter were to further investigate the molecular mechanisms responsible for the 1.1b$^{WT\ CYT}$-mediated cross-inhibition of phagocytosis. Here, I identified two signaling regions (i.e. tyrosine 453 and ITIMs) in the CYT of 1.1b$^{WT\ CYT}$ that are critical for sustaining inhibitory effects on 2.6b $^{ITAM\ CYT}$ -mediated phagocytosis. Coordinated recruitments of Csk and pSHP-2 molecules to phagocytic synapses upon co-crosslinking of IpLITR constructs likely contribute to inhibiting phagocytosis through down-regulation of the Erk1/2 signaling pathway. Overall, data presented in this chapter provide new insights into molecular details regarding the novel regulatory role of 1.1b$^{WT\ CYT}$ to cross-inhibit ITAM-driven phagocytosis via coordinated recruitments of specific inhibitory molecules.

The inhibitory role of 1.1b$^{WT\ CYT}$ was originally characterized in transfected NK cells and the first functional report showed that 1.1b$^{WT\ CYT}$ -mediated inhibition of NK cell killing is likely through recruitments of SHPs to ITIMs in the membrane distal CYT segment (10). Later studies revealed an ITIM-independent mechanism during the control of 1.1b$^{WT\ CYT}$-mediated inhibition

of NK cell killing responses. Specifically, the membrane proximal CYT region of $1.1b^{WT\ CYT}$ was shown capable of independently abrogating NK cell cytotoxicity and subsequent biochemical analysis confirmed that a Csk-binding motif (i.e. tyrosine 453) is likely responsible for this inhibitory activity (12). Interestingly, although cytotoxicity and phagocytosis are two functionally distinct cellular responses, similar synaptic structures (i.e. immunological and phagocytic synapses) are formed after encountering cognate targets, which provides a microenvironment for receptor clustering and recruitment of various signaling molecules that fine-tune effector responses. For example, in the context of NK cell-mediated cytotoxicity, the initial formation of an activating NK immunological synapse (aNKIS) is achieved by segregating key inhibitory proteins (e.g. SHPs) away from central supramolecular activation cluster (cSMAC), where activating receptors and associated components are resident and thus, local activity of tyrosine kinases would be favoured to propagate activating signals (172–174). Interestingly, similar mechanisms were also observed for the initiation of phagocytosis, in which engagement of Dectin-1 by β-glucan-opsonized particles result in local exclusion of transmembrane receptor tyrosine phosphatases (i.e. CD45 and CD148) from the receptor-enriched sites, thus allowing transduction of phosphotyrsosine-based signaling events (154). This observation leads to the "phagocytic synapses" model and later studies further reported that this mechanism is also used by classical phagocytic receptors (i.e. FcRs), suggesting that it may be relevant for all phagocytic receptors (157). With respect to the role of synaptic structures in inhibiting effector responses, a synaptic structure known as the inhibitory NKIS (iNKIS), is formed at the interface between the NK cells and normal host cells that engage ITIM-containing KIRs by cognate ligands (e.g. MHC-I molecules). These receptors are clustered in the central supramolecular inhibition cluster (cSMIC). This forms a platform for recruitments of

phosphatases (e.g. SHP1/2) to down-regulate activating signals and consequently, prevent NK cells from killing normal cells (173). Comparatively, although no "inhibitory phagocytic synapse" has been reported, inhibition of phagocytosis following co-crosslinking of activating and inhibitory receptors often results in stalled phenotype, where phagocytic targets are not completely internalized but still remain on the plasma membrane (131). This observation strongly suggests that similar synaptic structures are formed at the contact sites, beneath which the interplay between activating and inhibitory signals dictates the nature and magnitude of subsequent responses.

A set of inhibitory molecules that target proximal signaling events have been reported to down-regulate both phagocytosis and cytotoxicity. For example, both Csk and SHPs have been shown to inactivate critical signaling components required for the induction of phagocytosis and cytotoxicity (67,167,168,175–180). Collectively, these observations led me to formulate the hypothesis that membrane proximal and distal CYT segments of $1.1b^{WY\ CYT}$ may also independently control $2.6b^{ITAM\ CYT}$-mediated phagocytosis. To further determine if $1.1b^{WT\ CYT}$ uses similar mechanisms to cross-inhibit phagocytosis as was demonstrated for its inhibitory effects on cytotoxicity, I generated $1.1b^{CYT}$ constructs with combinations of tyrosines mutated to phenylalanine in their CYT regions and stably co-expressed these with $2.6b^{ITAM\ CYT}$ in AD 293 cells. Site-directed mutagenesis allowed me to test my hypothesis by disabling selected tyrosine motifs and then investigating if the rest of tyrosine motifs are sufficient to inhibit phagocytosis. For example, the mutant construct, $1.1b^{Distal\ CYT}$, has tyrosine motifs (i.e. ITIMs and ITSM) in the membrane distal region of $1.1b^{WT\ CYT}$ mutated to phenylalanine, thus potential inhibitory effects of tyrosine motifs in the membrane proximal region on phagocytosis can then be specifically examined.

Contrary to the observation in NK cells, the 1.1b$^{\text{Distal CYT}}$ constructs did not exert inhibitory effects on 2.6b$^{\text{ITAM CYT}}$-mediated phagocytosis even though it still has the potential of recruiting Csk molecules. Csk is a negative regulator of Src family kinases by specifically phosphorylating a conserved tyrosine residue (i.e. tyrosine 527) at C-terminus; thus rendering Src kinases in an auto-inhibitory conformation (66). Loss of Src kinase activity reduces phosphorylation of tyrosine within ITAMs, which results in the abrogation of various effector responses (181–185). However, several lines of evidence indicate that Src family kinases may not be indispensable for the initiation and completion of phagocytosis and macrophages lacking major Src kinases still able to engulf phagocytic targets, although in a delayed manner (186). It is proposed that a small number of Syk can constitutively associate with ITAM, which is sufficient to initiate and propagate signaling cascades after receptor ligation even in the absence of Src kinases (57,110,186). Therefore, recruitments of Csk alone to 1.1b$^{\text{Distal CYT}}$ signaling complex may not be sufficient to cross-inhibit phagocytosis. Interestingly, 2.6b $^{\text{ITAM CYT}}$-mediated phagocytosis was significantly inhibited after co-crosslinking with 1.1b$^{\text{Prox CYT}}$ constructs (i.e. tyrosine motifs, including the Csk-binding motif, in the membrane proximal segment are mutated) at 15 min but a robust phagocytic phenotype was restored at 30 min. This delay in phagocytosis suggests that inhibitory molecules (e.g. SHP2) recruited by 1.1b$^{\text{Prox CYT}}$ constructs may reduce but not completely abolish the activity of effector molecules critical for the progression of phagocytosis; thus failing to sustain the inhibitory effect. Indeed, a similar observation has been reported from mouse peritoneal macrophages lacking Abl kinases and reduced phosphorylation of a regulatory tyrosine residue (i.e. Y346) on Syk may account for the delay in phagocytosis (187). Collectively, these observations indicate that membrane proximal and distal CYT segments of 1.1b$^{\text{WT CYT}}$ are not able to independently sustain the inhibition of

2.6b $^{ITAM\ CYT}$-mediated phagocytosis; instead, tyrosine motifs from both CYT segments may be required for the initiation (1.1b$^{Distal\ CYT}$) and sustainment (1.1b$^{Prox\ CYT}$) of 1.1b$^{WT\ CYT}$-mediated cross-inhibition. Supporting this hypothesis, sustained inhibition of phagocytosis was observed after co-crosslinking 2.6b$^{ITAM\ CYT}$ with the 1.1b$^{3F\ CYT}$ constructs where the Csk-binding motif (i.e. Y453) and the CYT distal ITIMs (i.e. Y477 and Y499) remained intact, further suggesting that coordinated recruitments of multiple inhibitory molecules to CYT segments are required to cross-inhibit phagocytosis. Of note, the inhibition efficiency of 1.1b$^{3F\ CYT}$ is slightly reduced compared to 1.1b$^{WT\ CYT}$, indicating the other tyrosine motifs may also participate in sustaining inhibitory signals but the tyrosine-based signaling modules in 1.1b$^{3F\ CYT}$ constructs are minimally required to effectively cross-inhibit phagocytosis. Attempts to further mutate either tyrosine within ITIMs of 1.1b$^{3F\ CYT}$ constructs result in a significant reduction in its inhibition efficiency (data not shown).

Recruitments of endogenous Csk and pSHP-2 molecules to membrane proximal tyrosine 453 and the distal ITIMs of 1.1b$^{WT\ CYT}$, respectively were further confirmed by a co-immunoprecipitation assay. This is consistent with our previous biochemical data showing that recombinant GST-tagged 1.1b $^{WT\ CYT}$ constructs are co-immunoprecipitated with Csk and SHP-2 molecules (14). Interestingly, no immunoreactive band corresponding to Csk or pSHP-2 was observed upon independent engagement of 1.1b$^{WT\ CYT}$ constructs. This is consistent with the previous observation in Chapter V that independent crosslinking of 1.1b$^{WT\ CYT}$ constructs only result in the basal level of tyrosine phosphorylation. This leads to the hypothesis that co-crosslinking with 2.6b$^{ITAM\ CYT}$ constructs may be required to phosphorylate tyrosine motifs in the CYT region of 1.1b$^{WT\ CYT}$ for recruiting effector molecules to down-regulate 2.6b$^{ITAM\ CYT}$-mediated phagocytosis. In support of this hypothesis, co-immunoprecipitation of Csk and pSHP-

2 with 1.1b$^{WT\ CYT}$ constructs was observed only after co-crosslinking with 2.6b$^{ITAM\ CYT}$ constructs. This *trans*-phosphorylation mechanism that requires co-crosslinking of inhibitory receptors with their activating counterparts to produce inhibitory signals has also been reported in other immunoregulatory receptors and is vital for the control of various innate effector responses (152,188). For example, independent engagement of FcγRIIB failed to phosphorylate tyrosines within its CYT region; whereas after co-crosslinking, Src kinases (i.e. Lyn) recruited to the activating FcεRI also phosphorylated the ITIMs of FcγRIIB and consequently this facilitated recruitment of SHIPs required for the cross-inhibition of FcεRI-mediated degranulation in mast cells (152). Similarly, this may also account for the activation of 1.1b$^{WT\ CYT}$ as it likely does not endogenously associate with Src kinases but translocates to lipid rafts where Src kinases are resident after co-crosslinking with its activating counterparts. In return, phosphorylated 1.1b$^{WT\ CYT}$ constructs produce inhibitory signals to cross-inhibit signaling events downstream of 2.6b$^{ITAM\ CYT}$ activation. In this scenario, 2.6b$^{ITAM\ CYT}$ is not a passive target of inhibitory effectors but instead, actively participates in its own inhibition by recruiting kinases (e.g. Src family kinases) to phosphorylate 1.1b$^{WT\ CYT}$. In general, this may represent an intrinsic negative feedback loop for controlling 2.6b$^{ITAM\ CYT}$-mediated responses through receptor crosstalk.

In agreement with the above biochemical data, involvement of Csk and pSHP-2 molecules in regulating 2.6b$^{ITAM\ CYT}$-mediated phagocytosis was further confirmed by confocal microscopy. Following receptor co-crosslinking, Csk and pSHP-2 molecules translocate from cytosol to plasma membrane and specifically are enriched at phagocytic synapses. This brings Csk and pSHP-2 molecules into close proximity of 2.6b$^{ITAM\ CYT}$-1.1b$^{WT\ CYT}$ signaling complexes and act in concert to inactivate crucial signalling components indispensable for the ITAM-driven phagocytosis. Subsequent biochemical analysis further revealed that Erk1/2 signaling is a

downstream target affected during IpLITRs-mediated crosstalk. Erk1/2 is a critical component in the mitogen-activated protein kinase (MAPK) pathways that have been extensively characterized in regulating cell growth and differentiation upon cytokine-induced activation (189–191). Recent studies also suggest that Erk1/2 may participate in the regulation of phagocytosis at transcriptional and post-transcriptional levels. For example, Erk1/2 activation contributes to up-regulating the expression of inducible nitric oxide synthase (iNOS) and facilitating the production of reactive oxygen species (ROS), which are two potent bactericidal components synthesized during phagocytosis (192,193). In addition, a blockage of Erk1/2 phosphorylation reduces phagocytosis of *Francisella novicida* (194). Collectively, these observations suggest a regulatory role of Erk1/2 and reduced Erk1/2 activity can negatively impact phagocytosis.

In an attempt to expand the repertoire of recruited effector molecules involved in fine-tuning phagocytic signals, I further probed two potential inhibitory molecules (i.e. SHIP-2 and PTEN) that have been reported in negatively regulating phagocytosis by disrupting PI3K/Akt signaling axis (169,195–197). However, these two molecules are not co-immunoprecipitated with $1.1b^{WT\ CYT}$ (Fig. 6.3E-F). This may explain the observation that the level of phosphorylated Akt is not affected following receptor co-crosslinking. Currently, detailed mechanisms responsible for $1.1b^{WT\ CYT}$-mediated cross-inhibition of phagocytosis are far from understood and it is unlikely that Csk and SHP-2 are the only inhibitory molecules involved in this process. Another possible candidate is SHP-1, since recruitment of both SHP-1/2 molecules to ITIMs in the CYT of $1.1b^{WT\ CYT}$ have been shown previously (10,12). However, this phosphatase is restrictively expressed in hematopoietic cell lineages and not expressed in AD 293 cells (145). This may lead to recruitments of SHP-2 to compensate for the absence of SHP-1 in fibroblast cells, which further raises some interesting questions: i) which phosphatases are preferentially

recruited when both SHP1/2 are present and; ii) whether SHP-2 play a redundant role as SHP-1 in down-regulating phagocytosis. Future studies to identify potential inhibitory molecules along with their substrates in a more physiologically-relevant system (e.g. primary catfish immune cells) will provide a better understanding of mechanistic details regarding the inhibitory activities of teleost immunoregulatory receptors such as 1.1b$^{WT\ CYT}$.

In summary, in this chapter I have further investigated the molecular details regarding 1.1b$^{WT\ CYT}$-mediated cross-inhibition of ITAM-driven phagocytosis. For the first time, I have shown that receptor crosstalk is an important regulatory mechanism utilized by teleost immunoregulatory receptors to regulate important innate effector responses. As summarized in Fig. 6.7A, robust induction of phagocytosis and pro-inflammatory signals (i.e. Erk1/2 phosphorylation) were observed after co-crosslinking of 2.6b$^{ITAM\ CYT}$ with the mutant construct 1.1b$^{6YF\ CYT}$. These canonical ITAM-dependent signaling events likely require the participation of Src kinases to phosphorylate the tandem ITAM tyrosines, recruit Syk kinases and phosphorylate this enzyme to propagate downstream signaling cascades and promote phagocytosis. However, 2.6b$^{ITAM\ CYT}$-mediated phagocytosis was suppressed after co-crosslinking 2.6b$^{ITAM\ CYT}$ with the functional capable 1.1b$^{WT\ CYT}$ construct, and this response is likely due to recruitments of inhibitory molecules to the 2.6b$^{ITAM\ CYT}$-1.1b$^{WT\ CYT}$ complex, that suppress activities of Syk and Src family kinases (Fig. 6.7B). Indeed, two specific inhibitory molecules, Csk and SHP-2, were co-immunoprecipitated and recruited to phagocytic cups after co-crosslinking of 2.6b$^{ITAM\ CYT}$ and 1.1b$^{WT\ CYT}$. Presumably, the CYT region of 1.1b$^{WT\ CYT}$ is possibly *trans*-phosphorylated after co-crosslinking with 2.6b$^{ITAM\ CYT}$ and this initiates the production of inhibitory signals. Subsequent recruitments of Csk and SHP-2 molecules to the 2.6b$^{ITAM\ CYT}$-1.1b$^{WT\ CYT}$-containing synapse target specific substrates at different levels of phagocytic pathways to coordinately

down-regulate the Erk1/2 signaling pathway and thus cross-inhibit ITAM-driven phagocytosis. This represents the first report showing that teleost immunoregulatory receptors can regulate phagocytosis through receptor crosstalk and in general provides a new framework for investigating mechanistic details of receptor crosstalk in the regulation of various immunoregulatory receptor-driven innate immune effector responses in fish.

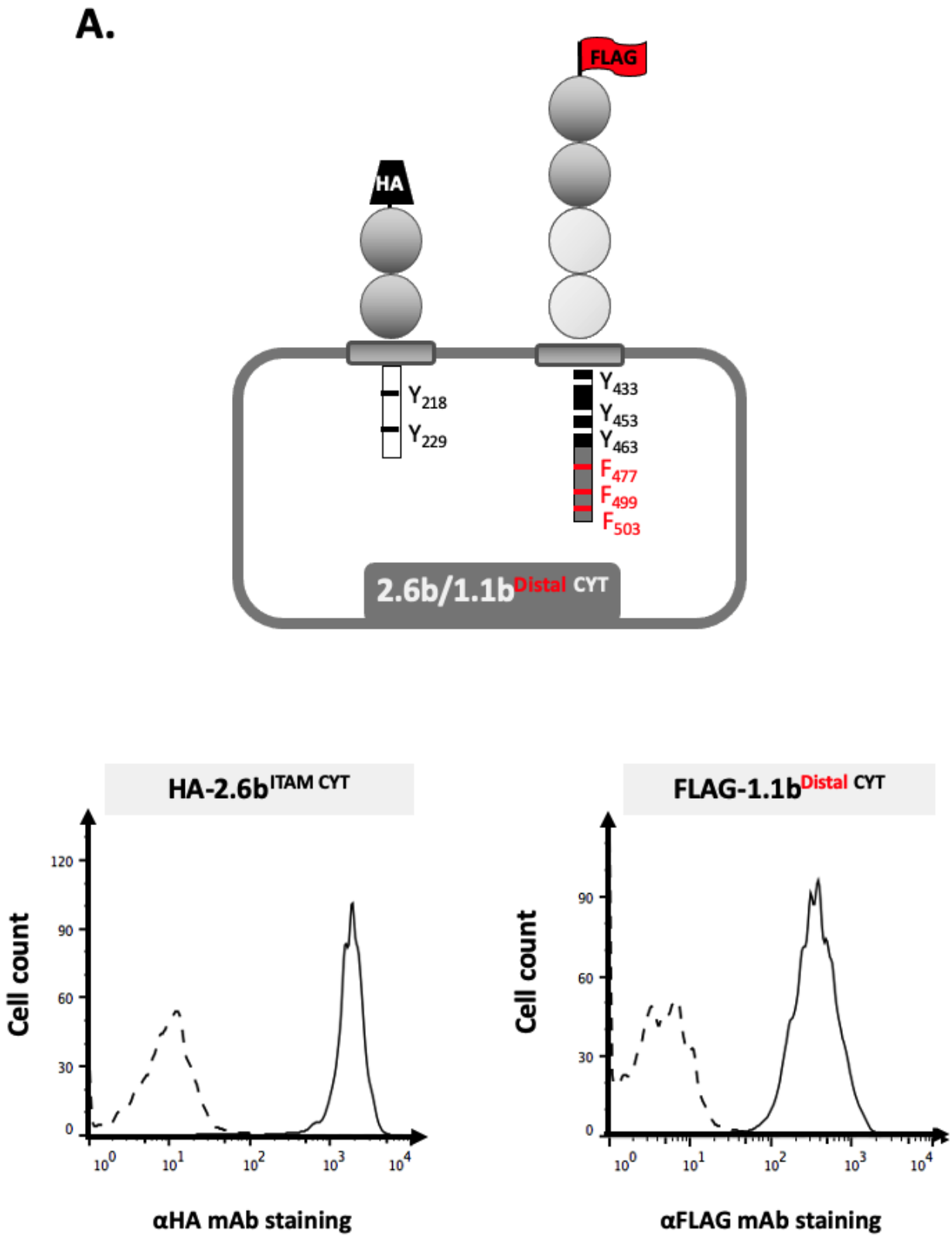
A.
FLAG
HA
Y218
Y229
Y433
Y453
Y463
F477
F499
F503
2.6b/1.1bDistal CYT
HA-2.6bITAM CYT
Cell count
120
90
60
30
0
10^0
10^1
10^2
10^3
10^4
αHA mAb staining
FLAG-1.1bDistal CYT
Cell count
90
60
30
0
10^0
10^1
10^2
10^3
10^4
αFLAG mAb staining

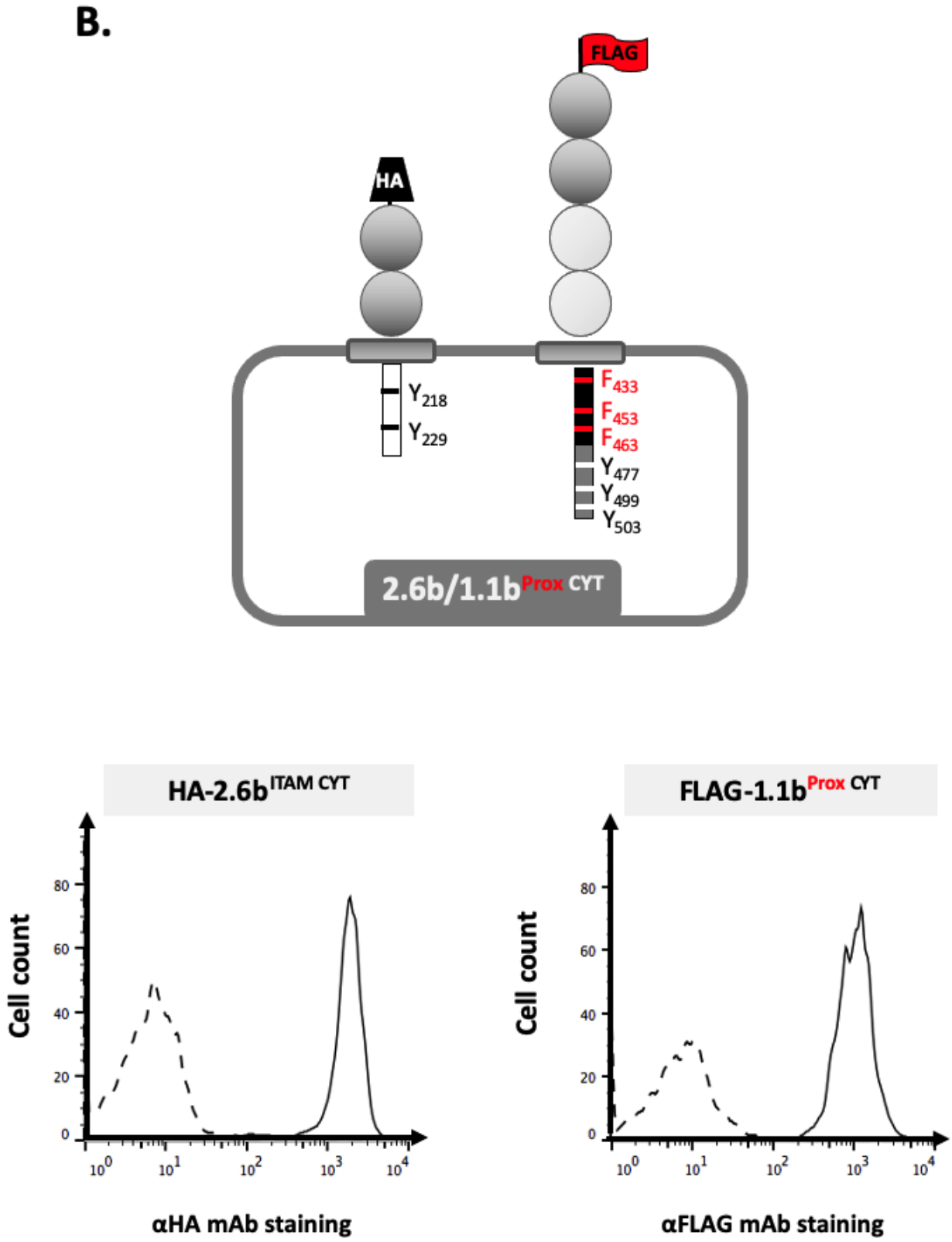
B.
FLAG
HA
Y218
Y229
F433
F453
F463
Y477
Y499
Y503
2.6b/1.1bProx CYT
HA-2.6bITAM CYT
Cell count
αHA mAb staining
FLAG-1.1bProx CYT
Cell count
αFLAG mAb staining

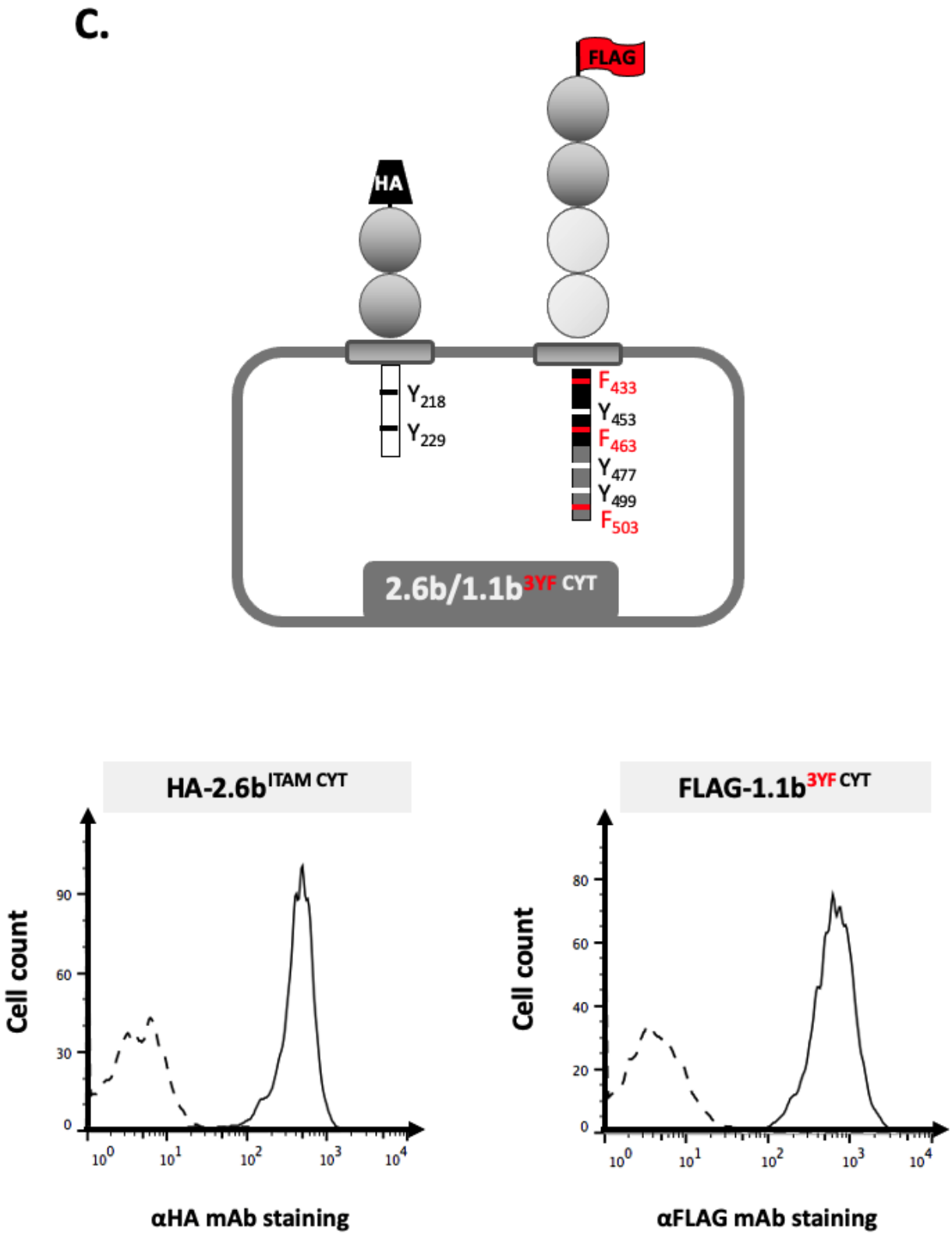
C.
FLAG
HA
Y218
Y229
F433
Y453
F463
Y477
Y499
F503
2.6b/1.1b3YF CYT
HA-2.6bITAM CYT
Cell count
αHA mAb staining
FLAG-1.1b3YF CYT
Cell count
αFLAG mAb staining

Figure 6.1. Generation and stable co-expression of N-terminal HA and FLAG epitope-tagged IpLITR constructs in AD293 cells. Stable AD 293 cells co-expressing 2.6b$^{ITAM\ CYT}$ and detection of the cell surface co-expression of 2.6b$^{ITAM\ CYT}$ with 1.1b$^{Distal\ CYT}$ (two ITIM and one ITSM in the distal region of the CYT were mutated to phenylalanine; referred to here as 2.6b/1.1b$^{Distal\ CYT}$,(A)) 1.1b$^{Prox\ CYT}$ (tyrosines, including Csk-binding motif Y453, in the proximal region of the CYT were mutated to phenylalanine; referred to here as 2.6b/1.1b $^{6YF\ CYT}$ (B)) and 1.1b$^{3F\ CYT}$ (Csk-binding motif and two ITIMs remain intact; referred to here as 2.6b/1.1b $^{3F\ CYT}$) respectively in transfected, selected and sorted AD 293 cells. Co-expression stable cells were stained by incubation with an αHA mAb (2.6b$^{ITAM\ CYT}$ staining, solid line, left panel), αFLAG mAb (1.1b^{CYT} constructs staining, solid line, right panel) or mouse IgG1 (isotype control, dash line) followed by staining with goat αmouse IgG pAb coupled to PE. Surface expression was then determined as an increase in fluorescence intensity in comparison with IgG1-stained cells. Shown are representative stains for each stable cell line.

A.

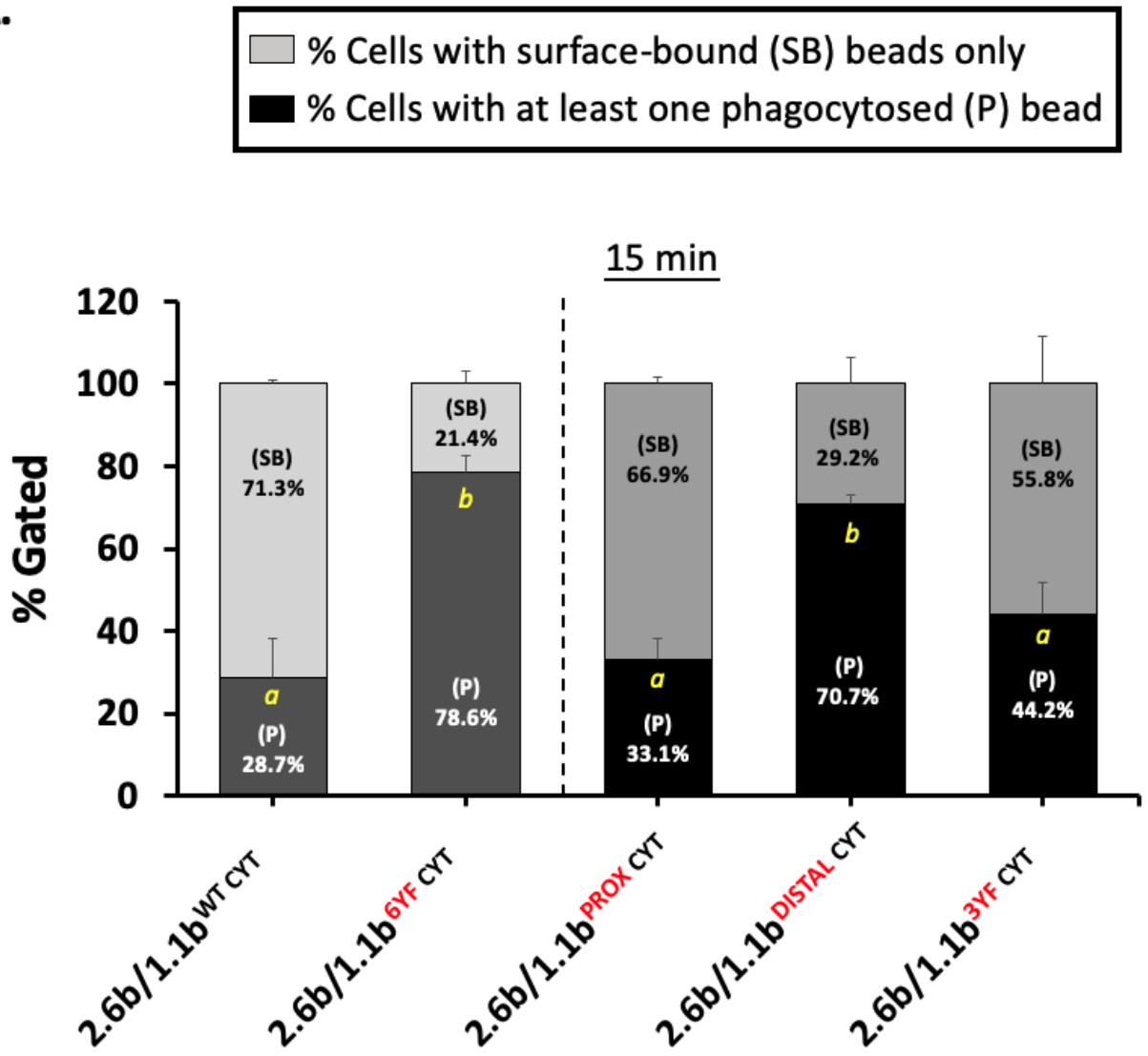
% Cells with surface-bound (SB) beads only
% Cells with at least one phagocytosed (P) bead
15 min
% Gated
120
100
80
60
40
20
0
(SB) 71.3%
a
(P) 28.7%
(SB) 21.4%
b
(P) 78.6%
(SB) 66.9%
a
(P) 33.1%
(SB) 29.2%
b
(P) 70.7%
(SB) 55.8%
a
(P) 44.2%
2.6b/1.1b WT CYT
2.6b/1.1b 6YF CYT
2.6b/1.1b PROX CYT
2.6b/1.1b DISTAL CYT
2.6b/1.1b 3YF CYT

B.

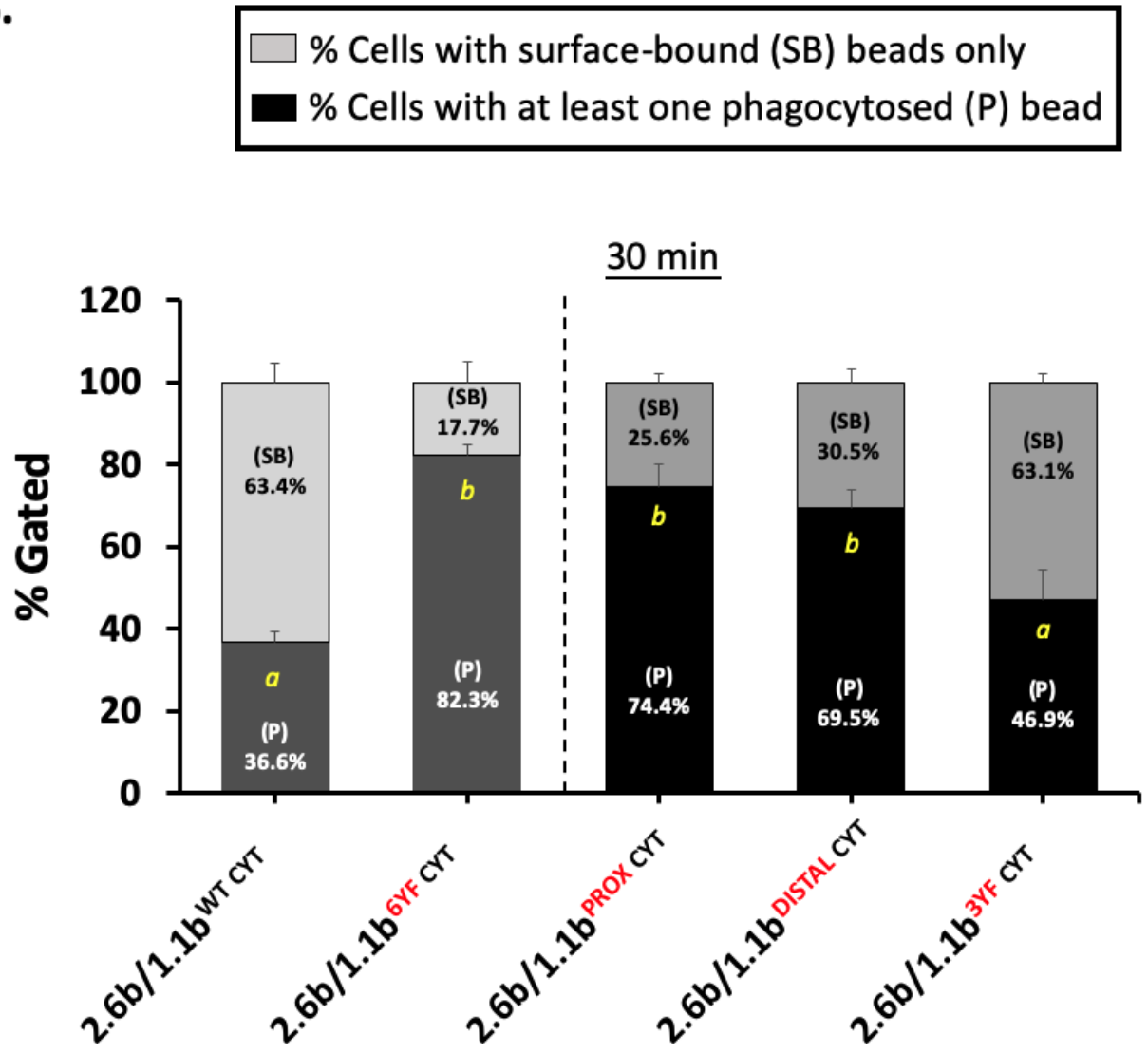
% Cells with surface-bound (SB) beads only
% Cells with at least one phagocytosed (P) bead
30 min
% Gated
120
100
80
60
40
20
0
(SB) 63.4%
a
(P) 36.6%
(SB) 17.7%
b
(P) 82.3%
(SB) 25.6%
b
(P) 74.4%
(SB) 30.5%
b
(P) 69.5%
(SB) 63.1%
a
(P) 46.9%
2.6b/1.1b WT CYT
2.6b/1.1b 6YF CYT
2.6b/1.1b PROX CYT
2.6b/1.1b DISTAL CYT
2.6b/1.1b 3YF CYT

C.

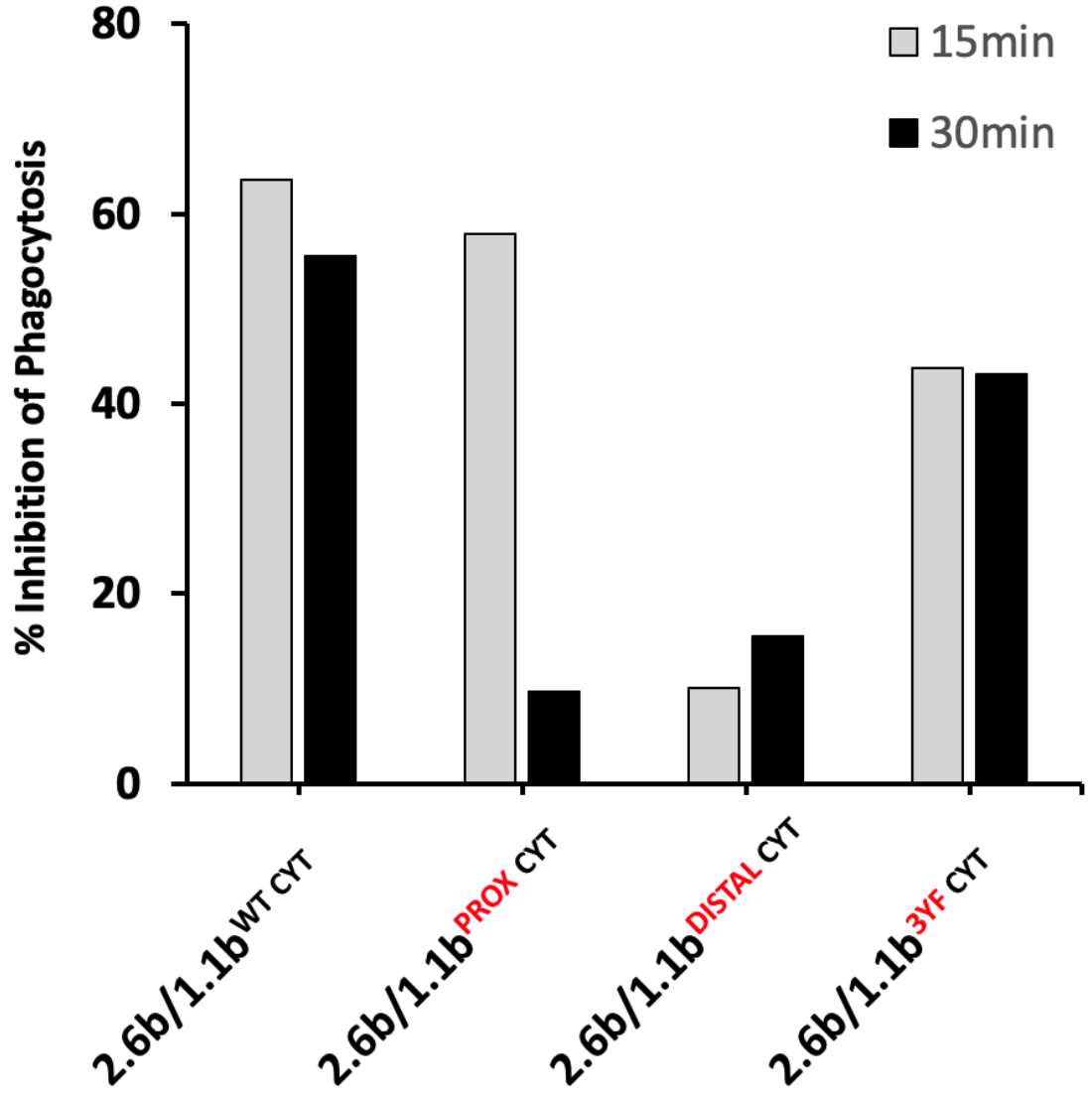
80
60
40
20
0
% Inhibition of Phagocytosis
15min
30min
2.6b/1.1b WT CYT
2.6b/1.1b PROX CYT
2.6b/1.1b DISTAL CYT
2.6b/1.1b 3YF CYT

Figure 6.2. Csk-binding motif (tyrosine 453) and ITIMs (tyrosine 477 and 499) in the cytoplasmic region of 1.1b$^{WT\ CYT}$ are required to sustain the inhibition on 2.6b$^{ITAM\ CYT}$-mediated phagocytosis. Stable cells (2×10^5) co-expressing 2.6b$^{ITAM\ CYT}$ and various 1.1b^{CYT} tyrosine mutant constructs (i.e.1.1b$^{Prox\ CYT}$, 1.1b$^{Distal\ CYT}$ and 1.1b$^{3F\ CYT}$) were incubated with 4.5μm YG beads (6×10^5) opsonized with αHA and αFLAG mAbs for 15 (A) and 30 min (B) at 37 ℃ prior to analysis of samples using the ImageStreamx Mark II instrument. Percentage of cells exhibiting two phenotypes is normalized and calculated as: % phagocytosis or surface-bound cells / % total bead-associated cells. Grey bars represent the percentage of cells with only surface-bound targets (i.e. no internalization) and black bars represent the percentage of cells with ≥1 fully internalized bead. Data representing phenotypes of 1.1b$^{WT\ CYT}$ (maximal inhibition on phagocytosis) and 1.1b$^{6YF\ CYT}$ (minimal inhibition on phagocytosis) from Figure 5.5 were also included and outlined by dash lines in the panel. Each bar represents the mean ± SEM of at least three independent experiments. Letters indicate statistical significance ($P \leq 0.05$) when comparing % of phagocytosis. (c) % of inhibition on phagocytosis was indexed in relative to the value from 2.6b/1.1b$^{6YF\ CYT}$ group and calculated as: [% phagocytosis of 2.6b/1.1b$^{6YF\ CYT}$ (maximal % phagocytosis) - % phagocytosis of each group) / (% phagocytosis of 2.6b/1.1b$^{6YF\ CYT}$]. % of inhibition on phagocytosis at 15 and 30 min was graphed as white and black bar respectively.

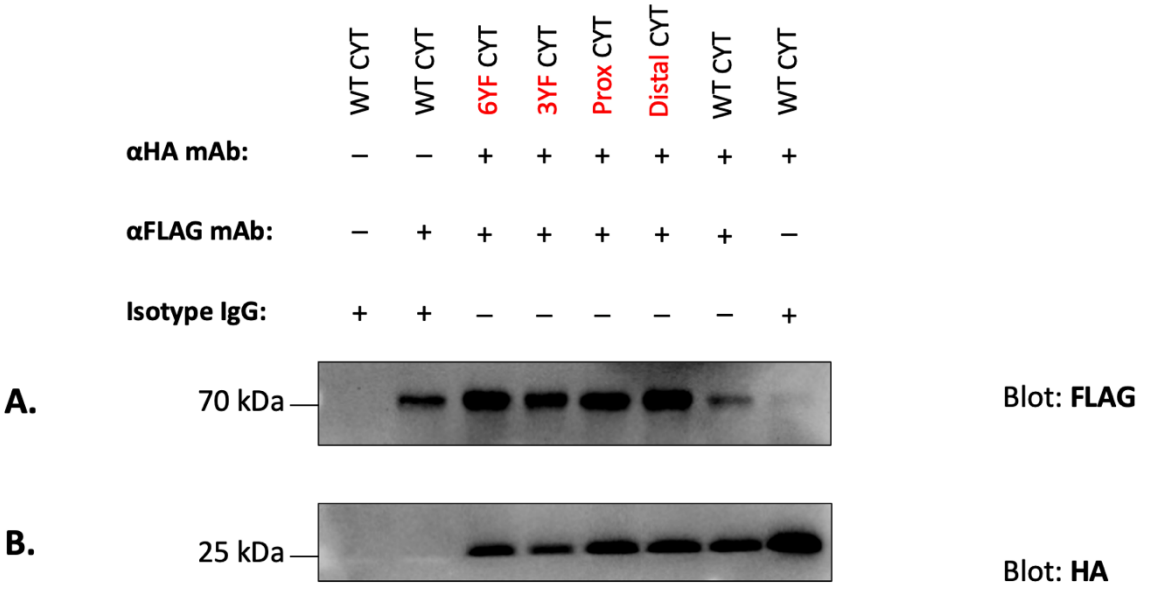
WT CYT
WT CYT
6YF CYT
3YF CYT
Prox CYT
Distal CYT
WT CYT
WT CYT
αHA mAb: – – + + + + + +
αFLAG mAb: – + + + + + + –
Isotype IgG: + + – – – – – +
A.
70 kDa
Blot: FLAG
B.
25 kDa
Blot: HA

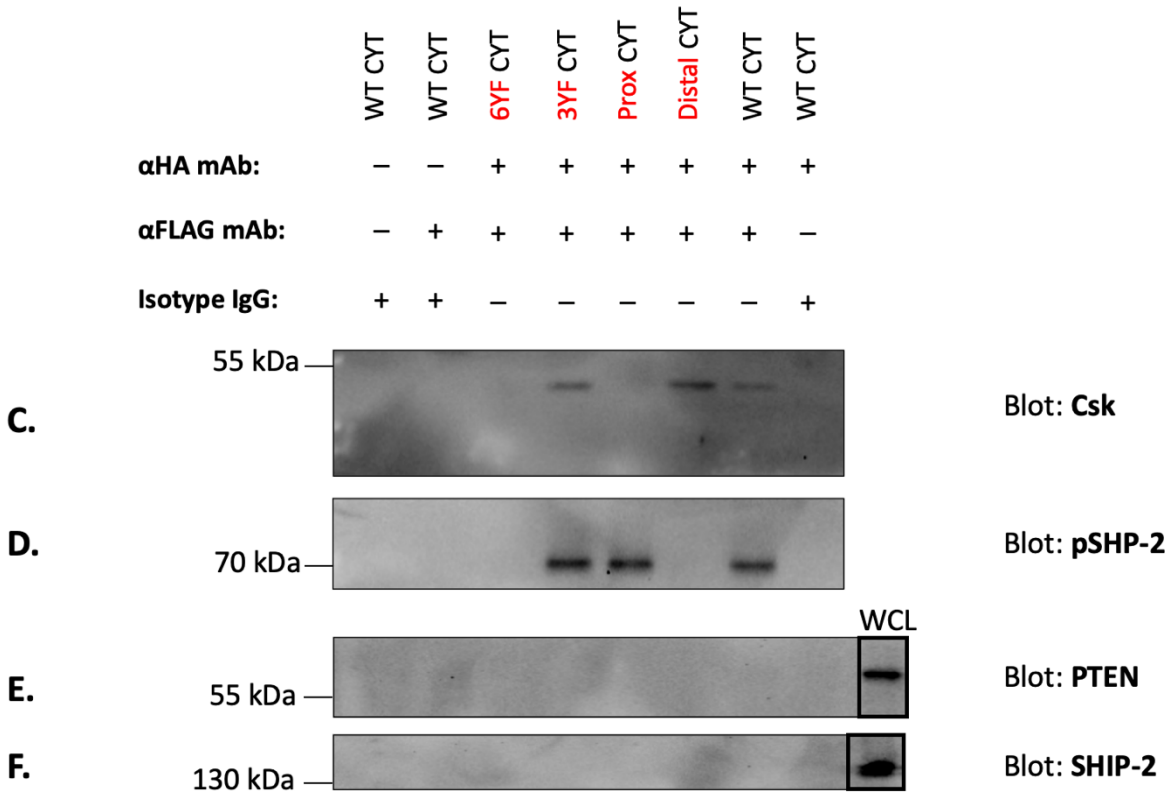
WT CYT
WT CYT
6YF CYT
3YF CYT
Prox CYT
Distal CYT
WT CYT
WT CYT
αHA mAb: – – + + + + + +
αFLAG mAb: – + + + + + + –
Isotype IgG: + + – – – – – +
55 kDa
C.
Blot: Csk
D.
70 kDa
Blot: pSHP-2
WCL
E.
55 kDa
Blot: PTEN
F.
130 kDa
Blot: SHIP-2

Figure 6.3. Selective recruitments of Csk and pSHP-2 molecules to tyrosine 453 and ITIMs in the CYT of 1.1b$^{WT\ CYT}$ following co-crosslinking with 2.6b$^{ITAM\ CYT}$. Stable cells (3×10^5) co-expressing 2.6b$^{ITAM\ CYT}$ and various 1.1b^{CYT} constructs were incubated with 3 μm magnetic beads (3×10^6). These magnetic beads were opsonized with indicated mAbs and isotype IgG ('+' and '-' indicate the presence and absence of corresponding proteins respectively during beads opsonization) to independently crosslink 2.6b$^{ITAM\ CYT}$ and 1.1b$^{WT\ CYT}$ or co-crosslinking 2.6b$^{ITAM\ CYT}$ with various 1.1b^{CYT} constructs. After 8 min incubation at 37 ℃, cells were immediately lysed on ice for 30 min and then magnetic beads were separated and washed three times before subjected to SDS-PAGE, transferred to nitrocellulose membrane and probed with αFLAG mAbs and αHA mAbs to examine successful pull-down of various 1.1b^{CYT} (A) and 2.6b$^{ITAM\ CYT}$ constructs (B). Co-immunoprecipitation of potential effector molecules was further examined by probing membrane with (C) an αCsk mAbs or stripping the membrane in (A) and reprobe with αpSHP-2 mAbs (D). Same batch of samples in the same order with the addition of whole cell lysates (WCL) in the rightmost lane were loaded and subjected for Western blot as described above and membranes were probed for PTEN (E) and SHIP-2 (F). Blots are representatives of at least two independent experiments.

A.

2.6b/1.1b$^{WT\ CYT}$

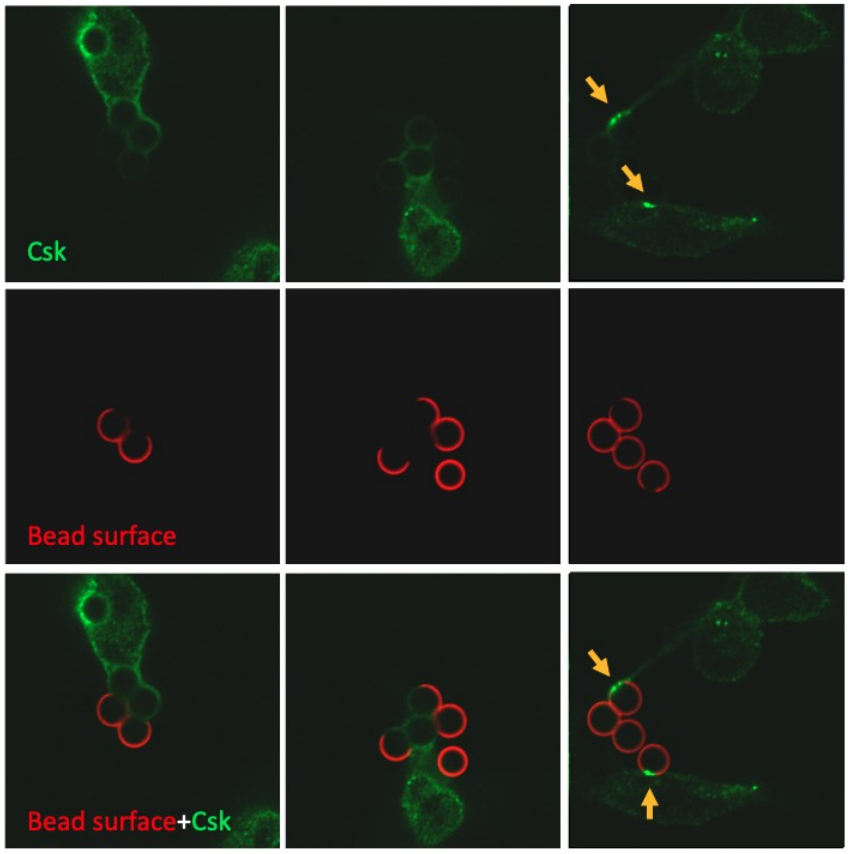

αHA mAb:	-	+	+
αFLAG mAb:	+	-	+
Isotype IgG:	+	+	-

B.

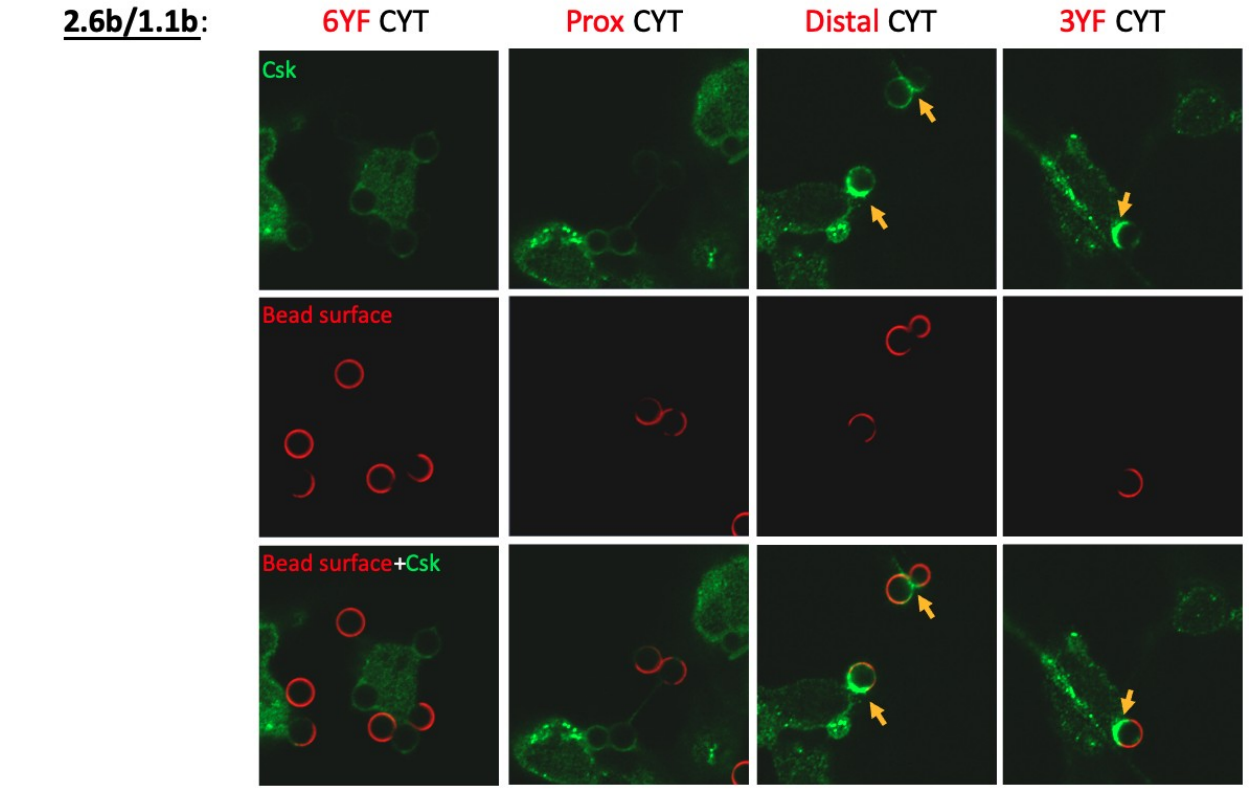
2.6b/1.1b:
6YF CYT
Prox CYT
Distal CYT
3YF CYT
Csk
Bead surface
Bead surface+Csk
αHA mAb: + + + +
αFLAG mAb: + + + +
Isotype IgG: - - - -

C.

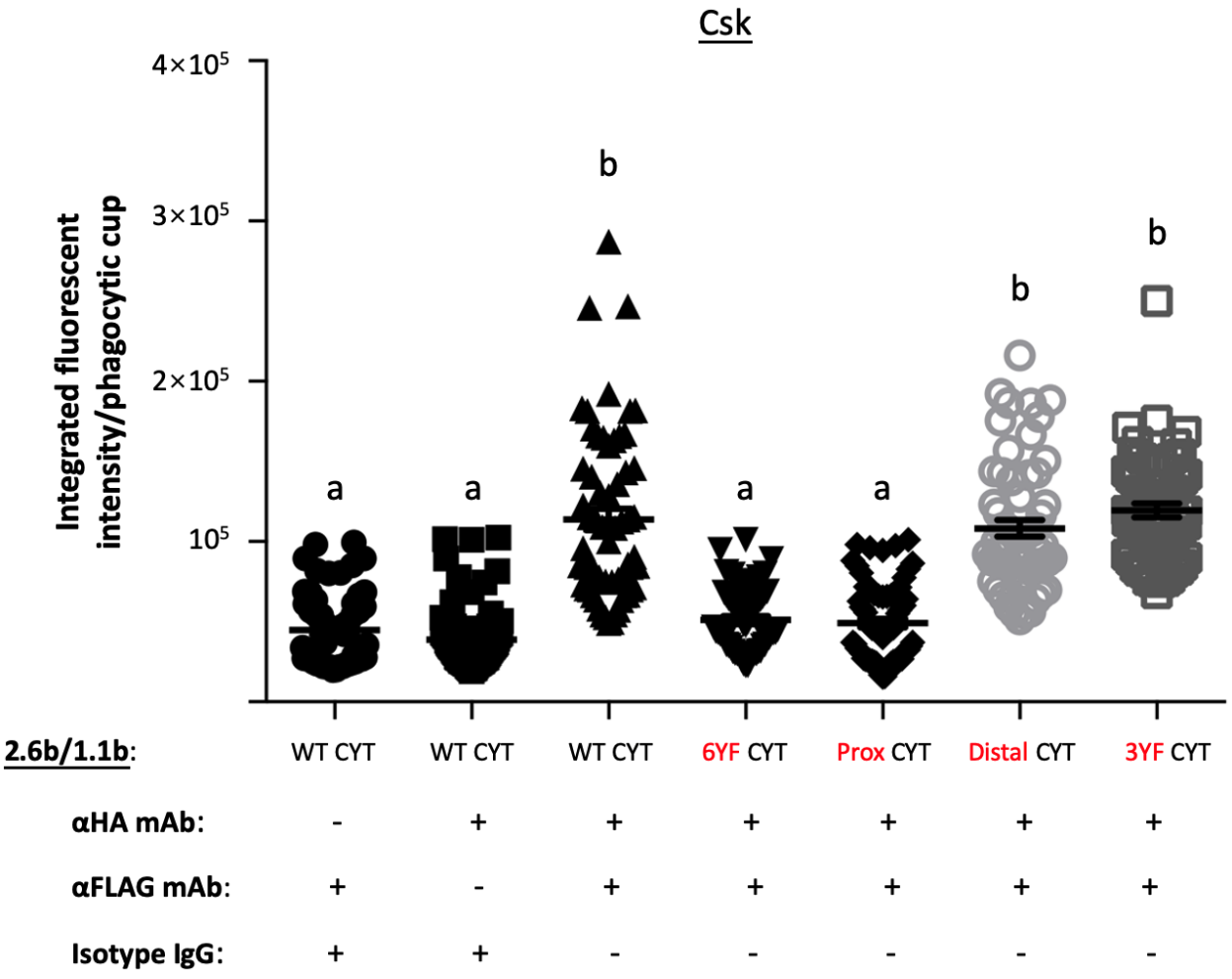
Csk
Integrated fluorescent intensity/phagocytic cup
4×10^5
3×10^5
2×10^5
10^5
a
a
b
a
a
b
b
2.6b/1.1b:
WT CYT
WT CYT
WT CYT
6YF CYT
Prox CYT
Distal CYT
3YF CYT
αHA mAb: - + + + + + +
αFLAG mAb: + - + + + + +
Isotype IgG: + + - - - - -

Figure 6.4. Confocal microscopy analysis of Csk recruitments to phagocytic cups following co-crosslinking of IpLITR constructs. Stable AD 293 cells (2×10^5) co-expressing $2.6b^{ITAM\ CYT}$ and $1.1b^{WT\ CYT}$ (A) or other $1.1b^{\ CYT}$ constructs with various tyrosine mutations (B) were grown on coverslips and incubated with 4.5 μm non-fluorescent (NF) beads opsonized with indicated mAbs and isotype IgG ('+' and '-' indicate the presence and absence of corresponding proteins respectively) at 37 ℃. After 8 min incubation, cells were fixed with 4% PFA for 10 min and partially internalized beads were then stained using Cy5-conjugated goat-anti-mouse secondary mAbs. After beads staining, cells were permeabilized and stained for recruitments of Csk molecules via first incubating with a rabbit αCsk mAbs and then a secondary goat-anti-rabbit mAbs conjugated to FITC. Z-stack images were then obtained at a magnification of 63× using a Zeiss LSM 710 scanning confocal microscope. Representative images from z-stack acquisitions are shown as images showing effector molecules of interest (green) staining alone, surface-bound beads (red) staining alone, merged-fluorescence images or brightfield-fluorescence merged images using the Zen 2009 imaging software. (C) Quantitative analyses of Csk molecules recruited to phagocytic cups under different conditions were performed as previously described in Figure 5.8 using Fiji software. At least 50 phagocytic cups from three independent experiments were analyzed and represented as mean integrated fluorescent intensity ± SEM. Letters indicate statistical significance ($P \leq 0.05$) between the means.

A.

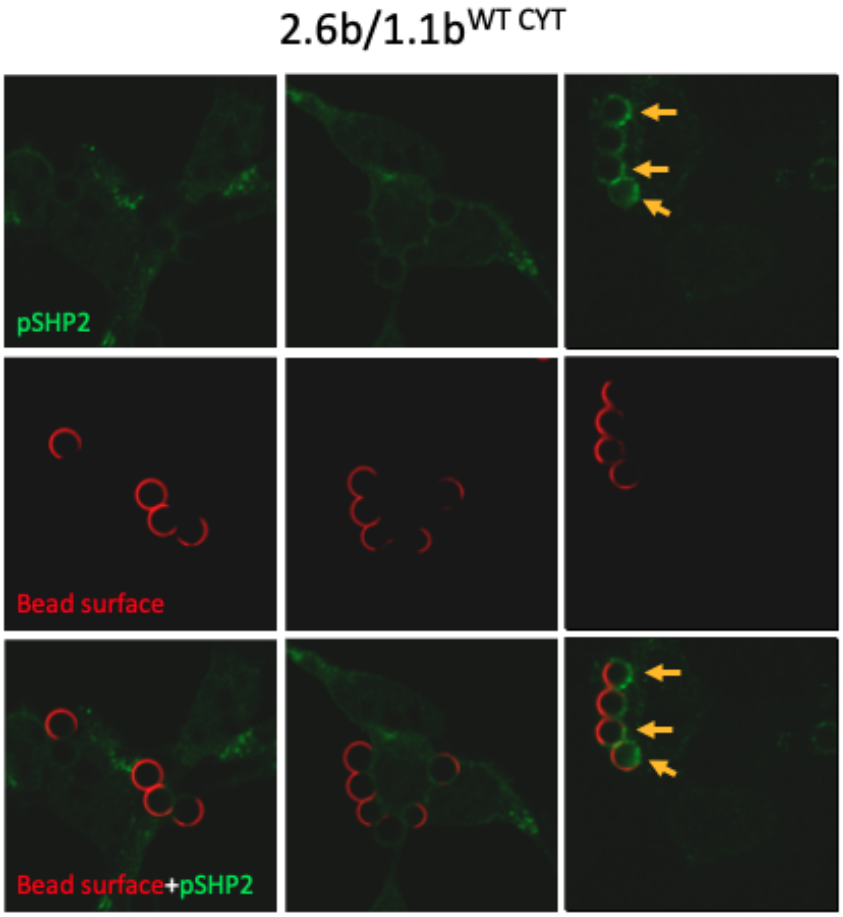

αHA mAb:	-	+	+
αFLAG mAb:	+	-	+
Isotype IgG:	+	+	-

B.

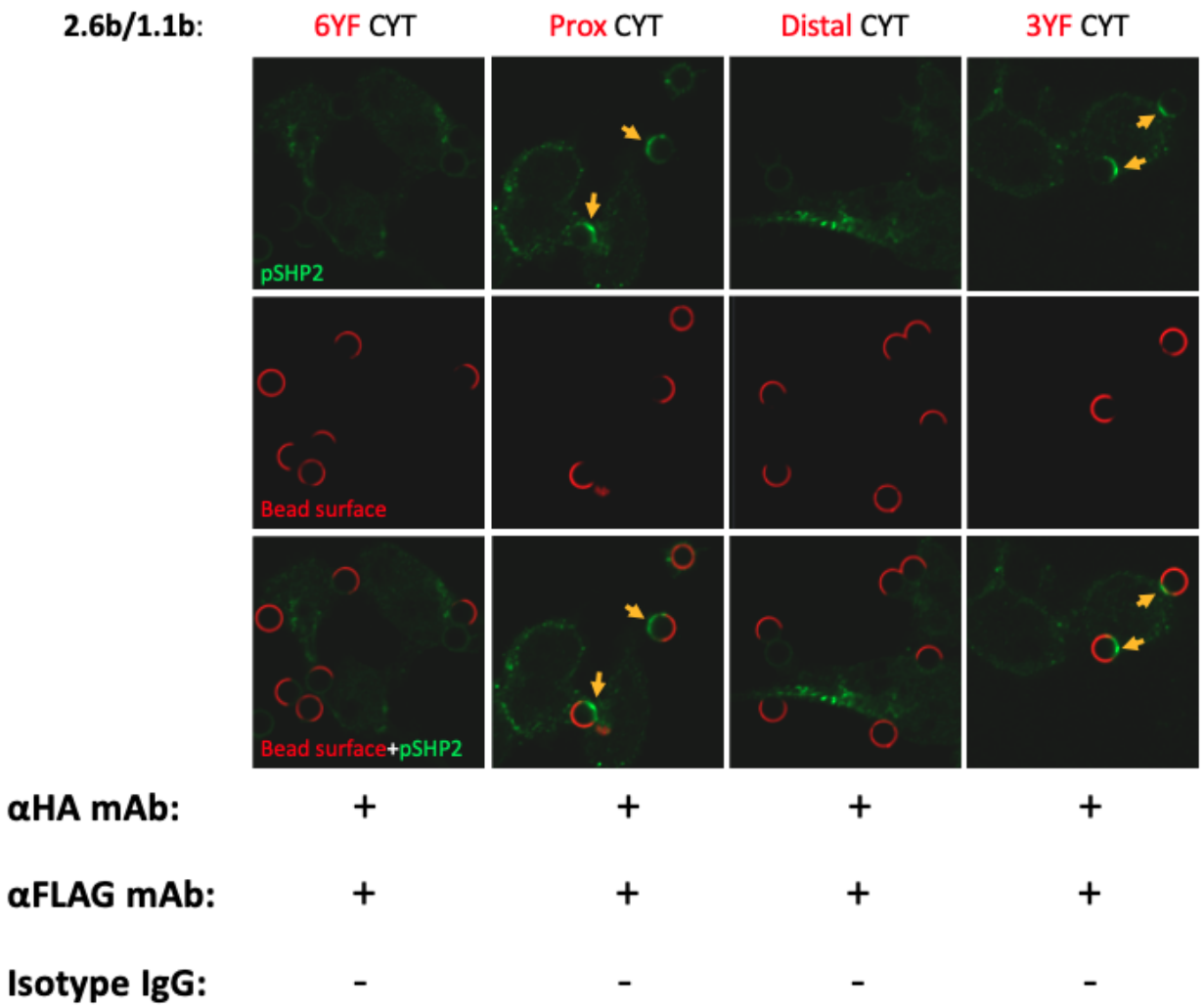
2.6b/1.1b:
6YF CYT
Prox CYT
Distal CYT
3YF CYT
pSHP2
Bead surface
Bead surface+pSHP2
αHA mAb: + + + +
αFLAG mAb: + + + +
Isotype IgG: - - - -

C.

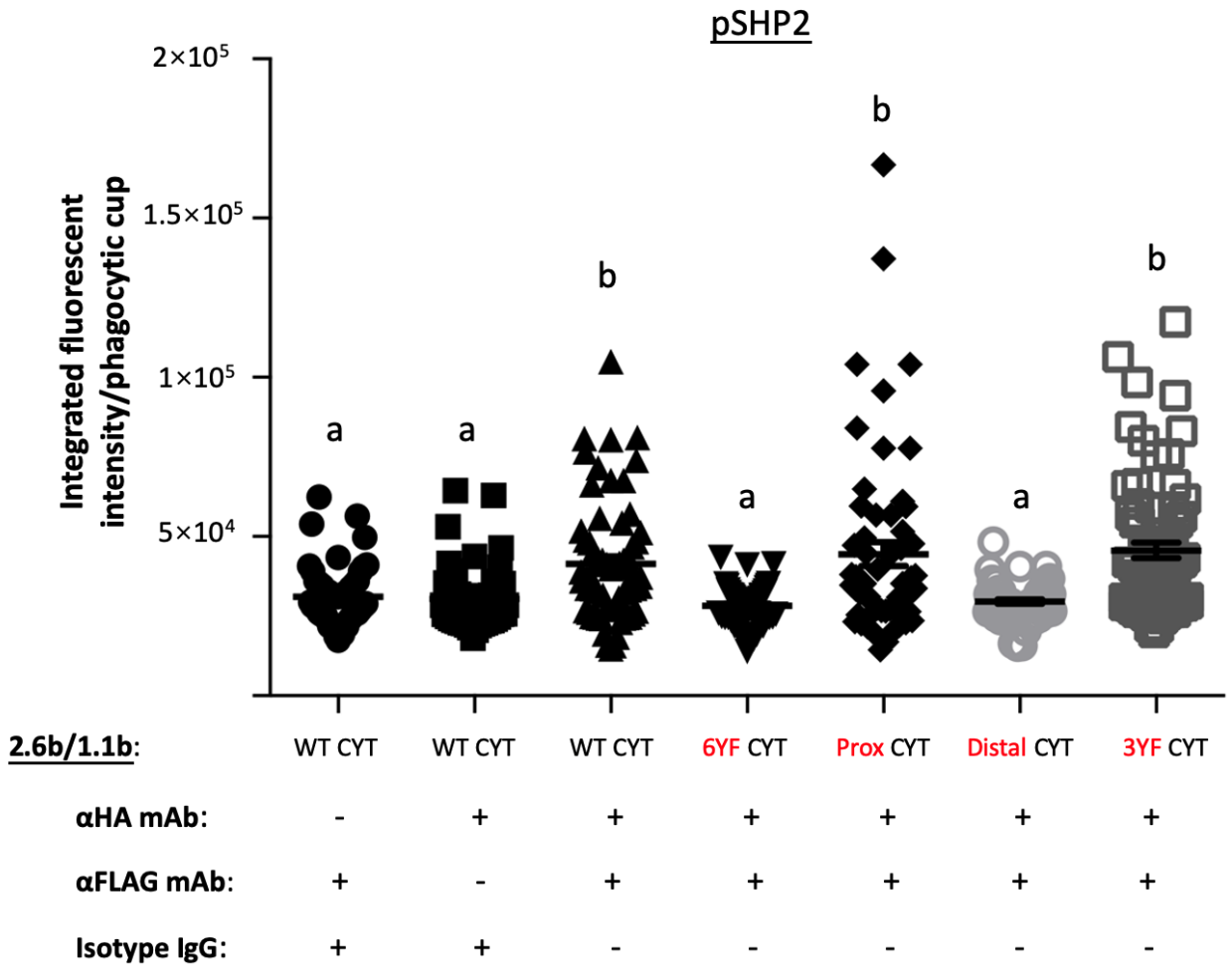
pSHP2
Integrated fluorescent intensity/phagocytic cup
2×10^5
1.5×10^5
1×10^5
5×10^4
a
a
b
a
b
a
b
2.6b/1.1b:
WT CYT
WT CYT
WT CYT
6YF CYT
Prox CYT
Distal CYT
3YF CYT
αHA mAb: - + + + + + +
αFLAG mAb: + - + + + + +
Isotype IgG: + + - - - - -

Figure 6.5. Confocal microscopy analysis of pSHP-2 recruitments to phagocytic cups following co-crosslinking of IpLITR constructs. Stable AD 293 cells (2×10^5) co-expressing $2.6b^{ITAM\ CYT}$ and $1.1b^{WT\ CYT}$ (A) or other $1.1b^{\ CYT}$ constructs with various tyrosine mutations (B) were grown on coverslips and incubated with 4.5 μm non-fluorescent (NF) beads opsonized with indicated mAbs and isotype IgG ('+' and '-' indicate the presence and absence of corresponding proteins respectively) at 37 ℃. After 8 min incubation, cells were fixed with 4% PFA for 10 min and partially internalized beads were then stained using Cy5-conjugated goat-anti-mouse secondary mAbs. After beads staining, cells were permeabilized and stained for recruitments of pSHP-2 molecules via first incubating with a rabbit αpSHP-2 mAbs and then a secondary goat-anti-rabbit mAbs conjugated to FITC. Z-stack images were then obtained at a magnification of 63× using a Zeiss LSM 710 scanning confocal microscope. Representative images from z-stack acquisitions are shown as images showing effector molecules of interest (green) staining alone, surface-bound beads (red) staining alone, merged-fluorescence images or brightfield-fluorescence merged images using the Zen 2009 imaging software. (C) Quantitative analyses of pSHP-2 molecules recruited to phagocytic cups under different conditions were performed as previously described in Figure 5.8 using Fiji software. At least 50 phagocytic cups from three independent experiments were analyzed and represented as mean integrated fluorescent intensity ± SEM. Letters indicate statistical significance ($P \leq 0.05$) between the means.

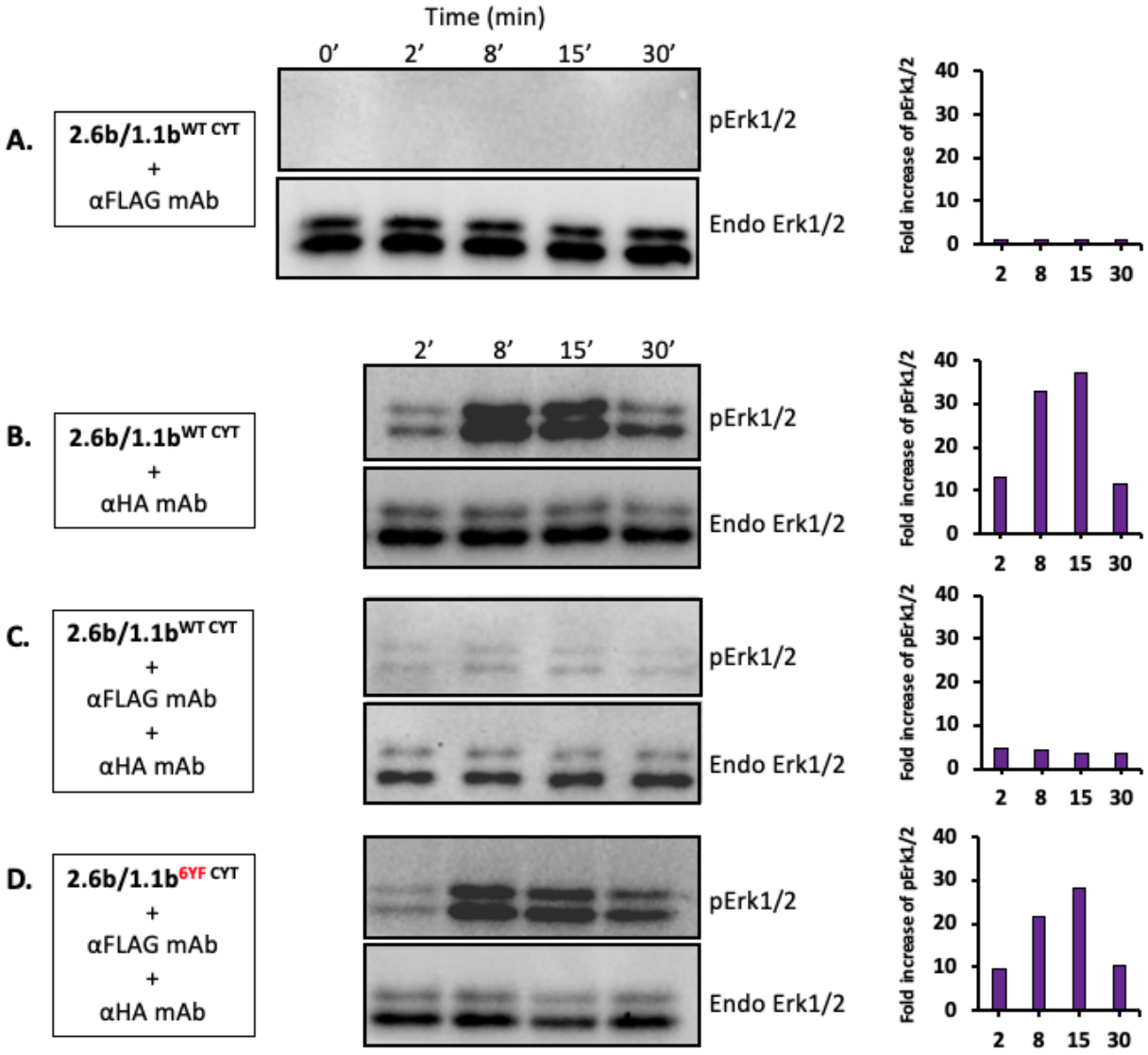
Time (min)
0′
2′
8′
15′
30′
A.
2.6b/1.1b WT CYT
+
αFLAG mAb
pErk1/2
Endo Erk1/2
Fold increase of pErk1/2
40
30
20
10
0
2
8
15
30
B.
2.6b/1.1b WT CYT
+
αHA mAb
C.
2.6b/1.1b WT CYT
+
αFLAG mAb
+
αHA mAb
D.
2.6b/1.1b 6YF CYT
+
αFLAG mAb
+
αHA mAb

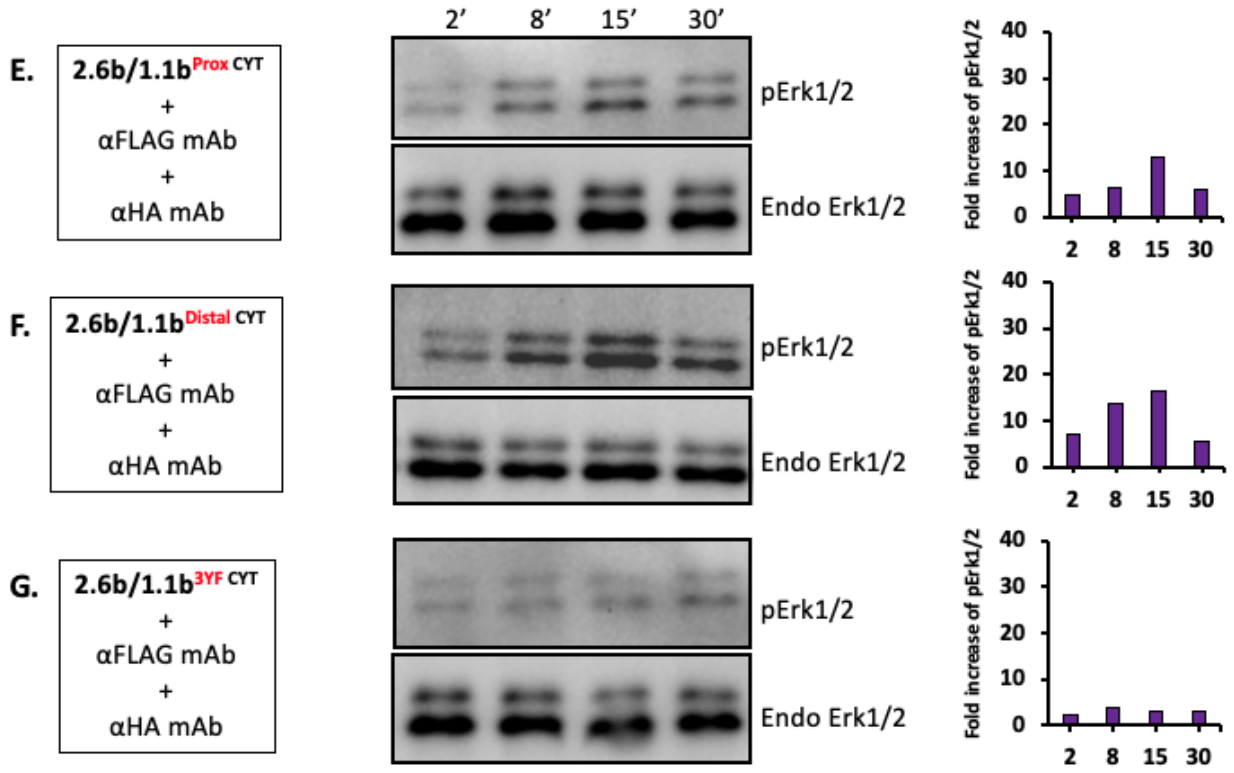

Figure 6.6. Examination of Erk1/2 activation in IpLITR-activated AD 293 cells. 2.6b/1.1b$^{WT\ CYT}$ stable cells (3×10^5) were incubated with 4.5 µm YG beads (9×10^5) opsonized with αFLGA or αHA mAbs to crosslink 1.1b$^{WT\ CYT}$ (A) and 2.6b$^{ITAM\ CYT}$ (B) constructs for indicated time points at 37℃, respectively. Cell lysates were then blotted with either α-phospho-p44/42 MAPR (Erk1/2) (Thr202/Tyr204) (E10) mouse mAb (A, B; top) or α-p44/42 MAPK (Erk1/2) mouse mAb (Endo; A, B; bottom) followed by a goat-α-mouse IgG (H+L) HRP-conjugated pAb. In co-crosslinking groups, same experimental procedures as described above were used except 4.5 µm YG beads were opsonized with both αFLGA and αHA mAbs to co-crosslink 2.6b$^{ITAM\ CYT}$ with various 1.1b^{CYT} constructs (C-G). Band intensity values were obtained by densitometry using Fiji software. Changes in phospho-Erk1/2 levels are reported as fold induction values relative to untreated 2.6b/1.1b$^{WT\ CYT}$ stable cells (i.e. 0 min), which is set to 1.0 (not shown on the graph) as calculated below. Phospho- Erk1/2 band intensity levels were corrected for endogenous molecule levels using the following equation: (phospho-molecules densitometry value for the time point/endo-molecules value for the time point). This corrected value was then divided by the value obtained from 0 min (i.e. unstimulated cells). Results are representative of 2 independent experiments that gave similar results.

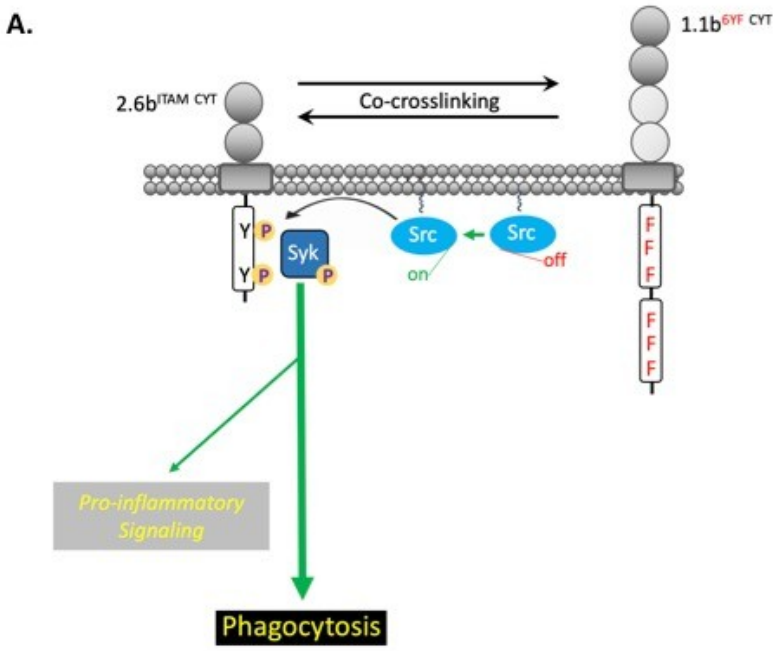
A.
1.1b6YF CYT
2.6bITAM CYT
Co-crosslinking
Y P
Y P
Syk
P
Src
on
Src
off
F
F
F
F
F
F
Pro-inflammatory Signaling
Phagocytosis

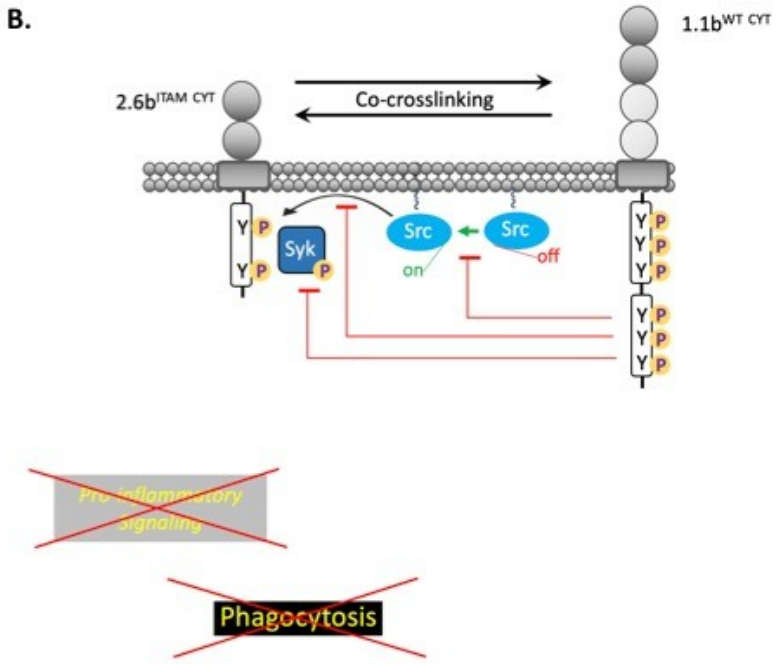
B.
1.1bWT CYT
2.6bITAM CYT
Co-crosslinking
Y P
Y P
Syk
P
Src
on
Src
off
Y P
Y P
Y P
Y P
Y P
Y P
Pro-inflammatory Signaling
Phagocytosis

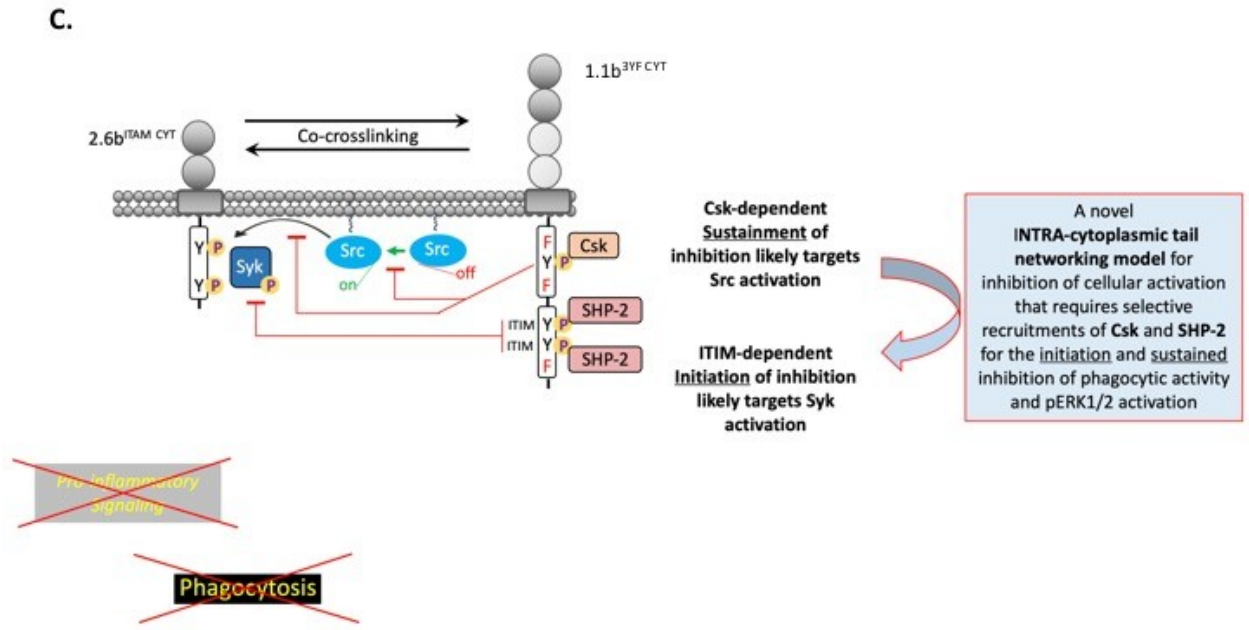

Figure 6.7. Hypothesized mechanism of 1.1b$^{WT\ CYT}$-mediated cross-inhibition of ITAM-driven phagocytosis. (A) Co-crosslinking 2.6b$^{ITAM\ CYT}$ and 1.1b$^{6YF\ CYT}$ constructs induce ITAM-dependent signaling events, including the activation of Src family kinases and recruitment of Syk to phosphorylated ITAMs. These proximal signaling events collectively promote downstream inflammatory signals and phagocytosis. However, these downstream events are cross-inhibited following co-crosslinking of 2.6b$^{ITAM\ CYT}$ and 1.1b$^{WT\ CYT}$ constructs and as demonstrated in (B), both Src family kinases and Syk may be targeted for the inhibitory effect. (C) An intro-cytoplasmic tail networking model is proposed to explain underlying mechanisms for the cross-inhibition of 2.6b$^{ITAM\ CYT}$-mediated phagocytosis. Following receptor co-crosslinking, tyrosine residues within CYT of 1.1b$^{WT\ CYT}$ were *trans*-phosphorylated by Src kinases recruited to 2.6b$^{ITAM\ CYT}$ and in return, this leads to the production of inhibitory signals. For example, recruitment of SHP-2 phosphatases to ITIMs of 1.1b$^{WT\ CYT}$ initiates the inhibition by reducing the activity of Syk; whereas inhibitory kinases (i.e Csk) recruited to the proximal region (i.e. tyrosine 453) of 1.1b$^{WT\ CYT}$ sustain the inhibitory effect by converting Src kinases back into auto-inhibitory conformation. Collectively, SHP-2 phosphatases and Csk kinases work in concert to target their specific substrates and exert inhibitory effects on Erk1/2 phosphorylation and phagocytosis.

CHAPTER VII

GENERAL DISCUSSION AND FUTURE DIRECTIONS

7.1 Summary of thesis findings

The functional characterization of IpLITRs has advanced our understanding of mechanistic details underlying the regulation of various innate effector responses. These teleost proteins share key characteristics with many paired immunoregulatory receptor-types in mammals including KIRs, LILRs and FcRs that regulate cytotoxicity, degranulation and phagocytosis (7–12). Therefore, IpLITRs are an excellent comparative vertebrate model that offers an opportunity to better understand the divergent and conserved aspects of regulating innate immune processes. Previous research in our lab primarily relied on heterologous overexpression in mammalian immune cell lines for examination of the functions of IpLITRs, which offered new information regarding the immunoregulatory potential of these teleost proteins in controlling various innate effector responses via a dynamic range of signaling versatility. For example, a putative inhibitory IpLITR type (i.e. $1.1b^{WT\ CYT}$) that contained ITIMs in its CYT region induced a distinct phagocytic phenotype when overexpressed in RBL-2H3 cells (4,13). These observations are consistent with the emerging theme of signaling versatility, suggesting that the functional outcome of immunoregulatory receptor engagement does not always coincide with the presence of canonical tyrosine-based motifs, as alternative mechanisms of ITAM- or ITIM-dependent signaling events may contribute to the functional plasticity. Further investigations regarding the dynamic signaling potentials of these teleost proteins using representative IpLITR types as models will significantly expand our knowledge of mechanistic details underlying this dual-regulatory property of innate effector responses. In my thesis research, I first established a new heterologous expression system using the AD293 fibroblast cell line and developed an imaging flow cytometry-based assay to further explore signaling

potentials of representative IpLITR types. This technical advancement allowed me to examine the signaling capabilities of various IpLITR types in a high throughput fashion and as demonstrated in my results, the 1.1b$^{WT\ CYT}$-mediated distinct phagocytic phenotype observed in RBL-2H3 cells was not recapitulated in AD293 cells, suggesting that engagement of 1.1b$^{WT\ CYT}$ results in selective recruitments of intracellular effectors for the intricate tuning of immune processes in a context-dependent manner. In chapter V, I demonstrated for the first time that IpLITR types can not only function independently, but that they also integrate proximal signaling events downstream via receptor crosstalk to modulate innate effector responses (i.e. phagocytosis). This represents the first report of IpLITR-mediated integrated control of phagocytosis via receptor crosstalk and significantly expands our understanding of potential roles of these immunoregulatory proteins. In chapter VI, I further investigated the mechanistic details underlying the cross-inhibition of phagocytosis and I proposed a model by which classical inhibitory molecules work in concert to diminish positive signals below an activation threshold, which added further insights of the regulatory mechanisms of IpLITR-mediated crosstalk inhibition of phagocytosis. The significance and contributions of my thesis findings summarized above will be further discussed below. Overall, my thesis research provides the first evidence for IpLITR-mediated crosstalk regulation of the phagocytic process and will serve as a stepping-stone for further investigation of the precise *in vivo* roles of IpLITRs.

Previous functional studies in our lab had focused on the characterization of two representative IpLITR members (i.e. 2.6b$^{ITAM\ CYT}$ and 1.1b$^{WT\ CYT}$). These studies revealed conserved and divergent aspects regarding immunoregulatory receptors in the control of various effector responses (4,10–16). For example, 2.6b$^{ITAM\ CYT}$ represents a classical stimulatory IpLITR-type that independently activates phagocytosis using classic ITAM-driven signaling

cascades (4,11,13). Comparatively, 1.1b$^{WT\ CYT}$ was originally characterized as an inhibitory receptor that blocked cytotoxic responses in NK cells through recruitment of Csk and SHP proteins (10,12). However, it was also shown that 1.1b$^{WT\ CYT}$ induced a distinct phagocytic phenotype using an alternative ITAM-independent signaling pathways when overexpressed in RBL-2H3 cells (i.e. 1.1b$^{WT\ CYT}$-expressing cells induced the formation of filopodia-like structures to capture and secure targets onto the plasma membrane (4,15)). Further confocal microscopic analysis revealed that 1.1b$^{WT\ CYT}$ is constitutively associated with Nck and upon encountering phagocytic targets, pSyk molecules were also recruited to 1.1b$^{WT\ CYT}$ in the filopodia-like structures, likely to initiate signaling cascades for targets uptake (16). This selective recruitment of distinct intracellular effectors for the intricate tuning of respective responses in a context-dependent manner is consistent with dual-regulatory features observed in the mammalian FCRL family. For instance, ligation of FCRL3 had potent co-stimulatory effects on TLR9-mediated activation of innate-like B cells, but repressed plasma B cell differentiation and antibody production (198). This dual-regulatory effects on B cell activity is likely dependent on the presence of both canonical ITIM and ITAM-like motifs in the CYT region that allows for networking through distinct signaling pathways. Of note, IpLITRs are distantly related to FCRLs and some IpLITR types (e.g. 1.1b$^{WT\ CYT}$) are also equipped with similar CYT configuration, in which ITIMs and other tyrosine-based motifs with various signaling potentials are found (7,8,13,14). This raises an interesting possibility that this dual-regulatory property might have been preserved as an efficient mechanism for regulating effector responses throughout evolution and the ability of 1.1b $^{WT\ CYT}$ to exert both inhibitory and activating effects on immune responses provides an alternative vertebrate model system to further understand conserved mechanistic details underlying this functional plasticity.

In chapter IV, I established a heterologous expression system using AD293 cells. The use of AD293 cells offers some advantages over heterologous expression systems previously used in our lab for exploring IpLITR-mediated signaling events underlying control of the phagocytic process. As fibroblasts, AD293 cells possess signalling components to control dynamic actin polymerization and membrane polarization but they do not express the classic phagocytic receptors that trigger the sub-membrane signaling events required for the internalization of foreign targets. This eliminates the potential for activation of endogenous phagocytic receptors expressed on immune cell-types that may interfere with IpLITR-mediated signaling events. Therefore, the AD293 cell line is a useful tool for investigating intracellular events during phagocytosis and has assisted in functionally characterizing a number of phagocytic receptors, including mammalian FcRs (123). Furthermore, unlike immune cell lines that suffer from low transfection efficiency, AD293 cells are easily transfectable and offer an opportunity to examine integrated control of phagocytic process using multiple IpLITR-types. As demonstrated in my results, the putative stimulatory IpLITR type (i.e. 2.6b$^{WT\ CYT}$) induced robust phagocytic responses in AD293 cells, which was similar to the phenotype observed in 2.6b$^{WT\ CYT}$-expressing RBL-2H3 cells (4,13). Furthermore, mutating tyrosines within IpFcRγ-L ITAMs completely abolished phagocytosis, suggesting this gain-of-function is specifically dependent on IpLITR-mediated ITAM-driven signaling cascades and further reinforce that AD293 cells are useful tools for investigating signaling potentials of IpLITR types in regulating phagocytosis. To re-examine the distinct phagocytic phenotype observed in 1.1b$^{WT\ CYT}$-expressing RBL-2H3 cells and to further characterize underlying molecular details using AD293 cells, I showed that ImageStream flow cytometry is a high throughput platform to accurately discriminate surface-bound targets (i.e. cells only with surface-bound targets) from those that are phagocytosed (i.e. cells with at

least one internalized target). This represents a technical advancement in comparison to the previous confocal microscopy-based method that is time-consuming and suffers from small sample sizes (e.g. usually hundreds of cells were manually examined for the analysis). Furthermore, the ImageStream-based method allows for an efficient screen of multiple constructs to identify signaling motifs that are involved in transducing signals during the phagocytic processes. My results show the observed phagocytic phenotype in RBL-2H3 cells is not recapitulated in $1.1b^{WT\ CYT}$-expressing AD293 cells, which only demonstrated basal level of phagocytosis (~9%). This discrepancy of observed results is likely due to the signaling versatility of $1.1b^{WT\ CYT}$ through selective recruitments of intracellular effectors in a context-dependent manner. Furthermore, the expression level and profile of signaling molecules vary between different cell types (i.e. myeloid vs. epithelioid cells), which may also influence the functional outcome. For example, co-crosslinking of FCRL5 with B cell receptors inhibits marginal zone B cell activation; whereas no inhibitory effect is observed following co-crosslinking in peritoneal cavity derived B-1 B cells due to comparatively lower SHP-1 levels (199). Overall, the establishment of this AD293 heterologous expression system coupled with a high throughput imaging flow cytometry-based assay provides a valuable platform to explore dynamic signaling potentials of IpLITRs in regulating phagocytosis. In addition, the re-examination of the signaling capabilities of representative IpLITR types (i.e. $1.1b^{WT\ CYT}$) suggests that ligation of $1.1b^{WT\ CYT}$ does not induce phagocytosis likely due to the activation of alternative signaling pathways in AD293 cells. This opens up new avenues for exploring the signaling potential of $1.1b^{WT\ CYT}$.

In Chapter V, I further explored the hypothesis that ligation of $1.1b^{WT\ CYT}$ in AD293 cells may result in the production of inhibitory signals. Unlike the active engulfment of phagocytic targets after activating $2.6b^{ITAM\ CYT}$ in AD293 cells, $1.1b^{WT\ CYT}$ cells only demonstrated a binding

activity after encountering targets. Similarly, engagement of the ITIM-containing human FcγRIIB receptor results in binding of opsonized targets, suggesting that FcγRIIB does not induce but rather can regulate phagocytosis via downstream (i.e. ITIM-mediated) signaling events (200). Further studies showed that FcRIIB cross-inhibits FcγRIIA-mediated phagocytosis following receptor co-crosslinking (131). This result, along with observations from studies on other immunoregulatory receptor families (e.g. KIRs and LILRs), suggests a common theme in regulating various effector responses through receptor crosstalk. Activating receptors and their inhibitory counterparts within the same receptor families are often co-expressed on immune cells and the extracellular domains of these paired receptors are highly similar, suggesting they bind the same ligand(s), resulting in the integrated control of downstream effector responses. Indeed, selected examples of paired receptors, including FcRs and KIRs, show that their effector responses (i.e. phagocytosis and cytotoxicity) are tightly controlled by integrated proximal signaling events due to receptor crosstalk mechanisms. Of note, stimulatory and inhibitory IpLITR-types are also likely co-expressed by catfish immune cell-types and thus, integrated signaling between these proteins may be important for their overall immunoregulatory functions. Furthermore, known IpLITRs (e.g. $2.6^{ITAM\ CYT}$ and $1.1b^{WT\ CYT}$) have very similar membrane distal Ig-like domains (D1-D2 of $2.6^{ITAM\ CYT}$ and $1.1b^{WT\ CYT}$ share ~91% amino acid identity), raising the possibility that $1.1b^{WT\ CYT}$ may also cross-inhibit $2.6b^{WT\ CYT}$-mediated phagocytosis as demonstrated in the studies of FcRs. To test this hypothesis, I co-expressed $1.1b^{WT\ CYT}$ and $2.6b^{ITAM\ CYT}$ in AD293 cells and after co-crosslinking with antibody-opsonized beads, my results show that $1.1b^{WT\ CYT}$ exerted an inhibitory effect on the $2.6b^{ITAM\ CYT}$-mediated induction of phagocytosis by down-regulating phosphotyrosine signaling cascades. It has been well-established that the induction of phagocytosis is often associated with increases in tyrosine

phosphorylation of various intracellular signaling molecules. Inhibitory phosphatases, that specifically dephosphorylate kinases (e.g. Syk) and adaptor molecules (e.g. Grb2) are recruited to ITIM-containing receptors to abrogate phagocytosis (164,201,202). Indeed, recruitment of SHPs to the CYT of 1.1b$^{WT\ CYT}$ has been observed in previous biochemical assays and this observation strongly suggests that conserved regulatory mechanisms are used by immunoregulatory receptors across evolution to control phagocytosis. Overall, this represents the first report of receptor crosstalk for teleost immunoregulatory receptors causing the abrogation of an effector response and provides the basis for further understanding the mechanistic details underlying this important regulatory process.

In Chapter VI, I further investigated the molecular mechanisms controlling the inhibitory actions of 1.1b$^{WT\ CYT}$ on 2.6$^{ITAM\ CYT}$-mediated phagocytosis. I first tested the hypothesis that the membrane proximal and distal CYT of 1.1b$^{WT\ CYT}$ are capable of independently exerting inhibitory effects on phagocytosis as demonstrated previously in NK cells (10,12). However, my results showed that tyrosine-based motifs (i.e. tyrosine 453 and ITIMs) within both CYT segments are minimally required to sustain the inhibition on 2.6b$^{ITAM\ CYT}$-mediated phagocytosis. Subsequent biochemical assays further revealed coordinated recruitments of endogenous Csk and SHP-2 molecules to the CYT of 1.1b$^{WT\ CYT}$ and down-regulation of Erk1/2 phosphorylation during receptor crosstalk. Collectively, these observations strongly suggest a novel regulatory mechanism that required participation of both Csk and SHP-2 molecules to coordinately control phagocytosis. At present, we are only beginning to understand molecular details regarding the inhibitory roles of 1.1b$^{WT\ CYT}$ in regulating phagocytosis. However, based on the observations obtained from biochemical and functional assays, I propose a model in which Csk and SHP-2 molecules, recruited to the 2.6b$^{ITAM\ CYT}$-1.1b$^{WT\ CYT}$ signaling complexes, target specific

substrates and coordinately contribute to inhibiting ITAM-driven phagocytosis. Presumably, recruitments of Csk molecules to the 2.6b$^{ITAM\ CYT}$-1.1b$^{WT\ CYT}$ complex constantly attenuate signals by specifically targeting Src family kinases and reduce phosphorylation of ITAMs in the CYT region of 2.6b$^{ITAM\ CYT}$; whereas SHP-2 molecules exert their inhibitory effects on substrates downstream of Src family kinases to further diminish activating signals. Overall, Csk and SHP-2 molecules act in concert to sustain the inhibitory effects on ITAM-driven phagocytosis. Although Csk is a potent inhibitor of Src family kinases, bone marrow-derived macrophages from triple knock-out mice (hck$^{-/-}$, lyn$^{-/-}$, Fgr$^{-/-}$) only exhibit partial impairments of FcR-mediated phagocytosis (186). This observation indicates that a blockage of Src family kinases activity alone are not sufficient to shut down phagocytic machinery under certain contexts in which other effector molecules (e.g. Syk) may compensate for the absence of Src family kinases. In agreement with this hypothesis, 2.6b/1.1b$^{Distal\ CYT}$-expressing cells induced a robust phagocytic response even though the recruitment of Csk molecules still occurred. It is likely that Src family kinases activity is not completely abrogated by Csk molecules; instead, low levels of Src family kinases actively phosphorylate tyrosine residues within the tail region of receptors. This residual Src family kinases activity may phosphorylate ITAMs in the CYT region of 2.6b$^{ITAM\ CYT}$ facilitating recruitment of a relatively low level of Syk molecules to the site. It has been reported that Syk can phosphorylate ITAMs *in vitro* and therefore, it is possible that after binding to phosphorylated ITAMs, Syk itself can phosphorylate additional neighbouring ITAMs and this generates a positive feedback loop to amplify the signaling cascades and consequently induce phagocytosis in 2.6b/1.1b $^{Distal\ CYT}$-expressing cells. Therefore, additional inhibitory molecules are required to act in concert with Csk to contain the strength of activating signals below the threshold of activation. SHP-2 is a ubiquitously expressed phosphatase and has

been shown to serve as a versatile regulator in signal transduction (203–205). In the context of immunity, recruitments of SHP-2 molecules to respective immunoregulatory receptors have been reported to inhibit various effector responses by dephosphorylating critical signaling components (176,206,207). Although specific substrate(s) targeted by SHP-2 to sustain the inhibition of 2.6b$^{ITAM\ CYT}$-mediated phagocytosis remain to be identified, one possibility is that recruited SHP-2 reduce the activity of Syk by dephosphorylating its regulatory tyrosines. Syk serves as a critical signaling hub during phagocytosis, which directly activates various downstream effector molecules through kinase activities but it also facilitates the formation of signaling complexes by virtue of recruiting SH2 domain-containing molecules to the phosphorylated regulatory tyrosines (44,57,144,208,209). Reduced phosphorylation of tyrosine 346 on Syk is responsible for delayed initiation of phagocytosis in mouse macrophage (187). This is consistent with the observation in 2.6b/1.1b$^{Prox\ CYT}$-expressing cells that recruitment of SHP-2 molecules alone can inhibit phagocytosis at early time points but this phosphatase fails to sustain the inhibitory effect over time. Furthermore, the peptide sequence, ESP**Y**ADPEE, that flanked the regulatory tyrosine 352 (in bold; the equivalent site of tyrosine 346 on mouse Syk) on human Syk is enriched with acidic amino acids (underlined). This fits the pattern of potential SHP-2 substrates based on an unbiased screen of peptide libraries (210). Furthermore, it has been reported that this regulatory tyrosine residue is also responsible for the binding and activation of PLCγ1 (211). Therefore, dephosphorylation of this regulatory tyrosine residue may reduce the activity of PLCγ1 and results in defective Ras activation, which is upstream of Erk1/2 phosphorylation (212,213). Indeed, lower magnitudes of Erk1/2 phosphorylation were observed after co-crosslinking 2.6b$^{ITAM\ CYT}$ with 1.1b$^{Prox\ CYT}$ (i.e. SHP-2 recruitments only) compared with 1.1b$^{Distal\ CYT}$ (i.e. Csk recruitments only) as shown in my biochemical assays. However, it is likely that Csk molecules

also contribute to down-regulating Erk1/2 phoshorylation since the induction of Erk1/2 molecules is further diminished when Csk and SHP-2 molecules are both recruited. Apart from regulating the activity of Syk, SHP-2 can also exert its inhibitory effects on other downstream substrates that are involved in phagocytic pathways. For example, paxillin is a substrate of SHP-2 and this cytoskeletal-associated protein is phosphorylated upon triggering of FcRs-mediated phagocytosis (214). Impaired phagocytosis is also observed in macrophages with reduced phosphorylation of paxillin as a consequence of viral infection (215). With respect to 1.1b$^{WT\ CYT}$-mediated cross-inhibition of phagocytosis, recruited SHP-2 molecules may also dephosphorylate paxillin to disrupt cytoskeletal rearrangement.

Taken together, my findings represent the first report regarding receptor crosstalk of teleost proteins, which expands our knowledge regarding the molecular details during the control of phagocytosis. A schematic diagram is provided to describe the potential molecular mechanisms underlining 1.1b$^{WT\ CYT}$-mediated inhibition of ITAM-driven phagocytosis (Fig. 6.7). This data provides alternative models to further explore dynamic signaling potentials of IpLITRs and will serve as an essential stepping-stone for understanding *in vivo* roles of this diverse receptor family in teleost immunity. Furthermore, my work also offers a framework for functional characterization of immunoregulatory receptor from non-model organisms in general.

7.2 Future directions

7.2.1 Characterization of the role of Csk and SHP-2 in 1.1b$^{WT\ CYT}$-mediated cross-inhibition of phagocytosis

My results support the notion that 1.1b$^{WT\ CYT}$ recruits Csk and SHP-2 during receptor-mediated crosstalk regulation of the phagocytic process, indicating that these molecules are both involved in the negative regulation of phagocytosis. However, no direct evidence is provided to

show that Csk and SHP-2 directly contribute to producing inhibitory signals. To further confirm the contribution of these two inhibitory molecules, one could design RNAi primers to specifically knock-down the expression of Csk or SHP-2 in 2.6b/1.1b$^{WT\ CYT}$ AD293 lines and then after co-crosslinking of 2.6b$^{ITAM\ CYT}$ and 1.1b$^{WT\ CYT}$ constructs, phagocytosis could be re-examined and compared to the value of wild type 2.6b/1.1b$^{WT\ CYT}$-expressing cells. If inhibition of phagocytosis is still observed after knocking down SHP-2 and Csk, although these molecules are recruited to signaling complexes, they may be dispensable for the observed inhibition of phagocytosis.

Since Csk is a strict regulator of Src kinases family, an alternative approach to confirm that Csk contributes to down-regulating phagocytosis would be to purify Src kinases using specific mAbs from 2.6b/1.1b$^{WT\ CYT}$ lysates after receptor co-crosslinking. Then the activity of isolated Src kinases could be examined based on the phosphorylation state of the regulatory tyrosine residue (i.e. tyrosine 527) at the C-terminus. Alternatively, these eluted Src kinases could be incubated with their substrates (e.g. tyrosine-containing peptides) to examine their abilities to phosphorylate tyrosines *in vitro*. Experiments described here would provide further evidence of Csk involvement in the crosstalk inhibition of phagocytosis.

Currently, it is evident that following receptor co-crosslinking, translocation of Csk and SHP-2 to phagocytic cups occurs. Additional experiments could be performed to obtain more information regarding temporal recruitments of these two molecules. For example, are Csk and SHP-2 simultaneously recruited to phagocytic cups? Do they stay on the membrane throughout the whole process or dissociate from the membrane after acting on their substrates? To address these questions, I could clone Csk and SHP-2 into a fluorescent epitope-tagged expression vector and then co-transfect into 2.6b/1.1b$^{WT\ CYT}$. This would allow me to add co-opsonized targets

directly to live cells and then monitor the location of Csk and SHP-2 simultaneously using live cell imaging.

7.2.2 Unbiased screen of potential effector molecules recruited to 2.6b$^{ITAM\ CYT}$ -1.1b$^{WT\ CYT}$ signaling complex during receptor crosstalk

I have identified Csk and SHP-2 molecules within the signaling complex during IpLITR-mediated crosstalk inhibition of the phagocytic response. However, it is likely that other effector molecules are also recruited to the site and contribute to producing or sustaining inhibitory signals. Furthermore, downstream substrates targeted by these inhibitory molecules are largely unknown and investigating the identity of these missing puzzles would help better understanding mechanisms underlying 1.1b$^{WT\ CYT}$-mediated inhibition. To address these questions, an unbiased and sensitive technique is required to examine the identify of effector molecules involved in this process. For example, a proximity-dependent biotin identification approach named BioID represents a sensitive technique to investigate protein-protein interactions. Specifically, this technique is based on fusing a promiscuous *E. coli* biotin protein ligase to a targeting protein (e.g. 1.1b$^{WT\ CYT}$) thus any protein that is a near-neighbor of this fusion protein will be biotinylated. Consequently, biotinylated proteins can be isolated by affinity capture and further identified using mass spectrometry (216). In the context of identifying effector molecules recruited by 1.1b$^{WT\ CYT}$ during receptor crosstalk, I would generate a chimeric construct that fuses an *E. coli* biotin protein ligase to the C-terminus of 1.1b$^{WT\ CYT}$ and stably co-express this with 2.6b$^{ITAM\ CYT}$ in AD293 cells. This BioID system coupled with mass spectrometry would serve as a valuable platform to investigate potential effector molecules involved in the process following receptor crosstalk. Furthermore, I could perform co-crosslinking of 2.6b$^{ITAM\ CYT}$ and 1.1b$^{WT\ CYT}$ constructs for various time points to monitor the change of effector molecules recruited to the site over time.

7.2.3 Establishing in vivo models for studying LITRs biology

The IpLITR research in our lab has primarily relied on heterologous expression of IpLITR types in representative mammalian cell lines. Although these functional studies offer novel information regarding signaling potentials of IpLITRs, *in vivo* roles of these teleost proteins in regulating various innate effector responses remain largely unknown. Of note, similarity searches using IpLITRs as queries revealed that LITRs are not exclusive to channel catfish but are likely ubiquitous among teleost fish (7,217). Therefore, expanding *in vitro* research to other well-established *in vivo* fish models will significantly broaden our appreciation of the functions of this diverse receptor family in teleost immunity.

Recent studies in our lab have successfully cloned LITRs sequences in zebrafish (Hima Gurupalli, unpublished data) and this offers a valuable opportunity to investigate various aspects of LITR biology in a well-established fish model. For example, zebrafish larvae survive with only innate effector responses since adaptive immunity becomes functionally mature only after 4-6 weeks post fertilization (218–220). This temporal segregation from adaptive immune responses offers an excellent system to study the contribution of LITRs to innate immunity *in vivo.* Larvae with mutated LITR genes could be challenged with various types of pathogens (e.g. gram positive/negative bacteria and fungi) and the consequent mortality rate would be a good indicator of pathogens that may be recognized by LITR types. Furthermore, transgenic zebrafish lines with GFP-tagged LITRs would be valuable tools to understand the expression of these receptors in specific cell-types under homeostasis conditions, over the course of and infection, and also during developmental stages of the animal.

In agreement with the idea that this diverse receptor family is likely ubiquitous among teleost species, LITR sequences have also been identified in immune cells isolated from goldfish

(Jiahui Wang, unpublished data). This provides an alternative model system to functionally characterize these teleost proteins using well-established primary kidney macrophage (PKM) cultures in goldfish (221). PKM represents three distinct subpopulations, including progenitor cells, monocytes and macrophages; upon supplementing with appropriate colony-stimulating factors, progenitor cells can differentiate into mature macrophages under two distinct pathways: one is consistent with the traditional pathway of macrophage development in mammals that progenitor cells differentiate into monocytes which further mature into macrophages; the other one represents an alternative pathway that progenitor cells directly differentiate into mature macrophages. It would be interesting to characterize the expression profile of LITRs at each developmental stage and could potentially be identified as specific markers for respective differentiation pathways.

7.2.4 Identification of IpLITR ligands

One of the most interesting and yet difficult questions yet to be addressed about IpLITRs is the identity of their endogenous ligands. Answering this question will not only add to a greater understanding of the *in vivo* roles that IpLITRs play in controlling effector responses but will also help to determine if IpLITRs are functional orthologs to other immunoregulatory receptors across evolution. Furthermore, identification of endogenous ligands will largely advance IpLITR research from solely relying on heterologous expression system to a more physiologically relevant models (e.g. primary fish cells) for understanding the contributions of IpLITRs in teleost immunity.

Previous sequence alignment and structural modelling of IpLITRs D1 and D2 domains suggest a relationship to the mammalian LILR receptor family and amino acid residues critical for binding of MHC-I molecules have been identified in similar positions within the D1 domain

of some IpLITR-types. To test the hypothesis that IpLITRs may be involved in self/non-self recognition via MHC-I interactions, I would first generate recombinant IpLITRs proteins with a fluorescent epitope-tag (e.g. GFP) fused to the C-terminus. Then a binding assay could be performed by incubating these recombinant proteins with transfected cells that overexpress channel catfish MHC-I molecules. Binding between MHC-I and respective recombinant IpLITRs proteins could then be detected as increased fluorescent intensity on the flow cytometry.

Alternatively, fish immunoglobulins play a vital role in regulating effector responses in teleost immunity. With respect to channel catfish, two Ig isoforms (i.e. IgM and IgD) have been identified so far and are responsible for the induction of antibody-dependent cellular cytotoxicity (ADCC) and degranulation in IgM^+ NK-like cells and IgD^+ granulocytes isolated from channel catfish, respectively (1,222). Although a FcR homolog (i.e. IpFcRI) has been identified in channel catfish, this represents a secreted form of teleost FcRs with no identifiable transmembrane/CYT or GPI-linkage motifs (223). Therefore, the identity of putative FcμR and FcδR expressed on catfish immune cells remain to be established. IpLITRs represent an attractive candidate for binding teleost Igs as i) this polymorphic and polygenetic receptor family shares phylogenetic relationships with mammalian FcRs and FCRLs, and; ii) representative IpLITR types are capable of inducing effector responses (e.g. phagocytosis and degranulation) that are mediated by FcRs in mammals (110). Therefore, it would be interesting to explore the possibility that IpLITRs may recognize and bind teleost Igs. To address this hypothesis, I would use IpLITRs-expressing AD293 stable lines generated in this thesis study and then incubate cells with purified IgM and IgD that are labeled with fluorescent dyes. Then potential binding of IgM and IgD to respective IpLITR types can be detected on flow cytometry. Of note, IpLITR types may not recognize or bind monomeric Igs with low affinity and thus, Igs could be aggregated via

high temperatures incubation as described in (224). Alternatively, anti-TNP IgMs could be generated and purified from catfish serum (225), which could be used to opsonized large particles (e.g. TNP-haptenated red blood cells/latex beads) to further increase the binding avidity when incubate with IpLITR-expressing cells.

7.3 Final summary

It has been an emerging theme that some immunoregulatory receptors-types are capable of exerting both inhibitory and activating effects on immune responses, a term referred to as functional plasticity. This blurs the definition of inhibitory and activating receptors based on key structural features of their CYT regions. Recent studies, including those presented in this thesis, are providing new insights into mechanistic details underlying this dual-regulatory effects on effector responses. Initially our lab reported that $1.1b^{WT\ CYT}$ induced a distinct phagocytic phenotype when overexpressed in RBL-2H3 cells. However, a re-examination of this observation in AD293 cells indicates that $1.1b^{WT\ CYT}$ displays dual-regulatory features and exerts potent inhibitory effects on $2.6b^{ITAM\ CYT}$-mediated induction of phagocytosis. This dynamic signaling potential of $1.1b^{WT\ CYT}$ is likely dependent on networking through distinct signaling pathways and consequently, facilitate intricate tuning of effector responses under different contexts. As such, my work provides new evidence in support of the hypothesis that the ability of certain immunoregulatory receptors to exhibit functional plasticity in regulating effector responses may represent a conserved yet important regulatory mechanism that has been preserved throughout evolution. Furthermore, my results also provide new insights into the regulation of innate effector responses and represents the first report of teleost immunoregulatory proteins operating during the crosstalk inhibition of phagocytosis. This information broadens our understanding of mechanistic details that occur during the control of phagocytosis and in

principle demonstrates that 1.1b$^{WT\ CYT}$ and its signaling capabilities can coordinately target specific signaling pathways to sustain the inhibitory effects. Overall, these foundational studies have set the stage for further exploring the dynamic signaling potentials controlled by immunoregulatory receptors and a path towards understanding the complex molecular mechanisms underlying immunoregulatory receptor functional plasticity features across vertebrates.

REFERENCES

1. Shen L, Stuge TB, Evenhuis JP, Bengtén E, Wilson M, Chinchar VG, Clem LW, Miller NW. Channel catfish NK-like cells are armed with IgM via a putative FcμR. *Developmental & Comparative Immunology* (2003) **27**:699–714. doi:10.1016/S0145-305X(03)00042-9

2. Shen L, Stuge TB, Zhou H, Khayat M, Barker KS, Quiniou SMA, Wilson M, Bengtén E, Chinchar VG, Clem LW, et al. Channel catfish cytotoxic cells: a mini-review. *Developmental & Comparative Immunology* (2002) **26**:141–149. doi:10.1016/S0145-305X(01)00056-8

3. Stuge TB, Wilson MR, Zhou H, Barker KS, Bengtén E, Chinchar G, Miller NW, Clem LW. Development and Analysis of Various Clonal Alloantigen- Dependent Cytotoxic Cell Lines from Channel Catfish. *The Journal of Immunology* (2000) **164**:2971–2977. doi:10.4049/jimmunol.164.6.2971

4. Lillico DM, Zwozdesky MA, Pemberton JG, Deutscher JM, Jones LO, Chang JP, Stafford JL. Teleost leukocyte immune-type receptors activate distinct phagocytic modes for target acquisition and engulfment. *Journal of leukocyte biology* (2015) **98**:235–48. doi:10.1189/jlb.2A0215-039RR

5. Litman GW, Hawke NA, Yoder JA. Novel immune-type receptor genes. (2001) Available at: https://www.ingentaconnect.com/content/mksg/imr/2001/00000181/00000001/art00021 [Accessed February 6, 2020]

6. Stet RJM, Hermsen T, Westphal AH, Jukes J, Engelsma M, Lidy Verburg-van Kemenade BM, Dortmans J, Aveiro J, Savelkoul HFJ. Novel immunoglobulin-like transcripts in teleost fish encode polymorphic receptors with cytoplasmic ITAM or ITIM and a new structural Ig domain similar to the natural cytotoxicity receptor NKp44. *Immunogenetics* (2005) **57**:77–89. doi:10.1007/s00251-005-0771-9

7. Stafford JL, Bengten E, Du Pasquier L, McIntosh RD, Quiniou SM, Clem LW, Miller NW, Wilson M. A novel family of diversified immunoregulatory receptors in teleosts is homologous to both mammalian Fc receptors and molecules encoded within the leukocyte receptor complex. *Immunogenetics* (2006) **58**:758–73. doi:10.1007/s00251-006-0134-1

8. Stafford JL, Bengten E, Du Pasquier L, Miller NW, Wilson M. Channel catfish leukocyte immune-type receptors contain a putative MHC class I binding site. *Immunogenetics* (2007) **59**:77–91. doi:10.1007/s00251-006-0169-3

9. Mewes J, Verheijen K, Montgomery BC, Stafford JL. Stimulatory catfish leukocyte immune-type receptors (IpLITRs) demonstrate a unique ability to associate with adaptor signaling proteins and participate in the formation of homo- and heterodimers. *Molecular immunology* (2009) **47**:318–31. doi:10.1016/j.molimm.2009.09.014

10. Montgomery BC, Mewes J, Davidson C, Burshtyn DN, Stafford JL. Cell surface expression of channel catfish leukocyte immune-type receptors (IpLITRs) and recruitment of both Src homology 2 domain-containing protein tyrosine phosphatase (SHP)-1 and SHP-2.

Developmental and comparative immunology (2009) **33**:570–82. doi:10.1016/j.dci.2008.10.006

11. Cortes HD, Montgomery BC, Verheijen K, Garcia-Garcia E, Stafford JL. Examination of the stimulatory signaling potential of a channel catfish leukocyte immune-type receptor and associated adaptor. *Developmental and comparative immunology* (2012) **36**:62–73. doi:10.1016/j.dci.2011.06.004

12. Montgomery BC, Cortes HD, Burshtyn DN, Stafford JL. Channel catfish leukocyte immune-type receptor mediated inhibition of cellular cytotoxicity is facilitated by SHP-1-dependent and -independent mechanisms. *Developmental and comparative immunology* (2012) **37**:151–63. doi:10.1016/j.dci.2011.09.005

13. Cortes HD, Lillico DM, Zwozdesky MA, Pemberton JG, O'Brien A, Montgomery BC, Wiersma L, Chang JP, Stafford JL. Induction of phagocytosis and intracellular signaling by an inhibitory channel catfish leukocyte immune-type receptor: evidence for immunoregulatory receptor functional plasticity in teleosts. *Journal of innate immunity* (2014) **6**:435–55. doi:10.1159/000356963

14. Zwozdesky MA, Fei C, Lillico DME, Stafford JL. Imaging flow cytometry and GST pulldown assays provide new insights into channel catfish leukocyte immune-type receptor-mediated phagocytic pathways. *Developmental & Comparative Immunology* (2017) **67**:126–138. doi:10.1016/j.dci.2016.10.011

15. Lillico DME, Pemberton JG, Stafford JL. Selective Regulation of Cytoskeletal Dynamics and Filopodia Formation by Teleost Leukocyte Immune-Type Receptors Differentially Contributes to Target Capture During the Phagocytic Process. *Front Immunol* (2018) **9**: doi:10.3389/fimmu.2018.01144

16. Lillico DME, Pemberton JG, Niemand R, Stafford JL. Selective recruitment of Nck and Syk contribute to distinct leukocyte immune-type receptor-initiated target interactions. *Cell Signal* (2020) **66**:109443. doi:10.1016/j.cellsig.2019.109443

17. Barrow AD, Trowsdale J. The extended human leukocyte receptor complex: diverse ways of modulating immune responses. *Immunological Reviews* (2008) **224**:98–123. doi:10.1111/j.1600-065X.2008.00653.x

18. Akula S, Mohammadamin S, Hellman L. Fc Receptors for Immunoglobulins and Their Appearance during Vertebrate Evolution. *PLoS ONE* (2014) **9**:e96903. doi:10.1371/journal.pone.0096903

19. Barclay AN. Membrane proteins with immunoglobulin-like domains—a master superfamily of interaction molecules. *Seminars in Immunology* (2003) **15**:215–223. doi:10.1016/S1044-5323(03)00047-2

20. Bezbradica JS, Medzhitov R. Role of ITAM signaling module in signal integration. *Current Opinion in Immunology* (2012) **24**:58–66. doi:10.1016/j.coi.2011.12.010

21. Li J, Barreda DR, Zhang Y-A, Boshra H, Gelman AE, LaPatra S, Tort L, Sunyer JO. B lymphocytes from early vertebrates have potent phagocytic and microbicidal abilities. *Nature Immunology* (2006) **7**:1116–1124. doi:10.1038/ni1389

22. Zhang Y-A, Salinas I, Li J, Parra D, Bjork S, Xu Z, LaPatra SE, Bartholomew J, Sunyer JO. IgT, a primitive immunoglobulin class specialized in mucosal immunity. *Nature Immunology* (2010) **11**:827–835. doi:10.1038/ni.1913

23. Engstad RE, Robertsen B. Recognition of yeast cell wall glucan by Atlantic salmon (Salmo salar L.) macrophages. *Developmental & Comparative Immunology* (1993) **17**:319–330. doi:10.1016/0145-305X(93)90004-A

24. Esteban MA, Meseguer J. Factors influencing phagocytic response of macrophages from the sea bass (Dicentrarchus labrax L.): An ultrastructural and quantitative study. *The Anatomical Record* (1997) **248**:533–541. doi:10.1002/(SICI)1097-0185(199708)248:4<533::AID-AR5>3.0.CO;2-M

25. Frøystad MK, Rode M, Berg T, Gjøen T. A role for scavenger receptors in phagocytosis of protein-coated particles in rainbow trout head kidney macrophages. *Developmental & Comparative Immunology* (1998) **22**:533–549. doi:10.1016/S0145-305X(98)00032-9

26. Shen L, Stuge TB, Bengtén E, Wilson M, Chinchar VG, Naftel JP, Bernanke JM, Clem LW, Miller NW. Identification and characterization of clonal NK-like cells from channel catfish (Ictalurus punctatus). *Developmental & Comparative Immunology* (2004) **28**:139–152. doi:10.1016/S0145-305X(03)00119-8

27. Vallejo AN, Miller NW, Harvey NE, Cuchens MA, Warr GW, Clem LW. Cellular Pathway(S) of Antigen Processing and Presentation in Fish APC: Endosomal Involvement and Cell-Free Antigen Presentation. *Developmental Immunology* (3) **3**:e82525. doi:https://doi.org/10.1155/1992/82525

28. Vallejo AN, Miller NW, Clem LW. Phylogeny of immune recognition: role of alloantigens in antigen presentation in channel catfish immune responses. *Immunology* (1991) **74**:165–168.

29. Chen K, Xu W, Wilson M, He B, Miller NW, Bengtén E, Edholm E-S, Santini PA, Rath P, Chiu A, et al. Immunoglobulin D enhances immune surveillance by activating antimicrobial, proinflammatory and B cell–stimulating programs in basophils. *Nature Immunology* (2009) **10**:889–898. doi:10.1038/ni.1748

30. Dezfuli BS, Giari L. Mast cells in the gills and intestines of naturally infected fish: evidence of migration and degranulation. *Journal of Fish Diseases* (2008) **31**:845–852. doi:10.1111/j.1365-2761.2008.00961.x

31. Katzenback BA, Belosevic M. Isolation and functional characterization of neutrophil-like cells, from goldfish (Carassius auratus L.) kidney. *Developmental & Comparative Immunology* (2009) **33**:601–611. doi:10.1016/j.dci.2008.10.011

32. Montgomery BC, Cortes HD, Mewes-Ares J, Verheijen K, Stafford JL. Teleost IgSF immunoregulatory receptors. *Developmental & Comparative Immunology* (2011) **35**:1223–1237. doi:10.1016/j.dci.2011.03.010

33. Rodríguez-Nunez I, Wcisel DJ, Litman GW, Yoder JA. Multigene families of immunoglobulin domain-containing innate immune receptors in zebrafish: Deciphering the differences. *Developmental & Comparative Immunology* (2014) **46**:24–34. doi:10.1016/j.dci.2014.02.004

34. Yoder JA, Litman GW. The phylogenetic origins of natural killer receptors and recognition: relationships, possibilities, and realities. *Immunogenetics* (2011) **63**:123–141. doi:10.1007/s00251-010-0506-4

35. Barclay AN. Ig-like domains: Evolution from simple interaction molecules to sophisticated antigen recognition. *PNAS* (1999) **96**:14672–14674. doi:10.1073/pnas.96.26.14672

36. Cannon JP, Haire RN, Magis AT, Eason DD, Winfrey KN, Prada JAH, Bailey KM, Jakoncic J, Litman GW, Ostrov DA. A Bony Fish Immunological Receptor of the NITR Multigene Family Mediates Allogeneic Recognition. *Immunity* (2008) **29**:228–237. doi:10.1016/j.immuni.2008.05.018

37. Yoder JA, Mueller MG, Wei S, Corliss BC, Prather DM, Willis T, Litman RT, Djeu JY, Litman GW. Immune-type receptor genes in zebrafish share genetic and functional properties with genes encoded by the mammalian leukocyte receptor cluster. *PNAS* (2001) **98**:6771–6776. doi:10.1073/pnas.121101598

38. Litman GW, Hawke NA, Yoder JA. Novel immune-type receptor genes. *Immunological Reviews* (2001) **181**:250–259. doi:10.1034/j.1600-065X.2001.1810121.x

39. Litman GW, Yoder JA, Cannon JP, Haire RN. Novel Immune-type Receptor Genes and the Origins of Adaptive and Innate Immune Recognition. *Integr Comp Biol* (2003) **43**:331–337. doi:10.1093/icb/43.2.331

40. Yoder JA. Form, function and phylogenetics of NITRs in bony fish. *Developmental & Comparative Immunology* (2009) **33**:135–144. doi:10.1016/j.dci.2008.09.004

41. Feng J, Call ME, Wucherpfennig KW. The Assembly of Diverse Immune Receptors Is Focused on a Polar Membrane-Embedded Interaction Site. *PLoS Biol* (2006) **4**:e142. doi:10.1371/journal.pbio.0040142

42. Küster H, Thompson H, Kinet JP. Characterization and expression of the gene for the human Fc receptor gamma subunit. Definition of a new gene family. *J Biol Chem* (1990) **265**:6448–6452.

43. Amoui M, Dráberová L, Tolar P, Dráber P. Direct interaction of Syk and Lyn protein tyrosine kinases in rat basophilic leukemia cells activated via type I Fcε receptors. *European Journal of Immunology* (1997) **27**:321–328. doi:10.1002/eji.1830270146

44. Mócsai A, Ruland J, Tybulewicz VLJ. The SYK tyrosine kinase: a crucial player in diverse biological functions. *Nature Reviews Immunology* (2010) **10**:387–402. doi:10.1038/nri2765

45. Bakker ABH, Wu J, Phillips JH, Lanier LL. NK cell activation: distinct stimulatory pathways counterbalancing inhibitory signals. *Human Immunology* (2000) **61**:18–27. doi:10.1016/S0198-8859(99)00160-3

46. Holowka D, Sil D, Torigoe C, Baird B. Insights into immunoglobulin E receptor signaling from structurally defined ligands. *Immunological Reviews* (2007) **217**:269–279. doi:10.1111/j.1600-065X.2007.00517.x

47. Lanier LL. Up on the tightrope: natural killer cell activation and inhibition. *Nature Immunology* (2008) **9**:495–502. doi:10.1038/ni1581

48. Underhill DM, Goodridge HS. The many faces of ITAMs. *Trends in Immunology* (2007) **28**:66–73. doi:10.1016/j.it.2006.12.004

49. Lanier LL, Corliss B, Wu J, Phillips JH. Association of DAP12 with Activating CD94/NKG2C NK Cell Receptors. *Immunity* (1998) **8**:693–701. doi:10.1016/S1074-7613(00)80574-9

50. Lanier LL, Corliss BC, Wu J, Leong C, Phillips JH. Immunoreceptor DAP12 bearing a tyrosine-based activation motif is involved in activating NK cells. *Nature* (1998) **391**:703–707. doi:10.1038/35642

51. Yoder JA, Orcutt TM, Traver D, Litman GW. Structural characteristics of zebrafish orthologs of adaptor molecules that associate with transmembrane immune receptors. *Gene* (2007) **401**:154–164. doi:10.1016/j.gene.2007.07.014

52. Takai T, Li M, Sylvestre D, Clynes R, Ravetch JV. FcR γ chain deletion results in pleiotrophic effector cell defects. *Cell* (1994) **76**:519–529. doi:10.1016/0092-8674(94)90115-5

53. Kinet J-P. The γ-ξ dimers of Fc receptors as connectors to signal transduction. *Current Opinion in Immunology* (1992) **4**:43–48. doi:10.1016/0952-7915(92)90122-U

54. Ghazizadeh S, Bolen JB, Fleit HB. Tyrosine phosphorylation and association of Syk with FcγRII in monocytic THP-1 cells. *Biochem J* (1995) **305**:669–674. doi:10.1042/bj3050669

55. Johnson SA, Pleiman CM, Pao L, Schneringer J, Hippen K, Cambier JC. Phosphorylated immunoreceptor signaling motifs (ITAMs) exhibit unique abilities to bind and activate Lyn and Syk tyrosine kinases. *The Journal of Immunology* (1995) **155**:4596–4603.

56. Crowley MT, Costello PS, Fitzer-Attas CJ, Turner M, Meng F, Lowell C, Tybulewicz VLJ, DeFranco AL. A Critical Role for Syk in Signal Transduction and Phagocytosis Mediated by Fcγ Receptors on Macrophages. *J Exp Med* (1997) **186**:1027–1039. doi:10.1084/jem.186.7.1027

57. Kiefer F, Brumell J, Al-Alawi N, Latour S, Cheng A, Veillette A, Grinstein S, Pawson T. The Syk Protein Tyrosine Kinase Is Essential for Fcγ Receptor Signaling in Macrophages and Neutrophils. *Molecular and Cellular Biology* (1998) **18**:4209–4220. doi:10.1128/MCB.18.7.4209

58. Park H, Cox D. Cdc42 Regulates Fcγ Receptor-mediated Phagocytosis through the Activation and Phosphorylation of Wiskott-Aldrich Syndrome Protein (WASP) and Neural-WASP. *MBoC* (2009) **20**:4500–4508. doi:10.1091/mbc.e09-03-0230

59. May RC, Caron E, Hall A, Machesky LM. Involvement of the Arp2/3 complex in phagocytosis mediated by FcγR or CR3. *Nature Cell Biology* (2000) **2**:246–248. doi:10.1038/35008673

60. Burshtyn DN, Lam AS, Weston M, Gupta N, Warmerdam PAM, Long EO. Conserved Residues Amino-Terminal of Cytoplasmic Tyrosines Contribute to the SHP-1-Mediated Inhibitory Function of Killer Cell Ig-Like Receptors. *The Journal of Immunology* (1999) **162**:897–902.

61. Burshtyn DN, Yang W, Yi T, Long EO. A Novel Phosphotyrosine Motif with a Critical Amino Acid at Position −2 for the SH2 Domain-mediated Activation of the Tyrosine Phosphatase SHP-1. *J Biol Chem* (1997) **272**:13066–13072. doi:10.1074/jbc.272.20.13066

62. Vivier E, Daëron M. Immunoreceptor tyrosine-based inhibition motifs. *Immunology Today* (1997) **18**:286–291. doi:10.1016/S0167-5699(97)80025-4

63. Sidorenko SP, Clark EA. The dual-function CD150 receptor subfamily: the viral attraction. *Nat Immunol* (2003) **4**:19–24. doi:10.1038/ni0103-19

64. Songyang Z, Shoelson SE, McGlade J, Olivier P, Pawson T, Bustelo XR, Barbacid M, Sabe H, Hanafusa H, Yi T. Specific motifs recognized by the SH2 domains of Csk, 3BP2, fps/fes, GRB-2, HCP, SHC, Syk, and Vav. *Mol Cell Biol* (1994) **14**:2777–2785. doi:10.1128/MCB.14.4.2777

65. Chong Y-P, Mulhern TD, Cheng H-C. C-terminal Src kinase (CSK) and CSK-homologous kinase (CHK)—endogenous negative regulators of Src-family protein kinases. *Growth Factors* (2005) **23**:233–244. doi:10.1080/08977190500178877

66. Okada M, Nada S, Yamanashi Y, Yamamoto T, Nakagawa H. CSK: a protein-tyrosine kinase involved in regulation of src family kinases. *J Biol Chem* (1991) **266**:24249–24252.

67. Sayós J, Martínez-Barriocanal A, Kitzig F, Bellón T, López-Botet M. Recruitment of C-terminal Src kinase by the leukocyte inhibitory receptor CD85j. *Biochemical and Biophysical Research Communications* (2004) **324**:640–647. doi:10.1016/j.bbrc.2004.09.097

68. Verbrugge A, Rijkers ESK, Ruiter T de, Meyaard L. Leukocyte-associated Ig-like receptor-1 has SH2 domain-containing phosphatase-independent function and recruits C-terminal Src kinase. *European Journal of Immunology* (2006) **36**:190–198. doi:10.1002/eji.200535226

69. Faure M, Long EO. KIR2DL4 (CD158d), an NK Cell-Activating Receptor with Inhibitory Potential. *The Journal of Immunology* (2002) **168**:6208–6214. doi:10.4049/jimmunol.168.12.6208

70. Newman Peter J., Newman Debra K. Signal Transduction Pathways Mediated by PECAM-1. *Arteriosclerosis, Thrombosis, and Vascular Biology* (2003) **23**:953–964. doi:10.1161/01.ATV.0000071347.69358.D9

71. Izawa K, Kitaura J, Yamanishi Y, Matsuoka T, Kaitani A, Sugiuchi M, Takahashi M, Maehara A, Enomoto Y, Oki T, et al. An Activating and Inhibitory Signal from an Inhibitory Receptor LMIR3/CLM-1: LMIR3 Augments Lipopolysaccharide Response through Association with FcRγ in Mast Cells. *The Journal of Immunology* (2009) **183**:925–936. doi:10.4049/jimmunol.0900552

72. Rajagopalan S, Fu J, Long EO. Cutting Edge: Induction of IFN-γ Production but Not Cytotoxicity by the Killer Cell Ig-Like Receptor KIR2DL4 (CD158d) in Resting NK Cells. *The Journal of Immunology* (2001) **167**:1877–1881. doi:10.4049/jimmunol.167.4.1877

73. Blank U, Launay P, Benhamou M, Monteiro RC. Inhibitory ITAMs as novel regulators of immunity. *Immunological Reviews* (2009) **232**:59–71. doi:10.1111/j.1600-065X.2009.00832.x

74. Pfirsch-Maisonnas S, Aloulou M, Xu T, Claver J, Kanamaru Y, Tiwari M, Launay P, Monteiro RC, Blank U. Inhibitory ITAM Signaling Traps Activating Receptors with the Phosphatase SHP-1 to Form Polarized "Inhibisome" Clusters. *Sci Signal* (2011) **4**:ra24–ra24. doi:10.1126/scisignal.2001309

75. Zhang Y, Zhou Y, Yang Q, Mu C, Duan E, Chen J, Yang M, Xia P, Cui B. Ligation of Fc gamma receptor IIB enhances levels of antiviral cytokine in response to PRRSV infection in vitro. *Veterinary Microbiology* (2012) **160**:473–480. doi:10.1016/j.vetmic.2012.06.021

76. Chemnitz JM, Parry RV, Nichols KE, June CH, Riley JL. SHP-1 and SHP-2 Associate with Immunoreceptor Tyrosine-Based Switch Motif of Programmed Death 1 upon Primary Human T Cell Stimulation, but Only Receptor Ligation Prevents T Cell Activation. *The Journal of Immunology* (2004) **173**:945–954. doi:10.4049/jimmunol.173.2.945

77. Shlapatska LM, Mikhalap SV, Berdova AG, Zelensky OM, Yun TJ, Nichols KE, Clark EA, Sidorenko SP. CD150 Association with Either the SH2-Containing Inositol Phosphatase or the SH2-Containing Protein Tyrosine Phosphatase Is Regulated by the Adaptor Protein SH2D1A. *J Immunol* (2001) **166**:5480–5487. doi:10.4049/jimmunol.166.9.5480

78. Mikhalap SV, Shlapatska LM, Berdova AG, Law C-L, Clark EA, Sidorenko SP. CDw150 Associates with Src-Homology 2-Containing Inositol Phosphatase and Modulates CD95-Mediated Apoptosis. *The Journal of Immunology* (1999) **162**:5719–5727.

79. Li C, Iosef C, Jia CYH, Han VKM, Li SS-C. Dual Functional Roles for the X-linked Lymphoproliferative Syndrome Gene Product SAP/SH2D1A in Signaling through the

Signaling Lymphocyte Activation Molecule (SLAM) Family of Immune Receptors. *J Biol Chem* (2003) **278**:3852–3859. doi:10.1074/jbc.M206649200

80. Brummer T, Schmitz-Peiffer C, Daly RJ. Docking proteins. *The FEBS Journal* (2010) **277**:4356–4369. doi:10.1111/j.1742-4658.2010.07865.x

81. Li W, Nishimura R, Kashishian A, Batzer AG, Kim WJ, Cooper JA, Schlessinger J. A new function for a phosphotyrosine phosphatase: linking GRB2-Sos to a receptor tyrosine kinase. *Molecular and Cellular Biology* (1994) **14**:509–517. doi:10.1128/MCB.14.1.509

82. Bohdanowicz M, Cosío G, Backer JM, Grinstein S. Class I and class III phosphoinositide 3-kinases are required for actin polymerization that propels phagosomes. *J Cell Biol* (2010) **191**:999–1012. doi:10.1083/jcb.201004005

83. Gu H, Saito K, Klaman LD, Shen J, Fleming T, Wang Y, Pratt JC, Lin G, Lim B, Kinet J-P, et al. Essential role for Gab2 in the allergic response. *Nature* (2001) **412**:186–190. doi:10.1038/35084076

84. Gotoh N. Regulation of growth factor signaling by FRS2 family docking/scaffold adaptor proteins. *Cancer Science* (2008) **99**:1319–1325. doi:10.1111/j.1349-7006.2008.00840.x

85. Gu H, Botelho RJ, Yu M, Grinstein S, Neel BG. Critical role for scaffolding adapter Gab2 in FcγR-mediated phagocytosis. *J Cell Biol* (2003) **161**:1151–1161. doi:10.1083/jcb.200212158

86. Bennett AM, Tang TL, Sugimoto S, Walsh CT, Neel BG. Protein-tyrosine-phosphatase SHPTP2 couples platelet-derived growth factor receptor beta to Ras. *PNAS* (1994) **91**:7335–7339. doi:10.1073/pnas.91.15.7335

87. Lowenstein EJ, Daly RJ, Batzer AG, Li W, Margolis B, Lammers R, Ullrich A, Skolnik EY, Bar-Sagi D, Schlessinger J. The SH2 and SH3 domain-containing protein GRB2 links receptor tyrosine kinases to ras signaling. *Cell* (1992) **70**:431–442. doi:10.1016/0092-8674(92)90167-B

88. Simon MA, Bowtell DDL, Dodson GS, Laverty TR, Rubin GM. Ras1 and a putative guanine nucleotide exchange factor perform crucial steps in signaling by the sevenless protein tyrosine kinase. *Cell* (1991) **67**:701–716. doi:10.1016/0092-8674(91)90065-7

89. Li N, Batzer A, Daly R, Yajnik V, Skolnik E, Chardin P, Bar-Sagi D, Margolis B, Schlessinger J. Guanine-nucleotide-releasing factor hSos1 binds to Grb2 and links receptor tyrosine kinases to Ras signalling. *Nature* (1993) **363**:85–88. doi:10.1038/363085a0

90. Araki N, Johnson MT, Swanson JA. A role for phosphoinositide 3-kinase in the completion of macropinocytosis and phagocytosis by macrophages. *J Cell Biol* (1996) **135**:1249–1260. doi:10.1083/jcb.135.5.1249

91. Cox D, Tseng C-C, Bjekic G, Greenberg S. A Requirement for Phosphatidylinositol 3-Kinase in Pseudopod Extension. *J Biol Chem* (1999) **274**:1240–1247. doi:10.1074/jbc.274.3.1240

92. Katzav S. Vav1: A hematopoietic signal transduction molecule involved in human malignancies. *The International Journal of Biochemistry & Cell Biology* (2009) **41**:1245–1248. doi:10.1016/j.biocel.2008.11.006

93. Hall AB, Gakidis MAM, Glogauer M, Wilsbacher JL, Gao S, Swat W, Brugge JS. Requirements for Vav Guanine Nucleotide Exchange Factors and Rho GTPases in FcγR- and Complement-Mediated Phagocytosis. *Immunity* (2006) **24**:305–316. doi:10.1016/j.immuni.2006.02.005

94. Schmitter T, Pils S, Sakk V, Frank R, Fischer K-D, Hauck CR. The Granulocyte Receptor Carcinoembryonic Antigen-Related Cell Adhesion Molecule 3 (CEACAM3) Directly Associates with Vav to Promote Phagocytosis of Human Pathogens. *The Journal of Immunology* (2007) **178**:3797–3805. doi:10.4049/jimmunol.178.6.3797

95. Pils S, Kopp K, Peterson L, Tascón JD, Nyffenegger-Jann NJ, Hauck CR. The Adaptor Molecule Nck Localizes the WAVE Complex to Promote Actin Polymerization during CEACAM3-Mediated Phagocytosis of Bacteria. *PLOS ONE* (2012) **7**:e32808. doi:10.1371/journal.pone.0032808

96. Frese S, Schubert W-D, Findeis AC, Marquardt T, Roske YS, Stradal TEB, Heinz DW. The Phosphotyrosine Peptide Binding Specificity of Nck1 and Nck2 Src Homology 2 Domains. *J Biol Chem* (2006) **281**:18236–18245. doi:10.1074/jbc.M512917200

97. Wang J, Wu Y, Hu H, Wang W, Lu Y, Mao H, Liu X, Liu Z, Chen B. Syk protein tyrosine kinase involves PECAM-1 signaling through tandem immunotyrosine inhibitory motifs in human THP-1 macrophages. *Cellular Immunology* (2011) **272**:39–44. doi:10.1016/j.cellimm.2011.09.009

98. Mendoza MC. Phosphoregulation of the WAVE regulatory complex and signal integration. *Seminars in Cell & Developmental Biology* (2013) **24**:272–279. doi:10.1016/j.semcdb.2013.01.007

99. Rougerie P, Miskolci V, Cox D. Generation of membrane structures during phagocytosis and chemotaxis of macrophages: role and regulation of the actin cytoskeleton. *Immunological Reviews* (2013) **256**:222–239. doi:10.1111/imr.12118

100. Lee WL, Mason D, Schreiber AD, Grinstein S. Quantitative Analysis of Membrane Remodeling at the Phagocytic Cup. *MBoC* (2007) **18**:2883–2892. doi:10.1091/mbc.e06-05-0450

101. Braun V, Fraisier V, Raposo G, Hurbain I, Sibarita J-B, Chavrier P, Galli T, Niedergang F. TI-VAMP/VAMP7 is required for optimal phagocytosis of opsonised particles in macrophages. *The EMBO Journal* (2004) **23**:4166–4176. doi:10.1038/sj.emboj.7600427

102. Cox D, Lee DJ, Dale BM, Calafat J, Greenberg S. A Rab11-containing rapidly recycling compartment in macrophages that promotes phagocytosis. *PNAS* (2000) **97**:680–685. doi:10.1073/pnas.97.2.680

103. Niedergang F, Colucci-Guyon E, Dubois T, Raposo G, Chavrier P. ADP ribosylation factor 6 is activated and controls membrane delivery during phagocytosis in macrophages. *J Cell Biol* (2003) **161**:1143–1150. doi:10.1083/jcb.200210069

104. Beemiller P, Zhang Y, Mohan S, Levinsohn E, Gaeta I, Hoppe AD, Swanson JA. A Cdc42 Activation Cycle Coordinated by PI 3-Kinase during Fc Receptor-mediated Phagocytosis. *MBoC* (2009) **21**:470–480. doi:10.1091/mbc.e08-05-0494

105. Ninomiya N, Hazeki K, Fukui Y, Seya T, Okada T, Hazeki O, Ui M. Involvement of phosphatidylinositol 3-kinase in Fc gamma receptor signaling. *J Biol Chem* (1994) **269**:22732–22737.

106. Bhattacharyya RP, Reményi A, Yeh BJ, Lim WA. Domains, Motifs, and Scaffolds: The Role of Modular Interactions in the Evolution and Wiring of Cell Signaling Circuits. *Annu Rev Biochem* (2006) **75**:655–680. doi:10.1146/annurev.biochem.75.103004.142710

107. Fei C, Lillico DME, Hall B, Rieger AM, Stafford JL. Connected component masking accurately identifies the ratio of phagocytosed and cell-bound particles in individual cells by imaging flow cytometry. *Cytometry Part A* (2017) **91**:372–381. doi:10.1002/cyto.a.23050

108. Jones LO, Stafford JL. Imaging flow cytometry and confocal microscopy-based examination of F-actin and phosphoinositide dynamics during leukocyte immune-type receptor-mediated phagocytic events. *Developmental & Comparative Immunology* (2019) **92**:199–211. doi:10.1016/j.dci.2018.11.018

109. Strzelecka-Kiliszek A, Kwiatkowska K, Sobota A. Lyn and Syk Kinases Are Sequentially Engaged in Phagocytosis Mediated by FcγR. *The Journal of Immunology* (2002) **169**:6787–6794. doi:10.4049/jimmunol.169.12.6787

110. Flannagan RS, Jaumouille V, Grinstein S. "The Cell Biology of Phagocytosis," in *Annual Review of Pathology: Mechanisms of Disease, Vol 7*, eds. A. K. Abbas, S. J. Galli, P. M. Howley, 61–98.

111. Aderem A, Underhill DM. Mechanisms of phagocytosis in macrophages. *Annual Review of Immunology* (1999) **17**:593–623. doi:10.1146/annurev.immunol.17.1.593

112. Freeman SA, Grinstein S. Phagocytosis: receptors, signal integration, and the cytoskeleton. *Immunological Reviews* (2014) **262**:193–215. doi:10.1111/imr.12212

113. Caron E, Hall A. Identification of two distinct mechanisms of phagocytosis controlled by different Rho GTPases. *Science* (1998) **282**:1717–1721. doi:10.1126/science.282.5394.1717

114. Allen L a. H, Aderem A. Molecular definition of distinct cytoskeletal structures involved in complement- and Fc receptor-mediated phagocytosis in macrophages. *Journal of Experimental Medicine* (1996) **184**:627–637. doi:10.1084/jem.184.2.627

115. Rieger AM, Hall BE, Barreda DR. Macrophage activation differentially modulates particle binding, phagocytosis and downstream antimicrobial mechanisms. *Developmental and Comparative Immunology* (2010) **34**:1144–1159. doi:10.1016/j.dci.2010.06.006

116. McFarlin BK, Williams RR, Venable AS, Dwyer KC, Haviland DL. Image-Based Cytometry Reveals Three Distinct Subsets of Activated Granulocytes Based on Phagocytosis and Oxidative Burst. *Cytometry Part A* (2013) **83A**:745–751. doi:10.1002/cyto.a.22330

117. Vranic S, Boggetto N, Contremoulins V, Mornet S, Reinhardt N, Marano F, Baeza-Squiban A, Boland S. Deciphering the mechanisms of cellular uptake of engineered nanoparticles by accurate evaluation of internalization using imaging flow cytometry. *Particle and Fibre Toxicology* (2013) **10**:2. doi:10.1186/1743-8977-10-2

118. Ploppa A, George TC, Unert KE, Nohe B, Durieux ME. ImageStream cytometry extends the analysis of phagocytosis and oxidative burst. *Scandinavian Journal of Clinical & Laboratory Investigation* (2011) **71**:362–369. doi:10.3109/00365513.2011.572182

119. Phanse Y, Ramer-Tait AE, Friend SL, Carrillo-Conde B, Lueth P, Oster CJ, Phillips GJ, Narasimhan B, Wannemuehler MJ, Bellaire BH. Analyzing Cellular Internalization of Nanoparticles and Bacteria by Multi-spectral Imaging Flow Cytometry. *Jove-Journal of Visualized Experiments* (2012)e3884. doi:10.3791/3884

120. Smirnov A, Solga MD, Lannigan J, Criss AK. An improved method for differentiating cell-bound from internalized particles by imaging flow cytometry. *Journal of Immunological Methods* (2015) **423**:60–69. doi:10.1016/j.jim.2015.04.028

121. Franzen CA, Simms PE, Van Huis AF, Foreman KE, Kuo PC, Gupta GN. Characterization of Uptake and Internalization of Exosomes by Bladder Cancer Cells. *Biomed Research International* (2014)619829. doi:10.1155/2014/619829

122. Rodrigues MA, Probst CE, Beaton-Green LA, Wilkins RC. Optimized automated data analysis for the cytokinesis-block micronucleus assay using imaging flow cytometry for high throughput radiation biodosimetry. *Cytometry Part A* (2016) **89A**:653–662. doi:10.1002/cyto.a.22887

123. Flannagan RS, Canton J, Furuya W, Glogauer M, Grinstein S. The phosphatidylserine receptor TIM4 utilizes integrins as coreceptors to effect phagocytosis. *MBoC* (2014) **25**:1511–1522. doi:10.1091/mbc.e13-04-0212

124. Somersan S, Bhardwaj N. Tethering and tickling a new role for the phosphatidylserine receptor. *J Cell Biol* (2001) **155**:501–504. doi:10.1083/jcb.200110066

125. McWhorter FY, Davis CT, Liu WF. Physical and mechanical regulation of macrophage phenotype and function. *Cell Mol Life Sci* (2015) **72**:1303–1316. doi:10.1007/s00018-014-1796-8

126. Underhill DM, Goodridge HS. Information processing during phagocytosis. *Nature Reviews Immunology* (2012) **12**:492–502. doi:10.1038/nri3244

127. Underhill DM, Gantner B. Integration of Toll-like receptor and phagocytic signaling for tailored immunity. *Microbes and infection / Institut Pasteur* (2004) **6**:1368–73. doi:10.1016/j.micinf.2004.08.016

128. Hajishengallis G, Lambris JD. More than complementing Tolls: complement-Toll-like receptor synergy and crosstalk in innate immunity and inflammation. *Immunological reviews* (2016) **274**:233–244. doi:10.1111/imr.12467

129. Gerber JS, Mosser DM. Stimulatory and inhibitory signals originatingfrom the macrophage Fcγ receptors. *Microbes and Infection* (2001) **3**:131–139. doi:10.1016/S1286-4579(00)01360-5

130. Hamerman JA, Lanier LL. Inhibition of Immune Responses by ITAM-Bearing Receptors. *Science Signaling* (2006) **2006**:re1–re1. doi:10.1126/stke.3202006re1

131. Hunter S, Indik ZK, Kim M-K, Cauley MD, Park J-G, Schreiber AD. Inhibition of Fcγ Receptor-Mediated Phagocytosis by a Nonphagocytic Fcγ Receptor. *Blood* (1998) **91**:1762–1768. doi:10.1182/blood.V91.5.1762

132. Nimmerjahn F. Activating and inhibitory FcγRs in autoimmune disorders. *Springer Semin Immun* (2006) **28**:305–319. doi:10.1007/s00281-006-0052-1

133. Lanier LL. Face off — the interplay between activating and inhibitory immune receptors. *Current Opinion in Immunology* (2001) **13**:326–331. doi:10.1016/S0952-7915(00)00222-3

134. Takai T, Ono M. Activating and inhibitory nature of the murine paired immunoglobulin-like receptor family. *Immunological Reviews* (2001) **181**:215–222. doi:10.1034/j.1600-065X.2001.1810118.x

135. Tridandapani S, Siefker K, Teillaud J-L, Carter JE, Wewers MD, Anderson CL. Regulated Expression and Inhibitory Function of FcγRIIb in Human Monocytic Cells. *J Biol Chem* (2002) **277**:5082–5089. doi:10.1074/jbc.M110277200

136. Joshi T, Ganesan LP, Cao X, Tridandapani S. Molecular analysis of expression and function of hFcγRIIbl and b2 isoforms in myeloid cells. *Molecular Immunology* (2006) **43**:839–850. doi:10.1016/j.molimm.2005.06.037

137. Jenkins MR, Tsun A, Stinchcombe JC, Griffiths GM. The Strength of T Cell Receptor Signal Controls the Polarization of Cytotoxic Machinery to the Immunological Synapse. *Immunity* (2009) **31**:621–631. doi:10.1016/j.immuni.2009.08.024

138. Ortaldo JR, Young HA. Mouse Ly49 NK receptors: balancing activation and inhibition. *Molecular Immunology* (2005) **42**:445–450. doi:10.1016/j.molimm.2004.07.024

139. Scalzo AA. Successful control of viruses by NK cells – a balance of opposing forces? *Trends in Microbiology* (2002) **10**:470–474. doi:10.1016/S0966-842X(02)02441-1

140. Eissmann P, Beauchamp L, Wooters J, Tilton JC, Long EO, Watzl C. Molecular basis for positive and negative signaling by the natural killer cell receptor 2B4 (CD244). *Blood* (2005) **105**:4722–4729. doi:10.1182/blood-2004-09-3796

141. Sivori S, Falco M, Marcenaro E, Parolini S, Biassoni R, Bottino C, Moretta L, Moretta A. Early expression of triggering receptors and regulatory role of 2B4 in human natural killer cell precursors undergoing in vitro differentiation. *PNAS* (2002) **99**:4526–4531. doi:10.1073/pnas.072065999

142. Coffey AJ, Brooksbank RA, Brandau O, Oohashi T, Howell GR, Bye JM, Cahn AP, Durham J, Heath P, Wray P, et al. Host response to EBV infection in X-linked lymphoproliferative disease results from mutations in an SH2-domain encoding gene. *Nature Genetics* (1998) **20**:129–135. doi:10.1038/2424

143. Sayos J, Wu C, Morra M, Wang N, Zhang X, Allen D, van Schaik S, Notarangelo L, Geha R, Roncarolo MG, et al. The X-linked lymphoproliferative-disease gene product SAP regulates signals induced through the co-receptor SLAM. *Nature* (1998) **395**:462–469. doi:10.1038/26683

144. Berton G, Mócsai A, Lowell CA. Src and Syk kinases: key regulators of phagocytic cell activation. *Trends in Immunology* (2005) **26**:208–214. doi:10.1016/j.it.2005.02.002

145. Poole AW, Jones ML. A SHPing tale: Perspectives on the regulation of SHP-1 and SHP-2 tyrosine phosphatases by the C-terminal tail. *Cellular Signalling* (2005) **17**:1323–1332. doi:10.1016/j.cellsig.2005.05.016

146. Feng GS, Hui CC, Pawson T. SH2-containing phosphotyrosine phosphatase as a target of protein-tyrosine kinases. *Science* (1993) **259**:1607–1611. doi:10.1126/science.8096088

147. Vogel W, Lammers R, Huang J, Ullrich A. Activation of a phosphotyrosine phosphatase by tyrosine phosphorylation. *Science* (1993) **259**:1611–1614. doi:10.1126/science.7681217

148. Lu W, Gong D, Bar-Sagi D, Cole PA. Site-Specific Incorporation of a Phosphotyrosine Mimetic Reveals a Role for Tyrosine Phosphorylation of SHP-2 in Cell Signaling. *Molecular Cell* (2001) **8**:759–769. doi:10.1016/S1097-2765(01)00369-0

149. Aman MJ, Walk SF, March ME, Su H-P, Carver DJ, Ravichandran KS. Essential Role for the C-Terminal Noncatalytic Region of SHIP in FcγRIIB1-Mediated Inhibitory Signaling. *Molecular and Cellular Biology* (2000) **20**:3576–3589. doi:10.1128/MCB.20.10.3576-3589.2000

150. Baran CP, Tridandapani S, Helgason CD, Humphries RK, Krystal G, Marsh CB. The Inositol 5′-Phosphatase SHIP-1 and the Src Kinase Lyn Negatively Regulate Macrophage Colony-stimulating Factor-induced Akt Activity. *J Biol Chem* (2003) **278**:38628–38636. doi:10.1074/jbc.M305021200

151. Damen JE, Ware MD, Kalesnikoff J, Hughes MR, Krystal G. SHIP's C-terminus is essential for its hydrolysis of PIP3 and inhibition of mast cell degranulation. *Blood* (2001) **97**:1343–1351. doi:10.1182/blood.V97.5.1343

152. Malbec O, Fong DC, Turner M, Tybulewicz VLJ, Cambier JC, Fridman WH, Daëron M. Fcε Receptor I-Associated lyn-Dependent Phosphorylation of Fcγ Receptor IIB During Negative Regulation of Mast Cell Activation. *The Journal of Immunology* (1998) **160**:1647–1658.

153. Stuart LM, Ezekowitz RAB. Phagocytosis: Elegant Complexity. *Immunity* (2005) **22**:539–550. doi:10.1016/j.immuni.2005.05.002

154. Goodridge HS, Reyes CN, Becker CA, Katsumoto TR, Ma J, Wolf AJ, Bose N, Chan ASH, Magee AS, Danielson ME, et al. Activation of the innate immune receptor Dectin-1 upon formation of a 'phagocytic synapse.' *Nature* (2011) **472**:471–475. doi:10.1038/nature10071

155. Latour S, Veillette A. Proximal protein tyrosine kinases in immunoreceptor signaling. *Current Opinion in Immunology* (2001) **13**:299–306. doi:10.1016/S0952-7915(00)00219-3

156. Waterman PM, Marschner S, Brandl E, Cambier JC. The inositol 5-phosphatase SHIP-1 and adaptors Dok-1 and 2 play central roles in CD4-mediated inhibitory signaling. *Immunology Letters* (2012) **143**:122–130. doi:10.1016/j.imlet.2012.02.009

157. Niedergang F, Di Bartolo V, Alcover A. Comparative Anatomy of Phagocytic and Immunological Synapses. *Front Immunol* (2016) **7**: doi:10.3389/fimmu.2016.00018

158. Salmond RJ, Filby A, Qureshi I, Caserta S, Zamoyska R. T-cell receptor proximal signaling via the Src-family kinases, Lck and Fyn, influences T-cell activation, differentiation, and tolerance. *Immunological Reviews* (2009) **228**:9–22. doi:10.1111/j.1600-065X.2008.00745.x

159. Sanderson MP, Wex E, Kono T, Uto K, Schnapp A. Syk and Lyn mediate distinct Syk phosphorylation events in FcεRI-signal transduction: Implications for regulation of IgE-mediated degranulation. *Molecular Immunology* (2010) **48**:171–178. doi:10.1016/j.molimm.2010.08.012

160. Lennartz MR. Phospholipases and phagocytosis: the role of phospholipid-derived second messengers in phagocytosis. *The International Journal of Biochemistry & Cell Biology* (1999) **31**:415–430. doi:10.1016/S1357-2725(98)00108-3

161. Bewley MA, Belchamber KBR, Chana KK, Budd RC, Donaldson G, Wedzicha JA, Brightling CE, Kilty I, Donnelly LE, Barnes PJ, et al. Differential Effects of p38, MAPK, PI3K or Rho Kinase Inhibitors on Bacterial Phagocytosis and Efferocytosis by Macrophages in COPD. *PLOS ONE* (2016) **11**:e0163139. doi:10.1371/journal.pone.0163139

162. Stephens L, Ellson C, Hawkins P. Roles of PI3Ks in leukocyte chemotaxis and phagocytosis. *Current Opinion in Cell Biology* (2002) **14**:203–213. doi:10.1016/S0955-0674(02)00311-3

163. Ganesan LP, Wei G, Pengal RA, Moldovan L, Moldovan N, Ostrowski MC, Tridandapani S. The Serine/Threonine Kinase Akt Promotes Fcγ Receptor-mediated Phagocytosis in Murine Macrophages through the Activation of p70S6 Kinase. *J Biol Chem* (2004) **279**:54416–54425. doi:10.1074/jbc.M408188200

164. Tridandapani S, Anderson CL. *Regulation of Phagocytosis by FcγRIIb and Phosphatases*. Landes Bioscience (2013). Available at: https://www.ncbi.nlm.nih.gov/books/NBK6112/ [Accessed February 9, 2020]

165. Ogawa A, Takayama Y, Sakai H, Chong KT, Takeuchi S, Nakagawa A, Nada S, Okada M, Tsukihara T. Structure of the Carboxyl-terminal Src Kinase, Csk. *J Biol Chem* (2002) **277**:14351–14354. doi:10.1074/jbc.C200086200

166. Wong L, Lieser SA, Miyashita O, Miller M, Tasken K, Onuchic JN, Adams JA, Woods VL, Jennings PA. Coupled Motions in the SH2 and Kinase Domains of Csk Control Src Phosphorylation. *Journal of Molecular Biology* (2005) **351**:131–143. doi:10.1016/j.jmb.2005.05.042

167. Suzuki T, Kono H, Hirose N, Okada M, Yamamoto T, Yamamoto K, Honda Z. Differential Involvement of Src Family Kinases in Fcγ Receptor-Mediated Phagocytosis. *The Journal of Immunology* (2000) **165**:473–482. doi:10.4049/jimmunol.165.1.473

168. Kant AM, De P, Peng X, Yi T, Rawlings DJ, Kim JS, Durden DL. SHP-1 regulates Fcγ receptor–mediated phagocytosis and the activation of RAC. *Blood* (2002) **100**:1852–1859.

169. Ai J, Maturu A, Johnson W, Wang Y, Marsh CB, Tridandapani S. The inositol phosphatase SHIP-2 down-regulates FcγR-mediated phagocytosis in murine macrophages independently of SHIP-1. *Blood* (2006) **107**:813–820. doi:10.1182/blood-2005-05-1841

170. Huang Z-Y, Hunter S, Kim M-K, Indik ZK, Schreiber AD. The effect of phosphatases SHP-1 and SHIP-1 on signaling by the ITIM- and ITAM-containing Fcγ receptors FcγRIIB and FcγRIIA. *Journal of Leukocyte Biology* (2003) **73**:823–829. doi:10.1189/jlb.0902454

171. Osada Y, Sunatani T, Kim I-S, Nakanishi Y, Shiratsuchi A. Signalling Pathway Involving GULP, MAPK and Rac1 for SR-BI-Induced Phagocytosis of Apoptotic Cells. *J Biochem* (2009) **145**:387–394. doi:10.1093/jb/mvn176

172. Krzewski K, Strominger JL. The killer's kiss: the many functions of NK cell immunological synapses. *Current Opinion in Cell Biology* (2008) **20**:597–605. doi:10.1016/j.ceb.2008.05.006

173. Vyas YM, Maniar H, Dupont B. Cutting Edge: Differential Segregation of the Src Homology 2-Containing Protein Tyrosine Phosphatase-1 Within the Early NK Cell Immune

Synapse Distinguishes Noncytolytic from Cytolytic Interactions. *The Journal of Immunology* (2002) **168**:3150–3154. doi:10.4049/jimmunol.168.7.3150

174. Yusa S, Catina TL, Campbell KS. SHP-1- and Phosphotyrosine-Independent Inhibitory Signaling by a Killer Cell Ig-Like Receptor Cytoplasmic Domain in Human NK Cells. *J Immunol* (2002) **168**:5047–5057. doi:10.4049/jimmunol.168.10.5047

175. Stebbins CC, Watzl C, Billadeau DD, Leibson PJ, Burshtyn DN, Long EO. Vav1 Dephosphorylation by the Tyrosine Phosphatase SHP-1 as a Mechanism for Inhibition of Cellular Cytotoxicity. *Molecular and Cellular Biology* (2003) **23**:6291–6299. doi:10.1128/MCB.23.17.6291-6299.2003

176. Dréan EL, Vély F, Olcese L, Cambiaggi A, Guia S, Krystal G, Gervois N, Moretta A, Jotereau F, Vivier E. Inhibition of antigen-induced T cell response and antibody-induced NK cell cytotoxicity by NKG2A: association of NKG2A with SHP-1 and SHP-2 protein-tyrosine phosphatases. *European Journal of Immunology* (1998) **28**:264–276. doi:10.1002/(SICI)1521-4141(199801)28:01<264::AID-IMMU264>3.0.CO;2-O

177. Nakamura MC, Niemi EC, Fisher MJ, Shultz LD, Seaman WE, Ryan JC. Mouse Ly-49A Interrupts Early Signaling Events in Natural Killer Cell Cytotoxicity and Functionally Associates with the SHP-1 Tyrosine Phosphatase. *J Exp Med* (1997) **185**:673–684. doi:10.1084/jem.185.4.673

178. Matalon O, Fried S, Ben-Shmuel A, Pauker MH, Joseph N, Keizer D, Piterburg M, Barda-Saad M. Dephosphorylation of the adaptor LAT and phospholipase C–γ by SHP-1 inhibits natural killer cell cytotoxicity. *Sci Signal* (2016) **9**:ra54–ra54. doi:10.1126/scisignal.aad6182

179. Dietrich J, Cella M, Colonna M. Ig-Like Transcript 2 (ILT2)/Leukocyte Ig-Like Receptor 1 (LIR1) Inhibits TCR Signaling and Actin Cytoskeleton Reorganization. *The Journal of Immunology* (2001) **166**:2514–2521. doi:10.4049/jimmunol.166.4.2514

180. Chang CC, Ciubotariu R, Manavalan JS, Yuan J, Colovai AI, Piazza F, Lederman S, Colonna M, Cortesini R, Dalla-Favera R, et al. Tolerization of dendritic cells by T S cells: the crucial role of inhibitory receptors ILT3 and ILT4. *Nature Immunology* (2002) **3**:237–243. doi:10.1038/ni760

181. Saijo K, Schmedt C, Su I -hsin, Karasuyama H, Lowell CA, Reth M, Adachi T, Patke A, Santana A, Tarakhovsky A. Essential role of Src-family protein tyrosine kinases in NF-κB activation during B cell development. *Nature Immunology* (2003) **4**:274–279. doi:10.1038/ni893

182. Parravicini V, Gadina M, Kovarova M, Odom S, Gonzalez-Espinosa C, Furumoto Y, Saitoh S, Samelson LE, O'Shea JJ, Rivera J. Fyn kinase initiates complementary signals required for IgE-dependent mast cell degranulation. *Nature Immunology* (2002) **3**:741–748. doi:10.1038/ni817

183. Miyazaki T, Sanjay A, Neff L, Tanaka S, Horne WC, Baron R. Src Kinase Activity Is Essential for Osteoclast Function. *J Biol Chem* (2004) **279**:17660–17666. doi:10.1074/jbc.M311032200

184. Mócsai A, Jakus Z, Vántus T, Berton G, Lowell CA, Ligeti E. Kinase Pathways in Chemoattractant-Induced Degranulation of Neutrophils: The Role of p38 Mitogen-Activated Protein Kinase Activated by Src Family Kinases. *The Journal of Immunology* (2000) **164**:4321–4331. doi:10.4049/jimmunol.164.8.4321

185. Mócsai A, Ligeti E, Lowell CA, Berton G. Adhesion-Dependent Degranulation of Neutrophils Requires the Src Family Kinases Fgr and Hck. *The Journal of Immunology* (1999) **162**:1120–1126.

186. Fitzer-Attas CJ, Lowry M, Crowley MT, Finn AJ, Meng F, DeFranco AL, Lowell CA. Fcγ Receptor–Mediated Phagocytosis in Macrophages Lacking the Src Family Tyrosine Kinases Hck, Fgr, and Lyn. *J Exp Med* (2000) **191**:669–682. doi:10.1084/jem.191.4.669

187. Greuber EK, Pendergast AM. Abl Family Kinases Regulate FcγR-Mediated Phagocytosis in Murine Macrophages. *JI* (2012) **189**:5382–5392. doi:10.4049/jimmunol.1200974

188. Malbec O, Cassard L, Albanesi M, Jönsson F, Mancardi D, Chicanne G, Payrastre B, Dubreuil P, Vivier E, Daëron M. Trans-inhibition of activation and proliferation signals by Fc receptors in mast cells and basophils. *Sci Signal* (2016) **9**:ra126–ra126. doi:10.1126/scisignal.aag1401

189. Katz M, Amit I, Yarden Y. Regulation of MAPKs by growth factors and receptor tyrosine kinases. *Biochimica et Biophysica Acta (BBA) - Molecular Cell Research* (2007) **1773**:1161–1176. doi:10.1016/j.bbamcr.2007.01.002

190. Dai J, Bercury KK, Macklin WB. Interaction of mTOR and Erk1/2 signaling to regulate oligodendrocyte differentiation. *Glia* (2014) **62**:2096–2109. doi:10.1002/glia.22729

191. Sun Y, Liu W-Z, Liu T, Feng X, Yang N, Zhou H-F. Signaling pathway of MAPK/ERK in cell proliferation, differentiation, migration, senescence and apoptosis. *Journal of Receptors and Signal Transduction* (2015) **35**:600–604. doi:10.3109/10799893.2015.1030412

192. Chan ED, Morris KR, Belisle JT, Hill P, Remigio LK, Brennan PJ, Riches DWH. Induction of Inducible Nitric Oxide Synthase-NO· by Lipoarabinomannan ofMycobacterium tuberculosis Is Mediated by MEK1-ERK, MKK7-JNK, and NF-κB Signaling Pathways. *Infection and Immunity* (2001) **69**:2001–2010. doi:10.1128/IAI.69.4.2001-2010.2001

193. Arthur JSC, Ley SC. Mitogen-activated protein kinases in innate immunity. *Nature Reviews Immunology* (2013) **13**:679–692. doi:10.1038/nri3495

194. Parsa KVL, Butchar JP, Rajaram MVS, Cremer TJ, Tridandapani S. The tyrosine kinase Syk promotes phagocytosis of Francisella through the activation of Erk. *Molecular Immunology* (2008) **45**:3012–3021. doi:10.1016/j.molimm.2008.01.011

195. Cao X, Wei G, Fang H, Guo J, Weinstein M, Marsh CB, Ostrowski MC, Tridandapani S. The Inositol 3-Phosphatase PTEN Negatively Regulates Fcγ Receptor Signaling, but Supports Toll-Like Receptor 4 Signaling in Murine Peritoneal Macrophages. *The Journal of Immunology* (2004) **172**:4851–4857. doi:10.4049/jimmunol.172.8.4851

196. Kim JS, Peng X, De PK, Geahlen RL, Durden DL. PTEN controls immunoreceptor (immunoreceptor tyrosine-based activation motif) signaling and the activation of Rac. *Blood* (2002) **99**:694–697. doi:10.1182/blood.V99.2.694

197. Mehta P, Wavreille A-S, Justiniano SE, Marsh RL, Yu J, Burry RW, Jarjoura D, Eubank T, Caligiuri MA, Butchar JP, et al. LyGDI, a Novel SHIP-Interacting Protein, Is a Negative Regulator of FcγR-Mediated Phagocytosis. *PLoS One* (2011) **6**: doi:10.1371/journal.pone.0021175

198. Li FJ, Schreeder DM, Li R, Wu J, Davis RS. FCRL3 promotes TLR9-induced B-cell activation and suppresses plasma cell differentiation. *European Journal of Immunology* (2013) **43**:2980–2992. doi:10.1002/eji.201243068

199. Davis RS. B-1 Cell Development and Function. *Ann N Y Acad Sci* (2015) **1362**:110–116. doi:10.1111/nyas.12771

200. Indik ZK, Pan XQ, Huang MM, McKenzie SE, Levinson AI, Schreiber AD. Insertion of cytoplasmic tyrosine sequences into the nonphagocytic receptor Fc gamma RIIB establishes phagocytic function. *Blood* (1994) **83**:2072–2080. doi:10.1182/blood.V83.8.2072.2072

201. Horan KA, Watanabe K, Kong AM, Bailey CG, Rasko JEJ, Sasaki T, Mitchell CA. Regulation of FcγR-stimulated phagocytosis by the 72-kDa inositol polyphosphate 5-phosphatase: SHIP1, but not the 72-kDa 5-phosphatase, regulates complement receptor 3–mediated phagocytosis by differential recruitment of these 5-phosphatases to the phagocytic cup. *Blood* (2007) **110**:4480–4491. doi:10.1182/blood-2007-02-073874

202. Cox D, Dale BM, Kashiwada M, Helgason CD, Greenberg S. A Regulatory Role for Src Homology 2 Domain–Containing Inositol 5′-Phosphatase (Ship) in Phagocytosis Mediated by Fcγ Receptors and Complement Receptor 3 (αMβ2; Cd11b/Cd18). *Journal of Experimental Medicine* (2001) **193**:61–72. doi:10.1084/jem.193.1.61

203. Feng G-S. Shp-2 Tyrosine Phosphatase: Signaling One Cell or Many. *Experimental Cell Research* (1999) **253**:47–54. doi:10.1006/excr.1999.4668

204. Kan C, Yang F, Wang S. SHP2-Mediated Signal Networks in Stem Cell Homeostasis and Dysfunction. *Stem Cells Int* (2018)8351374. doi:10.1155/2018/8351374

205. Matozaki T, Murata Y, Saito Y, Okazawa H, Ohnishi H. Protein tyrosine phosphatase SHP-2: A proto-oncogene product that promotes Ras activation. *Cancer Sci* (2009) **100**:1786–1793. doi:10.1111/j.1349-7006.2009.01257.x

206. Marengère LEM, Waterhouse P, Duncan GS, Mittrücker H-W, Feng G-S, Mak TW. Regulation of T Cell Receptor Signaling by Tyrosine Phosphatase SYP Association with CTLA-4. *Science* (1996) **272**:1170–1173. doi:10.1126/science.272.5265.1170

207. Lee K-M, Chuang E, Griffin M, Khattri R, Hong DK, Zhang W, Straus D, Samelson LE, Thompson CB, Bluestone JA. Molecular Basis of T Cell Inactivation by CTLA-4. *Science* (1998) **282**:2263–2266. doi:10.1126/science.282.5397.2263

208. Simon M, Vanes L, Geahlen RL, Tybulewicz VLJ. Distinct roles for the linker region tyrosines of Syk in FcepsilonRI signaling in primary mast cells. *J Biol Chem* (2005) **280**:4510–4517. doi:10.1074/jbc.M410326200

209. Moon KD, Post CB, Durden DL, Zhou Q, De P, Harrison ML, Geahlen RL. Molecular Basis for a Direct Interaction between the Syk Protein-tyrosine Kinase and Phosphoinositide 3-Kinase. *J Biol Chem* (2005) **280**:1543–1551. doi:10.1074/jbc.M407805200

210. Ren L, Chen X, Luechapanichkul R, Selner NG, Meyer TM, Wavreille A-S, Chan R, Iorio C, Zhou X, Neel BG, et al. Substrate Specificity of Protein Tyrosine Phosphatases 1B, RPTPα, SHP-1, and SHP-2. *Biochemistry* (2011) **50**:2339–2356. doi:10.1021/bi1014453

211. Law CL, Chandran KA, Sidorenko SP, Clark EA. Phospholipase C-gamma1 interacts with conserved phosphotyrosyl residues in the linker region of Syk and is a substrate for Syk. *Molecular and Cellular Biology* (1996) **16**:1305–1315. doi:10.1128/MCB.16.4.1305

212. Bivona TG, Pérez de Castro I, Ahearn IM, Grana TM, Chiu VK, Lockyer PJ, Cullen PJ, Pellicer A, Cox AD, Philips MR. Phospholipase Cγ activates Ras on the Golgi apparatus by means of RasGRP1. *Nature* (2003) **424**:694–698. doi:10.1038/nature01806

213. Zhang SQ, Yang W, Kontaridis MI, Bivona TG, Wen G, Araki T, Luo J, Thompson JA, Schraven BL, Philips MR, et al. Shp2 Regulates Src Family Kinase Activity and Ras/Erk Activation by Controlling Csk Recruitment. *Molecular Cell* (2004) **13**:341–355. doi:10.1016/S1097-2765(04)00050-4

214. Greenberg S, Chang P, Silverstein SC. Tyrosine phosphorylation of the gamma subunit of Fc gamma receptors, p72syk, and paxillin during Fc receptor-mediated phagocytosis in macrophages. *J Biol Chem* (1994) **269**:3897–3902.

215. Kedzierska K, Ellery P, Mak J, Lewin SR, Crowe SM, Jaworowski A. HIV-1 Down-Modulates γ Signaling Chain of FcγR in Human Macrophages: A Possible Mechanism for Inhibition of Phagocytosis. *J Immunol* (2002) **168**:2895–2903. doi:10.4049/jimmunol.168.6.2895

216. Kim DI, Jensen SC, Noble KA, Kc B, Roux KH, Motamedchaboki K, Roux KJ. An improved smaller biotin ligase for BioID proximity labeling. *MBoC* (2016) **27**:1188–1196. doi:10.1091/mbc.E15-12-0844

217. Fei C, Pemberton JG, Lillico DM, Zwozdesky MA, Stafford JL. Biochemical and Functional Insights into the Integrated Regulation of Innate Immune Cell Responses by Teleost Leukocyte Immune-Type Receptors. *Biology* (2016) **5**: doi:10.3390/biology5010013

218. Trede NS, Langenau DM, Traver D, Look AT, Zon LI. The Use of Zebrafish to Understand Immunity. *Immunity* (2004) **20**:367–379. doi:10.1016/S1074-7613(04)00084-6

219. Novoa B, Figueras A. Zebrafish: model for the study of inflammation and the innate immune response to infectious diseases. *Adv Exp Med Biol* (2012) **946**:253–275. doi:10.1007/978-1-4614-0106-3_15

220. Herbomel P, Thisse B, Thisse C. Ontogeny and behaviour of early macrophages in the zebrafish embryo. *Development* (1999) **126**:3735–3745.

221. Belosevic M, Hanington PC, Barreda DR. Development of goldfish macrophages in vitro. *Fish Shellfish Immunol* (2006) **20**:152–171. doi:10.1016/j.fsi.2004.10.010

222. Edholm E-S, Bengtén E, Stafford JL, Sahoo M, Taylor EB, Miller NW, Wilson M. Identification of Two IgD+ B Cell Populations in Channel Catfish, Ictalurus punctatus. *The Journal of Immunology* (2010) **185**:4082–4094. doi:10.4049/jimmunol.1000631

223. Stafford JL, Wilson M, Nayak D, Quiniou SM, Clem LW, Miller NW, Bengtén E. Identification and Characterization of a FcR Homolog in an Ectothermic Vertebrate, the Channel Catfish (Ictalurus punctatus). *The Journal of Immunology* (2006) **177**:2505–2517. doi:10.4049/jimmunol.177.4.2505

224. Jo/ssang T, Feder J, Rosenqvist E. Heat aggregation kinetics of human IgG. *J Chem Phys* (1985) **82**:574–589. doi:10.1063/1.448730

225. van Ginkel FW, Miller NW, Lobb CJ, Clem LW. Characterization of anti-hapten antibodies generated in vitro by channel catfish peripheral blood lymphocytes. *Developmental & Comparative Immunology* (1992) **16**:139–151. doi:10.1016/0145-305X(92)90014-4

APPENDIX

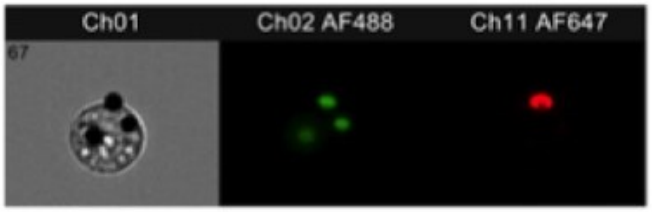

Mask	Description	Image
Peak(M02, Ch02 AF488, Bright 10)	Peak mask used to identify beads above background	
Dilate(Peak(M02, Ch02 AF488, Bright 10)1)	Dilate mask adds pixels to edge of peak mask to mask entire bead area	
Range(Dilate(Peak(M02, Ch02 AF488, Bright 10)1)15-5000)	Range mask selects size range for beads	
Component(1, Area, Range(Dilate(Peak(M02, Ch02 AF488, Bright, 10), 1), 15-5000, 0.3-1), Ascending)	Component 1 mask selects green bead with smallest masked area	
Component(2, Area, Range(Dilate(Peak(M02, Ch02 AF488, Bright, 10), 1), 15-5000, 0.3-1), Ascending)	Component 2 mask selects green bead with second smallest masked area	
Component(3, Area, Range(Dilate(Peak(M02, Ch02 AF488, Bright, 10), 1), 15-5000, 0.3-1), Ascending)	Component 3 mask selects green bead with largest masked area	

Appendix Figure A1. Masking description for connected component strategy. Outline of masks created to identify beads (peak, dilate, and range masks) and components (component 1–3). To show the mask, green beads were pseudo-coloured pink. And masked beads show up as purple. Component masks were created to identify beads with increasing pixel area (ascending area component mask). Each component mask is identified by a white arrow.